ABSTRACT

LIU, YANYUN. Simulation of Ocean Circulation around the Galápagos Archipelago using a Hybrid Coordinate Ocean Model (HYCOM). (Under the direction of Dr. Lian Xie and Dr. John M. Morrison).

The ocean circulation around the Galápagos Archipelago is simulated using the University of Miami's Hybrid Coordinate Ocean Model (HYCOM) using a high-resolution (0.04 degree resolution) nested domain. The model generally reproduces the major ocean circulation features around the Galapagos showing that the 0.04 degree resolution is sufficient for studying the circulation and water mass structure local to the Galápagos. A variety of winds forcing were tried with high frequency wind forcing (daily, 6-hrly) proving to be more reliable than the monthly forcing. The Archipelago has a large range in temperature and salinity associated with four different current systems and topographically and wind forced upwelling. West of Isabella and Fernandina Islands are the largest and most consistent upwelling zones, resulting from the collision of the Equatorial Undercurrent with the islands, bring relatively colder and salty waters to the surface in a region of topographically induced upwelling. This upwelling zone marks the location of high biological production at the surface with the EUC shoaling to approximately 20m from its normal depth of 50m just to the west of the islands. This results not only in a strong upwelling zone just to the west of the islands, but also in shallow mixed layers over the entire western portion of the Archipelago. The model results, which agree quite well with observations of the EUC by the TAO array, show a seasonal cycle in the speed and transport of the EUC, reaching a maximum during the late spring/early summer and minimum in the late fall. This seasonal cycle is disrupted during El Niño when the collapse of the westerlies results in a greatly weakened or even a

total lack of the undercurrent. The far northern region of the Archipelago is characterized with warmer, fresher water and had the deepest mixed layer depth as a result of Panama Current waters from the northeast. The water masses over the remainder of the region result from a mixing of cool Peru Current waters and upwelled Cold Tongue waters entering from the east to the southeast mixing with the upwelled EUC waters. The regional impact of global climate change and ENSO events on the ocean circulation and water mass characteristics around the Galápagos Archipelago is studied using the Hybrid Coordinate Ocean Model (HYCOM). The result indicates that with prescribed atmospheric forcing, the major characteristics of the ocean circulation and its variability in the Galapagos region, including the ENSO events, annual and seasonal cycles, upwelling system, local and regional current systems, and tropical instability waves, can be reproduced by the nested HYCOM model. Results show that the oceanic variability in the Galapagos region is sensitive to global climate change. The regional impact of global climate change in the Galapagos region varies from region to region. Results show the western Galapagos upwelling region is affected by the EUC and Panama currents; while central/east Galapagos is affected by both Peru and EUC currents. The north region is affected by the Panama Current only. The southeast region is affected by the Peru Current only. These regional differences explain the variability of the responses in different regions of the Galapagos Archipelago to global climate change.

Simulation of Ocean Circulation around the Galápagos Archipelago Using a Hybrid Coordinate Ocean Model (HYCOM)

by
Yanyun Liu

A dissertation submitted to the Graduate Faculty of
North Carolina State University
in partial fulfillment of the
requirements for the degree of
Doctor of Philosophy

Marine, Earth & Atmospheric Sciences

Raleigh, North Carolina

2010

APPROVED BY:

Dr. Dan L. Kamykowski	Dr. Fredrick H. M. Semazzi
Dr. John M. Morrison Co-Chair of Advisory Committee	Dr. Lian Xie Chair of Advisory Committee

BIOGRAPHY

Yanyun Liu was born in February, 1981, in Qingdao of Shandong province. In 1998, she attended Ocean University of Qingdao (now called Ocean University of China), receiving Bachelor of Science degree from double majors in Marine Meteorology and Computer Science in 2002, and Master of Science degree in Marine Meteorology in 2005. She joined the Department of Marine, Earth and Atmospheric Sciences of North Carolina State University in fall 2005 as a graduate student pursuing a Ph.D. degree.

ACKNOWLEDGMENTS

Here, I wish to acknowledge many great people during this work. First of all, I would like to express my great gratitude to my advisor, Dr. Lian Xie for his guidance, support throughout my graduate study. His encouragement and patience led me step-by-step to complete this work. I also benefited a lot from his methodology in ocean numerical modeling and his many thoughtful ideas. Great appreciation is expressed to my co-advisor Dr. John M. Morrison for his endless support and kindness, as well as his thoughtful input and advice on this research. I would also like to thank my advisory committee members, Dr. Daniel Kamykowski and Dr. Fredrick Semazzi, for their support, thoughtful discussions and helpful comments on this research. They are also very helpful in providing me with various resources for the study.

Great appreciation is extended to many faculty members whose lectures are the basis for marine science research. Thanks Dr. Gerald Janowitz and Connie Hockaday for the help during my graduate study. Thanks to Dr. Rainer Bleck and Dr. Alan Wallcraft for their help of the HYCOM model.

I also would like to thank all friends in the Coastal Fluid Dynamics Laboratory: Dr. Machuan Peng, Dr. Tingzhuang Yan, Dr. Xiaoming Liu, Dr. Huiqing Liu, Dr. Xuejin Zhang, Dr. Meng Xia and Dr. Bin Liu, Qianhong Tang, Yao Zhao for their help and suggestions in this study. Thanks for Elinor Keith and Katie Costa in my English

pronunciation and writing skills. Thanks are also given to Dr. William Sweet, Dr. Blake Schaeffer and Anita McCulloch for their help in this Galapagos study.

Finally, I would like to acknowledge my parents and sister. Without their continuous love, encouragement and support, I couldn't have completed this dissertation and faced the challenges in my life.

This study is funded by National Aeronautics Space Association (NASA) Biodiversity and Ecological Forecasting grant NNG04GL98G. The Counterpart US-AID No. 518-A-00-03-00152-00, UK Darwin Initiative Project No. 14-048 and the Department of Energy (DOE) also provided funding for this research. All modeling work is carried out in the Coastal Fluid Dynamical Lab of North Carolina State University using the High-Performance Computing (HPC) system.

TABLE OF CONTENTS

LIST OF FIGURES

Chapter 1

Chapter 3

Chapter 4

Chapter 5

Chapter 6

LIST OF TABLES

Chapter 3

Chapter 1

Introduction and Background

1 Scientific Background

The Galápagos Archipelago (Figure1) lies in the equatorial eastern Pacific Ocean, about 1000 km west of the coast of Ecuador, South America. It can reasonably claim to possess the most distinctive marine flora and fauna and unique species for any area of its size worldwide (Bustamante et al., 1999). In order to help preserve and protect the unique underwater environment, in March 1998, Ecuador created the Galápagos Marine Reserve (GMR), which is an extensive area, over 140,000 km^2, and consists of an extremely variable ecological system in space and time (Jennings 1994). It is the only place in the world where hammerhead sharks, penguins, and corals co-exist on the same sub-tidal reef. The principle reason why the GMR features such great diversity lies in its positioning in a complex transition zone between tropical, subtropical and upwelling zones. Hence, Galápagos provides an ideal "field laboratory" for assessing how rising global water temperature will impact marine ecosystems, as well as, the effects of events of extreme climate variability associated with ENSO. These conditions have allowed the presence of a rich diversity of endemic organisms. Edgar et al. (2004) divided the GMR based on the most comprehensive, on-going estimates of mobile macro-invertebrate and reef fish biodiversity within the GMR by divers from the Charles Darwin Research Station (CDRS). The results from the former indicate three unique major bio-zones – Far

northern, Western and remainder of the Archipelago, with the latter allowing further subdivisions of the Elizabeth, Northern and Central-Southeastern (Central-SE) bio-zones.

The Galápagos Archipelago ecosystem is mainly affected by several different surface and subsurface currents. On a larger scale, these currents are the westward North Equatorial Current (NEC), South Equatorial Current (SEC), eastward Equatorial Countercurrent (ECC) and Equatorial Undercurrent (EUC). The NEC usually lies between 10° and 20° N, while the SEC lies between 5° N and 10° S. Since the meteorological equator (Inter-Tropical Convergence Zone -- ITCZ) lies north of the geographical equator, the southern hemisphere trade winds cross the equator and result in a SEC that straddles the equator. The NEC and SEC are separated by the narrow ECC (flowing to the east in a belt and corresponding to the ITCZ). The SEC is the dominant surface current affecting the Galápagos, which drives superficial waters over the entire region around the Galápagos and is composed of the warmer Panama Current and cool Humboldt Current. The Panama Current influences the northern islands, while the cool Humboldt (Peru) Current influences the southern islands. The trade wind leads to the warm waters piling up in the western Equatorial and drains it from the eastern Pacific. The thermocline, which is the sharp vertical temperature gradient separating the warm surface layer from the cold deep ocean, is pushed down to a depth of 150m in the west, but shoals to 50m depth in the east. Sea level tends to reflect thermocline depth since water expands when heated. Thus, while the thermocline tilts downward towards the west along the equator, sea level rises to the west where it stands about 60cm higher than in

the eastern Pacific. The eastward EUC (also known as the Cromwell current) developed as a subsurface compensation against the eastward SEC, causing the upwelling in western archipelago. This upwelled water is relatively rich in iron, the micronutrient needed for growth by most organisms, and the production is high in many areas of the Galapagos and surrounding waters (Steger et al. 1998). The EUC, which is confined to a narrow region +/- 2° about the equator, rises from nearly 200m depth in the western Pacific and shallows to <50m in the east, feeding the Ekman divergence in the east Pacific (Wyrtki 1966). The EUC is found throughout the Archipelago at depths ~50m (Houvenaghel 1984). In addition, the Equatorial Undercurrent (EUC) flows eastward along the equator beneath the main equatorial currents. The EUC is the major oceanographic feature affecting production through the Galapagos Archipelago (Houvenaghel 1984).

The Galápagos are greatly affected by seasonal atmospheric and oceanographic variability (Houvenaghel 1984). During the hot wet season (from December to May), the Intertropical Convergence Zone (ITCZ) migrates southward towards the equator, the northeast trades become more prevalent, and warmer (>25°C), fresher (<34) and less-productive waters of the Panama Current flow southward into the Archipelago. During the dry Garúa season (from May to November), the ITCZ migrate to the north of the equator, the southeast trade winds become dominate, the major source waters for the SEC are the cold Peruvian ocean current and the Peruvian coastal current (the Humboldt Current), enhancing the contributions to the SEC with the colder (18°-20°C), saltier (>35) productive waters. The different source waters for the SEC as it flows though the

GMR, from both northern and southern hemispheres, as well as topographically induced upwelling which occurs when the eastward flowing EUC runs into the Galápagos platform are the cause of the tremendous diversity around the Archipelago.

A few studies have quantified the primary production around the Archipelago especially the higher concentrations west of Isabella (Feldman 1984, 1986) from the upwelling EUC. Houvenaghel (1984) discussed the oceanographic setting of the Galápagos and concluded that the EUC was the major oceanographic phenomena affecting the Galápagos. Hayes (1985) pointed out that the sea level differences across the Archipelago increase as the EUC strengthens, measured by shallow moored pressure gauges. Steger et al. (1998) found that the near-surface waters to the west of the Archipelago during November 1993 were predominately upwelled EUC waters, and as a consequence were cooler, saltier and higher in nutrients and iron than waters found over the eastern portion of the Archipelago. In addition, the extent of the plume shown by Feldman (1986) and the one observed by Steger et al. (1998) could only be maintained by upwelling of EUC waters that are cooler and high in nutrients. Steger et al. (1998) show that the waters of the EUC bifurcate when they run into the Galápagos platform, with water continuing to flow to the east both to the north and south of the platform. East of the Archipelago, Steger et al. (1998) found evidence that these north and south eastward flows most likely converge and reform a definable EUC. Steger et al. (1998) also found that the core of the EUC was south of the equator during a hot season, as did Christensen (1992), but with a strong branch also found north of the Galápagos. This variation in EUC displacement is not well enough

understood to determine whether it is due to seasonal variability or unstable flow conditions (Lukas 1986). Wyrtki (1967) showed by way of water mass analysis that some of the EUC waters re-circulate both north and south of the Archipelago, and Houvenaghel (1984) highlighted the areas within the Archipelago prone to upwelling due to the western exposure of landmasses to the eastward flowing EUC. Palacios (2004) found that the temporal variability of ocean color and SST around the Galapagos was dominated by the seasonal migration of the ITCZ and associated strengthening of the SEC and EUC. In summary, studies to this point indicate that the EUC is the major oceanographic feature affecting production in the Galápagos Marine Reserve.

However, the flow pattern of the EUC around the Galapagos has not been fully determined. How does the EUC propagate across the Galápagos platform? As the EUC runs into the Galápagos platform and is topographically "broken" in streams, how do these streams vary in position and strength, and route through the islands? It is quite probable that these topographical constrained flows and associated topographically induced upwelling are the most important defining physical process to influence the very high local production at certain sites. However, most of the prior studies of the Galápagos mainly focused on short term observational results, which necessarily have been rather limited in time and scope. Therefore, we propose to us a fully hydrodynamic, high-resolution numerical model to study these important processes. Numerical model results, especially of the current and water mass distributions will also allow us to make estimations of the effects of ocean warming and climate change on the biodiversity of the

Galápagos Marine Reserve. These local predictions may help to define the effects of climate change on global biodiversity – the Reserve is located at "ground zero" for ENSO!

Another distinctive feature associated with Galápagos coastal waters is that the greatest sea temperature anomalies occur during El Niño and La Niña events (Glynn and Ault, 2000). Recently the frequency and severity of El Niño events appear to have increased and this is a concern for the conservation of endangered species. El Niño events now occur 2–7 times more frequently than they did 7000–15,000 years ago (Riedinger et al., 2002; Rodbell et al., 1999). The 1982-83 and 1997-98 El Niño events, in particular, were the most extreme for many centuries, and had a devastating effect on marine life in the Galápagos region. During El Niño, the EUC weakens, the surface water warms, micronutrients are reduced, the primary production decreases (Chavez et al., 1999), and fish numbers diminish. Data from commercial fisheries indicated that the catch of mullets from the Galapagos during the 1997–1998 El Niño event were half that of the commercial catch in 1999, a "normal" year (Nicolaides and Murillo, 2001). Houvenaghel (1984) predicts that when the EUC is not present during intense El Niño's periods when the southeast trade winds collapse, biological activity within the Archipelago would be substantially reduced. This prediction is supported by SST and chlorophyll signatures from AVHRR and SeaWiFS satellite data during the final phase of the 1997/1998 El Niño when the Trade Winds resumed, driving upwelling in the Archipelago. Thus the relationship between El Niño events and EUC, as well as the relationship between extreme ENSO events and loss of marine biodiversity in Galápagos needs to be

investigated as a matter of local and global importance. Such a study has direct implications to predictions of loss of global biodiversity associated with ocean warming and climate change.

2. Purposes of the Study

The primary objective of this study is to describe ocean circulation and water mass characteristics around the Galapagos Archipelago. The emphasis is on the features and processes associated with the local upwelling of the EUC on the western side of the islands, since this phenomenon is responsible for sustaining the cold, highly productive conditions. One of the principle new findings from the US JGOFS Eq-Pac Process study in the central equatorial Pacific was that iron in the equatorial undercurrent (EUC) is the most important source of iron for driving biological new production and thus carbon cycling in this region.

Never the less, how the variation of the EUC around the Galapagos will be affected by climate change has not been fully determined. In addition, the flow pattern of the EUC around and through the Galápagos has not been fully determined. How does the EUC propagate across the Galápagos platform? As the EUC runs into the Galápagos platform and is topographically "broken" in streams, how do these streams vary in position and strength, and route through the islands? It is quite probably that these topographically constrained flows and associated topographically induced upwelling are the most

important defining physical process to influence the very high local production at certain sites.

This study will mainly focus on the oceanographic variability and forcing factors associated with biological productivity of the various marine pelagic ecosystems across the GMR using a fully hydrodynamic, ocean general circulation model, specifically the Hybrid Coordinate Ocean Model (HYCOM; Bleck, 2002; Chassignet et al., 2003; Halliwell, 2004). Specifically, the scientific objectives of this study are to,

1) Study the oceanographic variability and forcing factors associated with biological productivity and biogeography of the various marine pelagic ecosystems across the Galápagos Marine Reserve (GMR) using HYCOM model;
2) Simulate the water mass characteristics and currents around the GMR by using HYCOM and compare with the 2005/2006 cruises results, hoping to better understand the physical environment influencing the Galápagos Archipelago and human socio-economic response to climatological perturbations, such as ENSO;
3) Simulate the ENSO events using HYCOM and depict how the El Niño events affect the phytoplankton primary production around the GMR on a case by case basis. Sensitivity studies will be carried out to identify key physical processes that affect the water mass transport pathways and the local upwelling dynamics. This will include hind-casts during strong El Niño and La Niña conditions, as well as periods of "normal" conditions.

4) Model the potential impact of future climate change scenarios on the oceanographic variability in the Equatorial Pacific Ocean from mesoscale to basin scale as they affect the biodiversity of the marine pelagic ecosystems of the GMR using HYCOM. The outcome is a down-scaling assessment of the impact of global climate change scenarios on the ocean circulation and water mass structure in GMR region using a high-resolution nested grid HYCOM forced under selected climate change scenarios described by IPCC.

3. Hypotheses

Hypothesis 1: *The EUC is the major oceanographic feature affecting the production in the Galápagos Marine Reserve (GMR), and is likely strongly associated with local biogeography of marine species and endemism.*

The EUC is thought to be the major oceanographic feature affecting the production in the Galápagos Marine Reserve (GMR) and is important defining physical process to influence the very high local production at certain sites. Much of the energy input to the Galápagos archipelago is supported by nutrient influx to the euphotic zone from cold bathymetrically deflected upwelled water from the eastward flowing submarine EUC. The upwelling events impacting upon the west of the archipelago vary in strength, size and stability under the influence of localized current systems and forcing effects. The EUC flow pathways and upwelling are linked directly to the submarine topography,

which introduces obstacles to the eastward path of the undercurrent. This deflects water to the north in the northern hemisphere and to the south in the southern hemisphere. The EUC waters are cooler, saltier and higher in nutrients and iron than waters found over the eastern portion of the Archipelago and directly result in the large phytoplankton bloom observed in SeaWiFS and SST. The result indicates that when there is not an EUC present (for example, during intense El Niño's), the intense biological activity normally sustaining the GMR will be absent.

Hypothesis 2: *Galápagos marine pelagic ecosystem heterogeneity is a function of oceanographic pattern over small spatial, seasonal and inter-annual scales.*

A shift in the source of waters supplying the SEC as the ITCZ seasonally migrates is responsible for the seasonal climate changes of the Galapagos Islands. During the Garúa season (dry season – May to December) the ITCZ is well to the north of the equator and the major source waters for the SEC are the cold Peruvian Ocean Current and the Peruvian Coastal Current (the Humboldt Current). The southeast trade winds are very strong during the Garúa season, contributing to the process. The water has a temperature of 18 – 20 ℃, a salinity of 35, and is rich in marine fauna. In the warm season (wet season – December to May), the southeast trade winds vanish, as does the action of the Humboldt Current. The northeast trades become dominate, and warm waters head south from Panama and Columbia (Panama Flow). The water has a sea surface temperature range from 24 – 27 ℃, a lower salinity of 33.5, and is poor in organisms. As the ITCZ migrates to the south in this season, to within a few degrees north of the equator, the

warm waters again meet the Humboldt Current and form the SEC, which flows across the archipelago. During the Garúa season, the ITCZ is found north of the Equator, leading to strong southeast trades straddling the equator and a convergence of waters along the equator and ultimately to a compensating subsurface eastward flow is established, the Equatorial Undercurrent (EUC). This current gradually comes up in the water column as the thermocline shoals to the east, until it as found at a depth of ~ 50 m when it runs into the Galápagos. We are interested in what happens when this current runs into the Galápagos Platform.

The interaction of the different ocean currents within the Galápagos Archipelago divides the islands into distinct biogeographical zones. Harris (1969) proposed that the Galápagos Archipelago could be divided into five biogeographical zones based on a series of 300 snap-shot temperature records related to the influence of the different current systems impacting the area: the temperate north zone, two mixed central zones, South Equatorial Current (Humboldt) southern zone and Equatorial Undercurrent Current (Cromwell) upwelling zone to the west. The variable relationship among the boundaries associated with these biographical zones can provide a shorter time scale forcing to ecosystem structure/function to complement the El Niño/La Niña forcing (Longhurst, 1998). Wellington et al. (2001) verified that several distinct zones were identifiable, but differences between the historical zones appear less well defined than previously proposed. The most comprehensive estimates of marine biodiversity in the GMR

gathered by CDRS suggest that different biogeography exist for different groups and that endemism that is seen is related to areas of obvious EUC influence.

Hypothesis 3: *HYCOM model can generally reproduce the ocean circulation around the Galapagos and the major characteristics of ENSO events.*

This model allows high vertical resolution where it is most needed, over the shelf and in the mixed layer. Also the isopycnal coordinate reduces the need for high vertical resolution in deep water. The HYCOM simulations generate a stronger EUC that compares more favorably to observations than other models, such as the GFDL model (Chassignet et al. 1996). So HYCOM was a very good choice to simulate the ocean circulation around the GMR. Our hypotheses here need to be verified and to provide a basis of our future study, some sensitivity experiments need to be conducted using the HYCOM model.

Hypothesis 4: *Because of the location of the islands in the eastern Tropical Pacific Ocean and the extreme biodiversity of the waters surrounding the Archipelago, this is an ideal place to study the relationship between climate change and biodiversity as a matter of local and global importance. Such a study has direct implications for predictions of loss of global biodiversity associated with ocean warming and climate change.*

The water mass characteristics and currents around the GMR will be studied using

HYCOM in an effort to better understand the physical environment influencing the Galápagos Archipelago under future climate change scenarios as described by the Noble Peace Prize winning United Nations Intergovernmental Panel on Climate Change (IPCC). For example, it is well known that during El Niño, the lack of a strong Equatorial Undercurrent (EUC) essentially shuts off the upwelling of the cooler, saltier, higher nutrient and iron enriched waters found over the western portion of the Archipelago. Therefore, any influence of climate change on the frequency, duration and magnitude of El Nino at the basin scale is likely to be cascaded to the regional and local scales in the GMR.

Specifically, we will conduct three long-term model runs: 1) a 40 year simulation of the past climate change and its impact on the GMR ocean circulation (Case 1); 2) two long-term simulations (the exact length of simulation depends on the climate change scenarios to be selected) of future ocean circulation and water mass characteristics in the GMR under a global warming scenarios (Cases 2 and 3).

Case 1: For current climate (1951-2000), we will conduct the global and Pacific run. We will do high resolution runs near Galapagos for all El Niño, and La Niña years, and conduct ensemble analysis to see the differences of the local response to El Niño and La Nina, and also compare them with climatology, Historical data and data collected will be used to validate and calibrate the ocean model.

Case 2: We will run 2000-2050 climate change scenario runs, using the IPCC AR4 forcing scenarios. Then, we will analyze the average or weighted average of the Pacific and local circulation, and see if there is any noticeable difference at different spatial and temporal time scales.

Case 3 is a simulation of the regional and local ocean response in the GMR region to a global climate change scenario under the control scenario. We will simulate the response of the GMR ocean circulation to historical climate in the past 40 years using NCEP/NCAR reanalysis data as the climatic forcing. This simulation will provide a validation for the high resolution HYCOM model and a benchmark of assessing future climate change impacts.

4. Organization of the Dissertation

Data and ocean numerical model used in this research will be discussed in Chapter 2. The result of sensitivity tests on horizontal resolution and high-frequency atmospheric forcing will be included in Chapter 3. In Chapter 4, the simulated tropical ocean circulation around the GMR using QuikSCAT and NCEP forcing are demonstrated and compared with the observation cruise results. In Chapter 5, the ENSO simulation study and how ENSO events affected the ocean circulation around the Galapagos are presented. How the ocean circulation and water mass characteristics around the Galápagos Archipelago affected by climate change is studied in Chapter 6. In this chapter, the

different physical variables are specifically compared and analyzed around the GMR during the different El Nino and La Nina cases. How the different regions are influenced by different current will also be discussed. Finally, chapter 7 gives the concluding remarks and future work.

References

Bleck, R., 2002. An oceanic general circulation model framed in hybrid isopycnic-Cartesian coordinates. Ocean Modeling, 4, 55-88.

Bustamante, R., Collins, K. J. Bensted-Smith, R., 1999. Biodiversity conservation in the Galápagos Marine Reserve. Entomologie Supplement 68: 45-52.

Chassignet, E.P., Smith, L.T., Bleck, R., Bryan, F.O., 1996. A model comparison: numerical simulations of the north and equatorial Atlantic oceanic circulation in depth and isopycnic coordinates. J. Phys. Oceanogr. 26, 1849– 1867.

Chassignet, E.P., Smith, L.T., Halliwell, G.R., Bleck, R., 2003. North Atlantic Simulations with the Hybrid Coordinate Ocean Model (HYCOM): impact of the vertical coordinate choice, reference density, and thermobaricity. J. Phys. Oceanogr. 33, 2504–2526.

Chavez, F.P., Strutton, P.G., Friederich, G.E., Feely, R.A., Feldman, G.C., Foley, D.G., McPhaden, M.J., 1999. Biological and chemical response of the equatorial pacific ocean to the 1997–1998 El Niño. Science 286, 2126–2131.

Edgar, G. J., Banks, S., Farina, J. M., Calvopina, M. and Martınez, C., 2004. Regional biogeography of shallow reef fish and macro-invertebrate communities in the Galápagos archipelago. Journal of Biogeography 31: 1107-1124.

Feldman, G., Clark, D., Halpern, D., 1984. Satellite color observations of the phytoplankton distribution in the eastern equatorial Pacific during the 1982–1983 El Niño, Science 226 (4678), 1069–1071.

Feldman, G..,1986. Patterns of phytoplankton production around the Galápagos Islands. In M.J. Bowman, R.T. Barber & C.N.K. Mooers (Eds.), Lecture Notes on Coastal and Esutarine Studies: Tidal Mixing and Plankton Dynamics (pp. 77-106). Berlin: Springer

Glynn, P.W. and J.S. Ault. 2000. A biogeographic analysis and review of the far eastern Pacific coral reef region. *Coral Reefs* **19**: 1-23.

Halliwell Jr., G.R., 2004. Evaluation of vertical coordinate and vertical mixing algorithms in the Hybrid-Coordinate Ocean Model (HYCOM). Ocean Modelling. 7, 285–322.

Hayes, S. P. 1985. Sea level and near surface temperature variability at the Galápagos Islands, 1979-1983

Houvenaghel, G. T., 1978. Oceanographic conditions in the Galápagos Archipelago and their relationships with life on the islands. In: Boje, R., Tomczak, M. (Eds.), Upwelling Ecosystems. Springer, Berlin, pp. 181–200.

Houvenaghel, G. T., 1984. Oceanographic setting of the Galápagos Islands. In: Perry, R. (Ed.), Key Environments, Galápagos. Pergamon Press, Oxford, pp. 43–54.

Kistler, R., E. Kalnay, W. Collins, S. Saha, G. White, J. Woollen, M. Chelliah, W. Ebisuzaki, M. Kanamitsu, V. Kousky, H. van den Dool, R. Jenne, and M. Fiorino, 2001: The NCEP-NCAR 50-Year Reanalysis: Monthly Means CD-ROM and Documentation. Bull. Amer. Meteor. Soc., 82, 247-268.

Large, W.G., Mc Williams, J.C., Doney, S.C., 1994. Oceanic vertical mixing: review and a model with a nonlocal boundary layer parameterization. Rev. Geophys. 32, 363–403.

Levitus, S., Boyer, T., 1994. World Ocean Atlas 1994, Volume 4: Temperature. NOAA Atlas NESDIS 4. US Dept. of Commerce, Washington, DC.

Levitus, S., Burgett, R., Boyer, T., 1994. World Ocean Atlas 1994, Volume 3: Salinity. NOAA Atlas NESDIS 3. US Dept. of Commerce, Washington, DC.

Jennings, S., Brierley, A.S., & Walker, J.W. 1994. The inshore fish assemblages of the Galápagos Archipelago. Biological Conservation, 70, 49-57

Palacios, D.M. (2004). Seasonal patterns of sea-surface temperature and ocean color around the Galápagos: regional and local influences. *Deep-Sea Research II, 51,* 43-57

Riedinger, M.A., Steinitz-Kannan, M., Last, W.M., Brenner, M.,2002. A similar 6100 C-14C yr record of El Niño activity from the Galápagos Islands. Journal of aleolimnology 27, 1–7.

Rodbell, D.T., Seltzer, G.O., Anderson, D.M., Abbott, M.B., Enfield, D.B., Newman, J.H., 1999. An asymptotically equal to 15,000- Year Record of El Niño-Driven Alluviation in Southwestern Ecuador. Science 283, 516–519.

Steger, J. M., Collins, C. A., Chu, P. C., 1998. Circulation in the Archipielago de Colon (Galápagos Islands), November 1993. Deep-Sea Research II 45, 1093–1114.

Wyrtki, K., Kilonsky, B., 1984. Mean water and current structure during the Hawaii-to-Tahiti shuttle experiment. Journal of Physical Oceanography 14, 242–254.

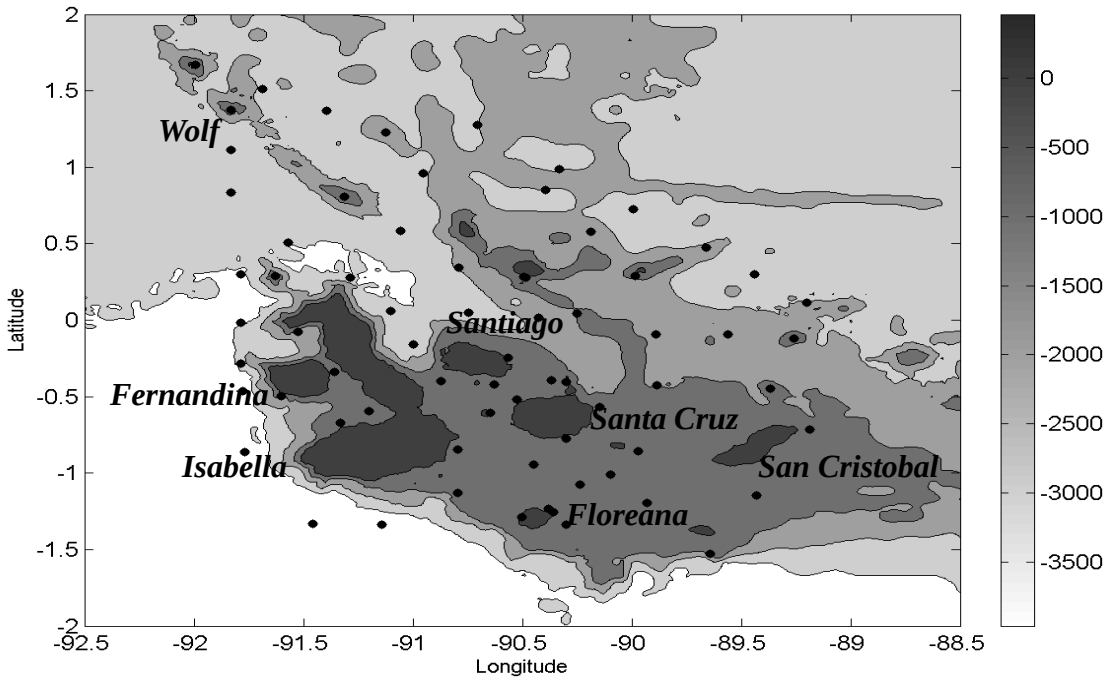

Figure 1: Bathymetry map and sampling stations of the Galápagos Archipelago.

Chapter 2

Data and Numerical Ocean Model

1 Data

The data used in this research include NCEP/NCAR Reanalysis data, IPCC AR4 HadCM3 data, COADS climatology, Levitus ocean data, and ETOP02 bathymetry. They are briefly described as below.

1.1 NCEP/NCAR Reanalysis Data

In order to get a sense of what past environments resemble, it is useful to analyze data from the National Center for Environmental Prediction (NCEP) and National Center for Atmospheric Research (NCAR) global reanalysis dataset. The NCEP/NCAR (Reanalysis project is using a state-of-the-art analysis/forecast system to perform data assimilation using past data from 1948 to the present. A large subset of this data is available from PSD in its original 4 times daily format and as daily averages. However, the data from 1948-1957 is a different in the regular (non-Gaussian) gridded data. That data was done at 8 times daily in the model, because the inputs available in that era were available at 3Z, 9Z, 15Z, and 21Z, whereas the 4x daily data has been available at 0Z, 6Z, 12Z, and 18Z. These latter times were forecasted and the combined result for this early era is 8 x daily. The local ingestion process took only the 0Z, 6Z, 12Z, and 18Z forecasted values, and

thus only those were used to make the daily time series and monthly means here. The products are of high temporal and spatial resolution, with a grid-spacing close to 1.875 ° longitude by 1.915 °latitude in the horizontal and with 17 levels and 28 sigma levels in the vertical. In our research, we will use this data for atmospheric forcing; we will mainly use the daily surface wind stress, surface air temperature, surface atmospheric specific humidity, net shortwave radiation, net long-wave radiation and precipitation fields obtained from NCEP reanalysis [Kalnay et al, 1997, Kistler, et al, 2001].

1.2 IPCC AR4 Data

The SRES refers to the scenarios described in IPCC Special Report on Emissions Scenarios (SRES, 2000). The SRES scenarios are grouped into four scenario families (A1, A2, B1 and B2) that explore alternative development pathways, covering a wide range of demographic, economic and technological driving forces and resulting GHG emissions. The emissions projections are widely used in the assessments of future climate change, and their underlying assumptions with respect to socio-economic, demographic and technological change serve as inputs to many recent climate change vulnerability and impact assessments. The A1 storyline assumes a world of very rapid economic growth, a global population that peaks in mid-century and rapid introduction of new and more efficient technologies. B1 describes a convergent world, with the same global population as A1, but with more rapid changes in economic structures toward a service and information economy. B2 describes a world with intermediate population and economic

growth, emphasizing local solutions to economic, social, and environmental sustainability. A2 describes a very heterogeneous world with high population growth, slow economic development and slow technological change. No likelihood has been attached to any of the SRES scenarios. Warming tends to reduce land and ocean uptake of atmospheric carbon dioxide, increasing the fraction of anthropogenic emissions that remains in the atmosphere. For the A2 scenario, for example, the climate-carbon cycle feedback increases the corresponding global average warming at 2100 by more than 1 ℃. In this study we will choose the A1B Emissions Scenario (A future world of very rapid economic growth, low population growth and rapid introduction of new and more efficient technology).

1.3 ETOP 02 and Galapagos bathymetry

This dataset is from National Geographical Data Center (NGDC). It contains digital data bases of seafloor and land elevations on a 2-minute latitude/longitude grid. The Galapagos bathymetry has a resolution of 0.01 ºfrom a data set put together by William Chadwick, Oregon State University (http://www.pmel.noaa.gov/vents/staff/chadwick/galapagos.html).

1.4 Levitus ocean data

This dataset is produced by NOAA National Oceanic Data Center (NODC). The atlas contains annual and monthly long term means for temperature and salinity at multiple depths as well as mixed layer depths as monthly long term means, the last derived both from potential temperature and potential density. The Levitus Climatology provides 13 raw fields of data (Temperature, Salinity, etc) from which specific seasons and years can be extracted. Data which contain any of several documented errors are flagged and be discarded, as we have done when using the raw data. An analyzed field for all years and individual seasons is also provided.

2 Ocean Numerical Model

HYCOM is a three-dimensional primitive equation ocean general circulation model using density, pressure, and sigma coordinates in the vertical coordinate. It has evolved from the Miami Isopycnic Coordinate Ocean Model (MICOM) and is isopycnal in the open stratified ocean, but reverts to a terrain-following coordinate in shallow coastal regions, and to z-level coordinates near the surface in the mixed layer (Bleck 2002). This generalized vertical coordinate approach is dynamic in space and time via the layered continuity equation, and permits the existence of zero thickness layers. HYCOM ability to accurately transition between deep and shallow water yield more reliable ocean circulation.

HYCOM, like MICOM, is a primitive-equation model containing 5 prognostic equations-- two for the horizontal velocity components, a mass continuity or layer thickness tendency equation, and two conservation equations for a pair of thermodynamic variables, such as salt and temperature or salt and density. The model equations, written in (x, y, s) coordinates, where s is an unspecified vertical coordinate, are

$$\frac{\partial \vec{v}}{\partial t_s} + \nabla_s \frac{\vec{v}^2}{2} + (\zeta + f)\vec{k} \times \vec{v} + \left(\dot{s} \frac{\partial p}{\partial s} \right) \frac{\partial \vec{v}}{\partial p} + \nabla_s M - p \nabla_s \alpha = -g \frac{\partial \vec{\tau}}{\partial p} + \left(\frac{\partial p}{\partial s} \right)^{-1} \nabla_s \cdot \left(\nu \frac{\partial p}{\partial s} \nabla_s \vec{v} \right) \quad (2.1)$$

$$\frac{\partial}{\partial t_s} \left(\frac{\partial p}{\partial s} \right) + \nabla_s \cdot \left(\vec{v} \frac{\partial p}{\partial s} \right) + \frac{\partial}{\partial s} \left(\dot{s} \frac{\partial p}{\partial s} \right) = 0 \quad (2.2)$$

$$\frac{\partial}{\partial t}(T \Delta p) + \underbrace{\nabla \cdot (\vec{v} T \Delta p)}_{advec} + \underbrace{\left(\dot{s} \frac{\partial p}{\partial s} T \right)_{bot} - \left(\dot{s} \frac{\partial p}{\partial s} T \right)_{top}}_{dia-diff} = \underbrace{\nabla \cdot (\upsilon \Delta p \Delta T)}_{iso-diff} + H_T \quad (2.3)$$

Where $\vec{v} = (u, v)$ is the horizontal velocity vector, p is pressure, T represents any one of the model's thermodynamic variable, $\alpha = \rho_{pot}^{-1}$ is the potential specific volume and $\zeta \equiv \partial v / \partial x_s - \partial u / \partial y_s$ is the relative vorticity, $M \equiv gz + p\alpha$ is Montgomery potential, $gz \equiv \Phi$ is the geopotential, f is the Coriolis parameter, $\vec{k}$ is the vertical unit vector, ν is a variable eddy viscosity/diffusivity coefficient, and $\vec{\tau}$ is the wind and/or bottom-drag induced shear stress vector. H_T represents the sum of diabatic source terms, including diapycnal mixing, acting on T. Subscripts indicate which variable is held constant during partial differentiation.

Other details of the HYCOM equations and numerical algorithms, along with a description and validation of the hybrid coordinate generator, can be found in Bleck (2002). Also, the HYCOM simulations generate a stronger EUC that compares more favorably to observations than other models, such as the GFDL model (Chassignet et al. 1996). As discussed above, since understanding the dynamics of the EUC is crucial to our study, HYCOM was the best choice to simulate the ocean circulation around the GMR. A variety of sensitivity studies were carried out using a nested modeling system centered on the Galapagos to identify the key physical processes that affect the water mass transport pathways and the local upwelling dynamics around the Galapagos Archipelago.

References

Bleck, R., 2002. An oceanic general circulation model framed in hybrid isopycnic-Cartesian coordinates. Ocean Modelling, 4, 55-88.

Chassignet, E.P., Smith, L.T., Bleck, R., Bryan, F.O., 1996. A model comparison: numerical simulations of the north and equatorial Atlantic oceanic circulation in depth and isopycnic coordinates. J. Phys. Oceanogr. 26, 1849–1867.

Chassignet, E.P., Smith, L.T., Halliwell, G.R., Bleck, R., 2003. North Atlantic Simulations with the Hybrid Coordinate Ocean Model (HYCOM): impact of the vertical coordinate choice, reference density, and thermobaricity. J. Phys. Oceanogr. 33, 2504–2526.

Large, W. G., J. C. Mc Williams, and S. C. Doney, 1994: Oceanic vertical mixing: a review and a model with a nonlocal boundary layer parameterization. Rev. Geophys. 32, 363-403.

Large, W. G., G. Danabasoglu, S. C. Doney, and J. C. McWilliams, 1997: Sensitivity to surface forcing and boundary layer mixing in a global ocean model: annual-mean climatology. J. Phys. Oceanogr., 27, 2418-2447.

Levitus, S., 1997: World Ocean Atlas, Washington DC, NOAA

Kalnay et al.,The NCEP/NCAR 40-year reanalysis project, Bull. Amer. Meteor. Soc., 77, 437-470, 1996.

Kistler, R., E. Kalnay, W. Collins, S. Saha, G. White, J. Woollen, M. Chelliah, W. Ebisuzaki, M. Kanamitsu, V. Kousky, H. van den Dool, R. Jenne, and M. Fiorino, 2001:

The NCEP-NCAR 50-Year Reanalysis: Monthly Means CD-ROM and Documentation. Bull. Amer. Meteor. Soc., 82, 247-268.

Mariano, A.J. and O.B. Brown, 1992: Ecient objective analysis of dynamically heterogeneous and nonstationary fields via the parameter matrix. Deep-Sea Res., 39, 1255-1271.

Mellor, G. L. and Yamada, T., 1982: Development of a turbulence closure model for geophysical fluid problems. *Rev. Geophys. Space Phys.*, **20**, 851-875.

Mellor, G. L., 1998: Users Guide for a Three-Dimensional, Primitive Equation Numerical Ocean Model. Available on the Princeton Ocean Model website.

Niiler, P.P. and E. B. Kraus, 1977: One-dimensional models. In Modeling and Prediction of the Upper Layers of the Ocean, E. B. Kraus, Editor. Pergamon, New York, 143-172
Price, J. F., R. A. Weller, and R. Pinkel, 1986: Diurnal cycling: Observations and models of the upper ocean response.

Chapter 3

Sensitivity of Numerical Simulation of Ocean Circulation around the Galápagos Archipelago to Spatial Resolution and Atmospheric Forcing Frequency

Abstract

The ocean circulation and water mass characteristics around the Galápagos Archipelago are studied using University of Miami's Hybrid Coordinate Ocean Model (HYCOM). A four-level nested-domain system with resolutions from 0.04° x 0.02° in the Galápagos region, 0.12° x 0.06° in the Eastern Tropical Pacific, 0.48° x 0.24° for the Pacific Ocean, to 1.44° x 0.72° covering the global ocean is used in the study. Ocean sensitivity to the frequency of the atmospheric forcing is examined. In a controlled experiment where the atmospheric forcing frequency was reduced from daily frequency to monthly, the results simulated by the ocean model are shown to be less accurate than those simulated using daily forcing. Simulations also are performed with four different scales (0.04°, 0.12°, 0.48°, 1.44°) centered on the Galápagos region under identical daily meteorological forcing fields and the results are compared. The improvements resulting from simulations under increasingly fine resolution are examined and the movement toward a more realistic spectrum of oceanographic variability is quantified. For example, the simulation with the resolution of 0.04° can depict the intra-seasonal signal from the tropical instability waves (TIW), as well as the annual and the inter-annual signals, whereas the low resolution global model failed to depict TIW signal. Finally, the El

Niño/Southern Oscillation (ENSO) variability in the Nino3.4 region was successfully simulated.

Keywords: HYCOM, Galápagos, GMR, ENSO, Simulation

1. Introduction

The Galápagos Archipelago (Figure1) lies in the equatorial eastern Pacific Ocean, about 1000 km west of the coast of Ecuador, South America. It can reasonably claim to possess the most distinctive marine flora and fauna and unique species for any area of its size worldwide [Bustamante et al., 1999]. Thus in March 1998, Ecuador created the Galápagos Marine Reserve (GMR), which is an extensive area, over 140,000 km^2, and consists of an extremely variable ecological system in space and time (Jennings 1994). The principle reason why the GMR features such great diversity lies in its positioning in a complex transition zone between tropical, subtropical and upwelling zones. The Galápagos archipelago ecosystem is mainly affected by three different surface and subsurface currents. The major currents affecting the Galápagos are the westward South Equatorial Current (SEC) and the eastward Equatorial Undercurrent [EUC, Boersma, 1977, 1978]. The SEC drives surface waters over the entire region around the Galápagos and is composed of the warmer Panama Current and cool Humboldt Current. The Panama Current influences the northern islands, while the cool Humboldt (Peru) Current influences the southern islands. To balance the westward SEC, the eastward EUC (also

known as the Cromwell current) develops as a subsurface compensation against the westward SEC, causing the upwelling in western archipelago. This upwelled water is relatively rich in iron, the often limiting micronutrient needed for growth by most organisms, and thus contributes to a higher production in many areas of the Galápagos and surrounding waters [Steger et al. 1998]. The EUC is the major oceanographic feature affecting production through the Galápagos Archipelago [Houvenaghel 1984].

The Galápagos are greatly affected by seasonal atmospheric and oceanographic variability [Houvenaghel 1984]. During the hot wet season (December to May), the Intertropical Convergence Zone (ITCZ) migrates southward towards the equator, the northeast trades become more prevalent, and warmer (>25 ° C), fresher (<34) and less-productive waters of the Panama Current flow southward into the Archipelago. During the dry Garúa season (May to November), the ITCZ migrates to the north of the equator, the southeast trade winds become dominate, the major source waters for the SEC are the cold Peruvian Ocean current and the Peruvian Coastal Current (the Humboldt Current), enhancing the contributions to the SEC with the colder (18 ° -20 ° C), saltier (>35) productive waters. The different source waters for the SEC from both northern and southern hemispheres as well as topographically induced upwelling which occurs when the eastward flowing EUC runs into the Galápagos platform are the cause of the tremendous diversity around the Archipelago.

A few studies have quantified the phytoplankton primary production around the Archipelago especially the higher concentrations west of Isabella [Feldman 1984, 1986] from the upwelling EUC. Houvenaghel [1984] discussed the oceanographic setting of the Galápagos and concluded that the EUC was the major oceanographic phenomena affecting the Galápagos. Hayes [1985] pointed out that the sea level differences across the Archipelago increase as the EUC strengthens, measured by shallow moored pressure gauges. Steger et al. [1998] found that the near-surface waters to the west of the Archipelago during November 1993 were predominately upwelled EUC waters, and as a consequence were cooler, saltier and higher in nutrients and iron than waters found over the eastern portion of the Archipelago. In addition, the extent of the plume shown by Feldman [1986] and of the one observed by Steger et al. [1998] could only be maintained by upwelling of EUC waters that are cooler and high in nutrients. Steger et al. [1998] showed that the waters of the EUC bifurcate when they run into the Galápagos platform, with water continuing to flow to the east both to the north and south of the platform. East of the Archipelago, Steger et al. [1998] found evidence that these north and south eastward flows most likely converge and reform a definable EUC. Steger et al. [1998] also found that the core of the EUC was south of the equator during a hot season, as did Christensen [1992], but with a strong branch also found north of the Galápagos. This variation in EUC displacement is not well enough understood to determine whether it is due to seasonal variability or unstable flow conditions [Lukas 1986]. Wyrtki [1967] showed by way of water mass analysis that some of the EUC waters re-circulate both north and south of the Archipelago, and Houvenaghel [1984] highlighted the areas within

the Archipelago prone to upwelling due to the western exposure of landmasses to the eastward flowing EUC. Palacios [2004] found that the temporal variability of ocean color and SST around the Galápagos was dominated by the seasonal migration of the ITCZ and associated strengthening of the SEC and EUC. In summary, studies to this point indicate that the EUC is the major oceanographic feature affecting production in the Galápagos Marine Reserve.

Another distinctive feature associated with Galápagos coastal waters is that the greatest sea temperature anomalies occur during El Niño and La Niña events [Glynn and Ault, 2000]. Recently the frequency and severity of El Niño events appear to have increased and this is a concern for the conservation of endangered species. El Niño events now occur 2–7 times more frequently than they did 7000–15,000 years ago [Riedinger et al., 2002; Rodbell et al., 1999]. The 1982-83 and 1997-98 El Niño events, in particular, were the most extreme for many centuries, and had a devastating effect on marine life in the Galápagos region. During El Niño, the EUC weakens, the surface water warms, micronutrients are reduced, the phytoplankton primary production decreases [Chavez et al., 1999], and fish numbers diminish. Data from commercial fisheries indicated that the catch of mullets from the Galápagos during the 1997–1998 El Niño event were half that of the commercial catch in 1999, a "normal" year [Nicolaides and Murillo, 2001]. Thus the relationship between El Niño events and EUC, as well as the relationship between extreme ENSO events and loss of marine biodiversity in Galápagos, will be investigated using a numerical model as a matter of local and global importance.

This chapter focuses on the oceanographic variability at four different spatial scales associated with the biological productivity and biogeography of the various marine ecosystems across the Galápagos Marine Reserve (GMR) as simulated by an ocean general circulation model. The objective is to quantify the relative improvements to the simulation of the equatorial Pacific (especially near GMR) in an OGCM arising from increased horizontal resolution. The model chosen for the present study is the Hybrid Coordinate Ocean Model [HYCOM; Bleck, 2002; Chassignet et al., 2003; Halliwell, 2004]. The rest of the paper is organized as follows: in section 2, we describe the HYCOM model configuration and the sensitivity experiments conducted. In section 3, the simulated tropical ocean circulation around the GMR using QuikSCAT and NCEP forcing are demonstrated and compared with the observation cruise results. Results are summarized in section 4.

2. Model description

HYCOM is a primitive equation ocean general circulation model using density, pressure, and sigma coordinates in the vertical coordinate. It has evolved from the Miami Isopycnic Coordinate Ocean Model (MICOM) and is isopycnal in the open stratified ocean, but reverts to a terrain-following coordinate in shallow coastal regions, and to z-level coordinates near the surface in the mixed layer. This generalized vertical coordinate approach is dynamic in space and time via the layered continuity equation, and permits

the existence of zero thickness layers. HYCOM ability to accurately transition between deep and shallow water yield more reliable ocean circulation.

Other details of the HYCOM equations and numerical algorithms, along with a description and validation of the hybrid coordinate generator, can be found in Bleck (2002). Also, the HYCOM simulations generate a stronger EUC that compares more favorably to observations than other models, such as the GFDL model (Chassignet et al. 1996). As discussed above, since understanding the dynamics of the EUC is crucial to our study, HYCOM was a good choice to simulate the ocean circulation around the GMR. A variety of sensitivity studies were carried out using a nested modeling system centered on the Galápagos to identify the key physical processes that affect the water mass transport pathways and the local upwelling dynamics around the Galápagos Archipelago.

3. Simulation results

3.1 Model configuration and numerical experiments

HYCOM simulations were carried out using a nesting scheme of 4 ever increasing resolution domains. The largest domain covers the entire global ocean with a grid size of 1.44° x 0.72° in zonal and meridional direction, respectively. The second domain embedded within the global domain uses a grid size of 0.48° x 0.24° covering the equatorial Pacific Ocean. The third higher resolution domain has a grid size of 0.12° x 0.06°. Finally, the highest resolution domain has a grid size of 0.04° x 0.02° (about 4.45

km x 2.21 km) that is centered on the GMR (92.16 °W - 88.96 °W, 1.68 °S - 1.68 °N). All domains have a vertical resolution of 26 layers that stretch or shrink vertically as a function of total depth according to the hybrid coordinate frame discussed above.

The model was initialized with temperature and salinity from the Levitus monthly climatology [Levitus et al., 1994] and run for 12 years. It was driven by daily surface wind stress, surface air temperature, surface atmospheric specific humidity, net shortwave radiation, net long-wave radiation and precipitation fields obtained from NCEP reanalysis [Kistler, et al, 2001]. The latent and sensible heat fluxes were calculated during model runs using the model sea surface temperature and the bulk formulation [Cayan 1992]. Boundary conditions were provided by buffer zones that were ten grid points wide within which temperature, salinity, and interface depth were relaxed to Levitus climatological values that had been vertically remapped to hybrid vertical coordinates. The KPP vertical mixing model of Large et al. [1994] was also used. For the experiments with the zonal resolution of 1.44 º, 0.48 ºand 0.12 º, the bathymetry was from ETOPO2, which contained digital data bases of seafloor and land elevations on a 2-minute latitude/longitude grid and was interpolated on the model grids of different resolutions. In the simulation with the resolution of 0.04 º(near the Galápagos Islands), the bathymetry had a resolution of 0.01 º from a data set put together by William Chadwick, Oregon State University (http://www.pmel.noaa.gov/vents/staff/chadwick/Galápagos.html). This sub-region was driven by wind fields interpolated from 25-km resolution QuikSCAT wind stress to drive both normal (EUC present) and El Niño conditions (EUC not present) simulations to

study the transport pathways of EUC waters. The model was spun up for twelve years from 1995 to 2006, and fields from the last two years of the simulation (year 2005 and 2006) are analyzed here.

3.2 Sensitivity tests

To test the ocean variability around the GMR, we conducted two types of sensitivity experiments. One was to test how marine meso-scale variability depended on different wind forcing; the other was to test how marine variability depended on different model horizontal resolutions. We also used the model to simulate observed ENSO variability to quantify the ability of the model to give realistic simulations of ENSO events around the islands.

3.2.1 Wind Forcing Experiments.

In the wind forcing experiments (Expt.1), we ran HYCOM model with four different winds forcings: monthly mean forcing, weekly mean forcing, daily mean forcing, and 6-hourly wind forcing. The high frequency daily mean forcing, and 6-hourly wind forcing were downloaded from http://www.cdc.noaa.gov/cdc/reanalysis/, while the monthly mean forcing and weekly mean forcing were computed by using the daily mean forcing data. Figure 2 shows the standard deviation of sea surface temperature (SST) with the four different wind forcing. From this figure, the simulation with the monthly wind

forcing had the largest standard deviation (0.7° C) over most of the GMR, while the standard deviations from the simulations with the high frequency wind forcing were similar but much smaller than that with the low frequency forcing. The result shows that monthly wind forcing is not adequate to resolve the ocean variability around the archipelago; therefore, especially in our region of interest, it is essential to use high frequency wind forcing.

3.2.2 Model Resolution Experiments

In the horizontal resolution experiments (Expt.2), we ran the model centered on the GMR (92.16 °W - 88.96 °W, 1.68 °S - 1.68 °N) with four different horizontal resolutions -- 0.04˚ (0.04 °x 0.02), 0.12˚ (0.12 °x 0.06 °), 0.48˚ (0.48 °x 0.24 °), 1.44˚ (1.44 °x 0.72 °).. Figure 3 displays the SST standard deviation in these different resolutions. From Figure 3, we see that the simulations around the GMR show that a 0.04˚ resolution is more suitable to study the variability in and around the Galápagos. Figure 4 shows the simulated mean SST with different horizontal resolutions (0.04˚, 0.12˚, 0.48˚, 1.44˚) and Figure 5 shows the vertical sections of mean temperature along the equator in the upper 200 m around the GMR with different horizontal resolutions. There appears to be very little difference when increasing the horizontal resolution around the Galápagos Islands. However there is only a cold bias around the Galápagos Islands under fine resolution.

In the equatorial Pacific Ocean, zonal transport is dominated by the eastward EUC and the westward SEC. The changes to the EUC are also found with different resolutions (Figures.6–7). Figure 6 presented the vertical sections of zonal current along the equator for the upper 200 m around the GMR with different horizontal resolutions. The core of the EUC is located at 50~100m. With increasing model resolution, the EUC speed is decreased and elevated to the surface with the inclusion of the Galápagos Islands under the fine 0.04˚ resolution. The meridional sections of zonal velocity at 91.44˚W and 90˚W for the upper 200 m around the GMR under different horizontal resolutions are shown in Figure 7. The core of EUC is located at ~100m. But for the fine case, upon meeting Isabela, a weak (10–20 cm/s) branch is directed south, and another is directed north of the barrier.

Figure 8 shows the region-averaged (within the whole GMR domain) SST simulated using four different horizontal resolutions (0.04˚, 0.12˚, 0.48˚, 1.44˚) and the region-averaged observed SST. The observational datasets used for comparison with model output came from the $2° \times 2°$ Reynolds and Smith (1994) optimal interpolation (OI) SST (often referred to "Reynolds"), with a period of 1990–2006. These figures show the simulated SST with a resolution of 0.04˚ is closest to the observed SST. The correlation coefficient between the two reaches 0.72 ($p<0.05$), while the correlation coefficients of between the simulated and observed SST using the different resolution of 0.12˚, 0.48˚, 1.44˚ are 0.67, 0.61 and 0.32, respectively. Figure 9 depicts the region-averaged (see Figure 9E: four different regions in eastern Pacific – Region 1: 97.2˚ W-92.88˚ W, 2.16˚

S-2.16˚ N; Region 2: 90˚ W-85.68˚ W, 2.16˚ S-2.16˚ N; Region 3: 90˚ W-85.68˚ W, 6.5˚ S-2.16˚ S; Region 4: 90˚ W-85.68˚ W, 2.16˚ N-6.5˚ N) simulated SST using three different horizontal resolutions (0.12˚, 0.48˚, 1.44˚) and the corresponding region-averaged observed SST. Table 1 shows the correlation coefficients of between the observed and simulated SST using the different resolution of 0.12˚, 0.48˚, 1.44˚ in the four different regions. The result shows that the simulation using higher resolution has the higher correlation. The highest correlation coefficient even reaches to 0.86.

Figure 10 shows the other simulated variables (SST, SSS and U/V velocity) using four different horizontal resolutions and Table 2 shows the correlation coefficients of between the simulated SST, Salinity and U/V velocity using the different resolution of 0.12˚, 0.48˚, 1.44˚. The result shows that the simulation using higher resolution has the higher correlation. The simulated SST and Salinity with the finest resolution of 0.04˚ has the same pattern as the results under the coarse resolution. But for the simulation of U/V velocity, there is a big difference when increasing the horizontal resolution (coarse vs. fine resolution) around the Galápagos Islands. Figure 11-14 show the power spectrum of SST, SSS and U/V velocity at 92˚W from 0.5S to equator under four different resolutions. Results also show there is no big difference for the simulation of SST and SSS for coarse and fine resolution. All simulations show the annual signals. But under fine resolution the simulations of U/V velocity show the interseasonal signal with the period of 20 days, as well as the annual and the inter-annual signals (Fig 13, 14). All above results show that the simulated variable using higher resolution (i.e. 0.04˚) resolution is more suitable to

study the variability in and around the Galápagos, especially for the simulation of U/V velocity.

3.2.3 ENSO Simulations

As a final test of the configurations to be used in this study we simulated El Niño/Southern Oscillation (ENSO) variability by using HYCOM driven by NCEP wind forcing. The SST anomalies in the Nino3.4 region (5°S-5°N, 150°W-90°W) are often used to index ENSO variability [Trenberth, 1997]. Figure 15 shows the observed (blue) and HYCOM simulated SST anomalies (red) in Nino3.4 region. The correlation coefficient between the simulate SSTA and observed SSTA is 0.883. This result shows that HYCOM generally simulates the major El Niño events especially the strong 1997-1998 events. Therefore, the HYCOM should give realistic simulations of ENSO events around the islands.

4. Summary

This paper focuses on the oceanographic variability and physical settings associated with the biological productivity and biogeography of the various marine ecosystems across the GMR using a general ocean circulation model (HYCOM). The model results were compared with data taken during oceanographic cruises in 2005/2006. Daily surface fields obtained from the NCEP and the wind forcing from QuikSCAT were used to drive the simulations. Sensitivity to different forcing conditions and resolutions are examined.

The sensitivity tests showed that frequency of wind forcing higher than weekly average is more reliable than monthly forcing in reproducing the observed oceanic features within the GMR. In a controlled experiment where the atmospheric forcing frequency was reduced from daily to monthly, the results simulated by the ocean model are shown to be less accurate than those simulated using daily forcing. In addition, the simulation around the GMR is greatly improved with the increase of horizontal resolutions. It was found the simulations under fine resolutions are more accurate and have multi-scale time periods. The simulation with the resolution of 0.04° can depict the intra-seasonal signal from the tropical instability waves (TIW), as well as the annual and the inter-annual signals, whereas the low resolution global model failed to depict TIW signal. Results also show that HYCOM generally simulates the major El Niño events especially the strong 1997-1998 events.

Acknowledgements

This project was funded by National Aeronautics Space Association (NASA) Biodiversity and Ecological Forecasting grant NNG04GL98G. The Counterpart US-AID No. 518-A-00-03-00152-00 and UK Darwin Initiative Project No. 14-048 also provided funding for this project. All modeling work is carried out in the Coastal Fluid Dynamical Lab of North Carolina State University using the High-Performance Computing (HPC) system.

Reference

Bleck, R., 2002. An oceanic general circulation model framed in hybrid isopycnic-Cartesian coordinates. Ocean Modeling, 4, 55-88.

Boersma, P.D. 1977. An ecological and behavioral study of the Galápagos Penguin. Living Bird 15: 43–93.

Boersma, P.D. 1978. Breeding patterns of Galápagos Penguins as an indicator of oceanographic conditions. Science 200: 1481–1483.

Bustamante, R., Collins, K. J. Bensted-Smith, R., 1999.Biodiversity conservation in the Galápagos Marine Reserve. Entomologie Supplement 68: 45-52.

Cayan, D., Latent and sensible heat flux anomalies over the Northern oceans: driving the sea surface temperature, J. Phys. Oceanogr., *22*, 859–881, 1992.

Cayan, 1992: Latent and sensible heat flux anomalies over the northern ocean: The connection to monthly atmospheric circulation. JClim, 5, 354--369

Chassignet, E.P., Smith, L.T., Bleck, R., Bryan, F.O., 1996. A model comparison: numerical simulations of the north and equatorial Atlantic oceanic circulation in depth and isopycnic coordinates. J. Phys. Oceanogr. 26, 1849– 1867.

Chassignet, E.P., Smith, L.T., Halliwell, G.R., Bleck, R., 2003. North Atlantic Simulations with the Hybrid Coordinate Ocean Model (HYCOM): impact of the vertical coordinate choice, reference density, and thermobaricity. J. Phys. Oceanogr. 33, 2504–2526.

Chavez, F.P., Strutton, P.G., Friederich, G.E., Feely, R.A., Feldman, G.C., Foley, D.G., McPhaden, M.J., 1999. Biological and chemical response of the equatorial pacific ocean to the 1997–1998 El Niño. Science 286, 2126–2131.

Edgar, G. J., Banks, S., Farina, J. M., Calvopina, M. and Martınez, C., 2004. Regional biogeography of shallow reef fish and macro-invertebrate communities in the Galápagos archipelago. Journal of Biogeography 31: 1107-1124.

Feldman, G., Clark, D., Halpern, D., 1984. Satellite color observations of the phytoplankton distribution in the eastern equatorial Pacific during the 1982–1983 El Niño, Science 226 (4678), 1069–1071.

Feldman, G..,1986. Patterns of phytoplankton production around the Galápagos Islands. In M.J. Bowman, R.T. Barber & C.N.K. Mooers (Eds.), Lecture Notes on Coastal and Esutarine Studies: Tidal Mixing and Plankton Dynamics (pp. 77-106). Berlin: Springer

Glynn, P.W. and J.S. Ault. 2000. A biogeographic analysis and review of the far eastern Pacific coral reef region. *Coral Reefs* **19**: 1-23.

Halliwell Jr., G.R., 2004. Evaluation of vertical coordinate and vertical mixing algorithms in the Hybrid-Coordinate Ocean Model (HYCOM). Ocean Modelling. 7, 285–322.

Hayes, S. P. 1985. Sea level and near surface temperature variability at the Galápagos Islands, 1979-1983

Houvenaghel, G. T., 1978. Oceanographic conditions in the Galápagos Archipelago and their relationships with life on the islands. In: Boje, R., Tomczak, M. (Eds.), Upwelling Ecosystems. Springer, Berlin, pp. 181–200.

Houvenaghel, G. T., 1984. Oceanographic setting of the Galápagos Islands. In: Perry, R. (Ed.), Key Environments, Galápagos. Pergamon Press, Oxford, pp. 43–54.

Kistler, R., E. Kalnay, W. Collins, S. Saha, G. White, J. Woollen, M. Chelliah, W. Ebisuzaki, M. Kanamitsu, V. Kousky, H. van den Dool, R. Jenne, and M. Fiorino, 2001: The NCEP-NCAR 50-Year Reanalysis: Monthly Means CD-ROM and Documentation. Bull. Amer. Meteor. Soc., 82, 247-268.

Large, W.G., Mc Williams, J.C., Doney, S.C., 1994. Oceanic vertical mixing: review and a model with a nonlocal boundary layer parameterization. Rev. Geophys. 32, 363–403.

Levitus, S., Boyer, T., 1994. World Ocean Atlas 1994, Volume 4: Temperature. NOAA Atlas NESDIS 4. US Dept. of Commerce, Washington, DC.

Levitus, S., Burgett, R., Boyer, T., 1994. World Ocean Atlas 1994, Volume 3: Salinity. NOAA Atlas NESDIS 3. US Dept. of Commerce, Washington, DC.

Jennings, S., Brierley, A.S., & Walker, J.W. 1994. The inshore fish assemblages of the Galápagos Archipelago. Biological Conservation, 70, 49-57

Palacios, D.M. (2004). Seasonal patterns of sea-surface temperature and ocean color around the Galápagos: regional and local influences. *Deep-Sea Research II, 51*, 43-57

Riedinger, M.A., Steinitz-Kannan, M., Last, W.M., Brenner, M.,2002. A similar 6100 C-14C yr record of El Niño activity from the Galápagos Islands. Journal of aleolimnology 27, 1–7.

Rodbell, D.T., Seltzer, G.O., Anderson, D.M., Abbott, M.B., Enfield, D.B., Newman, J.H., 1999. An asymptotically equal to 15,000- Year Record of El Niño-Driven Alluviation in Southwestern Ecuador. Science 283, 516–519.

Steger, J. M., Collins, C. A., Chu, P. C., 1998. Circulation in the Archipielago de Colon (Galápagos Islands), November 1993. Deep-Sea Research II 45, 1093–1114.

Trenberth, K.E., Hoar, T.J., 1997. El Niño and climate change. Geophysical Research Letters 24, 3057–3060.

Trenberth, K.E., 1997. The Definition of El Niño. Bulletin-American Meteorological Society 78, 2771–2778.

Wyrtki, K., Kilonsky, B., 1984. Mean water and current structure during the Hawaii-to-Tahiti shuttle experiment. Journal of Physical Oceanography 14, 242–254.

Figure Caption:

Figure 1: Bathymetry map and sampling stations of the Galápagos Archipelago.

Figure 2: The standard deviation of simulated SST with different winds forcing, from (a) the 6-hourly wind, (b) daily mean wind, (c) weekly mean wind, to (d) the monthly wind forcing.

Figure 3: The standard deviation of simulated SST with different horizontal resolutions (0.04˚, 0.12˚, 0.48˚, 1.44˚)

Figure 4: The simulated mean SST with different horizontal resolutions (0.04˚, 0.12˚, 0.48˚, 1.44˚)

Figure 5: Vertical sections of mean temperature (℃) along the equator in the upper 200 m around the GMR with different horizontal resolutions (a) 0.04˚, b) 0.12˚, c) 0.48˚, d) 1.44˚)

Figure 6: Vertical sections of zonal current (m/s) along the equator for the upper 200 m around the GMR with different horizontal resolutions (a) 0.04˚, b)0.12˚, c) 0.48˚, d)1.44˚)

Figure 7: Meridional sections of zonal velocity(m/s) at 91.44W and 90W for the upper 200 m around the GMR under different horizontal resolutions (a) 0.04˚, b)0.12˚, c) 0.48˚, d)1.44˚)

Figure 8: The region-averaged around GMR (92.16° W-88.96° W, 1.68° S-1.68° N) simulated SST under four different horizontal resolutions (0.04˚, 0.12˚, 0.48˚, 1.44˚) and the region-averaged observed SST

Figure 9: The region-averaged (four different regions in eastern Pacific, see figure 5E, region 1: 97.2˚W-92.88˚W, 2.16˚S-2.16˚N; region 2: 90˚W-85.68˚W, 2.16˚S-2.16˚N; region 3: 90˚W-85.68˚W, 6.5˚S-2.16˚S; region 4: 90˚W-85.68˚W, 2.16˚N-6.5˚N) simulated SST under three different horizontal resolutions (0.12˚, 0.48˚, 1.44˚) and the region-averaged observed SST.

Figure 10: shows the other simulated variables (SST, SSS and U/V velotiy) using four different horizontal resolutions.

Figure 11: The spectrum of surface temperature at 92˚W from 0.5S to equator under four different resolutions

Figure 12: The spectrum of surface salinity at 92˚W from 0.5S to equator under four different resolutions

Figure 13: The spectrum of surface zonal velocity at 92˚W from 0.5S to equator under four different resolutions
Figure 14: The spectrum of surface meridional velocity at 92˚W from 0.5S to equator under four different resolutions

Figure 15: The observed (solid) and HYCOM simulated SST anomalies (dashed) in Nino3.4 region. The grey shaded areas indicate the four cruise periods.

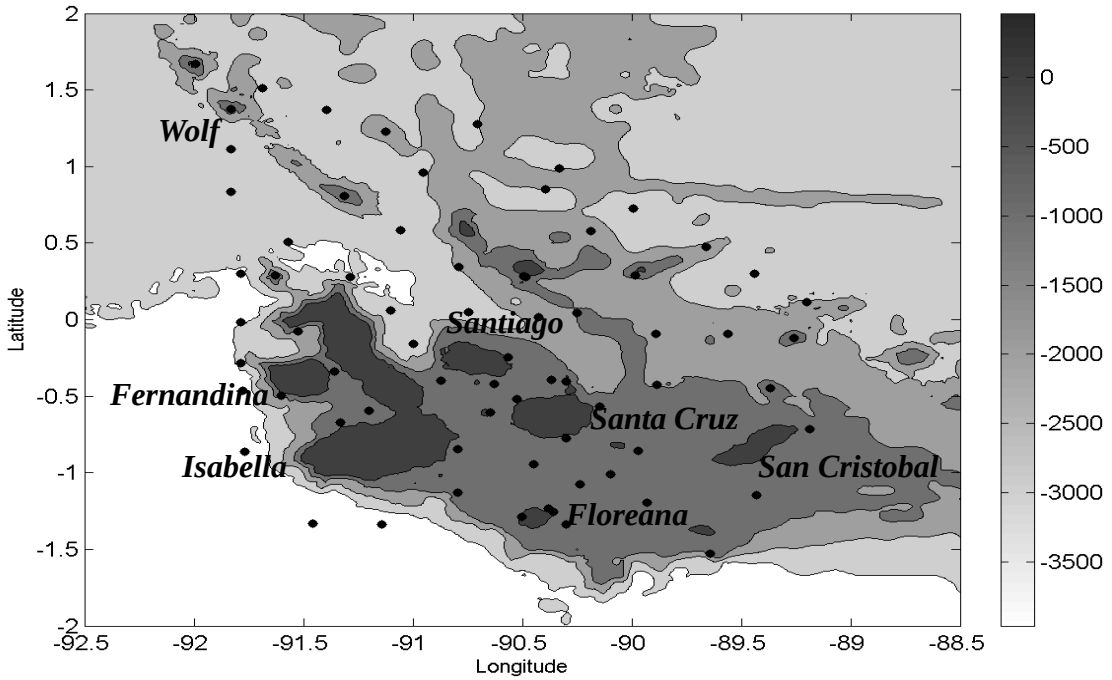

Figure 1: Bathymetry map and sampling stations of the Galápagos Archipelago.

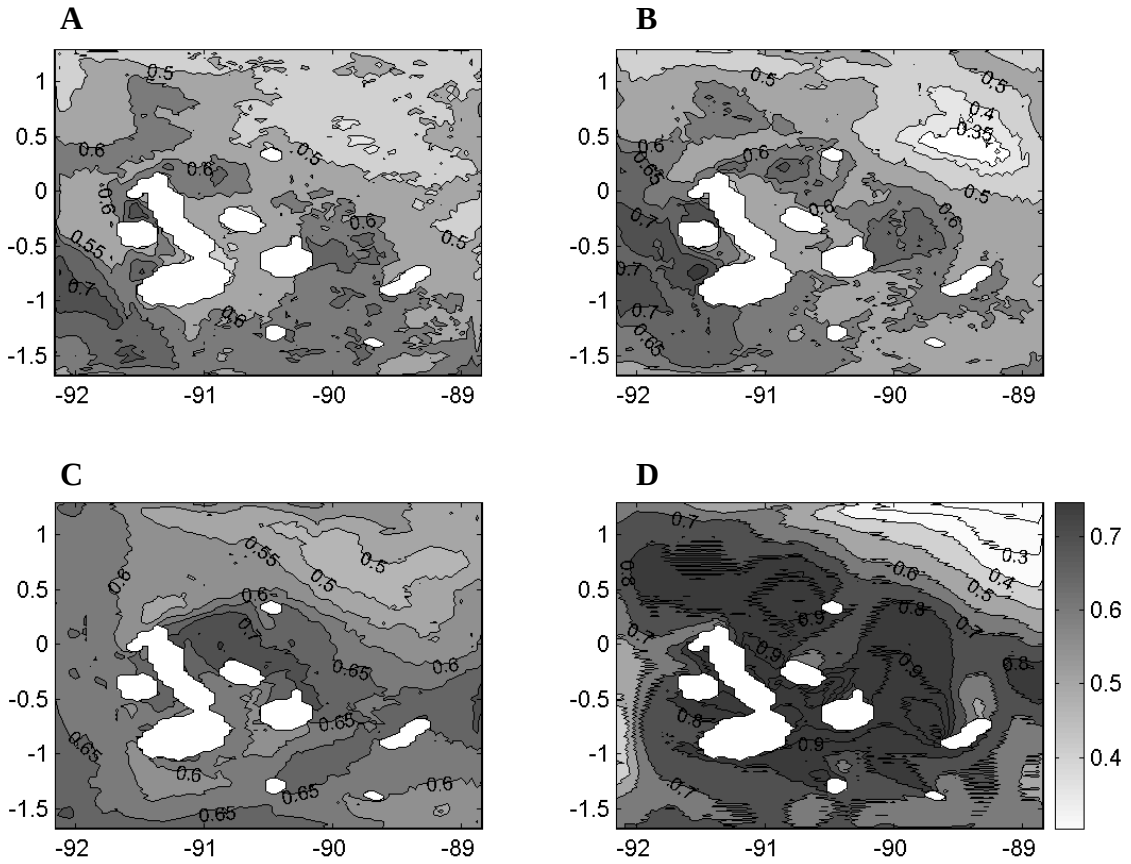

Figure 2: The standard deviation of simulated SST with different winds forcing, from (a) the 6-hourly wind, (b) daily mean wind, (c) weekly mean wind, to (d) the monthly wind forcing.

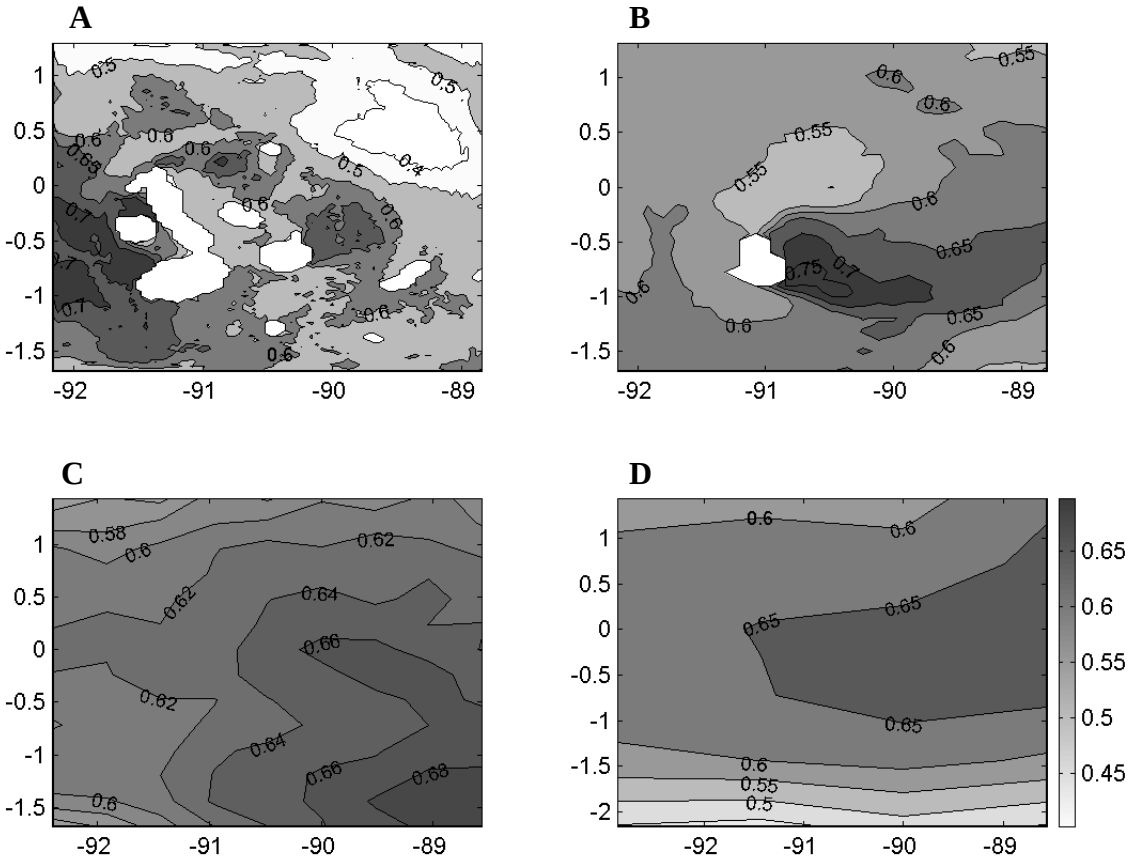

Figure 3: The standard deviation of simulated SST with different horizontal resolutions (0.04˚, 0.12˚, 0.48˚, 1.44˚).

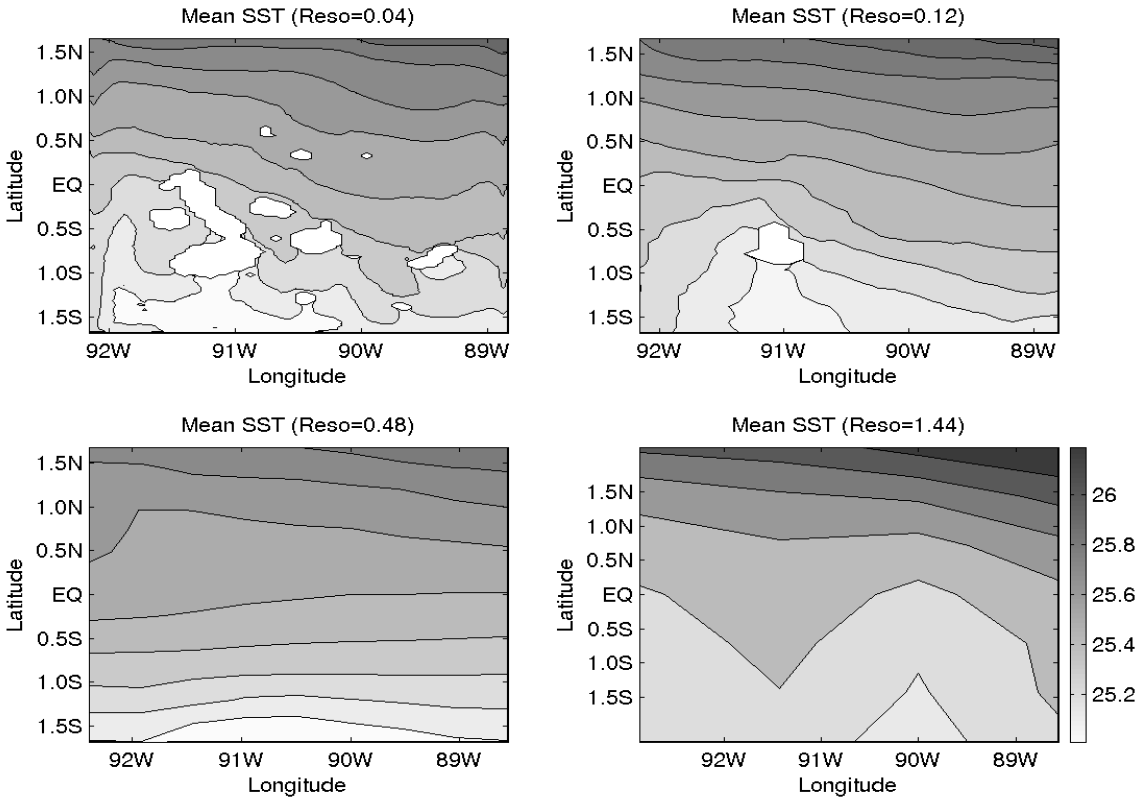

Figure 4: The simulated mean SST with different horizontal resolutions (0.04˚, 0.12˚, 0.48˚, 1.44˚).

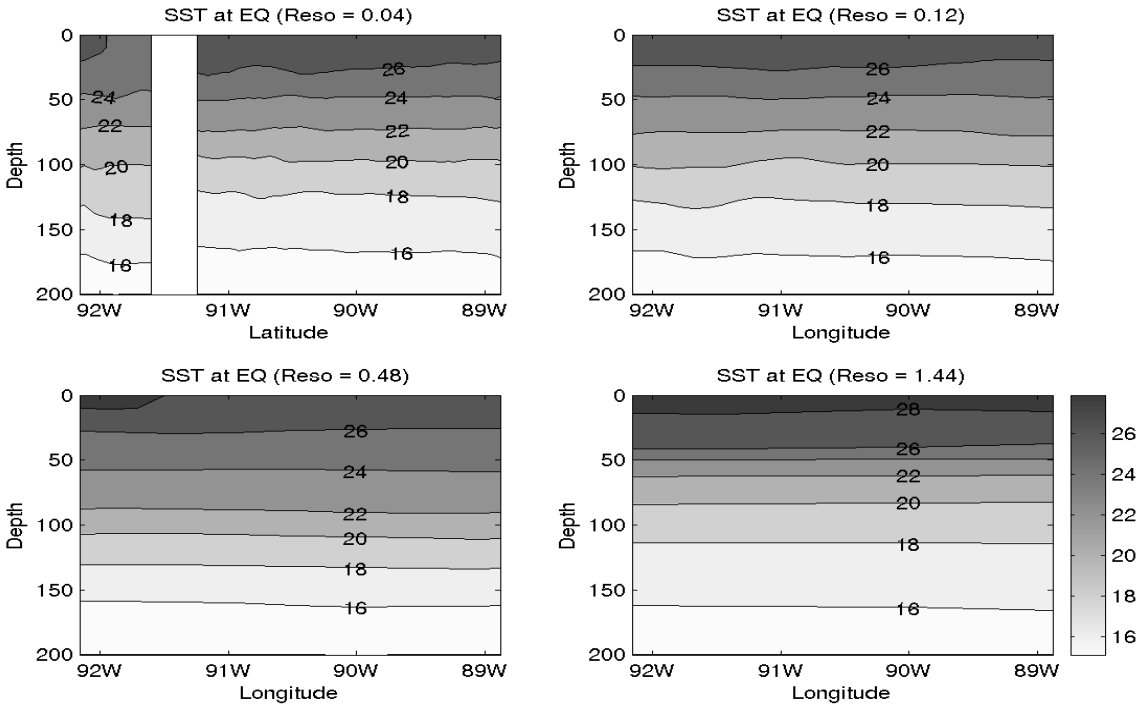

Figure 5: Vertical sections of mean temperature (℃) along the equator in the upper 200 m around the GMR with different horizontal resolutions (a) 0.04˚, b) 0.12˚, c) 0.48˚, d) 1.44˚).

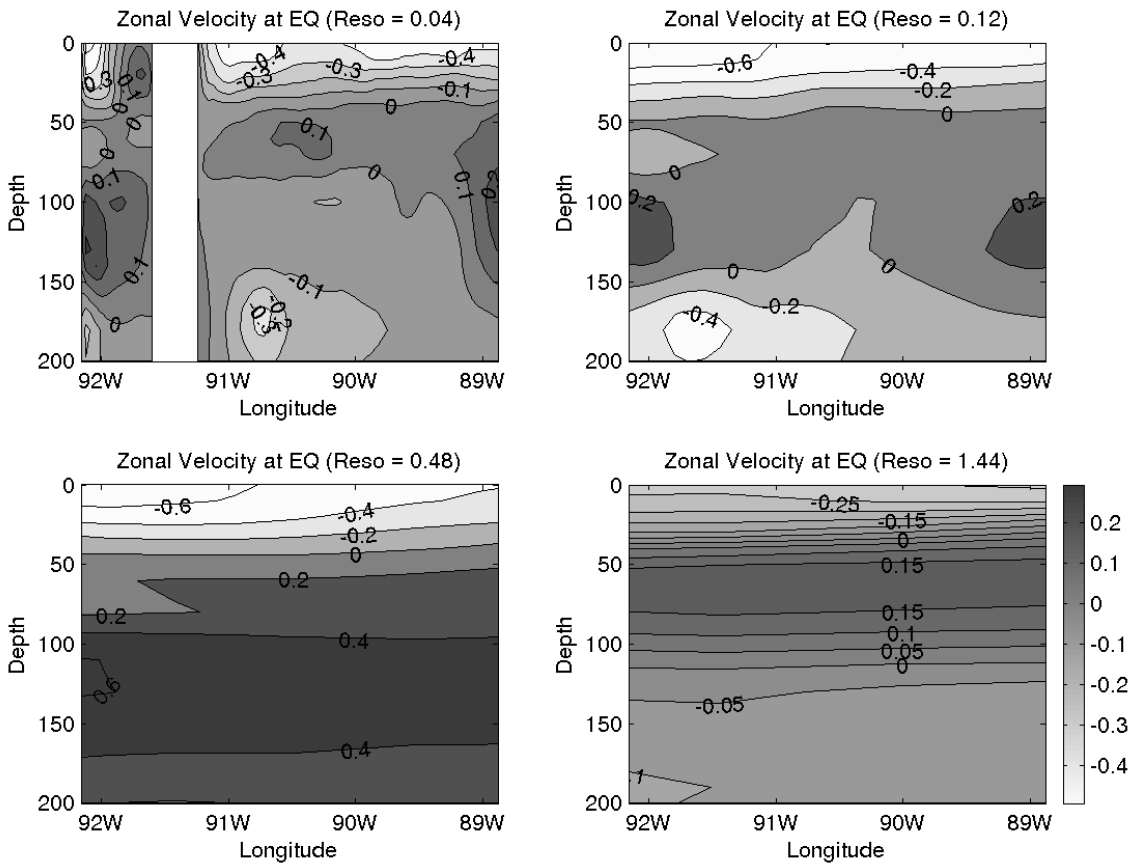

Figure 6: Vertical sections of zonal current (m/s) along the equator for the upper 200 m around the GMR with different horizontal resolutions (a) 0.04˚, b)0.12˚, c) 0.48˚, d)1.44˚)

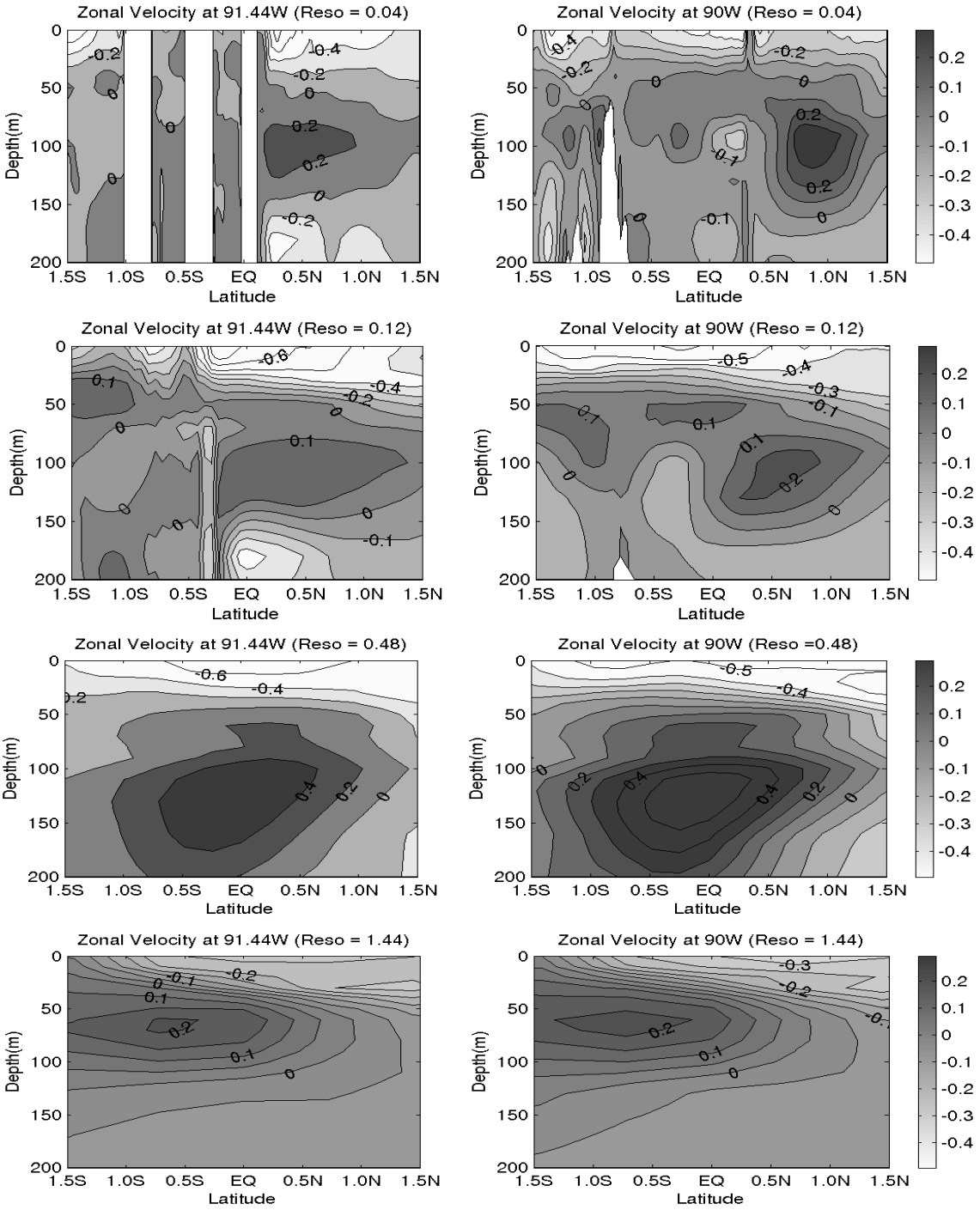

Figure 7: Meridional sections of zonal velocity (m/s) at 91.44W and 90W for the upper 200 m around the GMR under different horizontal resolutions (a) 0.04˚, b)0.12˚, c) 0.48˚, d)1.44˚)

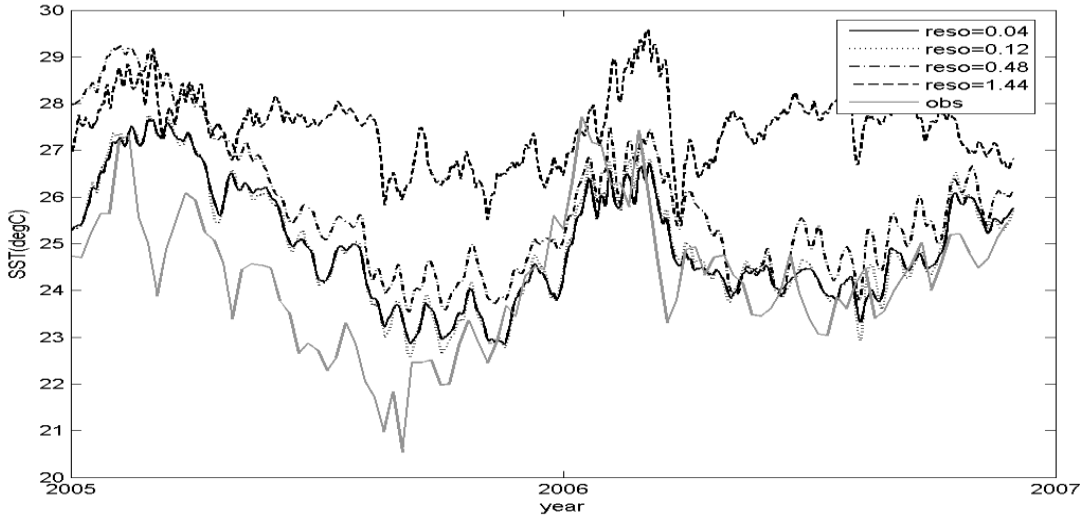

Figure 8: The region-averaged around GMR (92.16 ° W-88.96 ° W, 1.68 ° S-1.68 ° N) simulated SST under four different horizontal resolutions (0.04˚, 0.12˚, 0.48˚, 1.44˚) and the region-averaged observed SST.

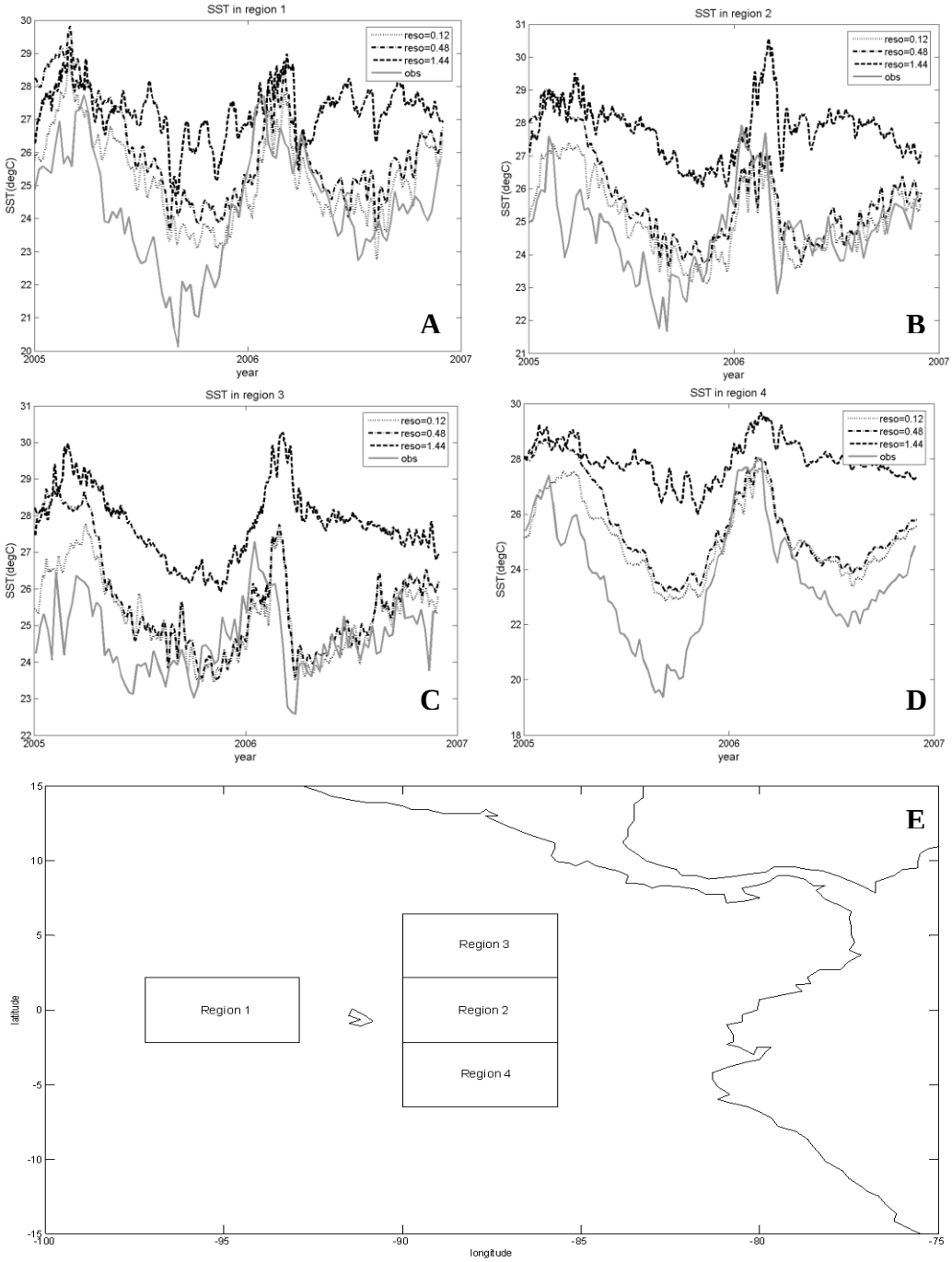

Figure 9: The region-averaged (four different regions in eastern Pacific, see figure 5E, region 1: 97.2˚W-92.88˚W, 2.16˚S-2.16˚N; region 2: 90˚W-85.68˚W, 2.16˚S-2.16˚N; region 3: 90˚W-85.68˚W, 6.5˚S-2.16˚S; region 4: 90˚W-85.68˚W, 2.16˚N-6.5˚N) simulated SST under three different horizontal resolutions (0.12˚, 0.48˚, 1.44˚) and the region-averaged observed SST.

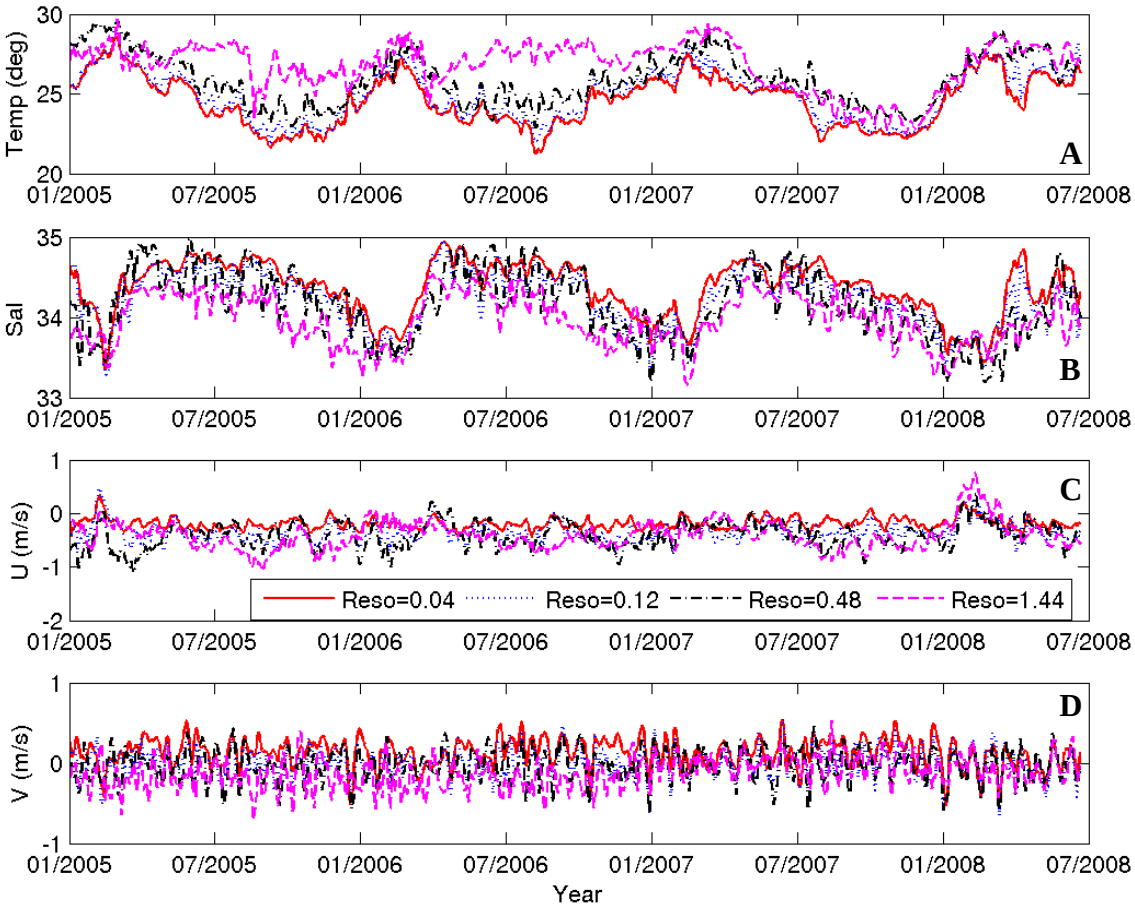

Figure 10: shows the other simulated variables (SST, SSS and U/V velocity) using four different horizontal resolutions.

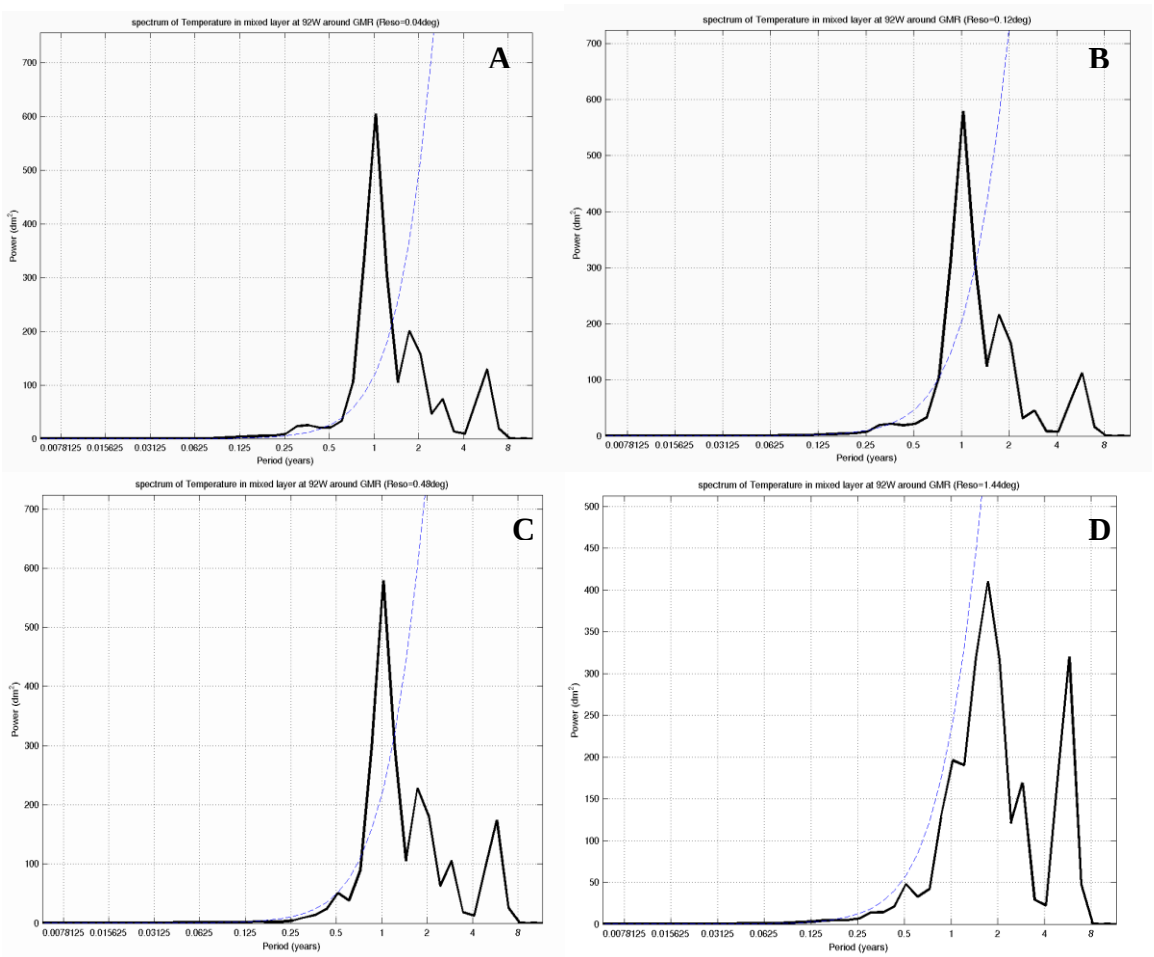

Figure 11: The spectrum of surface temperature at 92˚W from 0.5S to equator under four different resolutions of A) 0.04˚, B) 0.12˚, C) 0.48˚, D) 1.44˚.

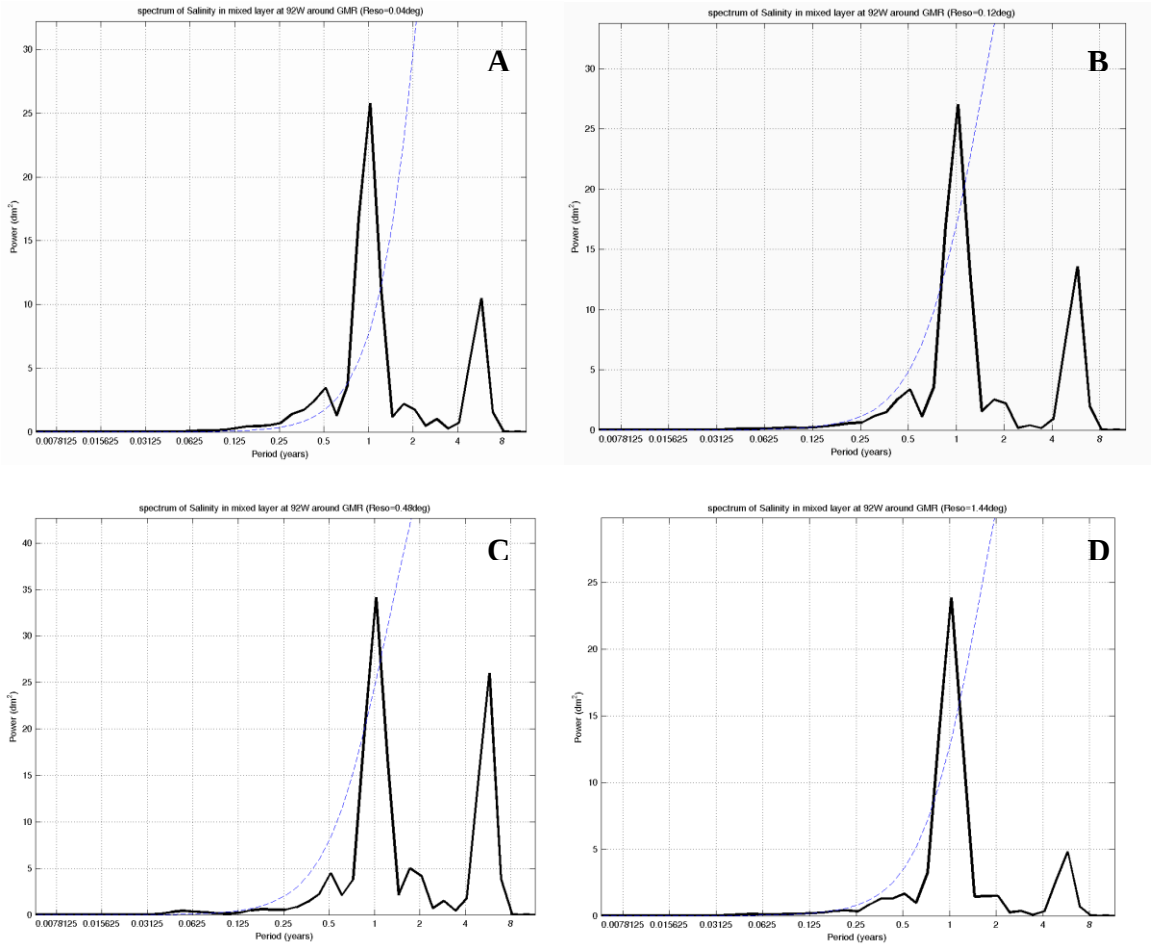

Figure 12: The spectrum of surface salinity at 92˚W from 0.5S to equator under four different resolutions of A) 0.04˚, B) 0.12˚, C) 0.48˚, D) 1.44˚.

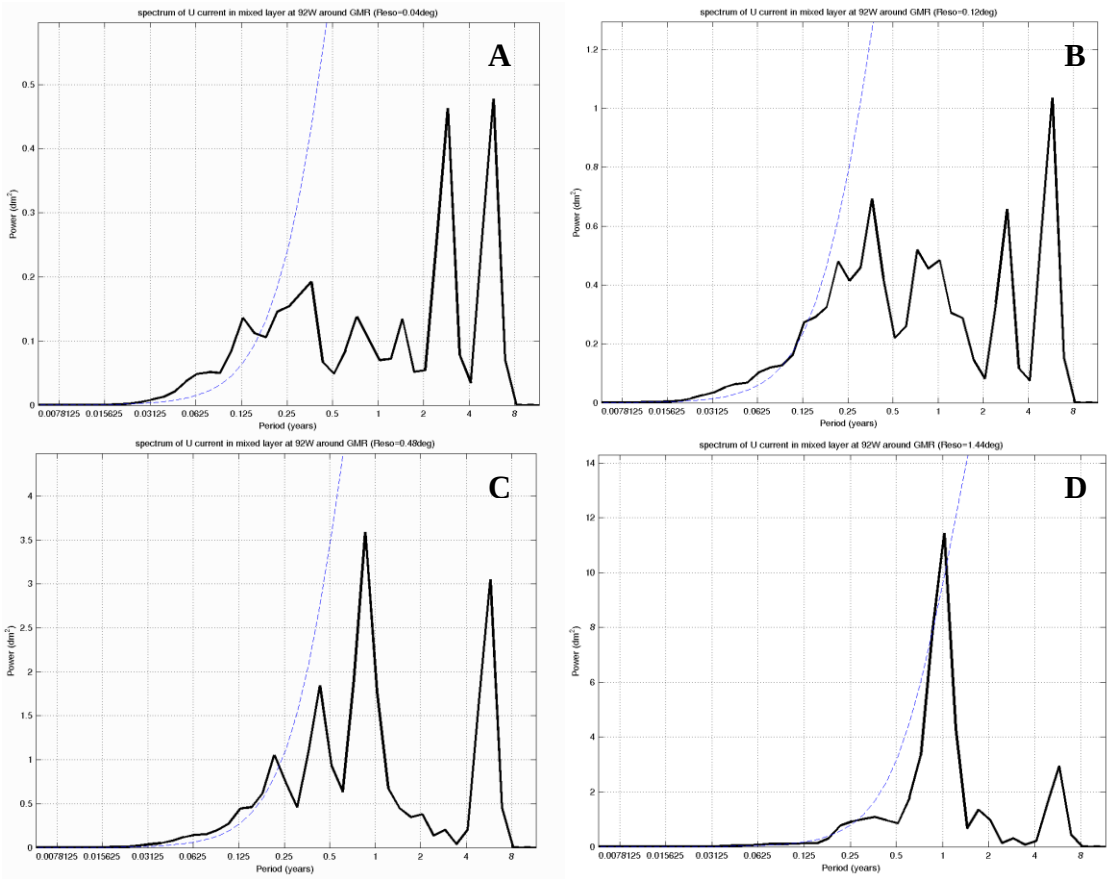

Figure 13: The spectrum of surface zonal velocity at 92˚W from 0.5S to equator under four different resolutions of A) 0.04˚, B) 0.12˚, C) 0.48˚, D) 1.44˚.

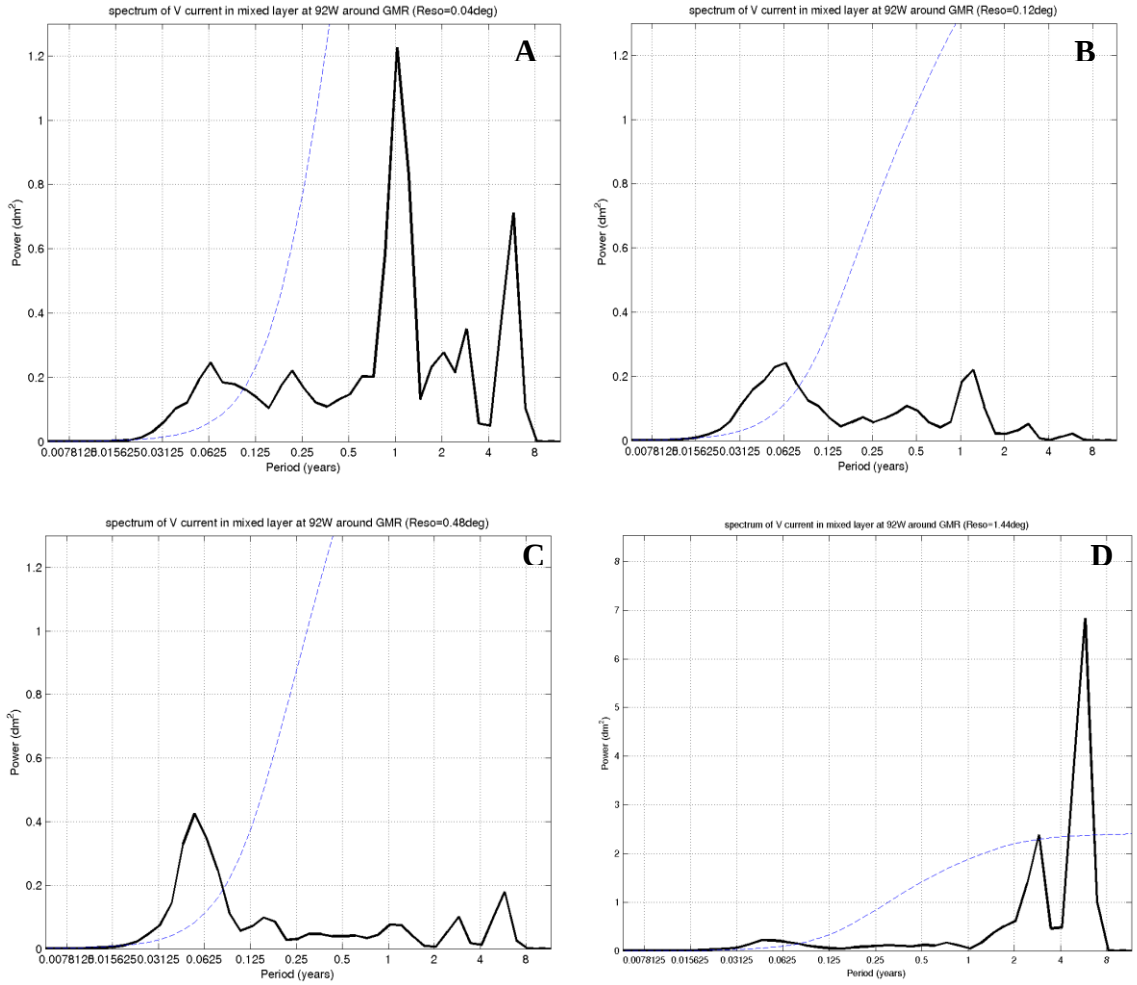

Figure 14: The spectrum of surface meridional velocity at 92˚W from 0.5S to equator under four different resolutions A) 0.04˚, B) 0.12˚, C) 0.48˚, D) 1.44˚.

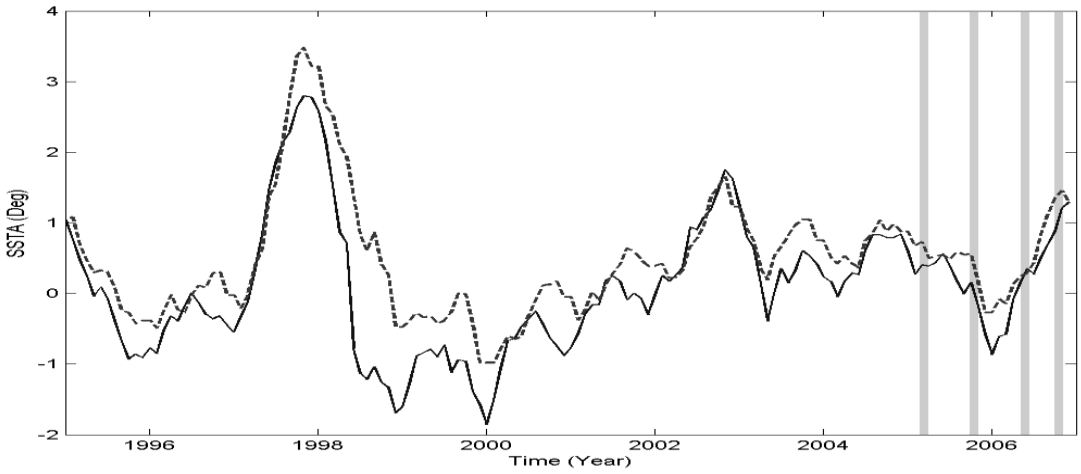

Figure 15: The observed (solid) and HYCOM simulated SST anomalies (dashed) in Nino3.4 region. The grey shaded areas indicate the four cruise periods.

Table 1: The correlation coefficients between the observed and simulated SST under the different resolution of 0.12˚, 0.48˚, 1.44˚ in four different regions.

SST corrcoef	Region 1	Region 2	Region 3	Region 4
Reso = 0.12˚ & obs	0.70	0.62	0.50	0.86
Reso = 0.48˚ & obs	0.67	0.57	0.49	0.82
Reso = 1.44˚ & obs	0.56	0.39	0.26	0.69

Table 2: The correlation coefficients of between the simulated SST, Salinity and U/V velocity using the different resolution of 0.12˚, 0.48˚, 1.44˚.

Correlation coefficient	SST	Salinity	U_velocity	V velocity
Reso = 0.12˚ & 0.04˚	0.988	0.950	0.803	0.738
Reso = 0.48˚ & 0.04˚	0.911	0.805	0.298	0.427
Reso = 1.44˚ & 0.04˚	0.56	0.746	0.294	0.062

Chapter 4

Ocean Circulation and Water Mass Characteristics around the Galápagos Archipelago Simulated by a Multi-Scale Nested Ocean Circulation Model

Abstract

The ocean circulation and water mass characteristics around the Galápagos Archipelago are studied using University of Miami's Hybrid Coordinate Ocean Model (HYCOM). A four-level nested-domain system with resolutions from of 0.04 °x 0.02 °in the Galápagos region, to 0.12 °x 0.06 °in the Eastern Tropical Pacific, to 0.48 °x 0.24 °for the Pacific Ocean, to 1.44 °x 0.72 °covering the global ocean is used in the study. Daily meteorological forcing fields were used to drive the ocean model.

Waters surrounding the Archipelago show a large range of temperature and salinity values in association with 4 different current systems and topographically and wind-forced upwelling. West of Isabella and Fernandina Islands are the largest and most consistent upwelling zones, resulting from the collision of the Equatorial Undercurrent (EUC) with the islands, bring relatively colder and salty waters to the surface in a region of topographically induced upwelling. This upwelling zone marks the location of highest biological production at the surface with the EUC shoaling to approximately 20m from its normal depth of 50m just to the west of the islands. This results not only in a strong upwelling zone just to the west of the islands, but also in a shallow mixed layers over the entire western portion of the Archipelago. The model results, which agree quite well with

observations of the EUC by the TAO array, show a seasonal cycle in the speed and transport of the EUC, reaching a maximum during the late spring/early summer and minimum in the late fall. This seasonal cycle is disrupted during El Niño when the collapse of the westerlies results in a greatly weakened to a total lack of the undercurrent. The far northern region of the Archipelago is characterized with warmer, fresher water and had the deepest mixed layer depth as a result of Panama Current waters from the northeast. The water masses over the remainder of the region result from a mixing of cool Peru Current waters and upwelled Cold Tongue waters entering from the east to the southeast mixing with the upwelled EUC waters.

Keywords: HYCOM, Galápagos, GMR, ENSO, Simulation

1. Introduction

The Galápagos Archipelago (Figure1) lies in the equatorial eastern Pacific Ocean, about 1000 km west of the coast of Ecuador, South America. It can reasonably claim to possess the most distinctive marine flora and fauna and unique species for any area of its size worldwide (Bustamante et al., 1999). Thus in March 1998, Ecuador created the Galápagos Marine Reserve (GMR), which is an extensive area, over 140,000 km^2 and consists of an extremely variable ecological system in space and time (Jennings 1994). The principle reason why the GMR features such great diversity lies in its positioning in a complex transition zone between tropical, subtropical and upwelling zones. Because of

this strong temporal and spatial variability, it would be extremely difficult to monitor the sources of the ecological variability using an observing system alone. During 2006 – 2007 a series of 5 archipelago-wide ship-borne surveys, supported by moorings in 5 of the major upwelling regions were carried out by a joint program of the University of North Carolina Wilmington, North Carolina State University, Mote Marine Laboratory, Charles Darwin Research Station and the Galápagos Nation Park Service which was supported by NASA's Biodiversity and Ecological Monitoring and Biological Oceanography Programs. This effort also supported the modeling effort described in this document, with the observed ocean spatial and time series data used to validate the modeling effort which is the subject of this paper. As might be expected, the biological response to physical forcing within the Galápagos Marine Reserve is the ultimate goal of this activity. The biological response is also being simulated by a nutrient – phytoplankton – zooplankton – detritus model (NPZD, Oschlies 2001) coupled to the inner nest of the hydrodynamic model. These efforts have only recently been begun as we now feel that we have a physical model with sufficient resolution to meet the needs of the biological simulations. Wiggert et al. (2005) conclude that the greatest challenge in ecological modeling appears to involve reproducing observed levels of physical variability (e.g., upwelling and rapid mixing events, filaments and mesoscale eddies). They further concluded that high frequency physical processes are directly responsible for major biogeochemical events that are, in turn, responsible for a large fraction of annual production and export flux. Until physical variability is resolved and their biogeochemical effects accounted for, understanding of biogeochemical variability will

not be impacted by increasing ecosystem model complexity.

The Galápagos archipelago ecosystem is mainly affected by three different surface and subsurface currents. The major currents affecting the Galápagos are the westward South Equatorial Current (SEC) and the eastward Equatorial Undercurrent (EUC, Boersma, 1977, 1978). The SEC drives surface waters over the entire region around the Galápagos and is composed of the warmer Panama Current and cool Humboldt Current. The Panama Current influences the northern islands, while the cool Humboldt (Peru) Current influences the southern islands. To balance the westward SEC, the eastward EUC (also known as the Cromwell current) develops as a subsurface compensation against the westward SEC, causing the upwelling in western archipelago. This upwelled water is relatively rich in iron, the micronutrient needed for growth by most organisms, and the production is high in many areas of the Galápagos and surrounding waters (Steger et al. 1998). The EUC is the major oceanographic feature affecting production through the Galápagos Archipelago (Houvenaghel 1984).

The Galápagos are greatly affected by seasonal atmospheric and oceanographic variability (Houvenaghel 1984). During the hot wet season (December to May), the Intertropical Convergence Zone (ITCZ) migrates southward towards the equator, the northeast trades become more prevalent, and warmer (>25 °C), fresher (<34) and less-productive waters of the Panama Current flow southward into the Archipelago. During the dry Garúa season (May to November), the ITCZ migrates to the north of the equator,

the southeast trade winds become dominate, the major source waters for the SEC are the cold Peruvian Ocean current and the Peruvian Coastal Current (the Humboldt Current), enhancing the contributions to the SEC with the colder (18 °-20 °C), saltier (>35) productive waters. The different source waters for the SEC as it flows though the GMR, from both northern and southern hemispheres, as well as topographically induced upwelling which occurs when the eastward flowing EUC runs into the Galápagos platform are the cause of the tremendous diversity around the Archipelago.

A few studies have quantified the phytoplankton primary production around the Archipelago, especially the higher concentrations west of Isabella (Feldman 1984, 1986) associated with the upwelling EUC. Houvenaghel (1984) discussed the oceanographic setting of the Galápagos and concluded that the EUC was the major oceanographic phenomena affecting the Galápagos. Hayes (1985) pointed out that the sea level differences across the Archipelago increase as the EUC strengthens, measured by shallow moored pressure gauges. Steger et al. (1998) found that the near-surface waters to the west of the Archipelago during November 1993 were predominately upwelled EUC waters, and as a consequence were cooler, saltier and higher in nutrients and iron than waters found over the eastern portion of the Archipelago. In addition, the extent of the plume shown by Feldman (1986) could only be maintained by upwelling of EUC waters that are cooler and higher in nutrients than the waters surrounding the plume. Palacios (2004) also found that the temporal variability of ocean color and SST around the

Galápagos was dominated by the seasonal migration of the ITCZ and associated strengthening of the SEC and EUC.

Another distinctive feature associated with Galápagos coastal waters is that the greatest sea temperature anomalies occur during El Niño and La Niña events (Glynn and Ault, 2000). Recently, the frequency and severity of El Niño events appear to have increased and this is a concern for the conservation of endangered species. El Niño events now occur 2–7 times more frequently than they did 7000–15,000 years ago (Riedinger et al., 2002; Rodbell et al., 1999). The 1982- 83 and 1997- 98 El Niño events, in particular, appear to have been the most extreme for many centuries, and have had a devastating effect on marine life in the Galápagos region. During the El Niño event period, the Equatorial Undercurrent weakens, the surface water warms, micronutrients are reduced, the primary production decreases (Chavez et al., 1999), and fish numbers diminish. Data from commercial fisheries indicated that the catch of mullets from the Galápagos during the 1997–1998 El Niño event were half that of the commercial catch in 1999 when there was no El Niño event (Nicolaides and Murillo, 2001). So the relationship between extreme ENSO events and loss of marine biodiversity in Galápagos needs to be investigated as a matter of local and global importance. Such a study has direct implications to predictions of loss of global biodiversity associated with ocean warming and climate change.

This paper focuses on the oceanographic variability at four different spatial scales associated with the biological productivity and biogeography of the various marine ecosystems across the Galápagos Marine Reserve (GMR) as simulated by an ocean general circulation model, specifically, the Hybrid Coordinate Ocean Model (HYCOM; Bleck, 2002; Chassignet et al., 2003; Halliwell, 2004). The rest of the paper is organized as follows: in section 2, we describe the HYCOM model configuration and do some sensitivity experiments. In section 3, the simulated tropical ocean circulation around the GMR using QuikSCAT and NCEP forcing are demonstrated and compared with the observation cruise results. Results are discussed in section 4 and 5 and summarized in section 6.

2. HYCOM model and Data

2.1 Model description

HYCOM is a primitive equation ocean general circulation model (OGCM) using density, pressure, and sigma coordinates in the vertical coordinate. It has evolved from the Miami Isopycnic Coordinate Ocean Model (MICOM) and is isopycnal in the open stratified ocean, but reverts to a terrain-following coordinate in shallow coastal regions, and to z-level coordinates near the surface in the mixed layer. This generalized vertical coordinate approach is dynamic in space and time via the layered continuity equation, and permits the existence of zero thickness layers. HYCOM's ability to seamlessly transition between deep and shallow water yield more reliable ocean circulation makes it

ideal to apply to the GMR. The islands lie in the Pacific Ocean about 1,000 km from the South American coast and straddling the Equator. There are 13 large islands, 6 smaller ones and 107 islets and rocks, with a total land area of about 8,000 square kilometers. The islands are volcanic in origin and several volcanoes in the west of the archipelago are still very active. These volcanoes rise from a depth of > 3500 m with the main platform at ~ 500 m depth. As shown by Chassignet et al. (1996), HYCOM was able to generate a more realistic EUC than several other popular OGCMs (Chassignet et al. 1996). Since understanding the dynamics of the EUC is crucial to this study, HYCOM is an appropriate choice for simulating the ocean circulation around the GMR.

The details of the HYCOM equations and numerical algorithms, along with a description and validation of the hybrid coordinate generator, can be found in Bleck (2002).

2.2 Model configuration and numerical experiments

A suite of HYCOM simulations were carried out using a nesting scheme of 4 ever increasing resolution domains. The largest domain covers the entire global ocean with a grid size of 1.44 °x 0.72 °in the zonal and meridional direction, respectively. The second domain embedded within the global domain uses a grid size of 0.48 °x 0.24 °covering the equatorial Pacific Ocean. The third domain has a grid size of 0.12 °x 0.06 °. Finally, the highest resolution domain has a grid size of 0.04 °x 0.02 °(about 4.45 km x 2.21 km) that is centered on the GMR (92.16 °W-88.96 °W, 1.68 °S-1.68 °N). All domains have a

vertical resolution of 26 layers that stretch or shrink vertically as a function of total depth according to the hybrid coordinate frame discussed above.

The model was initialized with temperature and salinity from the Levitus monthly climatology (Levitus et al., 1994) and run for 12 years. It was driven by daily surface wind stress, surface air temperature, surface atmospheric specific humidity, net shortwave radiation, net long-wave radiation and precipitation fields obtained from NCEP reanalysis (Kistler, et al, 2001). The latent and sensible heat fluxes were calculated during model runs using the model sea surface temperature and the bulk formulation (Cayan 1992). Boundary conditions were provided by buffer zones that are ten grid points wide within which temperature, salinity, and interface depth are relaxed to Levitus climatological values that have been vertically remapped to hybrid vertical coordinates. The KPP vertical mixing model of Large et al. (1994) was used. For the experiments with the resolution of 1.44 º, 0.48 ºand 0.12 º, the bathymetry was derived from ETOPO2, which is a digital data base of seafloor and land elevations on a 2-minute latitude/longitude grid and is interpolated onto the various model grids. The bathymetry for the simulation of the resolution of 0.04 º(near the Galápagos Islands) domain is derived from the 0.01 º bathymetry of William Chadwick at Oregon State University (http://www.pmel.noaa.gov/vents/staff/chadwick/Galapagos.html). The wind field used to drive the ocean circulation in this sub-region was derived from the 25-km resolution QuikSCAT wind field instead of the NCEP/NCAR reanalysis. The model was run for

twelve years from 1995 to 2007, and fields from the last three years of the simulation (year 2005, 2006 and 2007) are analyzed here.

2.3 Sensitivity experiments

The simulations with these four different simulations have been performed under identical daily meteorological forcing fields and the results compared between model grids with coarse and fine resolutions. It was found that the simulations under fine resolutions are more accurate and have a more realistic spectrum of oceanographic variability. For example, the simulation with the resolution of 0.04° can depict the intra-seasonal signal from the tropical instability waves (TIW), as well as the annual and the inter-annual signals, whereas the low-resolution global model failed to depict TIW signal. The ocean is also sensitive to the frequency of the atmospheric forcing. In a controlled experiment where the atmospheric forcing frequency was reduced from daily frequency to monthly, the results simulated by the ocean model are shown to be less accurate than those simulated using daily forcing (Liu et al, in review).

El Niño /Southern Oscillation (ENSO) variability was also simulated from 1995-2006 driven by NCEP atmospheric forcing using the above configuration. The SST anomalies in the Nino3.4 region (5° S-5° N, 170° W-120° W) are often used to index ENSO variability (Trenberth, 1997). Figure 2 shows the observed (blue) and HYCOM simulated SST anomalies (red) in Nino3.4 region. The correlation coefficient between the simulate SSTA and observed SSTA is 0.883. This result shows that HYCOM can

reasonably simulate the major El Niño events including the strong 1997-1998 events. Therefore, we feel confident the HYCOM should give realistic simulations of the large-scale circulation around the islands during ENSO events as well as normal years.

3. Model simulations compared to observations

3.1 Simulation of T-S and ocean currents around GMR

Here we will compare the simulated circulation around the GMR to observational cruise results; focusing on the surface water mass characteristics and flow patterns. It should be noted that it is not expected that the modeled fields accurately portray the observed fields, but they should portray the major features of the water masses and currents. Data assimilation, which consists in combining available data with a dynamical model to provide an efficient and accurate estimate of the underlying state of the system, is now recognized as the most powerful tool to improve the consistency between the model and data (Ghil and Malanotte- Rizzoli, 1991). There currently is an ongoing effort to add data assimilation to HYCOM (HYCOM Consortium for Data Assimilation Modeling, http://hycom.rsmas.miami.edu/data_assimilation.html).

The observation data used in the study were collected during four surveys (see station positions in Figure 1) conducted 17-28 March, 2005 (Mar 05), November 22-December 3 (Nov 05), 2005, June 26-July 4, 2006 (Jun 06) and 14 -23 November 2006 (Nov 06) onboard the Galápagos National Park Service's M/N Sierra Negra. Each cruise was 8 to

12 days long and occupied ~70 hydrographic stations around the GMR. Surface data included underway measurements of temperature, salinity, dissolved oxygen and fluorescence data using a Seabird Electronics SBE 19+ system (CTD) that were averaged into 30 min time intervals.

a) March 2005

The March 2005 cruise occurred during the hot, wet season, a period characterized by warm SST associated with the southward advection of warmer, northern waters from the Panama current and a weakening of the southeast trade winds. Figures 3a and 4a display the simulated and observed SST. Figure 5a, 6a display the simulated and observed sea surface salinity (SSS). Figure 7a displays the simulated mixed layer depth (MLD) to compare with the observed chlorophyll (Figure 8a) during March 2005. From Figure 3a and 5a, the warmest and less salty waters are located within the north and south regions of the GMR and the coolest and saltiest waters are found west of Isabella and Fernandina, indicative of topographically induced upwelling of the EUC (Feldman 1986). These results are consistent with the observation cruise T-S characteristics (see Figures 4a, 6a). Also the MLD (Figure 7a) was the shallowest (~10m) in the west of Isabella and Fernandina during the March 2005 cruise. The coldest and saltiest water had the highest chlorophyll concentration (see Figure 8a). The highest surface chlorophyll *a* concentrations observed of 3.25 mg m^{-3} was found to the west of Isabella Island and north of Fernandina Island. The minimum chlorophyll *a* concentration observed was 0.05 mg m^{-3} located directly southeast of Isabella Island.

The simulated surface layer flow (Figure 9a) showed the westward flow of the SEC collided with the eastward flow of the EUC both north and south of Isabella Island. Nearing the Archipelago, the SEC splinters into northward and southward lobes that continue to the west a few degrees off the equator (Wyrtki and Kilonsky 1984). The mixed layer flow (Figure 10a) is mainly dominated by the eastward flow of EUC around the Galápagos. The EUC is quite strong (150 cm/s), has its core below the thermocline and drives an eastward flow near surface (~20m). The mixed layer depth shoals to 15m in west of Isabella and Fernandina Islands, which indicates the upper reach of a weakened, centrally located EUC.

b) November/December 2005

The November/December 2005 cruise occurred during a transition from the Garúa to the wet season with a lessening of the southeast trades. The simulated mean SST was cooler than climatology by approximately -0.5°C during the transition, as seen from the ENSO anomaly (Figure 2, grey area). Figures 3b and 4b display the simulated and observed SST. Figures 5b, 6b display the simulated and observed sea surface salinity (SSS). Figure 9b displays the simulated mixed layer depth (MLD) to compare with the observed chlorophyll (Figure 8a) during November/December 2005. During this period, the modeled coldest (20 °C, see Figure 3b) and saltiest (34.7, see Figure 5b) waters were found to the west of Isabella Island and north of Fernandina Island, and corresponded with the largest upwelling zones found in late spring/early summer as the EUC

strengthened. These features were consistent with the *in situ* T-S characteristics observed during this cruise period (see Figures 4b, 6b). Figure 7b shows the MLD was slightly shallower in the west nearing the cooler, upwelling region. The warmest (25.0 °C) and freshest (33.7) waters were found in north of the Archipelago. The far northern region was characterized with warmer, fresher water and had the deepest MLD, and the other regions fell between the range of upwelling region and far north region. Both the SST and SSS distributions showed an east-to-west gradient associated with higher values of chlorophyll concentrations indicative of higher phytoplankton biomass. The maximum values of chlorophyll *a* were found west of Isabella Island, and the minimum chlorophyll *a* concentrations were observed along the equator in the GMR (Figure 8b). Also, the shallowest MLD was simulated over the cooler waters at depth (Figures 7b, 3b), another indication of strong upwelling. The modeled surface layer flow (Fig 9b) was completely dominated by the westward flow of the SEC throughout the GMR during this period. The EUC (Figure 10b) had weakened considerably.

c) June 2006

The June/July 2006 cruise occurred during a transition period, leaving the wet season and entering the Garúa season, with the strengthening of southeast trade winds and SST significantly (+1.2 ℃) above climatology (Figure 2). Figures 5c and 6c display the simulated and observed SST. Figures 5c, 6c display the simulated and observed sea surface salinity (SSS). Figure 7c displays the simulated mixed layer depth (MLD) to compare with the observed chlorophyll (Figure 8c) during June 2006. The model mean

temperature was 24.35+/-1.69 ^{o} C throughout the GMR (Figure 3c) with the warmest waters, 26.04 °C, found north of the Archipelago and the coldest waters, 24.2^{o}C , found to the west of Isabella and Fernandina Islands (Figure 3c). The simulated SST was warmest (26.04 ℃) and SSS was freshest in northeast of the Archipelago, forming an increasing gradient to the west with the highest salinity, 35, in areas of coldest waters west of Isabella and Fernandina Islands (Figure 5c). The model generally simulated the main T-S characteristics observed around the Galápagos Archipelago (see Figures 4c, 6c). The modeled MLD (Figure 7c) shoaled to ~20m in west of Isabella Island and was deepest about 65m to the north of the Archipelago. The simulated SSS has higher values which in general corresponded to lower temperatures (Figures 3c, 5c). Freshest waters (33.76) were found towards the northeast and steadily increased to the southwest, reaching a maximum (34.9) to the west of Isabella Island where the observed chlorophyll *a* concentrations (Figure 12c) also reached the maximum compared with the other cruises.

The model results also indicated surface expression of the EUC (Figure 9c) was quite similar to those of Mar05, with a strong velocity core (100cm/s) centered just below the mixed layer. During this period the EUC rose close to the surface and drove an eastward surface flow through the GMR. The eastward EUC (Figure 10c) reached to ~20m depth beneath the westward SEC.

d) November 2006

The November 2006 cruise occurred at the end of the Garúa season and at the

beginning of a mild El Niño (Figure 2). During this period, the model mean surface temperature was 25.87 +/-1.67^{o}C throughout the GMR (Figure 3d). The warmest waters (27 ℃) were north of the Archipelago and the coldest waters (24.2^{o}C) west of Isabella and Fernandina Islands. The mean SST was 33.5 with freshest waters found northeast of the Archipelago, forming an increasing westward salinity gradient with the highest salinity (34.6) west of Isabella Island (Figures 3d, 5d). Because this period was during the onset of an El Niño event, the MLD (Figure 7d) was the deepest and warmest during this period to the west of Isabella Island. These results were consistent with the cruise observation results (see Figures 4d, 6d). In addition, the observed chlorophyll *a* concentrations (Figure 8d) around the GMR were greatly reduced during this period of reduced upwelling. The maximum observed chlorophyll *a* (1.17 mg m^{-3}) was south of Santa Cruz Island and north of Floreana and Española Islands, and minimum chlorophyll *a* (0.17 mg m^{-3}) observed directly northwest of Isabella Island. The surface currents (Figure 9d) during this period were dominated by the westward flowing SEC. The EUC (Figure 10d) was greatly weakened, leading to the weaker upwelling to the west of Isabella Island.

4. Four cruises comparison and discussions

The March 2005 cruise occurred during the wet season, a period characterized by warm SST and near the later stages of the weak 2004-05 El Niño. During this period, warmer waters from the Panama Current were advected southward and the southeast

trade winds weakened (characteristic of an El Niño period). The region west of Isabella and Fernandina was characterized by the coolest and saltiest waters observed, indicative of the productive zone upwelling of the EUC and of the re-establishment of the EUC with the end of El Niño conditions. The simulated surface flow (Figure 9a) showed the eastward flow of the EUC collided with the westward flow of the SEC both north and south of Isabella Island. Nearing the Archipelago, the SEC splintered into northward and southward lobes that continued to the west a few degrees off of the equator.

The November/December 2005 cruise occurred during a transition from the Garúa to the wet season with the lowest SST compared with other three cruise periods. The modeled coldest and saltiest water were found to the west of Isabella Island and north of Fernandina Island, corresponded with the largest upwelling zone observed during 2005 - 2006. The modeled surface layer flow (Figure 9b) was completely dominated by the westward flow of the SEC throughout the GMR during this period. The EUC was relatively weak and even diminished.

The June 2006 cruise occurred during a transition period, leaving the wet season and entering the Garúa characterized by a strengthening of the southeast trade winds. The EUC characteristics (Figure 9c) are similar to those of Mar05 (see Figure 9a) and the EUC core was centered near the mixed layer, and extends to the surface and drives a warm eastward flow through the GMR. The coldest and saltiest waters were found to the west of Isabella and Fernandina Islands (Figure 3c) were associated with the highest chlorophyll concentration and most productive upwelling zone during this time of the

year (Fig 8c). Model results also indicated that the eastward EUC existed ~20m above the thermocline, beneath the westward SEC. During this period, the mixed layer depth was the shallowest throughout the Archipelago compared with other cruises period.

The November 2006 cruise occurred at the end of the Garúa and at the beginning of a mild El Niño. This transition was also characterized by weaker upwelling to the west of Isabella Island associated with a weakening of the EUC. The thermocline was the deepest and warmest during the November 2006 cruise west of Isabella Island. The chlorophyll *a* around the GMR was greatly reduced.

The model results are in good agreement with observations. All four cruises had warm, fresher water in the east part of the GMR supplied by the SEC, with the relative cold and salty water in west of Isabella Island indicating the productive upwelling zone (Houvenaghel 1978, 1984). A gradient formed from east to west with increasing salinity and decreasing temperature.

5. How the ENSO events affected the GMR

Since the model is able to accurately simulate the internnual variability in the tropical ocean. We will use two case studies to study how El Niño/La Niña events affect the ocean circulation and water mass around the Galápagos Archipelago. This study include simulating the 2006 El Niño and 2007 La Niña events and investigate key physical

processes that affect the water mass transport pathways and the local upwelling dynamics for comparison to observed conditions (Schaeffer et al., 2008, Sweet et al, 2007). Sensitivity studies using the nested modeling system have been carried out to identify key physical processes that affect the water mass transport pathways and the local upwelling dynamics. Other possible cases include simulations (hinecasts) of strong El Niño (eg., 1982/3 and 1997/8) and La Niña conditions, as well as periods of "normal" conditions. By quantifying and studying the mechanisms through which the extreme temperature anomalies affect biological productivity and the survival of species in Galápagos, we should be able to identify recovery processes that minimize ecosystem disruption through biological resilience.

Here we chose the 2006-2007 El Niño events and 2007-2008 La Niño events. We selected Jan 2007 as El Niño event period and selected Dec 2007/Jan 2008 as La Niño period (see the SST anomalies from Figure 10). Figure 11 is the observed and simulated SST in Jan 2007 (A: observed SST, C: simulated SST) and Dec 2007 (B: observed SST, D: simulated SST). Figure 11E) and F) are the simulated SSS in Jan 2007 and Dec 2007. We could see that the HYCOM can generally simulated the temperature and salinity during the 2007 El Niño and Dec 2007/Jan 2008 La Niño Events. Figure 12 and 13 show the vertical sections of zonal current along four sections including 92^{o}W, 91.8^{o}W, 90^{o}W and 89^{o}W for the upper 200 m around the GMR in Jan 2007 and Dec 2007. During the El Niño event (Jan 2007), there are warm and less salty waters during the whole GMR region, while the less warm and saltier water are found west of Isabella and Fernandina,

indicative of topographically reduced upwelling of the EUC. The EUC is weakened and its core is at ~100m. While during the La Niño event (Dec 2007), there are cold and salty waters during the whole GMR region, while the colder and saltier water are found west of Isabella and Fernandina, indicative of topographically increased upwelling of the EUC. The EUC is greatly strengthened and EUC core depth is increasing from ~100m to ~150m during this La Niño event.

6. Summary

This paper focuses on the oceanographic variability and physical settings associated with the biological productivity and biogeography of the various marine ecosystems across the GMR using a general ocean circulation model (HYCOM). The model results were compared with data taken during oceanographic cruises in 2005/2006. Daily surface fields obtained from the NCEP and the wind forcing from QuikSCAT were used to drive the simulations. Sensitivity to different forcing conditions and resolutions are tested. The sensitivity tests showed that frequency wind forcing higher than weekly average is more reliable than monthly forcing in generating the observed fields within the GMR. In addition, the simulation around the GMR is greatly improved with the increase of horizontal resolutions. A 0.04˚ resolution is deemed suitable for studying the ocean circulation in and around Galápagos Archipelago.

There is a large spatial variability in temperature and salinity across the Galápagos

Archipelago. West of Isabella and Fernandina Islands, the largest upwelling and productive zones, corresponds with relatively colder and salty waters. The effects of the EUC and local upwelling are easily resolved in the simulations and compare well with the highly productive zones observed in cruise and satellite data. The model results show that the EUC around the Galápagos shoals to nearly 20m from the normal 50m, seen from shallow mixed layers in western Galápagos. The EUC collides with the islands and breaks into a number of well defined flows through the islands. The EUC is strongest during the late spring/early summer and weakened in the late fall. The collapse of the westerlies with the onset of El Niño event in 2006 resulted in a collapse of the EUC flow in the vicinity of the Galápagos and effectively shut off the major upwelling regions. The property distributions in the far northern region of the GMR are characterized by warmer, fresher waters from the Panama Current and had the deepest MLD. Properties in the remainder of the Archipelago fell between the range of upwelling region and Far North Region. The Jan 2007 and Dec 2007 cases also show that the HYCOM model can generally simulate the ocean circulation around the GMR during the El Niño and La Niño events. The EUC became stronger during the La Niño events and the EUC core depth is increasing from ~100m to ~150m.

Acknowledgements

This project was funded by National Aeronautics Space Association (NASA) Biodiversity and Ecological Forecasting grant NNG04GL98G. The Counterpart US-AID No. 518-A-00-03-00152-00 and UK Darwin Initiative Project No. 14-048 also provided

funding for this project. All modeling work is carried out in the Coastal Fluid Dynamical Lab of North Carolina State University using the High-Performance Computing (HPC) system.

Reference:

Bleck, R., 2002. An oceanic general circulation model framed in hybrid isopycnic-Cartesian coordinates. Ocean Modelling, 4, 55-88.

Boersma, P.D. 1977. An ecological and behavioral study of the Galápagos Penguin. Living Bird 15: 43–93.

Boersma, P.D. 1978. Breeding patterns of Galápagos Penguins as an indicator of oceanographic conditions. Science 200: 1481–1483.

Bustamante, R., Collins, K. J. Bensted-Smith, R., 1999.Biodiversity conservation in the Galápagos Marine Reserve. Entomologie Supplement 68: 45-52.

Cayan, D., Latent and sensible heat flux anomalies over the Northern oceans: driving the sea surface temperature, J. Phys. Oceanogr., *22*, 859–881, 1992.

Cayan, 1992: Latent and sensible heat flux anomalies over the northern ocean: The connection to monthly atmospheric circulation. JClim, 5, 354--369

Chassignet, E.P., Smith, L.T., Bleck, R., Bryan, F.O., 1996. A model comparison: numerical simulations of the north and equatorial Atlantic oceanic circulation in depth and isopycnic coordinates. J. Phys. Oceanogr. 26, 1849– 1867.

Chassignet, E.P., Smith, L.T., Halliwell, G.R., Bleck, R., 2003. North Atlantic Simulations with the Hybrid Coordinate Ocean Model (HYCOM): impact of the vertical coordinate choice, reference density, and thermobaricity. J. Phys. Oceanogr. 33, 2504–2526.

Chavez, F.P., Strutton, P.G., Friederich, G.E., Feely, R.A., Feldman, G.C., Foley, D.G., McPhaden, M.J., 1999. Biological and chemical response of the equatorial pacific ocean to the 1997–1998 El Niño. Science 286, 2126–2131.

Edgar, G. J., Banks, S., Farina, J. M., Calvopina, M. and Martınez, C., 2004. Regional biogeography of shallow reef fish and macro-invertebrate communities in the Galápagos archipelago. Journal of Biogeography 31: 1107-1124.

Feldman, G., Clark, D., Halpern, D., 1984. Satellite color observations of the phytoplankton distribution in the eastern equatorial Pacific during the 1982–1983 El Niño, Science 226 (4678), 1069–1071.

Feldman, G..,1986. Patterns of phytoplankton production around the Galápagos Islands. In M.J. Bowman, R.T. Barber & C.N.K. Mooers (Eds.), Lecture Notes on Coastal and Esutarine Studies: Tidal Mixing and Plankton Dynamics (pp. 77-106). Berlin: Springer

Ghil, M., Malanotte-Rizzoli, P., 1991. Data assimilation in meteorology and oceanography. Adv. Geophys. 33, 141–266.

Glynn, P.W. and J.S. Ault. 2000. A biogeographic analysis and review of the far eastern Pacific coral reef region. *Coral Reefs* **19**: 1-23.

Halliwell Jr., G.R., 2004. Evaluation of vertical coordinate and vertical mixing algorithms in the Hybrid-Coordinate Ocean Model (HYCOM). Ocean Modelling. 7, 285–322.

Hayes, S. P. 1985. Sea level and near surface temperature variability at the Galápagos Islands, 1979-1983

Houvenaghel, G. T., 1978. Oceanographic conditions in the Galápagos Archipelago and

their relationships with life on the islands. In: Boje, R., Tomczak, M. (Eds.), Upwelling Ecosystems. Springer, Berlin, pp. 181–200.

Houvenaghel, G. T., 1984. Oceanographic setting of the Galápagos Islands. In: Perry, R. (Ed.), Key Environments, Galápagos. Pergamon Press, Oxford, pp. 43–54.

Kistler, R., E. Kalnay, W. Collins, S. Saha, G. White, J. Woollen, M. Chelliah, W. Ebisuzaki, M. Kanamitsu, V. Kousky, H. van den Dool, R. Jenne, and M. Fiorino, 2001: The NCEP-NCAR 50-Year Reanalysis: Monthly Means CD-ROM and Documentation. Bull. Amer. Meteor. Soc., 82, 247-268.

Large, W.G., Mc Williams, J.C., Doney, S.C., 1994. Oceanic vertical mixing: review and a model with a nonlocal boundary layer parameterization. Rev. Geophys. 32, 363–403.

Levitus, S., Boyer, T., 1994. World Ocean Atlas 1994, Volume 4: Temperature. NOAA Atlas NESDIS 4. US Dept. of Commerce, Washington, DC.

Levitus, S., Burgett, R., Boyer, T., 1994. World Ocean Atlas 1994, Volume 3: Salinity. NOAA Atlas NESDIS 3. US Dept. of Commerce, Washington, DC.

Liu, Y., Xie, L., Morrison, J.M., Kamykowski, D., Sweet, W., 2009, Sensitivity of Numerical Simulation of Ocean Circulation around the Galápagos Archipelago to Spatial Resolution and Atmospheric Forcing Frequency. In Review.

Jennings, S., Brierley, A.S., & Walker, J.W. 1994. The inshore fish assemblages of the Galápagos Archipelago. Biological Conservation, 70, 49-57

Oschlies, A., 2001. Model-derived estimates of new production: New results point towards lower values, *Deep-Sea Research II*, **48**, 2173-2197.

Palacios, D.M., 2004. Seasonal patterns of sea-surface temperature and ocean color around the Galápagos: regional and local influences. *Deep-Sea Research II, 51,* 43-57

Riedinger, M.A., Steinitz-Kannan, M., Last, W.M., Brenner, M.,2002. A similar 6100 C-14C yr record of El Niño activity from the Galápagos Islands. Journal of aleolimnology 27, 1–7.

Rodbell, D.T., Seltzer, G.O., Anderson, D.M., Abbott, M.B., Enfield, D.B., Newman, J.H., 1999. An asymptotically equal to 15,000- Year Record of El Niño-Driven Alluviation in Southwestern Ecuador. Science 283, 516–519.

Steger, J. M., Collins, C. A., Chu, P. C., 1998. Circulation in the Archipielago de Colon (Galápagos Islands), November 1993. Deep-Sea Research II 45, 1093–1114.

Trenberth, K.E., Hoar, T.J., 1997. El Niño and climate change. Geophysical Research Letters 24, 3057–3060.

Trenberth, K.E., 1997. The Definition of El Niño. Bulletin-American Meteorological Society 78, 2771–2778.

Wiggert, J. D., R.R. Hood, K. Banse and J.C. Kindle. 2005. Monsoon-driven biogeochemical processes in the Arabian Sea. Progress In Oceanography 65 (2-4), pp. 176-213

Wyrtki, K., Kilonsky, B., 1984. Mean water and current structure during the Hawaii-to-Tahiti shuttle experiment. Journal of Physical Oceanography 14, 242–254.

Figure Caption:

Figure 1: Bathymetry map and sampling stations of the Galápagos Archipelago.

Figure 2: The observed (blue, dashed) and HYCOM simulated SST anomalies (red, solid) in Nino3.4 region. The grey shaded areas indicate the four cruise periods.

Figure 3: HYCOM Simulated sea surface temperature for (A) March 2005, (B) November/December 2005, (C) June/July 2006, and (D) November 2006.

Figure 4: The observed sea surface temperature for (A) March 2005, (B) November/December 2005, (C) June/July 2006, and (D) November 2006 cruises

Figure 5: HYCOM Simulated sea surface salinity for (A) March 2005, (B) November/December 2005, (C) June/July 2006, and (D) November 2006.

Figure 6: The observed sea surface salinity for (A) March 2005, (B) November/December 2005, (C) June/July 2006, and (D) November 2006 cruises

Figure 7: HYCOM Simulated Mixed Layer Depth for (A) March 2005, (B) November/December 2005, (C) June/July 2006, and (D) November 2006.

Figure 8: Chlorophyll for (A) March 2005, (B) November/December 2005, (C) June/July 2006, and (D) November 2006.

Figure 9: Hydrodynamic model surface layer flow of the SEC and EUC throughout the GMR for (A) March 2005, (B) November/December 2005, (C) June/July 2006, and (D) November 2006.

Figure 10: Hydrodynamic model mix layer flow of the SEC and EUC throughout the

GMR for (A) March 2005, (B) November/December 2005, (C) June/July 2006, and (D) November 2006.

Figure 11: The observed and simulated SST in Jan 2007 (A: observed SST, C: simulated SST) and Dec 2007 (B: observed SST, D: simulated SST). Figure 11E) and F) are the simulated SSS in Jan 2007 and Dec 2007.

Figure 12: Vertical sections of zonal current (m/s) along 92W, 91.8W, 90W and 89W for the upper 200 m around the GMR in Jan 2007

Figure 13: Vertical sections of zonal current (m/s) along 92W, 91.8W, 90W and 89W for the upper 200 m around the GMR in Dec 2007

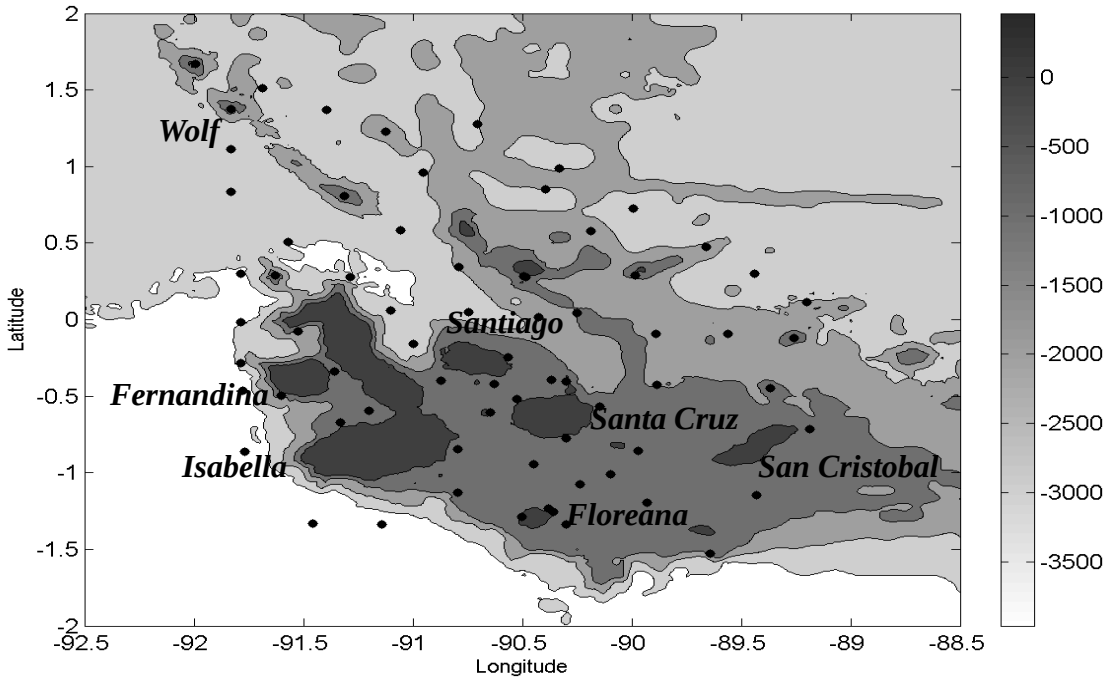

Figure 1: Bathymetry map and sampling stations of the Galápagos Archipelago.

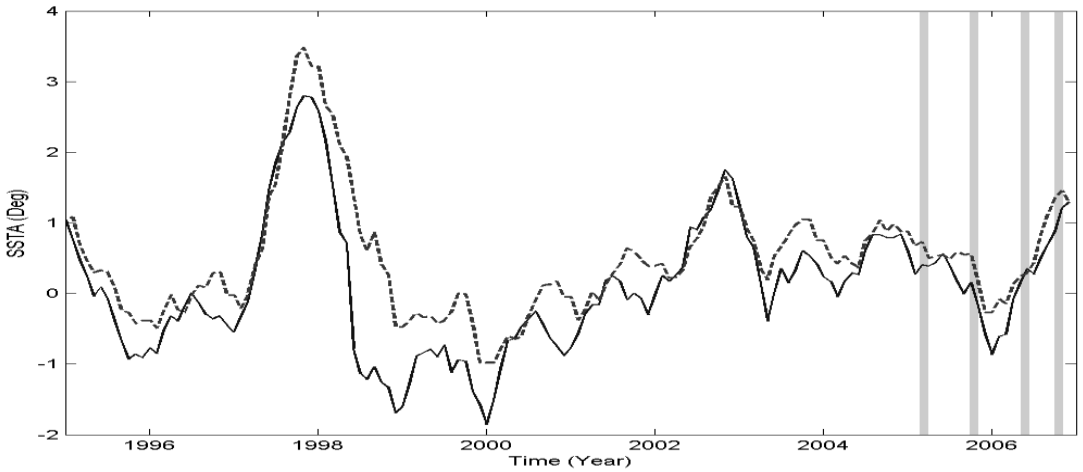

Figure 2: The observed (solid) and HYCOM simulated SST anomalies (dashed) in Nino3.4 region. The grey shaded areas indicate the four cruise periods.

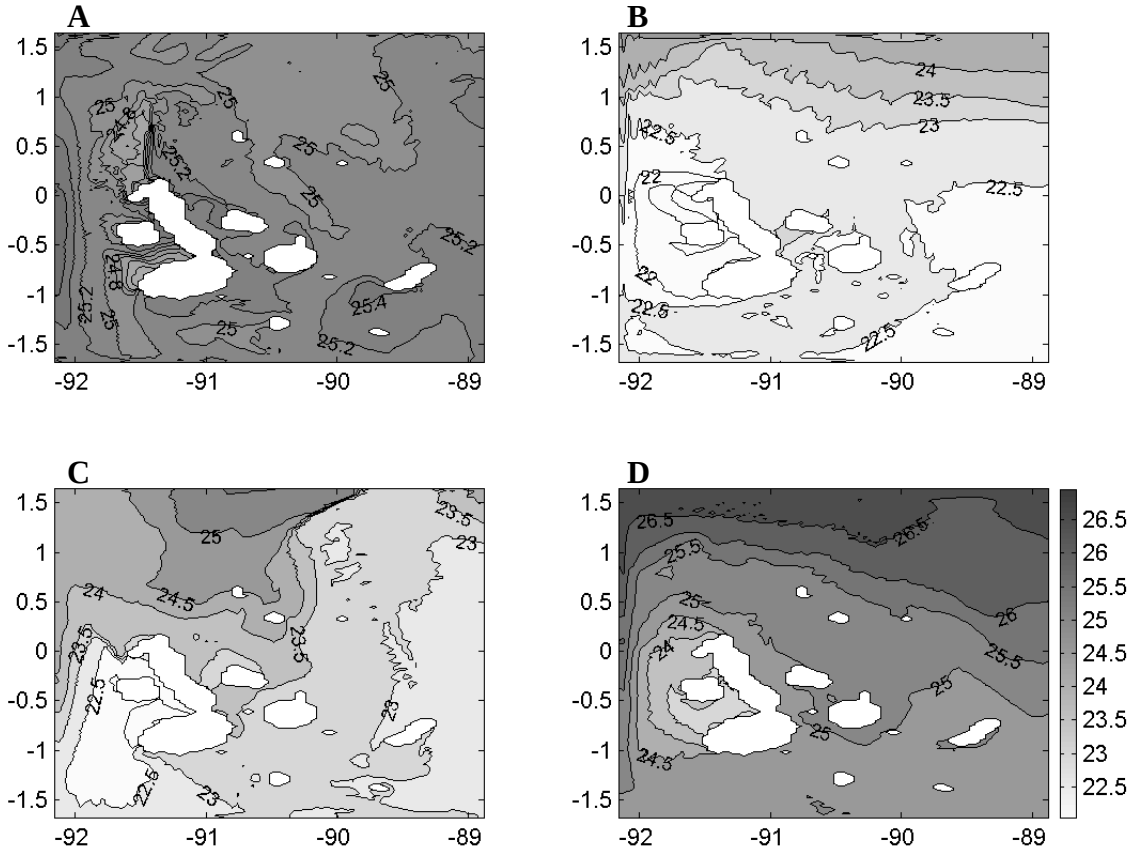

Figure 3: HYCOM Simulated sea surface temperature for (A) March 2005, (B) November/December 2005, (C) June/July 2006, and (D) November 2006.

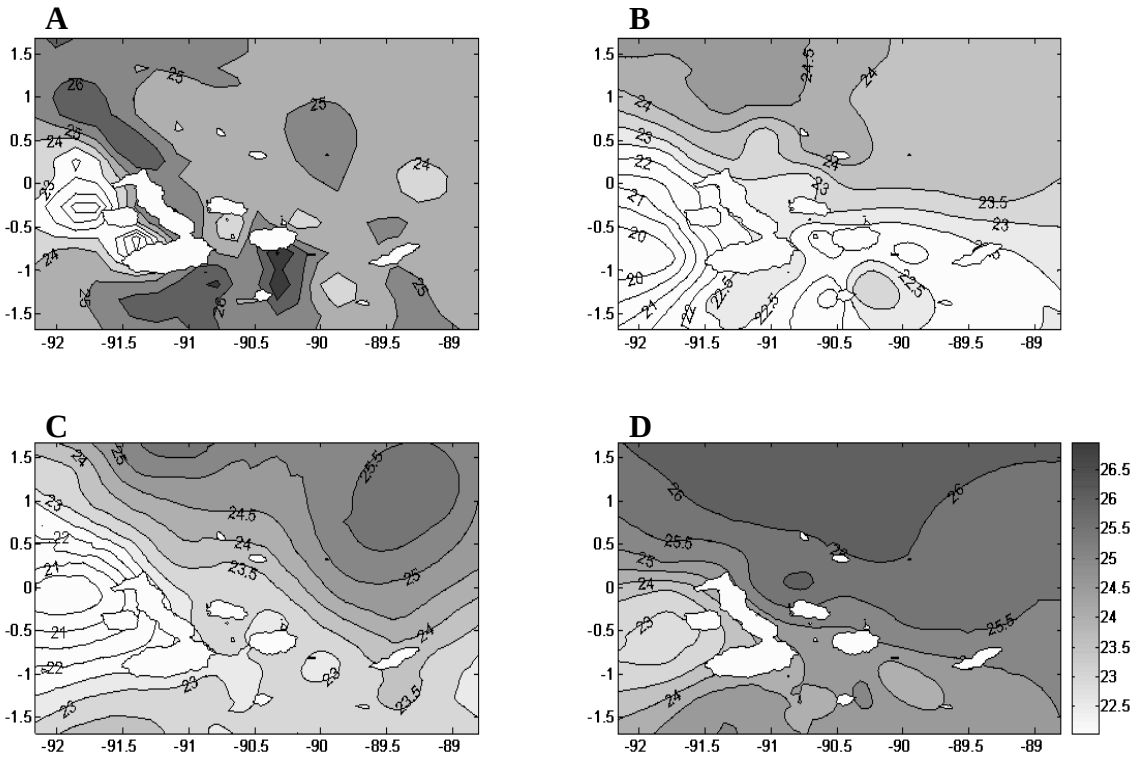

Figure 4: The observed sea surface temperature for (A) March 2005, (B) November/December 2005, (C) June/July 2006, and (D) November 2006 cruises.

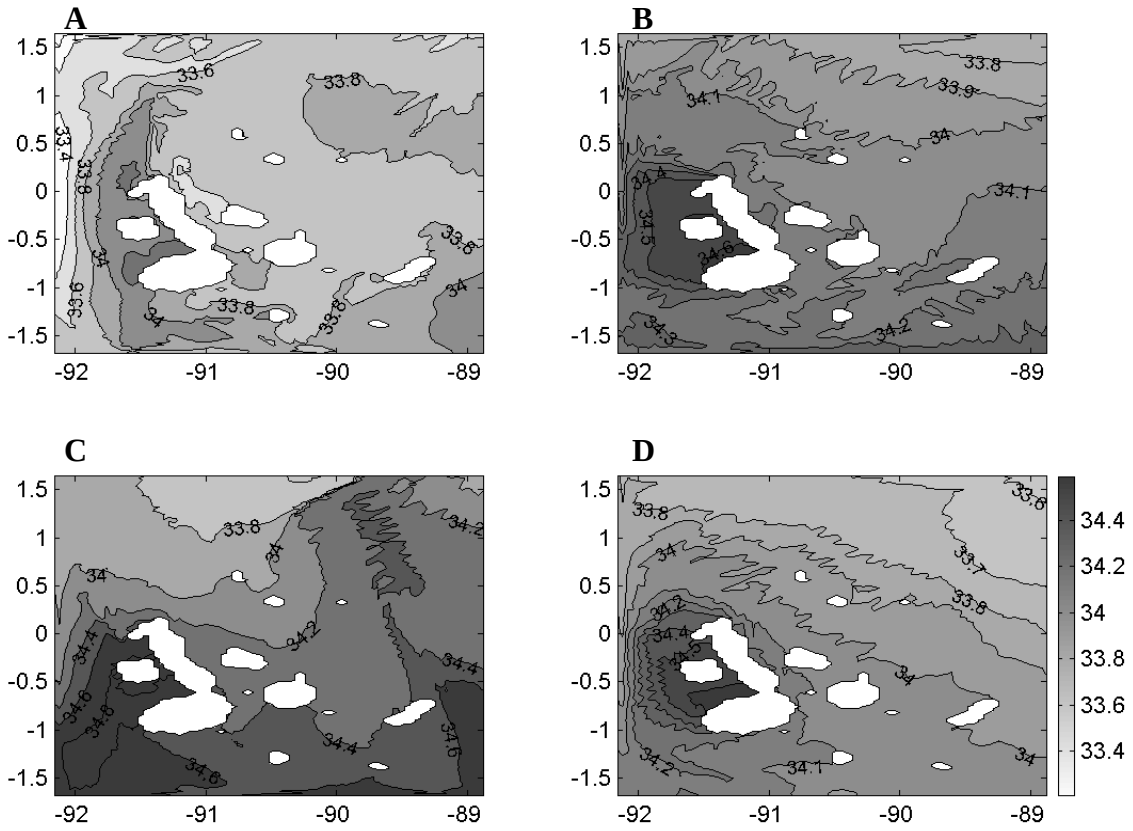

Figure 5: HYCOM Simulated sea surface salinity for (A) March 2005, (B) November/December 2005, (C) June/July 2006, and (D) November 2006.

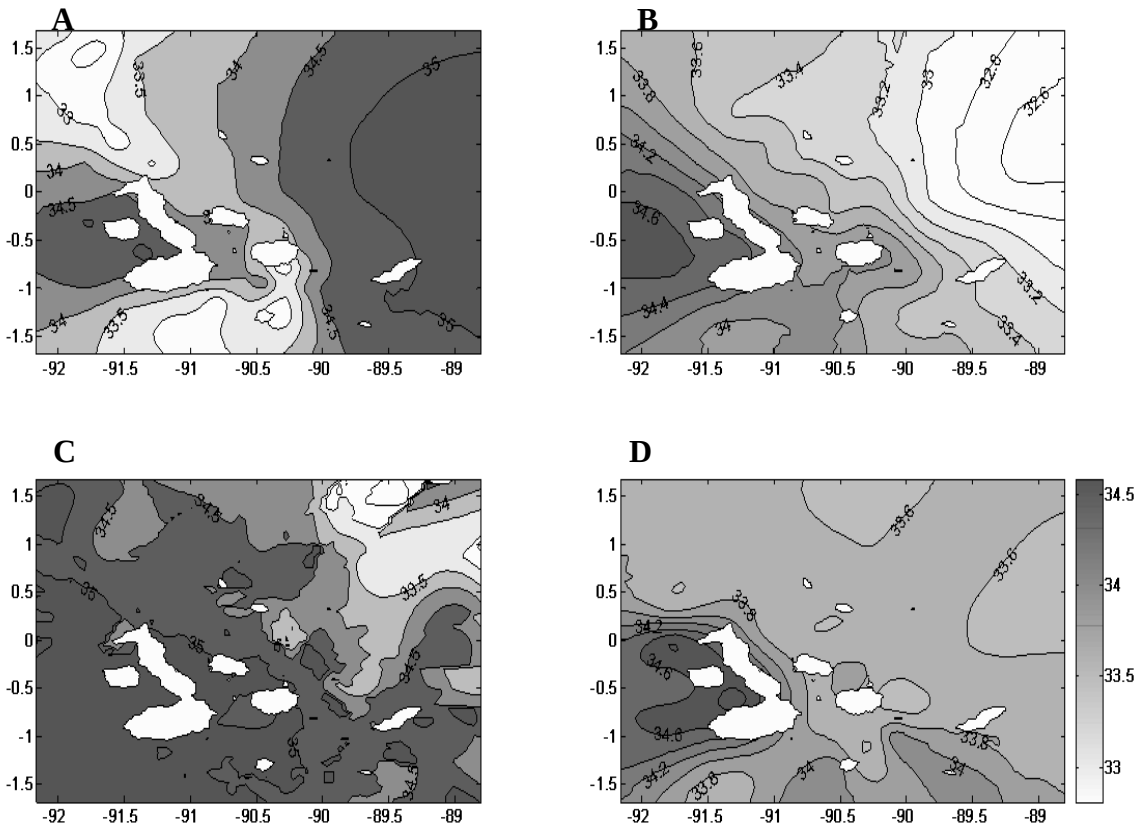

Figure 6: The observed sea surface salinity for (A) March 2005, (B) November/December 2005, (C) June/July 2006, and (D) November 2006 cruises.

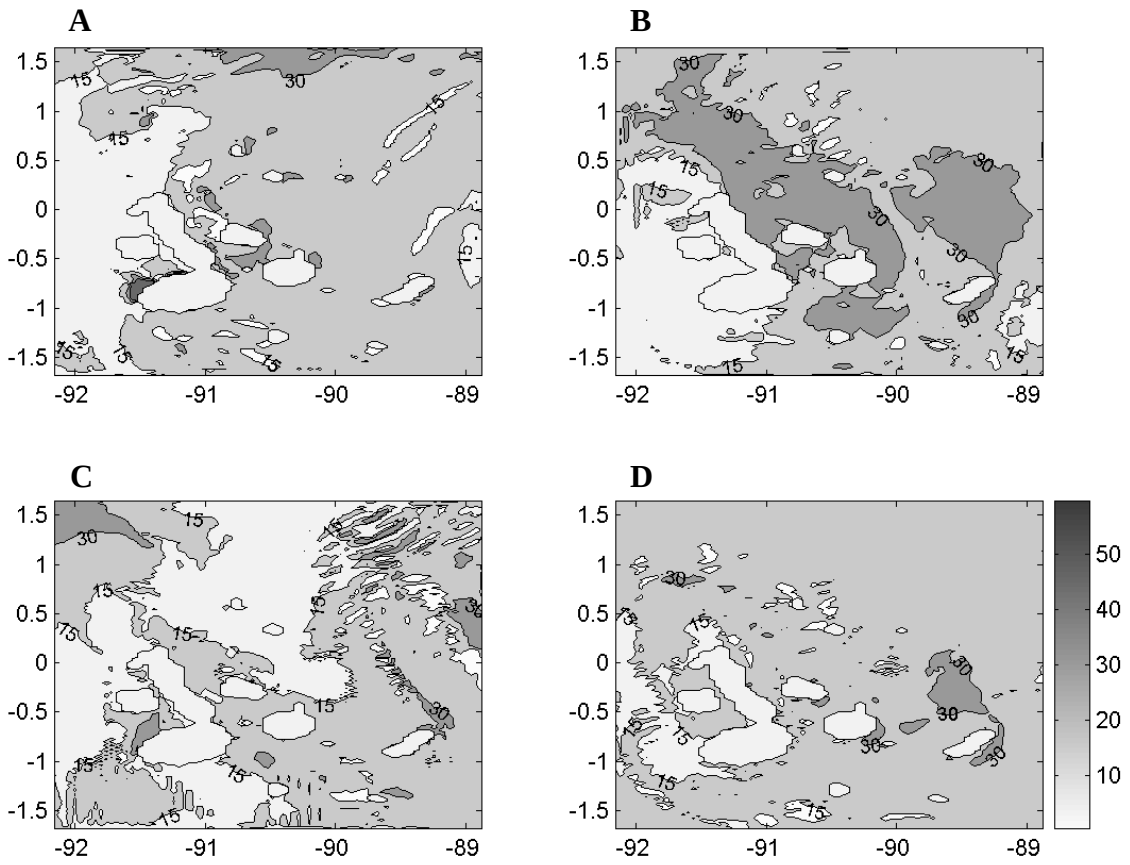

Figure 7: HYCOM Simulated Mixed Layer Depth for (A) March 2005, (B) November/December 2005, (C) June/July 2006, and (D) November 2006.

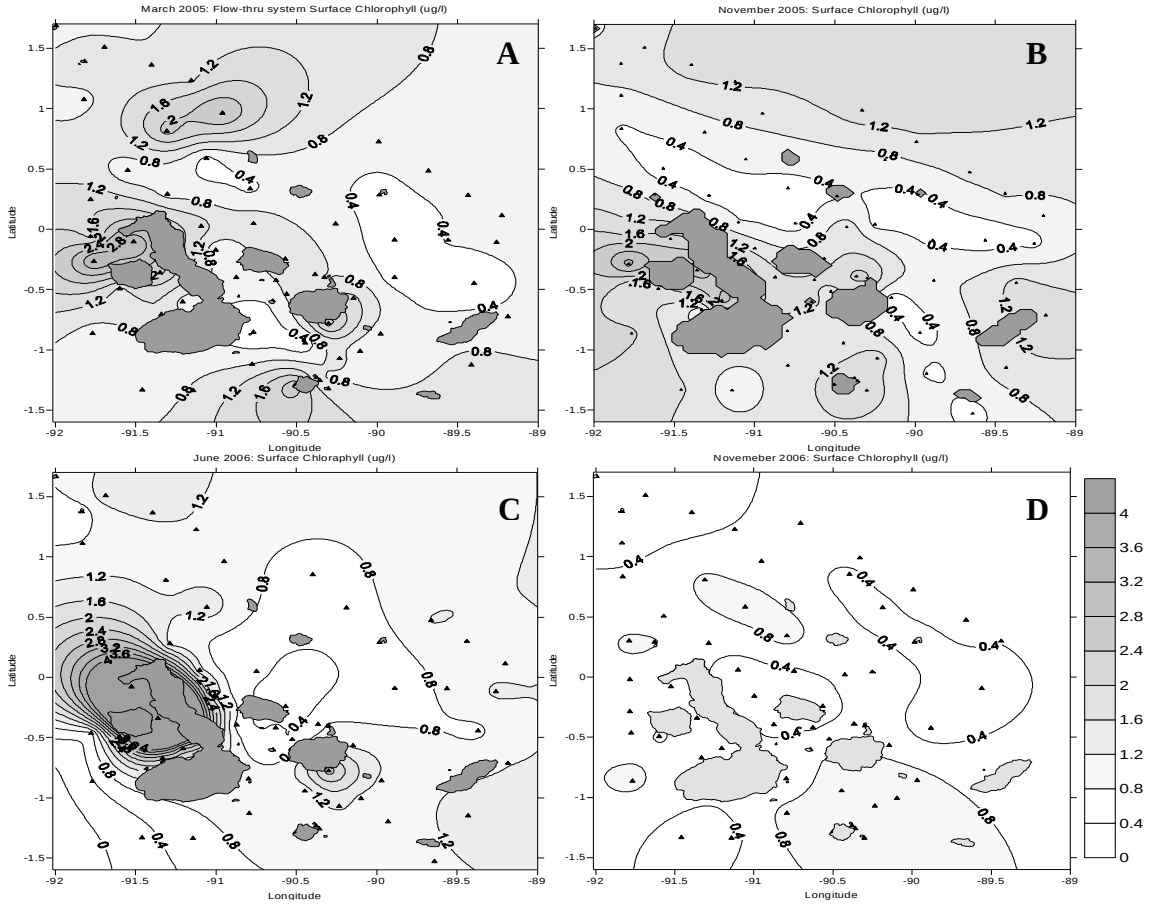

Figure 8: Chlorophyll for (A) March 2005, (B) November/December 2005, (C) June/July 2006, and (D) November 2006.

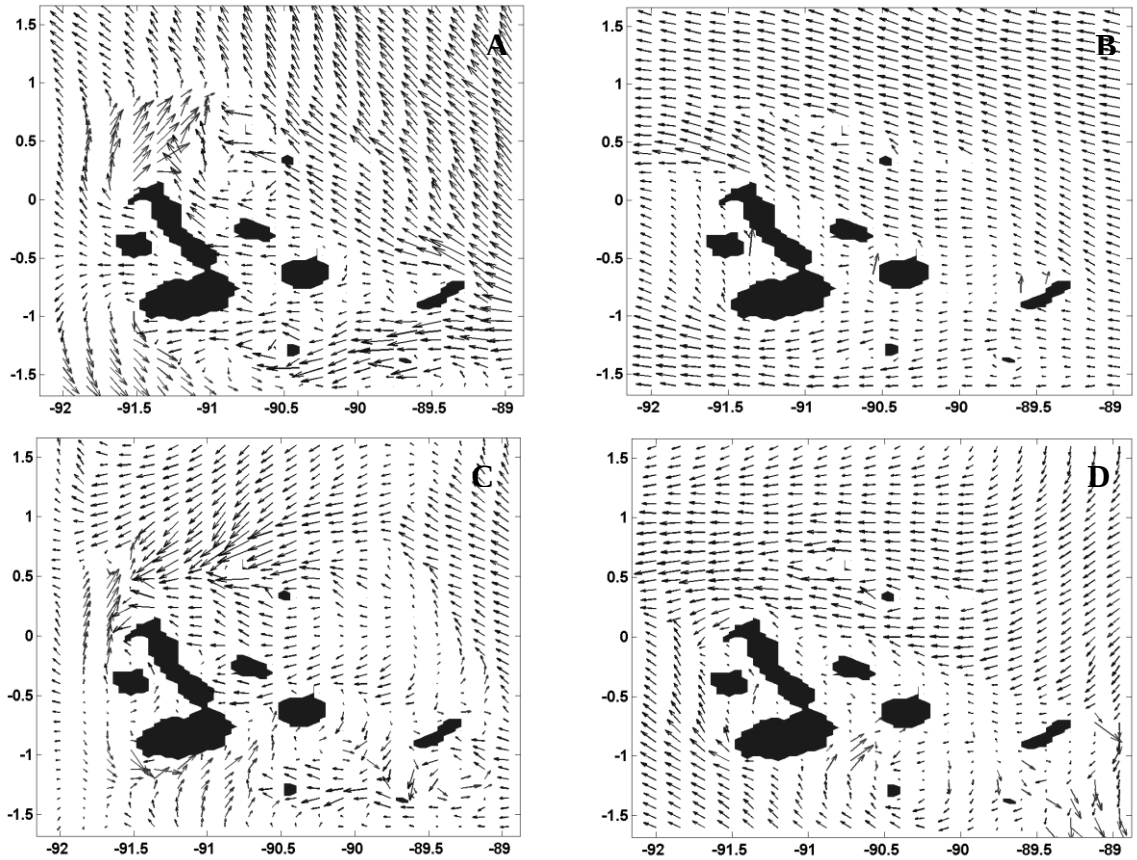

Figure 9: Hydrodynamic model surface layer flow of the SEC and EUC throughout the GMR for (A) March 2005, (B) November/December 2005, (C) June/July 2006, and (D) November 2006.

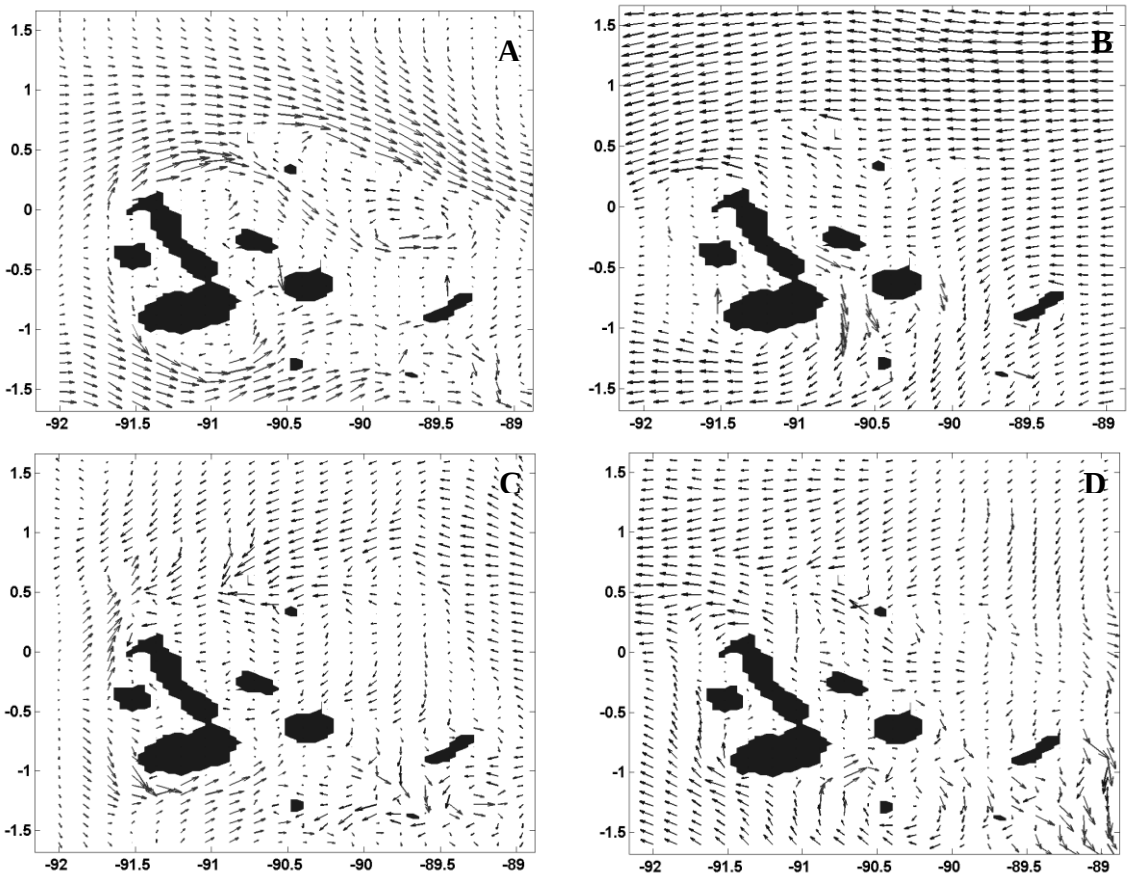

Figure 10: Hydrodynamic model mix layer flow of the SEC and EUC throughout the GMR for (A) March 2005, (B) November/December 2005, (C) June/July 2006, and (D) November 2006.

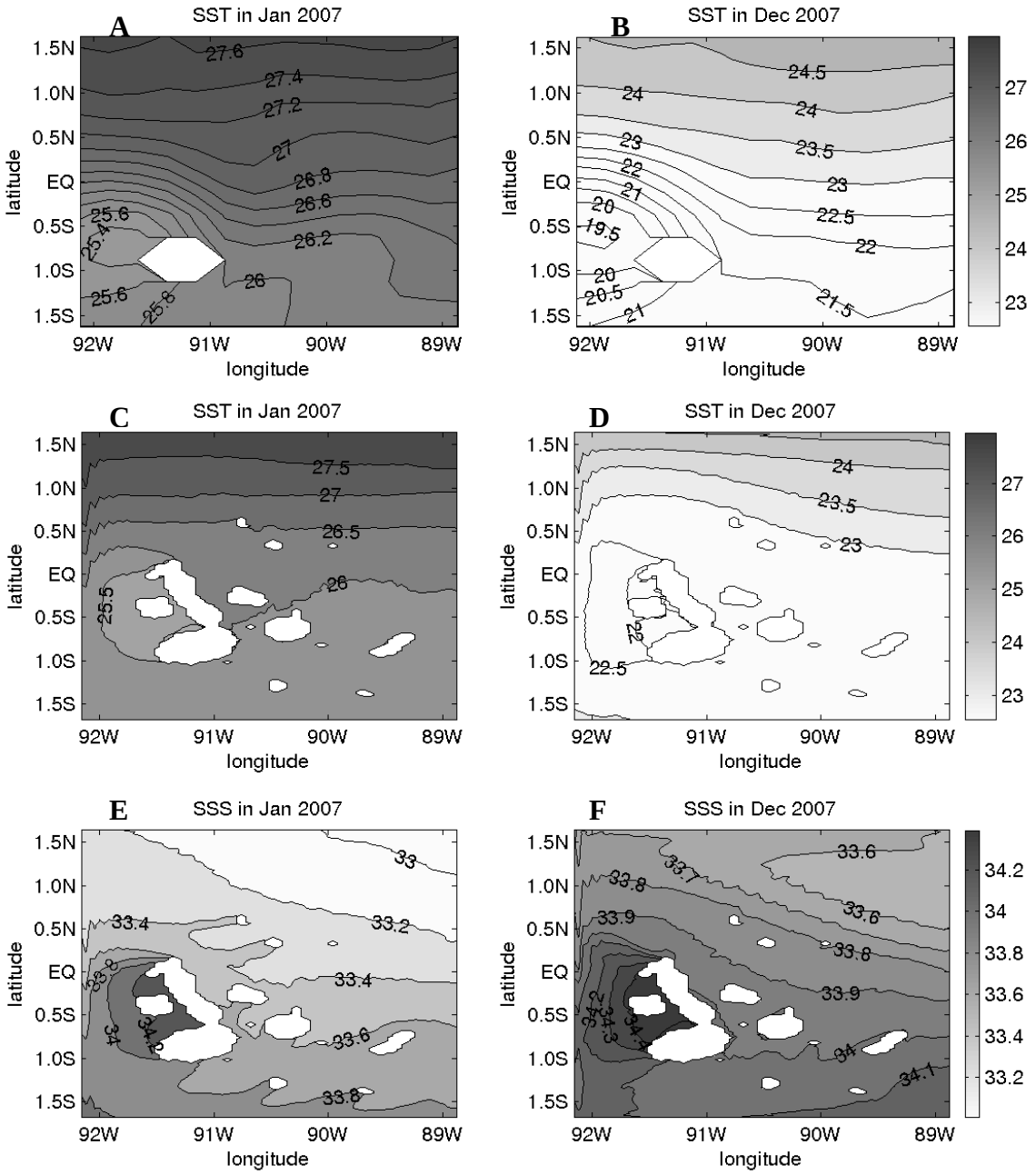

Figure 11: The observed and simulated SST in Jan 2007 (A: observed SST, C: simulated SST) and Dec 2007 (B: observed SST, D: simulated SST). Figure 11E) and F) are the simulated SSS in Jan 2007 and Dec 2007.

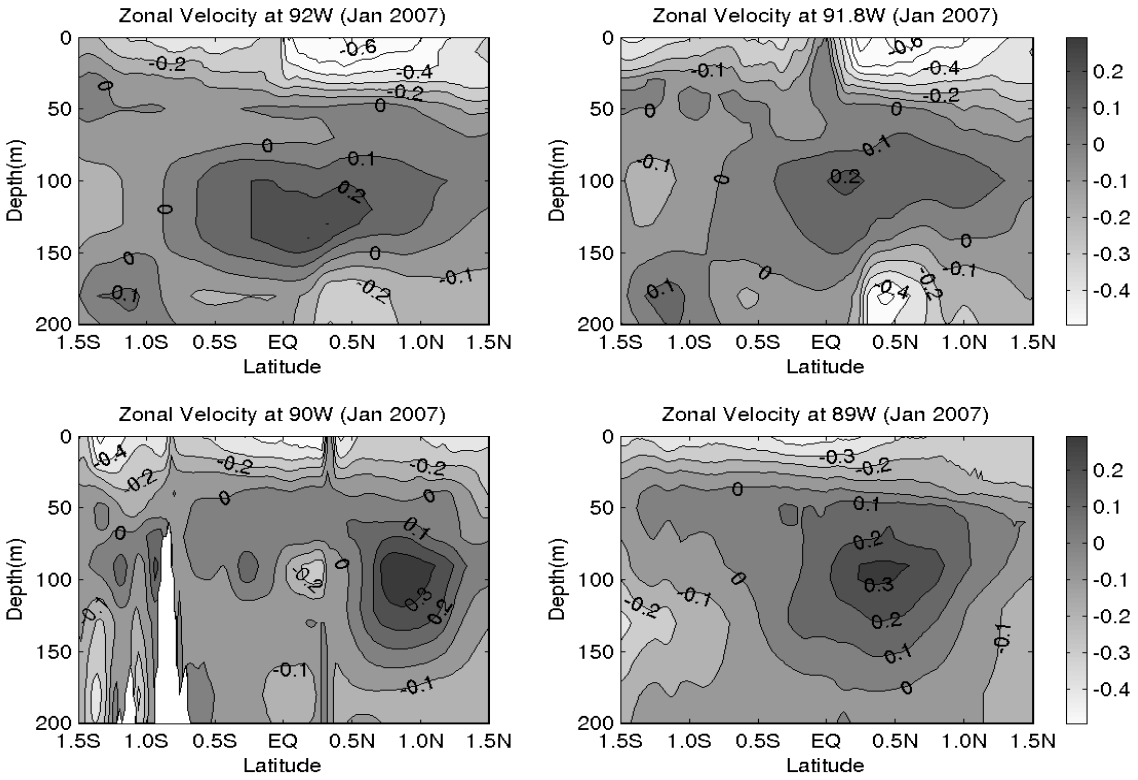

Figure 12: Vertical sections of zonal current (m/s) along 92W, 91.8W, 90W and 89W for the upper 200 m around the GMR in Jan 2007.

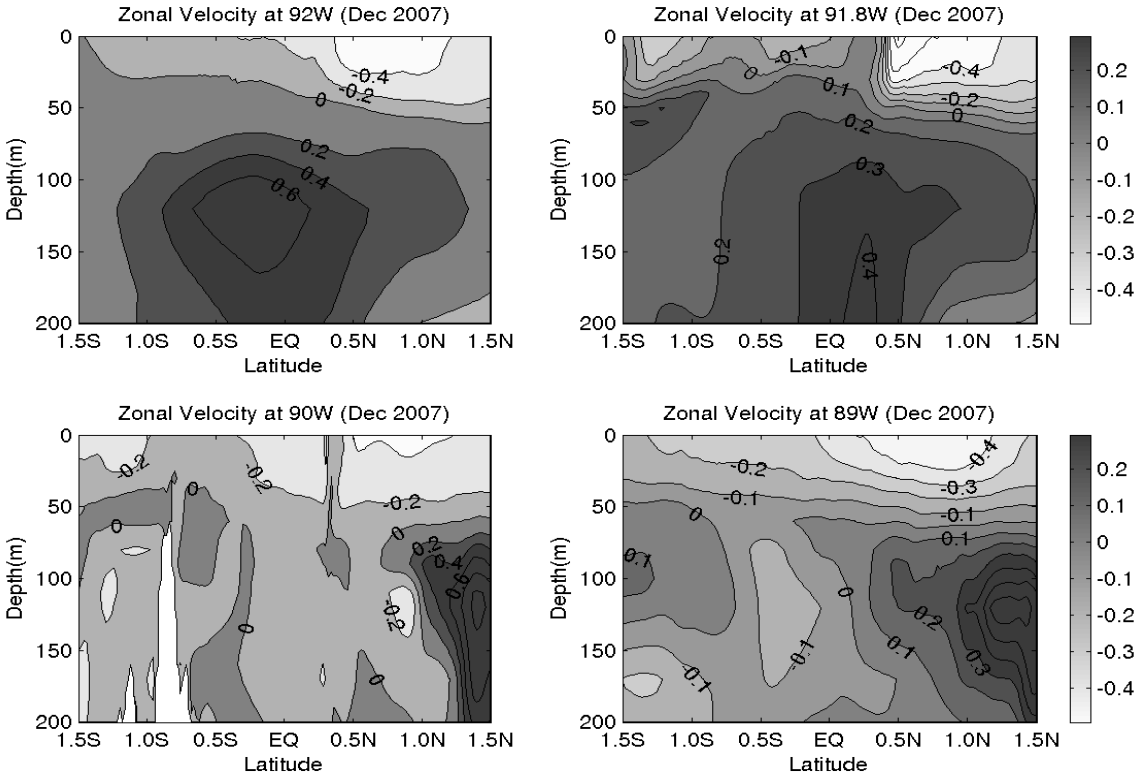

Figure 13: Vertical sections of zonal current (m/s) along 92W, 91.8W, 90W and 89W for the upper 200 m around the GMR in Dec 2007.

Chapter 5

Simulation of El Nino-Southern Oscillation (ENSO) Using a Hybrid Coordinate Ocean Model (HYCOM)

Abstract

El Nino and Southern Oscillation (ENSO) is an atmosphere-ocean coupled phenomenon that exhibits interannual variability in tropical Pacific Ocean and plays an important role in modulating the interannual variability of regional climate globally. In this study, the ENSO events are simulated using the Hybrid Coordinate Ocean Model (HYCOM) with daily atmospheric forcing derived from the NCEP/NCAR reanalysis dataset for the period of 1951-2006. The result indicates that with prescribed atmospheric forcing, the HYCOM model can accurately simulate the major characteristics of ENSO events. The correlation coefficient between the simulated Sea Surface Temperature (SST) anomalies and observed SST anomalies in the Niño3.4 region is 0.73. However, the simulated SST anomalies (SSTA) have an anomalous rising trend compared with the observed SSTA. SST can be influenced by horizontal advection, radiation flux, sensible and latent heat flux and entrainment/detrainment process. Two choices of bulk parameterization schemes of surface fluxes due to different latent and sensible heat exchange coefficients are used in HYCOM. Sensitivity analysis shows the unrealistic rising trend produced by the model was more due to weak model mixing than to trends in the surface forcing. However, extracting the interannual band of the simulated tropical

Pacific SST from the model data shows a near-perfect match between the model data and the observations at the interannual band. This suggests that even with the presence of erroneous trends in the simulated data, the model was able to accurately simulate the internnual variability in the tropical ocean. The Jan 2007 and Dec 2007 cases also show that the HYCOM model can generally simulate the ocean circulation around the GMR during the El Nino and La Nina events.

Keywords: HYCOM, ENSO, air-sea interaction, Simulation

1. Introduction

El Niño and Southern Oscillation (ENSO) is an atmosphere-ocean coupled phenomenon that exhibits interannual variability in tropical Pacific Ocean and plays an important role in modulating the interannual variability of regional climate globally. El Niño is defined by the appearance and persistence, for 6-18 month, of anomalously warm water in the coastal and equatorial ocean off Peru and Ecuador (Trenberth, 1997) and is a perturbation of the coupled ocean-atmosphere system. It is dynamically linked to the Southern Oscillation, a see-saw in surface atmospheric pressure between the Australian–East Asian region and the eastern tropical Pacific. Bjerkness (1969) first hypothesized that a positive ocean-atmosphere feedback involved the Walker circulation is responsible for the SST warming observed in the equatorial eastern and central Pacific. An initial positive sea surface temperature (SST) anomaly in the equatorial eastern Pacific reduces

the east-west SST gradient and hence the strength of the Walker circulation (Gill, 1980; Lindzen and Nigam, 1987), resulting in weaker trade winds around the equator. A decrease of the equatorial easterlies weakens the equatorial upwelling, thereby the eastern equatorial Pacific becomes warmer and supplies heat also to the atmosphere above it. The weaker trade winds in turn drive the ocean circulation changes that further reinforce SST anomaly. This positive ocean-atmosphere feedback leads to the occurrence of El Niño.

During El Niño events, the trade winds weakened and may reverse, thus removing the driving force for upwelling. At the same time, ocean dynamical processes depress the thermocline in the eastern and central equatorial Pacific, and along the coasts of North and South America. The supply of nutrients to the euphotic zone drops or may be cut off entirely. The lack of a strong Equatorial Undercurrent essentially shut off upwelling of the cooler, saltier and higher in nutrients and iron waters found over the eastern Pacific. During the El Niño events, there are two important types of wave motions in the equatorial Pacific: Rossby wave and equatorial Kelvin waves. Away from the equator the principle balance in the ocean is the geostrophic one between Coriolis and pressure gradient forces. This balance is characteristic of Rossby waves. The vanishing of coriolis parameter at the equator allows another low frequency wave-form, the equatorial wave. While the Rossby waves generated by the wind propagate westward, the Kelvin wave carried energy eastward. The eastward Kelvin wave deepened the mixed layer and thermocline, with the result that the water mixed into the surface layer is warmer than before and decreased primary productivity, the decreases in primary productivity affect

the entire food web. We know the principal source for nutrients, away from the areas of significant coastal runoff, is the thermocline. Small organisms that have died near the surface decay as they slowly sink out of the euphotic zone. These processes create a pool of nutrients and carbon in the thermocline which, when upwelled into the euphotic zone, are available for uptake by phytoplankton. And coastal upwelling is mainly responsible for the great biological production that feeds the different tropical levels of the coastal environment. The upwelled water is high in mcronutrients such as nitrate, phosphate, silicate and carbon dioxide, as well as micronutrient such as iron (Chavez and Barber, 1987). If the primary production decreases, zooplankton that feed on phytoplankton will also decrease in abundance. Fish, sea birds and marine mammals die off or migrate to more productive regions in search of food. Undernourished sea birds and marine mammals may experience reproductive failures or abandon young when food becomes scarce. In extreme cases, decimated populations may require one or more years to fully rebound. Also, by quantifying and studying the mechanisms through which the extreme temperature anomalies affect biological productivity and the survival of species in Galápagos, we should be able to identify recovery processes that minimize ecosystem disruption through biological resilience.

The Galápagos coastal waters are greatly affected by the El Niño and La Niña events (Glynn and Ault, 2000). Recently the frequency and severity of El Niño events appear to have increased and this is a concern for the conservation of endangered species. El Niño events now occur 2–7 times more frequently than they did 7000–15,000 years ago

(Riedinger et al., 2002; Rodbell et al., 1999). The 1982-83 and 1997-98 El Niño events, in particular, were the most extreme for many centuries, and had a devastating effect on marine life in the Galápagos region. During El Niño, the EUC weakens, the surface water warms, micronutrients are reduced, the primary production decreases (Chavez et al., 1999), and fish numbers diminish. Data from commercial fisheries indicated that the catch of mullets from the Galapagos during the 1997–1998 El Niño event were half that of the commercial catch in 1999, a "normal" year (Nicolaides and Murillo, 2001). Houvenaghel (1984) predicts that when the EUC is not present during intense El Niño's periods when the southeast trade winds collapse, biological activity within the Archipelago would be substantially reduced. This prediction is supported by SST and chlorophyll signatures from AVHRR and SeaWiFS satellite data during the final phase of the 1997/1998 El Niño when the Trade Winds resumed, driving upwelling in the Archipelago. Thus the relationship between El Niño events and EUC, as well as the relationship between extreme ENSO events and loss of marine biodiversity in Galápagos, will be investigated using a numerical model as a matter of local and global importance.

In this study, we will first test the ENSO simulation ability of HYCOM. The ENSO events are simulated using the HYCOM with daily atmospheric forcing derived from the NCEP/NCAR reanalysis dataset. Then we will discuss how the El Nino and La Nino events affect the ocean circulation around the Galapagos.

2. Model configuration and numerical experiments

ENSO simulations were carried out using HYCOM with a grid size of 1.44 °x 0.72 °in zonal and meridional direction, respectively. The experiment domain covers the entire global ocean and has a vertical resolution defined by 26 layers that stretch or shrink vertically as a function of total depth according to the hybrid coordinate frame. The model was driven by daily surface wind stress, surface air temperature, surface atmospheric specific humidity, net shortwave radiation, net long-wave radiation and precipitation fields obtained from NCEP/NCAR reanalysis dataset for the period of 1949-2006 (Kistler, et al, 2001). The model was initialized with temperature and salinity from the Levitus monthly climatology (Levitus et al., 1994) and ran for 58 years. The latent and sensible heat fluxes were calculated during model runs using the model sea surface temperature and the bulk formulation (Cayan 1992). The KPP vertical mixing model of Large et al (1994) was also used and the bathymetry was from ETOPO2, and is interpolated on the model grids. The model was run for 58 years from 1949 to 2006.

3. Preliminary results about ENSO simulation using HYCOM

ENSO variability from 1949 to 2006 was simulated using HYCOM with NCEP NCAR reanalysis atmospheric forcing. The area-averaged SST anomalies in the Nino3.4 region (5 °S-5 °N, 150 °W-90 °W) are often used to index ENSO variability (Trenberth, 1997). Fig 1 shows the observed (solid) and HYCOM simulated (dashed) SST anomalies in

Niño3.4 region from 1949 to 2006. The correlation coefficient between the simulated SSTA and observed SSTA is 0.721. The power spectrum of the SST anomalies (Fig 2) showed that the main ENSO period in the model is approximately from 3 to 7 years, similar to the observations. The peak amplitude of the power spectrum is comparable in the model and observations. This result indicates that the HYCOM can generally simulate major El Niño events especially the strong 1997-98 events.

However, the simulated SST anomalies (SSTA) in Niño3.4 region have an anomalous rising trend compared with the observed SSTA (see Fig 1). If we remove the trend from the SST anomalies series, the simulated SSTA is closer to the observations (see Fig 3). The correlation coefficient between the simulated SSTA and observed SSTA increases to 0.836. To extract the main signal with a period from 2-7 year, the SST anomalies in Niño3.4 region are band-pass filtered using a wavelet filter. Fig 4 shows the band-pass filtered observed (dashed) and HYCOM simulated SST anomalies (solid) in Nino3.4 region from 1950 to 2006. The correlation coefficient between the simulated SSTA and observed SSTA increases to 0.913, which shows a near-perfect match between the model data and the observations at the interannual band. This suggests that even with the presence of erroneous trends in the simulated data, the model was able to accurately simulate the internnual variability in the tropical ocean.

3.1 Diagnostic study of ENSO simulation

Diagnostic analysis of the ENSO simulations by HYCOM was carried out to try to understand the reasons for the simulated trend in the SSTA. In order to study the reason for this trend, we need to identify the factors which affect the sea surface temperature. The sea surface temperature can be influenced by horizontal advection, radiation flux, sensible and latent heat flux and entrainment/detrainment process. In HYCOM, the temperature governing equation in isopycnic coordinate is

$$\frac{\partial}{\partial t}(T\Delta p)+\underbrace{\nabla\cdot(\vec{u}T\Delta p)}_{advec}+\underbrace{\left(\dot{s}\frac{\partial p}{\partial s}T\right)_{bot}-\left(\dot{s}\frac{\partial p}{\partial s}T\right)_{top}}_{dia-diff}=\underbrace{\nabla\cdot(\upsilon\Delta p\Delta T)}_{iso-diff}+H_T$$

where Δp is the thickness of the layer with temperature T; γ is the eddy viscosity/diffusion coefficient and H_T is the radiative exchanges. The expression $\left(\dot{s}\frac{\partial p}{\partial s}\right)$ is the vertical mass flux. The first term on left hand side (LHS) is the change of temperature in the mixed layer; the second term on the LHS is the horizontal advection term; the third is diapycnic diffusion term. On the right hand side, the first term is the isopycnic diffusion and the second term H_T the radiative term. The advection term is mainly determined by wind stress. Entrainment/ Detrainment processes depend on both wind stress and buoy fluxes which are affected by sensible and latent heat fluxes and radiation.

In this study, HYCOM is driven by daily surface wind stress, surface air temperature,

surface atmospheric specific humidity, net shortwave radiation, net longwave radiation and precipitation fields. The latent and sensible heat fluxes can be calculated during model runs using the model sea surface temperature and the bulk formulation. There are two choices for bulk parameterization schemes of surface fluxes due to different latent and sensible heat exchange coefficients in HYCOM. The first is the standard constant bulk coefficients. The second is the complex parameterization algorithm of Kara *et al.* (2000) for evaporation and air-sea heat fluxes that has been included in HYCOM. The main difference of the two choices is due to the different parameterization of latent and sensible heat exchange coefficients. For the first choice, the exchange coefficients are constant but for the second, they are related to wind speed and air-sea temperature difference. In addition, the wind stress also has a great effect on the change of temperature via mechanical energy transfer.

The effect of ocean-atmosphere exchanges (bulk formula) on the mixed layer is summed as follows:

$$B = R + H + \xi$$

where R is the net radiative exchanges, H is sensible heat flux and ξ is latent heat flux.

The sensible heat flux

$$H = C_{Pair} E_x (T_s - T_a);$$

where E_x is an exchange coefficient such that $E_x = \rho_a C_T W$, ρ_a means Mass/volume of the air; C_T is heat transfer coefficient; C_{Pair} is specific heat of the air; T_s is sea surface

temperature; T_a is temperature in the atmosphere boundary layer; W is wind velocity.

The latent heat flux

$$\xi = E_x L(H_u - E_v).$$

Where L is latent heat of vaporization; H_u is specific humidity; E_v is evaporation.

A possible reason for the rising trend of SST anomaly in Nino3.4 region may come from the surface forcing. Fig 5 showed the shortwave radiation and net radiation flux anomaly in Nino3.4 region from 1950 to 2006 from NCEP/NCAR dataset. The radiation heat fluxes also showed a rising trend. Fig 6 depicted the observed and simulated latent heat flux anomaly and sensible heat flux anomaly in Nino3.4 region from 1950 to 2006. Simulated results showed that the latent heat flux can been generally simulated by HYCOM, while the sensible heat flux, which also has a rising trend, has a large difference with the observed sensible flux. The reasons for this phenomenon may be associated with the rising trend of the simulated SST anomaly. The net heat flux also has a rising trend, similar to the shortwave heat flux. Fig 7 shows the HYCOM simulated SST anomalies in Nino3.4 region from 1950 to 2006 using the classic bulk formula method and Kara, 2000). The SST simulations do not exhibit a big difference in these three schemes. So there is a hypothesis that the rising trend of SST anomaly came from the surface forcing.

Another possible reason for the unrealistic rising trend produced in the model was

due to weak model mixing relative to trends in the surface forcing. To test this hypothesis, we increased the mixing coefficient to 10 times of the original one. Figure 8 is the observed (dashed) and HYCOM simulated SST anomalies (solid) in Nino3.4 region from 1949 to 2007. The blue line is HYCOM simulated SST anomalies with the increased (10 times of the original) mixing coefficient. We could see from this figure that if we increased the mixing coefficient, the rising trend decreased. The correlation coefficient between the simulated SSTA and observed SSTA became 0.816 from the original 0.721. Also if we divided the whole time series from the year 1975, the rising trend is decreased greatly during the year from 1976 to 2006. Figure 9 is the observed (red, dashed) and HYCOM simulated SST anomalies (black, solid) in Nino3.4 region from 1950 to 1975 and from 1976 to 2006. The blue line is HYCOM simulated SST anomalies with the increased (10 times of the original) mixing coefficient; which is an artificial value and is used to increase model mixing. The weak model mixing could possibly be caused by weak wind stress in Tropics in NCEP/NCAR re-analysis (Smith et al. 2001). Their research showed that NCEP underestimated surface winds over most of tropics. The trend could be caused by weak wind stress in Tropics in NCEP/NCAR re-analysis. From these figures, we could see that Sensitivity analysis shows the unrealistic rising trend produced by the model was more due to weak model mixing than to trends in the surface forcing.

4. How the ENSO events affected the Galapagos Archipelago

Since the model is able to accurately simulate the internnual variability in the tropical ocean. We will use two case studies to study how El Niño/La Niña events affect the Galapagos Archipelago. Potential studies include simulating the 2006 El Niño event and investigate key physical processes that affect the water mass transport pathways and the local upwelling dynamics for comparison to observed conditions (Schaeffer et al., 2008, Sweet et al, 2007). Sensitivity studies using the nested modeling system have been carried out to identify key physical processes that affect the water mass transport pathways and the local upwelling dynamics. Other possible cases include simulations (hinecasts) of strong El Niño (eg., 1982/3 and 1997/8) and La Niña conditions, as well as periods of "normal" conditions. By quantifying and studying the mechanisms through which the extreme temperature anomalies affect biological productivity and the survival of species in Galápagos, we should be able to identify recovery processes that minimize ecosystem disruption through biological resilience. The vertical velocity (W) is determined by vertically integrating the continuity equation downward from the surface. To estimate W profiles at HYCOM grid points, the horizontal velocity components were re-gridded to constant high-resolution depth levels before integration. Data from the simulation includes daily values of U, V, and SST that are produced every third day. Modeled time series data is averaged over ~0.5 °box centered about a specific location and the daily latitudinal profiles are a smoothed by a loess algorithm with a one-degree polynomial and a 0.1 sampling proportion.

Here we chose the 2006-2007 El Nino events and 2007-2008 La Nina events. We selected Jan 2007 as El Nino event period and selected Dec 2007/Jan 2008 as La Nina period (see the SST anomalies from Figure 10). Figure 11 is the observed and simulated SST in Jan 2007 (A: observed SST, C: simulated SST) and Dec 2007 (B: observed SST, D: simulated SST). Figure 11E) and F) are the simulated SSS in Jan 2007 and Dec 2007. The HYCOM can generally simulated the temperature and salinity during the 2007 El Nino and Dec 2007/Jan 2008 La Nina Events. Figure 12 and 13 show the vertical sections of zonal current along 92W, 91.8W, 90W and 89W for the upper 200 m around the GMR in Jan 2007 and Dec 2007. During the El Nino event (Jan 2007), there are warm and less salty waters throughout the whole GMR region, while the less warm and saltier water is found west of Isabella and Fernandina, indicative of topographically reduced upwelling of the EUC. During the La Nina event (Dec 2007), there are cold and salty waters throughout the whole GMR region, while colder and saltier water are found west of Isabella and Fernandina, indicative of topographically increased upwelling of the EUC. Figure 14 and 15 show the vertical sections of zonal current along 1S, 0.5S, EQ and 0.5N for the upper 200m around the GMR in Jan 2007 and Dec 2007. These figures indicate during the 2007 El Nino event, the EUC is greatly weakened, while during the La Nina events, the EUC is greatly strengthened especially in west Galapagos. Figure 16 show the hydrodynamic model flow of the SEC and EUC throughout the GMR for layer 1 (surface), layer 5 (~ 40m), layer 8 (~100m) and layer 10 (~ 200m) in Jan 2007 and Dec 2007. These current figures described the surface current is primarily dominated by

westward SEC, while in the deep layers (~100m), the eastward EUC is strong, especially during the 2007 La Nina event, the EUC is strengthened at deeper layers (~200m).

5. Summary

El Nino and Southern Oscillation is an atmosphere-ocean coupled phenomenon that exhibits interannual variability in tropical Pacific Ocean and plays an important role in modulating the interannual variability of regional climate globally. In this study, the ENSO events are simulated using the Hybrid Coordinate Ocean Model (HYCOM) with daily atmospheric forcing derived from the NCEP/NCAR reanalysis dataset for the period of 1949-2006. The result indicates that with prescribed atmospheric forcing, the HYCOM model can accurately simulate the major characteristics of ENSO events. The correlation coefficient between the simulated Sea Surface Temperature (SST) anomalies and observed SST anomalies in the Niño3.4 region is 0.73. However, the simulated SST anomalies (SSTA) have an anomalous rising trend compared with the observed SSTA. SST can be influenced by horizontal advection, radiation flux, sensible and latent heat flux and entrainment/detrainment process. Two choices of bulk parameterization schemes of surface fluxes due to different latent and sensible heat exchange coefficients are used in HYCOM. Sensitivity analysis shows the unrealistic rising trend produced by the model was more due to weak model mixing than to trends in the surface forcing. However, extracting the interannual band of the simulated tropical Pacific SST from the model data shows a near-perfect match between the model data and the observations at the

interannual band. This suggests that even with the presence of erroneous trends in the simulated data, the model was able to accurately simulate the internnual variability in the tropical Pacific Ocean. The Jan 2007 and Dec 2007 cases also show that the HYCOM model can generally simulate the ocean circulation around the GMR during the El Nino and La Nina events.

Acknowledgements

This study was funded by National Aeronautics Space Association (NASA) Biodiversity and Ecological Forecasting grant NNG04GL98G. The Counterpart US-AID No. 518-A-00-03-00152-00 and UK Darwin Initiative Project No. 14-048 also provided funding for this project. All modeling work is carried out in the Coastal Fluid Dynamical Lab of North Carolina State University using the High-Performance Computing (HPC) system.

References

Bjerkness, J. 1969: Atmospheric teleconnections from the equatorial Pacific. Monthly Weather Review, 97, 163-172.

Bleck, R., 2002. An oceanic general circulation model framed in hybrid isopycnic-Cartesian coordinates. Ocean Modeling, 4, 55-88.

Cayan, D. R., 1992: Latent and sensible heat flux anomalies over the northern oceans: Driving the sea surface temperature. *J. Phys. Oceanogr*., 22, 859-881.

Chavez, F.P., Strutton, P.G., Friederich, G.E., Feely, R.A., Feldman, G.C., Foley, D.G., McPhaden, M.J., 1999. Biological and chemical response of the equatorial pacific ocean to the 1997–1998 El Niño. Science 286, 2126–2131.

Glynn, P.W. and J.S. Ault. 2000. A biogeographic analysis and review of the far eastern Pacific coral reef region. *Coral Reefs* **19**: 1-23.

Levitus, S., Boyer, T., 1994. World Ocean Atlas 1994, Volume 4: Temperature. NOAA Atlas NESDIS 4. US Dept. of Commerce, Washington, DC.

Lindzen, R.S., and S. Nigam, 1987: On the role of sea surface temperature gradients in forcing low level winds and conver-gence in the tropics. *J. Atmos. Sci., 44*, 2440-2458.

Kara A.B., P.A. Rochford and H.E. Hurlburt, An optimal definition for ocean mixed layer depth, *J. Geophys. Res.* **105** (2000), pp. 16,803–16,821.

Kistler, R., E. Kalnay, W. Collins, S. Saha, G. White, J. Woollen, M. Chelliah, W. Ebisuzaki, M. Kanamitsu, V. Kousky, H. van den Dool, R. Jenne, and M. Fiorino, 2001:

The NCEP-NCAR 50-Year Reanalysis: Monthly Means CD-ROM and Documentation. Bull. Amer. Meteor. Soc., 82, 247-268.

Riedinger, M.A., Steinitz-Kannan, M., Last, W.M., Brenner, M.,2002. A similar 6100 C-14C yr record of El Nino activity from the Galapagos Islands. Journal of aleolimnology 27, 1–7.

Rodbell, D.T., Seltzer, G.O., Anderson, D.M., Abbott, M.B., Enfield, D.B., Newman, J.H., 1999. An asymptotically equal to 15,000- Year Record of El Nino-Driven Alluviation in Southwestern Ecuador. Science 283, 516–519.

Schaeffer, B.A., Morrison, J., Kamykowski, D., Feldman, G., Xie, L., Liu, Y., Sweet, W.V., McCulloch, A., & Banks, S., 2008: Phytoplankton biomass distribution and seasonal change within the Galápagos Marine Reserve. Remote Sensing of Environment. 112(6), pp. 3044-3054

Smith, S. R., D. M. Legler and K.V. Verzone, Quantifying uncertainties in NCEP reanalyses using high quality research vessel observations. *J. Climate*, *14*, 4062-4072. 2001.

Steger, J. M., Collins, C. A., Chu, P. C., 1998. Circulation in the Archipielago de Colon (Galápagos Islands), November 1993. Deep-Sea Research II 45, 1093–1114.

Sweet, W.V., J.M. Morrison, D. Kamykowski, B.A. Schaeffer, S. Banks, A. McCulloch, 2007: Water mass seasonal variability in the Galápagos Archipelago. Deep-Sea Research I 54, 2023-2035.

Trenberth, K.E., 1997. The Definition of El Niño. Bulletin American Meteorological Society 78, 2771–2778.

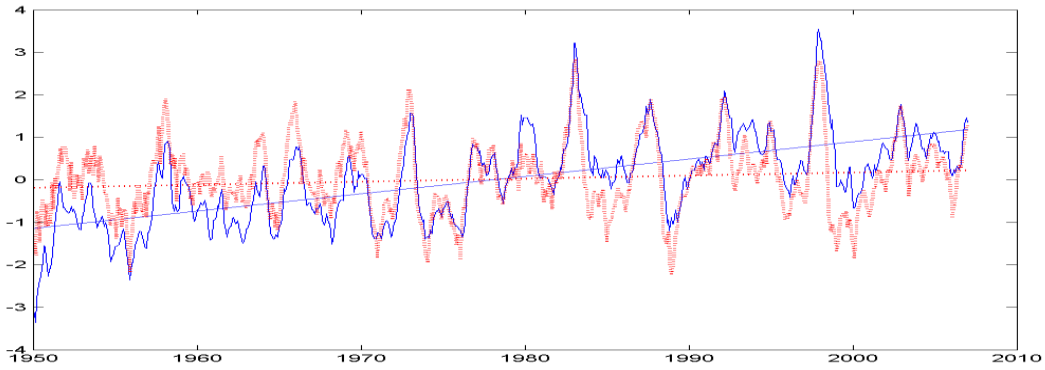

Figure 1: The observed (red, dashed) and HYCOM simulated SST anomalies (blue, solid) in Nino3.4 region from 1950 to 2006.

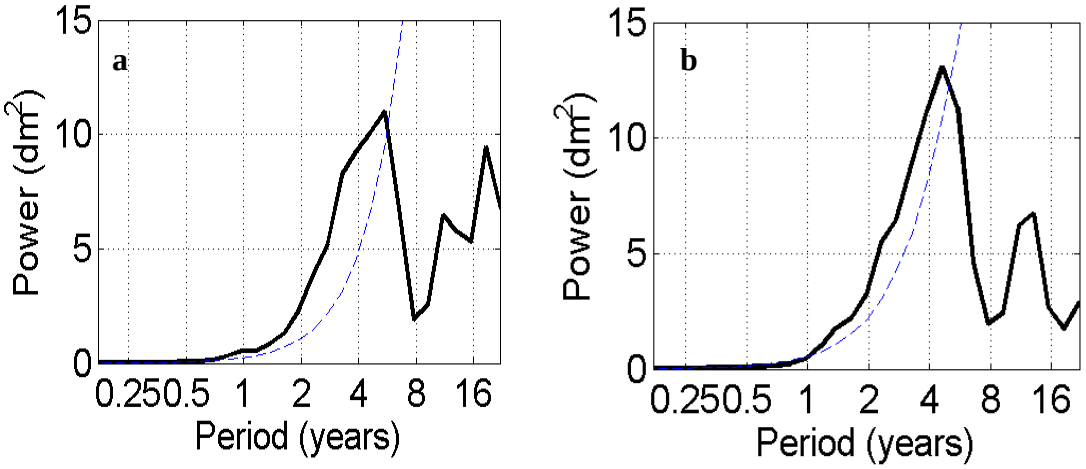

Figure 2: The power spectrum of the SST anomalies in the Niño3 region during 1950-2006: a) Model simulation; b) Observation.

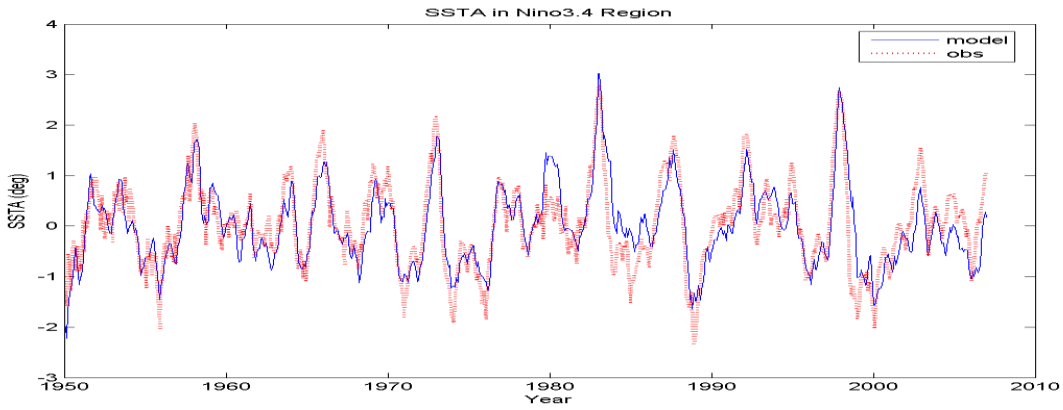

Figure 3: The observed (red, dashed) and HYCOM simulated SST anomalies (blue, solid) in Nino3.4 region from 1950 to 2006 after subtracting the trend.

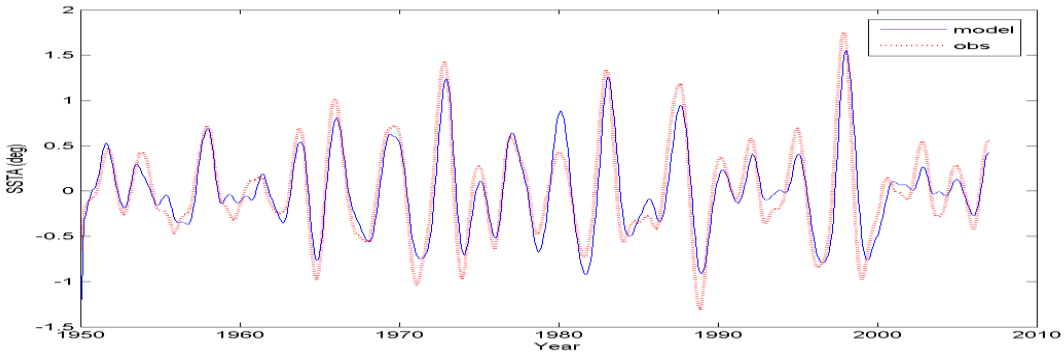

Figure 4: The bandpass filtered observed (red, dashed) and HYCOM simulated SST anomalies (blue, solid) in Nino3.4 region from 1950 to 2006.

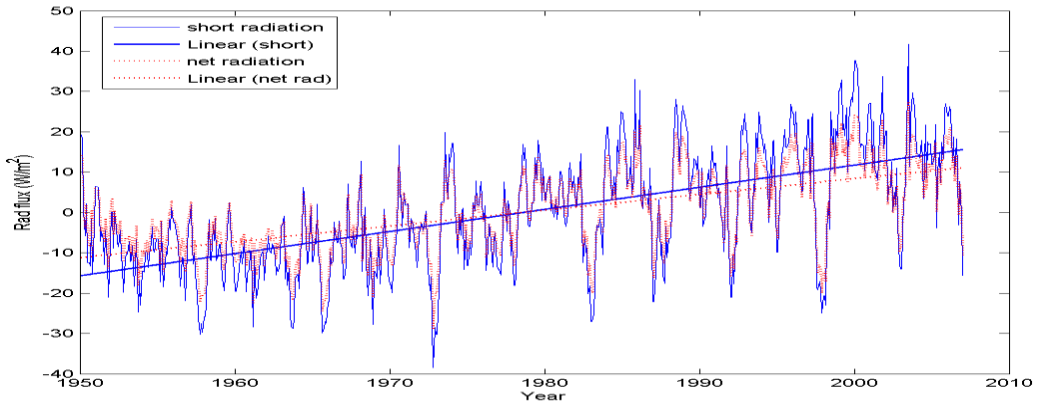

Figure 5: The shortwave radiation anomaly (blue, solid) and net radiation flux anomaly (red, dashed) in Nino3.4 region from 1950 to 2006 from NCEP dataset.

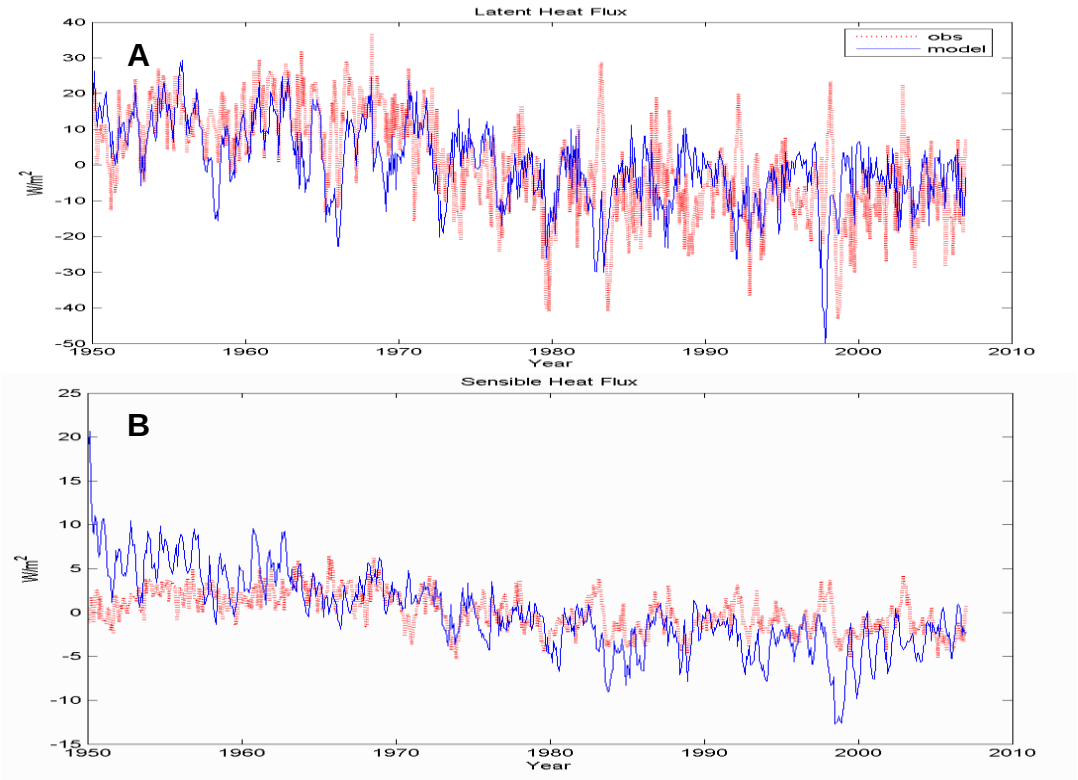

Figure 6: The observed (red, dashed) and simulated (blue, solid) a) Latent heat flux anomaly and b) Sensible heat flux anomaly in Nino3.4 region from 1950 to 2006.

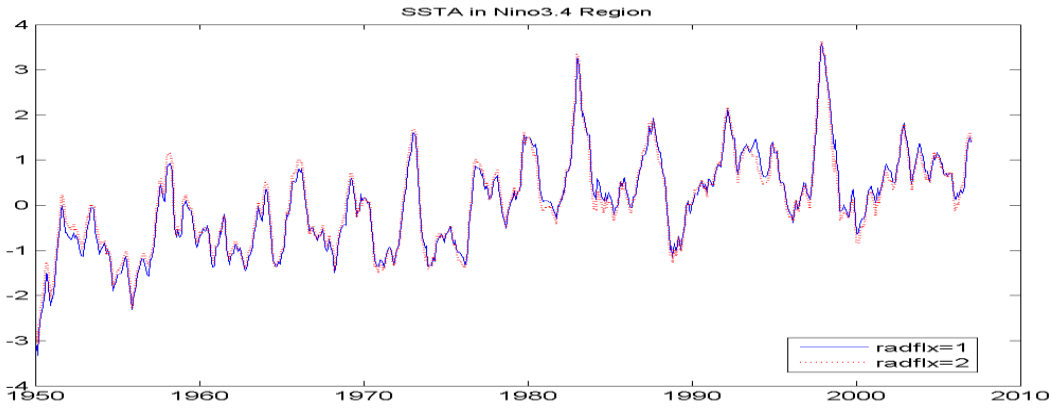

Figure 7: The HYCOM simulated SST anomalies in Nino3.4 region from 1950 to 2006 a) using the classic bulk formula method, b) using Kara (2000) calculating method.

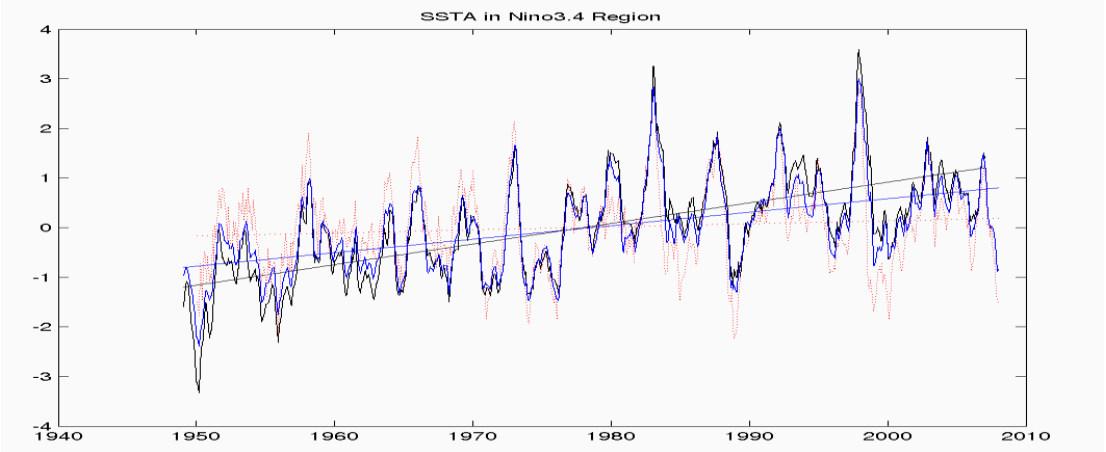

Figure 8: The observed (red, dashed) and HYCOM simulated SST anomalies (black, solid) in Nino3.4 region from 1949 to 2007. The blue line is HYCOM simulated SST anomalies with the increased (10 times of the original) mixing coefficient.

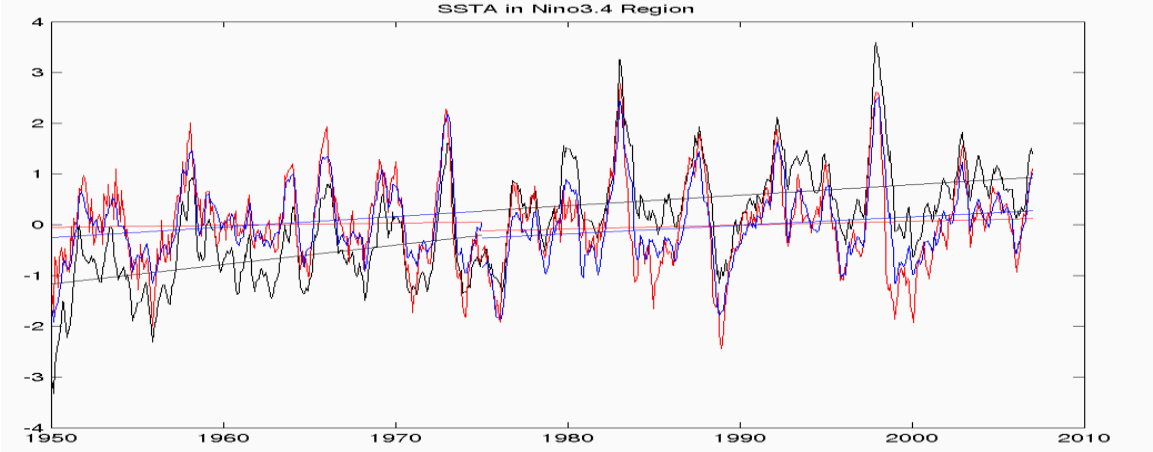

Figure 9: The observed (red, dashed) and HYCOM simulated SST anomalies (black, solid) in Nino3.4 region from 1950 to 1975 and from 1976 to 2006. The blue line is HYCOM simulated SST anomalies with the increased (10 times of the original) mixing coefficient.

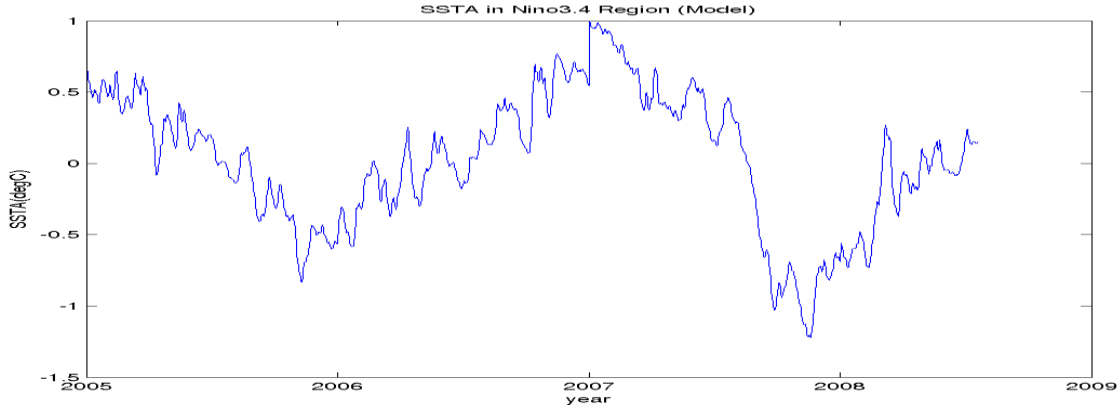

Figure 10: The HYCOM simulated SST anomalies in Nino3.4 region from 2005 to 2008.

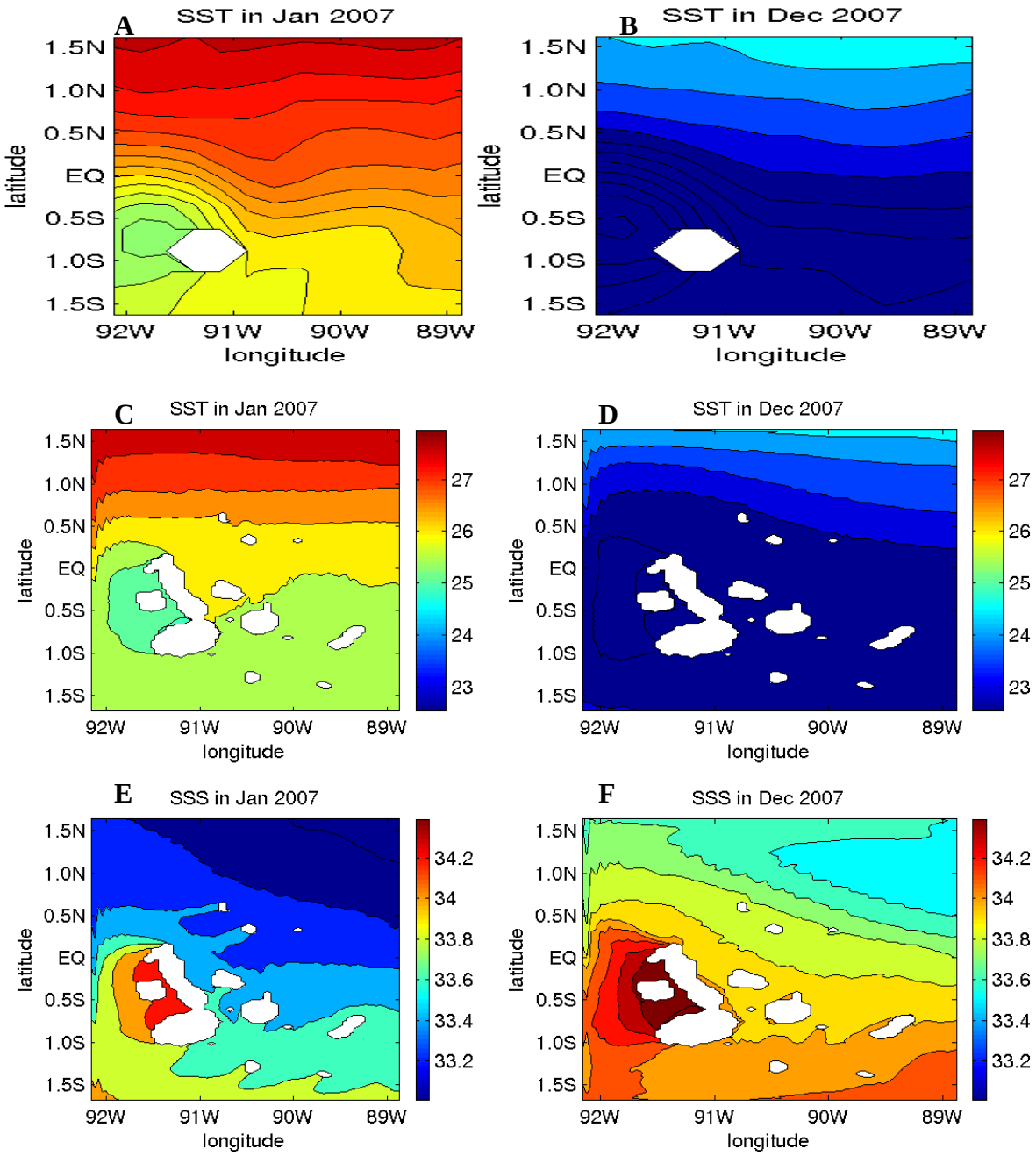

Figure 11: The observed and simulated SST in Jan 2007 (A: observed SST, C: simulated SST) and Dec 2007 (B: observed SST, D: simulated SST). Figure 11E) and F) are the simulated SSS in Jan 2007 and Dec 2007.

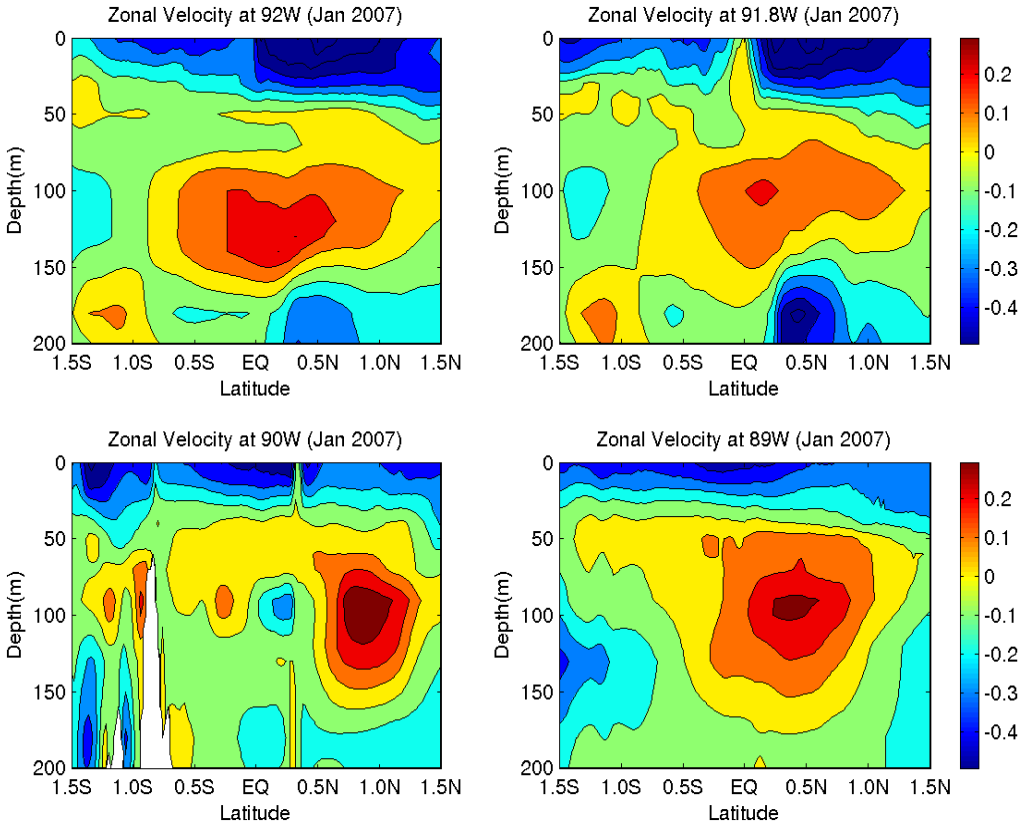

Figure 12: Vertical sections of zonal current (m/s) along 92W, 91.8W, 90W and 89W for the upper 200 m around the GMR in Jan 2007.

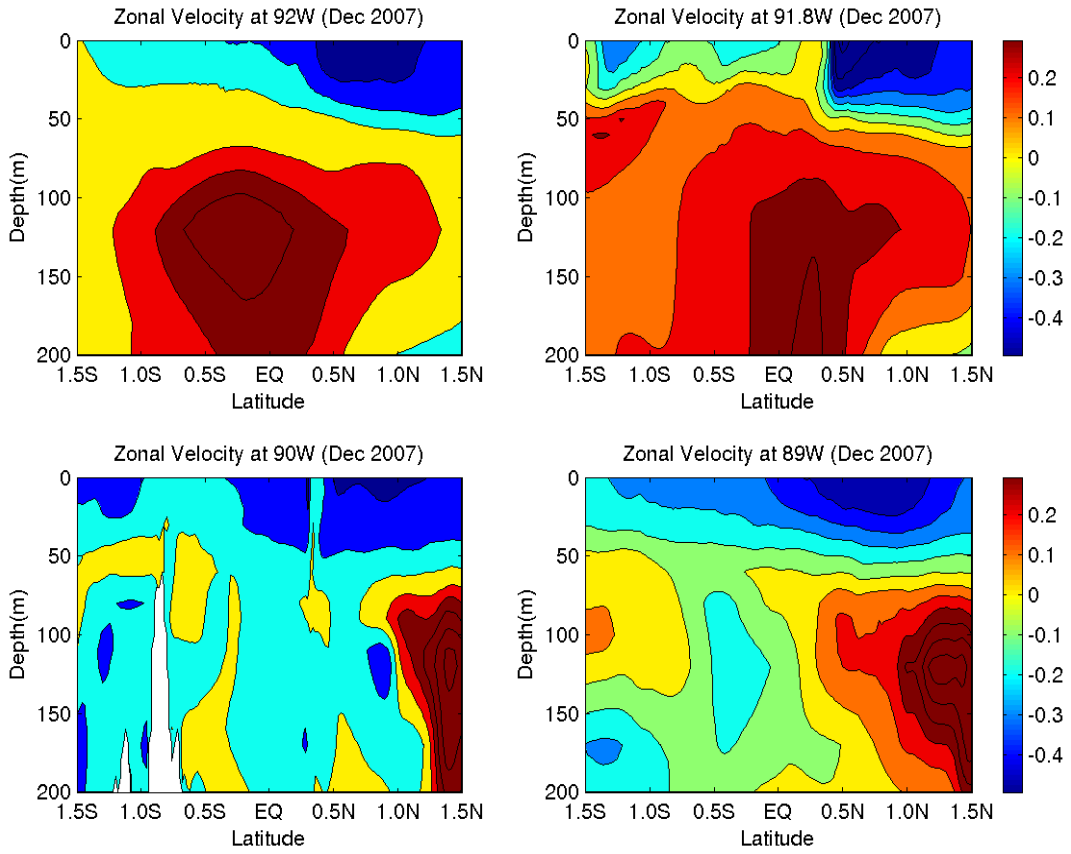

Figure 13: Vertical sections of zonal current (m/s) along 92W, 91.8W, 90W and 89W for the upper 200 m around the GMR in Dec 2007.

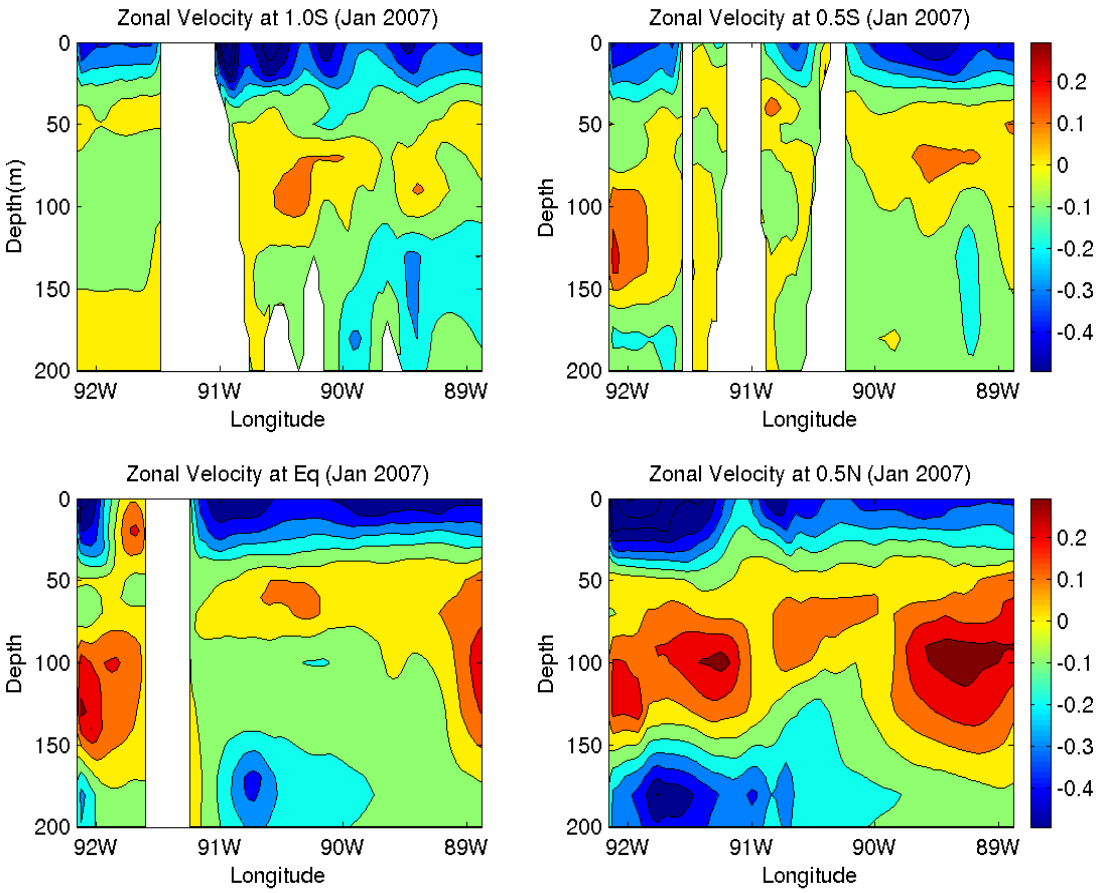

Figure 14: Vertical sections of zonal current (m/s) along 1S, 0.5S, EQ and 0.5N for the upper 200 m around the GMR in Jan 2007.

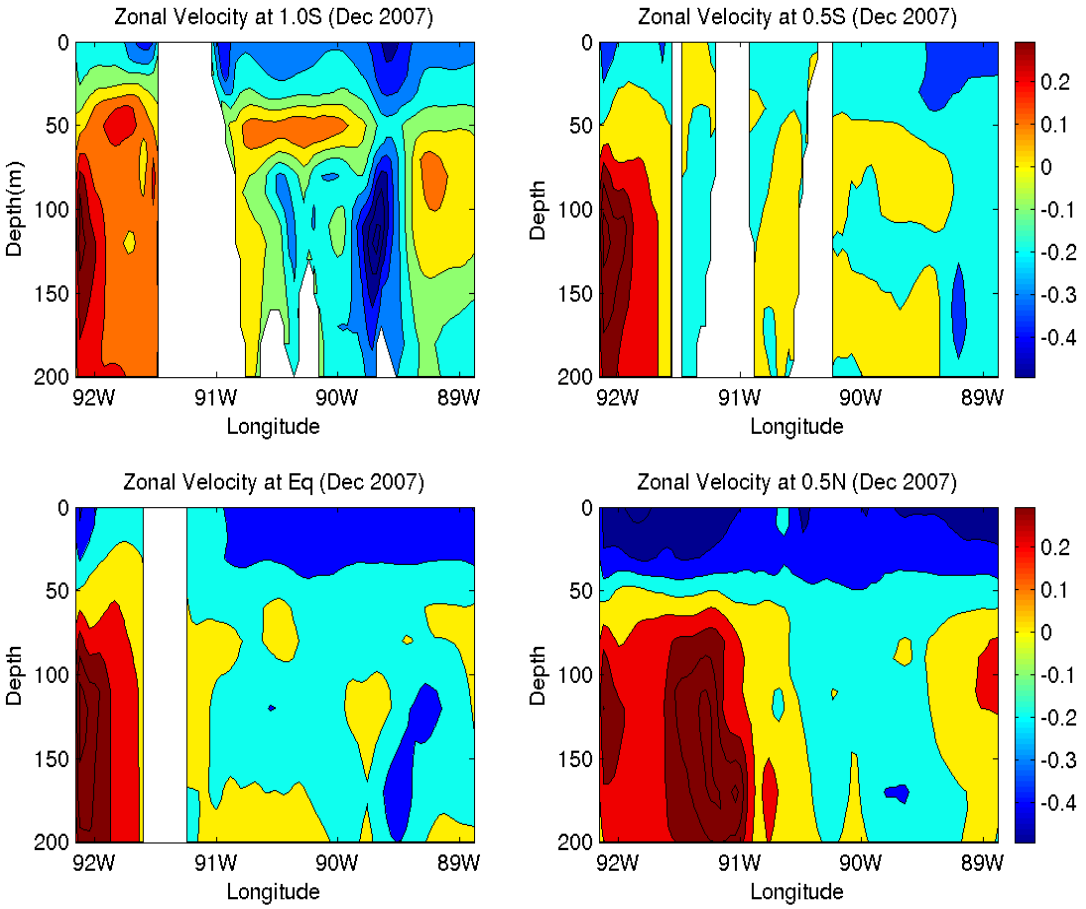

Figure 15: Vertical sections of zonal current (m/s) along 1S, 0.5S, EQ and 0.5N for the upper 200 m around the GMR in Dec 2007.

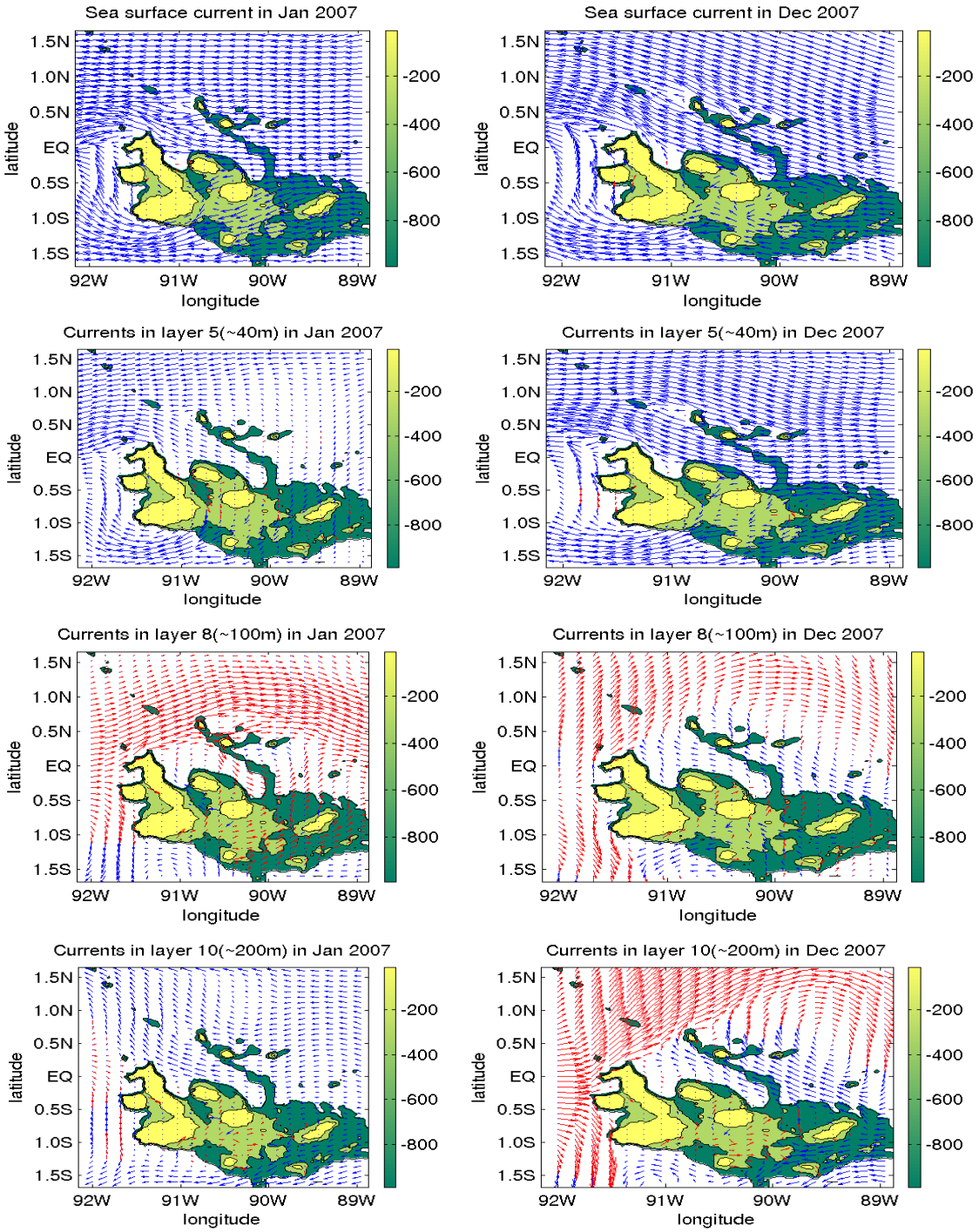

Figure 16: Hydrodynamic model flow of the SEC and EUC throughout the GMR for layer 1 (surface), layer 5 (~ 40m), layer 8 (~100m) and layer 10 (~ 200m) in Jan 2007 and Dec 2007.

Chapter 6

Dynamic Downscaling of the Impact of Climate Change on the Ocean Circulation in the Galápagos Archipelago

Abstract

The regional impact of global climate change on the ocean circulation and water mass characteristics around the Galápagos Archipelago is studied using the Hybrid Coordinate Ocean Model (HYCOM). A four-level nested-domain system with resolutions from 0.06° x 0.03° in the Galapagos region, 0.18° x 0.09° in the Eastern Tropical Pacific, 0.72° x 0.36° for the Pacific Ocean, to 2.88° x 1.44° covering the global ocean is used in the study to downscale the global climate change impact to the regional scale centered around the Galapagos Archipelago. First, the ocean circulation driven by the past and current climate is simulated using HYCOM with daily atmospheric forcing derived from the NCEP/NCAR reanalysis dataset for the period of 1951-2007 (Expt1). The result indicates that with prescribed atmospheric forcing, the major characteristics of the ocean circulation and its variability in the Galapagos region, including the ENSO events, annual and seasonal cycles, upwelling system, local and regional current systems, and tropical instability waves, can be reproduced by the nested HYCOM. For example, there is a high correlation (r=0.73) between the simulated Sea Surface Temperature (SST) anomalies and the observed SST anomalies in the Niño3.4 region. The response of the ocean circulation in the Galapagos region to future climate change scenarios is studied using the IPCC AR4

SRES A1b scenario as an example. The monthly IPCC (AR4) SRES A1b Emissions Scenario from 2001-2050 is used as the atmospheric forcing to drive the nested HYCOM in the future climate change scenario simulation (Expt2). The results show that the oceanic variability in the Galapagos region is sensitive to global climate change. However, the regional impact of global climate change in the Galapagos region varies from region to region. The SST trend is also dependent on the time scales. The upwelling region has the lowest warming trend, and occasionally experiences a decreasing trend at decadal time scales. This indicates that the upwelling zone may be less affected by global warming compared with other regions. Power spectrum analysis shows that the frequency for the occurrence of ENSO events seems unchanged (4-5yr) by climate change, while the amplitude of ENSO events is increased. The surface temperature, salinity and current as well as the undercurrent around Galápagos Archipelago are simulated under increasingly finer resolution. These variables are specifically compared and analyzed around the Galapagos Marine Reserve with a resolution of 0.06° x 0.03° for El Niño and La Niña cases, respectively. The results show that for the El Niño cases, the EUC will be greatly weakened, leading to weaker upwelling to the west of Isabella Island. While during the La Niña event, the EUC will be greatly strengthened and the EUC may come up to the sea surface. The EUC core is located around 0.5˚N. The volume transport variations in the entire equatorial band of the Pacific and in its eastern part are quantified using both in situ data and an ocean general circulation model, in which the current data from the TAO/TRITON moorings and simulated current at the equator are compared. The north branch of the EUC accounts for most (58%) of the volume transport. The effect

of different currents (EUC, Panama and Peru) on different areas of the Galapagos Archipelago is studied. The results show that the western Galapagos upwelling region is affected mainly by the EUC and Panama currents; while central/east Galapagos is predominantly affected by both Peru and EUC currents. The north region is primarily affected by the Panama Current whereas the southeast region by Peru Current. These regional differences explain the variability of the responses in different regions of the Galapagos Archipelago to global climate change.

1. Introduction

The Galápagos Islands (Figure1) are an oceanic archipelago located near the equator in the eastern tropical Pacific. It reasonably claims to possess the most distinctive marine flora and fauna and unique species for any area of its size worldwide [Bustamante et *al.*, 1999]. The principle reason why the GMR features such great diversity lies in its positioning in a complex transition zone between tropical, subtropical and upwelling zones. The Galápagos archipelago ecosystem is mainly affected by three different surface and subsurface currents. The major currents affecting the Galapagos are the westward South Equatorial Current (SEC) and the eastward Equatorial Undercurrent [EUC, Boersma, 1977, 1978]. The EUC is thought to be the major oceanographic feature affecting the production in the Galápagos Marine Reserve (GMR) and is important defining physical process to influence the very high local production at certain sites. Much of the energy input to the Galápagos archipelago is supported by nutrient influx to

the euphotic zone from cold bathymetrically deflected upwelled water from the eastward flowing submarine EUC. The upwelling events impacting upon the west of the archipelago vary in strength, size and stability under the influence of localized current systems and forcing effects. The EUC flow pathways and upwelling are linked directly to the submarine topography, which introduces obstacles to the eastward path of the undercurrent. This deflects water to the north in the northern hemisphere and to the south in the southern hemisphere. The EUC waters are cooler, saltier and higher in nutrients and iron than waters found over the eastern portion of the Archipelago and directly result in the large phytoplankton bloom observed in SeaWiFs and AVHRR. The result indicates that when there is not a EUC present (for example, during intense El Niño events), the intense biological activity normally sustaining the GMR will be absent.

Besides, the equatorial EUC plays an important role in El Nino and decadal variability. One distinctive feature associated with Galápagos coastal waters is that the greatest sea temperature anomalies occur during El Niño and La Niña events [Glynn and Ault, 2000]. Recently the frequency and severity of El Niño events appear to have increased and this is a concern for the conservation of endangered species. El Niño events now occur 2–7 times more frequently than they did 7000–15,000 years ago [Riedinger et al., 2002; Rodbell et al., 1999]. The 1982-83 and 1997-98 El Niño events, in particular, were the most extreme for many centuries, and had a devastating effect on marine life in the Galápagos region. During El Niño, the EUC weakens, the surface water warms, micronutrients are reduced, the primary production decreases [Chavez et al., 1999], and

fish numbers diminish. Data from commercial fisheries indicated that the catch of mullets from the Galapagos during the 1997–1998 El Niño event were half that of the commercial catch in 1999, a "normal" year [Nicolaides and Murillo, 2001]. For example, it is well known that during El Niño, the lack of a strong Equatorial Undercurrent (EUC) essentially shuts off the upwelling of the cooler, saltier with higher nutrients and iron waters found over the western portion of the Archipelago.

Houvenaghel [1984] discussed the oceanographic setting of the Galápagos and concluded that the EUC was the major oceanographic phenomena affecting the Galápagos. Hayes [1985] pointed out that the sea level differences across the Archipelago increase as the EUC strengthens, measured by shallow moored pressure gauges. Steger et al. [1998] found that the near-surface waters to the west of the Archipelago during November 1993 were predominately upwelled EUC waters, and as a consequence were cooler, saltier and higher in nutrients and iron than waters found over the eastern portion of the Archipelago. Steger et al. [1998] show that the waters of the EUC bifurcate when they run into the Galápagos platform, with water continuing to flow to the east both to the north and south of the platform. East of the Archipelago, Steger et al. [1998] found evidence that these north and south eastward flows most likely converge and reform a definable EUC. Steger et al. [1998] also found that the core of the EUC was south of the equator during a hot season, as did Christensen [1992], but with a strong branch also found north of the Galápagos. This variation in EUC displacement is not well understood to determine whether it is due to seasonal variability or unstable flow conditions [Lukas

1986]. In summary, studies to this point indicate that the EUC is the major oceanographic feature affecting production in the Galápagos Marine Reserve, but more studies are need to understand the physical mechanisms for its temporal and spatial variability. In fact, there are several unanswered questions. For example, how the variation of the EUC around the Galapagos will be affected by climate change? How does the EUC flux transport propagate across the Galápagos platform? What is the impact of climate change on the ocean circulation of the Galápagos Archipelago?

There are two point views about whether there is a warming trend around the Galapagos. Conroy et al. [2009] found that there is a warming trend and the eastern tropical Pacific ocean SST warmed up by about 0.8 degrees in the past 40 years, while other research show there is no warming trend (A flat trend line, Reilly 2008). Is there a warming trend around the GMR? If so, is this trend uniform for the whole GMR region? How about the occurrence of ENSO events affected by future climate change? This paper will focus on studying water mass characteristics and currents around the GMR using a 3-dimensional ocean general circulation model (HYCOM) in an effort to better understand the physical environment influencing the Galápagos Archipelago under future climate change scenarios as described by Intergovernmental Panel on Climate Change (IPCC). The objective is to model the potential impact of future climate change scenarios on the oceanographic variability in the Equatorial Pacific Ocean from mesoscale to basin scale around the GMR using HYCOM. The outcome is a down-scaling assessment of the impact of global climate change scenarios on the ocean circulation and water mass

structure in GMR region using a high-resolution nested grid HYCOM forced under selected climate change scenarios described by IPCC. The rest of the paper is organized as follows: in section 2, we describe the HYCOM model configuration and the experiments conducted. In section 3, the simulated tropical ocean circulation around the GMR using NCEP and IPCC scenario forcing are demonstrated and compared. The different physical variables are specifically compared and analyzed around the GMR during the different El Nino and La Nina cases in this section. How the different regions are influenced by different current will be discussed in section 4. Results are summarized in section 5.

2. Model and Data Description

HYCOM is a primitive equation ocean general circulation model using density, pressure, and sigma coordinates in the vertical coordinate. It has evolved from the Miami Isopycnic Coordinate Ocean Model (MICOM) and is isopycnical in the open stratified ocean, but reverts to a terrain-following coordinate in shallow coastal regions, and to z-level coordinates near the surface in the mixed layer. This generalized vertical coordinate approach is dynamic in space and time via the layered continuity equation, and permits the existence of zero thickness layers.

HYCOM ability to accurately transition between deep and shallow water yield more reliable ocean circulation, which is important in our case as the Galápagos platform with

an average depth of approximately 250m rises from the depths of the ocean > 4000 m. Other details of the HYCOM equations and numerical algorithms, along with a description and validation of the hybrid coordinate generator, can be found in Bleck (2002). Also, the HYCOM simulations generate a stronger EUC that compares more favorably to observations than other models, such as the GFDL model (Chassignet et al. 1996). As discussed above, since understanding the dynamics of the EUC is crucial to our study, HYCOM was a good choice to simulate the ocean circulation around the GMR.

A four-level nested-domain system is used in the study. There are 26 layers in the vertical. The simulations with these four different simulations have been performed under identical daily meteorological forcing fields and the results compared between model grids with coarse and fine resolutions. It was found that the simulations under fine resolutions are more accurate and have a more realistic spectrum of oceanographic variability. For example, the simulation with the resolution of $0.04°$ can depict the intra-seasonal signal from the tropical instability waves (TIW), as well as the annual and the inter-annual signals, whereas the low-resolution global model failed to depict TIW signal (Sweet, 2009). The ocean is also sensitive to the frequency of the atmospheric forcing. In a controlled experiment where the atmospheric forcing frequency was reduced from daily frequency to monthly, the results simulated by the ocean model are shown to be less accurate than those simulated using daily forcing (Liu, 2010)

The nested-grid HYCOM was driven by daily surface wind stress, surface air

temperature, surface atmospheric specific humidity, net shortwave radiation, net long-wave radiation and precipitation fields. For the Expt1, the atmospheric forcing was obtained from NCEP/NCAR reanalysis dataset for the period of 1949-2006 [Kistler, et al, 2001], while for the Expt2, the atmospheric forcing is derived from IPCC AR4 SERS scenario from 2001-2050. The SRES refers to the scenarios described in IPCC Special Report on Emissions Scenarios (SRES, 2000). The SRES scenarios are grouped into four scenario families (A1, A2, B1 and B2) that explore alternative development pathways, covering a wide range of demographic, economic and technological driving forces and resulting Green House Gas (GHG) emissions. The emissions projections are widely used in the assessments of future climate change, and their underlying assumptions with respect to socio-economic, demographic and technological change serve as inputs to many recent climate change vulnerability and impact assessments. The A1 storyline assumes a world of very rapid economic growth, a global population that peaks in mid-century and rapid introduction of new and more efficient technologies. B1 describes a convergent world, with the same global population as A1, but with more rapid changes in economic structures toward a service and information economy. B2 describes a world with intermediate population and economic growth, emphasizing local solutions to economic, social, and environmental sustainability. A2 describes a very heterogeneous world with high population growth, slow economic development and slow technological change. No likelihood has been attached to any of the SRES scenarios. Warming tends to reduce land and ocean uptake of atmospheric carbon dioxide, increasing the fraction of anthropogenic emissions that remains in the atmosphere (IPCC AR4 Special Report on

Emissions Scenarios, 2007).

2.1 Experiment Design

Two kinds of long-term model runs are conducted. One is to study how the ocean circulation and water mass characteristics around the GMR was affected by the past base climate overlaid with anthropogenic current climate change using HYCOM with daily atmospheric forcing derived from the NCEP/NCAR reanalysis dataset for the period of 1951-2007 (Expt1); the other is to study the ocean circulation and water mass characteristics in the GMR under a global warming scenarios forced by IPCC AR4 SRES A1B Emissions Scenario from 2001-2050 (Expt2). The high resolution runs are conducted near the Galapagos for all El Niño, and La Niña years from 2001 to 2050 observed in Experiment 1.

The HYCOM simulations were carried out using a nesting scheme of 4 ever increasing resolution domains. The largest domain covers the Pacific Ocean with a grid size of 2.88 ° x 1.44 ° in zonal and meridional direction, respectively. The second and third domain embedded within the Pacific domain uses a grid size of 0.72 ° x 0.36 ° and 0.18 ° x 0.09 ° covering the Eastern Pacific Ocean. Finally, the highest resolution domain has a grid size of 0.06 ° x 0.03 ° (about 6.67 km x 3.32 km) that is centered on the GMR (92.16 ° W - 88.74 ° W, 1.71 ° S - 1.71 ° N). All domains have a vertical resolution of 26 layers that stretch or shrink vertically as a function of total depth according to the hybrid coordinate

frame discussed above. The model was initialized with temperature and salinity from the Levitus monthly climatology [Levitus et al., 1994] and run for 50 years. For the current and future climate, the monthly IPCC (AR4) SRES A1b Emissions Scenario from 2001-2050 is used as the atmospheric forcing to perform the simulation (Expt2).

The latent and sensible heat fluxes were calculated during model runs using the model sea surface temperature and the bulk formulation [Cayan 1992]. Boundary conditions were provided by buffer zones that are ten grid points wide within which temperature, salinity, and interface depth are relaxed to Levitus climatological values [Levitus et al., 1994] that have been vertically remapped to hybrid vertical coordinates. The KPP vertical mixing model of Large et al. [1994] was also used. For the experiments with the grid size of 2.88 º, 0.72 º and 0.18 º on zonal direction, the bathymetry was derived from the ETOPO2 data [National Geophysical Data Center (NGDC)], which contains digital data bases of seafloor and land elevations on a 2-minute latitude/longitude grid and is interpolated on the model grids of different resolutions. In the simulation with the resolution of 0.06 º (near the Galapagos Islands), the bathymetry was drived from the 0.01 º data processed by William Chadwick, Oregon State University (http://www.pmel.noaa.gov/vents/staff/chadwick/galapagos.html). The model was spun up for fifty years from 2001 to 2050. We will discuss the results in the next section.

3. Results

3.1 The impact of past and current climate on the ocean variability around the GMR

For Expt1, the historical data can be used to validate and calibrate the ocean model. The response of the GMR ocean circulation to historical climate in the past fifty years is simulated using the NCEP/NCAR reanalysis data as the climatic forcing. This simulation provides a validation for the high resolution HYCOM model and a benchmark of assessing future climate change impacts. The global run occurred using HYCOM, with a grid size of 1.44° x 0.72° in zonal and meridional directions, respectively. The experiment domain covers the entire global ocean and has a vertical resolution defined by 26 layers that stretch or shrink vertically as a function of total depth according to the hybrid coordinate frame.

The results indicate that with prescribed atmospheric forcing, the nested HYCOM model can reproduce the major characteristics of the ocean circulation and its variability in the Galapagos region, including the ENSO events, annual and seasonal cycles, upwelling system, local and regional current systems. The area-averaged SST anomalies in the Nino3.4 region (5°S-5°N, 150°W-90°W) are used to index ENSO variability [Trenberth, 1997]. Fig 2 shows the observed (solid) and HYCOM simulated (dashed) SST anomalies in Niño3.4 region from 1949 to 2006. The SST anomalies are computed from the departure of the monthly mean SST from average climatology SST. The

climatology SST is the average condition computed from the climatological base period of 1949-2006. The observational datasets used for comparison with model output came from the $2° \times 2°$ Reynolds and Smith (1994) optimal interpolation (OI) SST (often referred to "Reynolds SST"), from 1949 to 2006. The correlation coefficient between the simulated SSTA and Reynolds SSTA is 0.721. The power spectrum of the SST anomalies (Fig 3) showed that the main ENSO period in the model is approximately 3 to 7 years, similar to the observed period. The peak amplitude of the simulated power spectrum is comparable to that of the Reynolds. This result indicates that the HYCOM can generally simulate major El Niño events.

However, the simulated SST anomalies (SSTA) in Niño3.4 region show a rising trend compared with the Reynolds SSTA (Fig 2). It is not clear whether this trend is a model artifact or something real but missing from the Reynolds SSTA. Recent studies by Conroy et al. [2009] indicate that there was significant warming trend in Eastern tropical Pacific in the past 40 years. Therefore, the simulated trend in Nino3.4 SSTA may not be entirely artificial. If we compare "apple to apple" by removing the trend from the simulated SST anomalies series, the de-trended simulated SSTA is in much better agreement with the de-trended Reynolds SSTA (see Fig 4). The correlation coefficient between the de-trended simulated SSTA and Reynolds SSTA increases to 0.836. An alternative to comparing the interannual signal is to extract the main signal with a period of 2-7 year from the SST anomalies in Niño3.4 region using a band-pass wavelet filter. Fig 5 shows the band-pass filtered Reynolds (dashed) and HYCOM simulated SST

anomalies (solid) in the Nino3.4 region from 1950 to 2006. The correlation coefficient between the simulated SSTA and Reynolds SSTA in the 2-7 year band increases to 0.913, which shows a near-perfect match between the model data and the observations at the 2-7 year band. This suggests that the model was able to accurately simulate the inter-annual variability in the tropical ocean.

3.2 The impact of future climate on the ocean variability around the GMR

The response of the GMR ocean circulation to future climate in the next fifty years is simulated using the monthly IPCC (AR4) SRES A1bE missions Scenario from 2001-2050 as the atmospheric forcing (Expt 2), with the goal to better understand the impact of global climate change on the ocean circulation and water mass structure around the GMR region. The results from the 50-yr simulation will be shown and analyzed in the following.

Figure 6 shows the simulated SST in Nino3.4 region from 1950 to 2006 forced by NCEP atmospheric forcing and the simulated SST in the Nino3.4 region from 2001 to 2070 forced by IPCC AR4 SERS A1b atmospheric forcing using HYCOM model. Results indicate that the ocean variability is greatly affected by global climate change. There is a 2 °C rising trend in the SST anomaly in the Nino3.4 region during ??? fifty years(2001-2050 which 50 years?, not clear). Besides, during the overlapping years of 2001-2007 for Expt1 and Expt2, the SST in the Nino3.4 region is consistent. The wavelet

power spectrum of the simulated SSTA in the Nino 3.4 region from 1949 to 2061 (Fig 7) shows that there is an obvious ENSO period of approximately 5-yr and a PDO period of approximately 8-10yr. Power spectrum analysis shows that the frequency for the occurrence of ENSO events seems unchanged (4-5yr) by climate change compared with Figure 3 and Figure 7. The interannual variability, increased SST may suggest a warmer mean state of the eastern Pacific Ocean, perhaps due to weaker Walker Circulation or a more southerly ITCZ, which would weaken the trade winds, deepen the thermocline and increase local convection.

Figure 8 shows the simulated SST anomalies in the Niño3.4 region from 2001 to 2060. The results indicate that there is an obvious global warming around the GMR. Fig 9 and 10 shows the simulated SST anomalies after subtracting the trend and using the band-pass filter, which greatly help us to recognize the future El Nino/La Nina events, for example the El Nino events in 2013, 2017, 2027, 2030, 2040, 2044 and the La Nina events in 2014, 2018, 2026, 2031, 2041, 2045. Figure 11 and 12 show the 10-yr average SST and salinity around the GMR simulated with the 0.18° x 0.09° resolution grids from 2001- 2050. The results indicate that there is about ~1.6°C temperature increase around the GMR, while the salinity around the GMR is little changed (Figure 12). The 10-yr average water temperature at 40m around the GMR (Figure 13) shows a pattern similar to that of the SST, with the lowest temperature around the west portion of Galápagos. The 10-yr average salinity at 40m around the GMR (Figure 14) increases slightly with time.

3.3 Case studies

In this section, the El Niño and La Niña cases from 2001 to 2050 are chosen to study how these ENSO events affect the ocean circulation and water mass characteristics around the GMR under future climate change scenario. We choose the December-February to represent the El Niño season and August-October for the La Niña season. The El Niño cases include 2013-2014, 2017-2018, 2027-2028 and 2044-2045 El Niño events and the La Niña cases include 2014, 2018, 2026 and 2045 La Niña events. Fig 15 and 16 indicate the SST around the GMR during the El Niño cases (Fig 15) and La Niña cases (Fig 16), respectively, while Fig 17 and 18 indicate the surface salinity around the GMR during the El Niño cases (Fig 17) and La Niña cases (Fig 18). During the El Niño events, there are warm and less salty waters around the whole GMR region, while less warm and saltier water are found west of Isabella and Fernandina, indicative of topographically reduced upwelling of the EUC. While during the La Niña event, there are cold and salty waters around the whole GMR region, while colder and saltier water are found west of Isabella and Fernandina, indicative of topographically increased upwelling of the EUC. Figures 19 and 20 show the surface current around the GMR during the El Niño cases and the La Niña cases, respectively. Figures 21 and 22 show the current in the mixed layer around the GMR during the El Niño cases and the La Niña cases, respectively. During the El Niño events, the surface currents during this period were dominated by the westward flowing SEC. The EUC was greatly weakened, leading to weaker upwelling to the west of Isabella Island. During the La Niña cases, the simulated

surface layer flow showed that the westward flow of the SEC collided with the eastward flow of the EUC both north and south of Isabella Island.

Figures 23 and 25 show the vertical sections of the zonal current along 92W, 91.8W, 90W and 89W for the upper 200m around the GMR in the Dec-Feb 2014 El Niño event, and the Aug-Oct 2014 La Niña event, Figures 24 and 26 show the vertical sections of zonal current (m/s) along 1S, 0.5S, EQ and 0.5N for the upper 200 m around the GMR in the Dec-Feb 2014 El Niño event and the Aug-Oct 2014 La Niña event. These results also show that during the El Niño cases, the EUC will be greatly weakened, leading to a weaker upwelling to the west of Isabella Island. While during the La Niña event, the EUC will be greatly strengthened and even reach the sea surface. The EUC core is located around 0.5˚N. During El Niño, the SEC is diminished in strength during its respective annual cycle, as is the EUC, whose core also sinks tens of meters (Johnson et al. 2002). In addition, a decreased Ekman divergence and evaporation (Xie 1994) and eastward migration of the warm SST pool contribute to a reduced upwelling and warming of the SST (Fieldler and Talley 2006). The opposite response occurs during La Niña. The surface salinity changes little (Fielder and Talley 2006), fresher (saltier) during El Niño (La Niña) as upwelling within the equatorial cold tongue is suppressed (heightened).

To study the weighted average of the GMR region of SST variability, and find whether there is any noticeable difference at different spatial and temporal time scales, the SST trend contour is plotted around GMR (Figure 27) for different time scales from 10 year to

30 year: a) 10yr from 2005-2014, b) 15yr from 2005-2019, c) 20yr from 2005-2024, d) 25yr from 2005-2029 and e) 30yr from 2005-2029. The positive (negative) values in the plot indicate positive (negative) trend in the region for the period of trend calculation. The presence of different values and signs in the trend field indicate that SST values in the GMR region experience varying trends in different regions and for different time periods.

As shown from the contour figure, if we define the west Galapagos as the upwelling region, this upwelling zone is less affected by global warming compared with other regions. For the 10-year and 15-year SST trends, there is even a cold trend around most of the GMR region, especially the upwelling region, while there is a warm trend around the GMR for the longer time period (for example, 20-year, 25-year and 30-year). In summary, the regional impact of global climate change in the Galapagos region varies from region to region. The SST trend is also dependent on the time scales. The upwelling region has the lowest warming trend, and occasionally experiences a decreasing trend at decadal time scales. This indicates that the upwelling zone may be less affected by global warming compared with other regions. Power spectrum analysis shows that the frequency for the occurrence of ENSO events seems unchanged (4-5yr) for the period of 2001-2060 under IPCC AR4 A1B scenario. The results show that the oceanic variability in the Galapagos region is sensitive to global climate change. However, the regional impact of global climate change in the Galapagos region varies from region to region. The SST trend is also dependent on the time scales.

4. Study of the EUC using TAO moored data and model data

4.1 Definitions of EUC time series from TAO/TRITON data and numerical model

In this section the CTD/ADCP data are used to calculate the EUC volume flux transport during Tropical Atmosphere-Ocean/Triangle Trans-Ocean Buoy Network (TAO/ TRITON) buoy array cruises, which is an ocean observing system of instrumented moorings spanning the entire equatorial Pacific for monitoring seasonal-to-interannual climate variability (McPhaden et al., 1998). The TAO/TRITON array consists of approximately 70 moorings between 170 °W and 95 °W which measures subsurface temperature. At some locations, current meters and acoustic Doppler current profiler (ADCP) measurements are available. To study the EUC volume flux, we use the current from TAO mooring along the equator at 140 ºW and at 110 ºW from 2001 to 2007.

In the calculation of volume fluxes, the EUC and SEC are objectively defined below.

EUC: The EUC is defined as the zonal currents (U) which satisfy the following criteria: U > 0 m/s and 25 m < z < 300 m (or less depending on data availability). The sensitivity to the choice of the criteria was tested and appeared insignificant for the variability of EUC volume flux. The mean transport of EUC is defined as:

$$U_{EUC/eq} = \int_{EUC} u dz$$

where $U_{EUC/eq}$ is the volume transport per unit width in m^2/s obtained by integrating the zonal current at the equator over all depth where EUC is defined.

SEC: the SEC is defined similar to EUC but with zonal current U <0.

In the HYCOM model, the same criteria are used to define the EUC and SEC. Because the high-resolution model domain does not include 95 ºW, for convenience, the simulated EUC volume flux at 140 ºW and 110 ºW will be computed using the simulated currents from the 0.72 ° x 0.36 °domain. In the model, there is a proportionality between the zonal current integrated only vertically right at the equator over the depth of EUC ($U_{EUC/eq}$) and the current integrated over the whole EUC section (U_{EUC}). For a better comparison, we use a meridional width L of about 100km. $U_{EUC} = L * U_{EUC/eq}$. Figure 28 shows the comparison between model and in-situ (TAO) EUC (SEC) volume flux transport at 140 ºW and 110 ºW, which indicate that the simulated EUC volume flux transport is consistent with the TAO in-situ data, especially with respect to the annual/interannual cycle. This means that the constructed EUC/SEC time series obtained from the in-situ data from 2001-2007 could be used to study the EUC variability and to validate the simulated EUC in ocean model. In the next section, we will use the ocean model to study the EUC in more details.

4.2 Study of EUC using numerical model (HYCOM)

Because of the scarcity of current data, the numerical model (HYCOM) is used to study the EUC/SEC volume flux variability and the effect of three currents on the different regions of the Galapagos. Figure 29 shows the simulated EUC, SEC (including Panama Current and Peru Current) volume flux transport from 2005 to 2035 around GMR. The blue line is the simulated flux transport computed using the simulated currents from the high resolution (0.06° x 0.03°) domain, while the red line represents the simulated flux transport computed using the simulated currents from the relatively low resolution (0.72° x 0.36°) domain. For the low resolution domain, we defined the EUC: U>0 m/s and 0 m < z < 300 m and defined the EUC volume flux transport per unit width in m^2/s obtained by integrating the zonal current over the whole EUC section between 3°S and 3°N over all depth where EUC is defined. The SEC is defined similar to EUC but with U<0 m/s. It consists of the Panama Current and the Peru Current. The Panama current is defined by U<0 m/s and V< 0 m/s, while the Peru current is defined by U<0 m/s but V>0 m/s. In the high resolution domain, because of the limitation of the domain size (92.16° W - 88.74° W, 1.71° S - 1.71° N), we can only define the portions of EUC/SEC within the domain (1.71° S - 1.71° N). All the simulated volume flux transports within the high resolution domain is smaller than those with the low resolution due to the difference in covered area. The correlation coefficient of the EUC volume flux transports between these two resolutions is 0.793; while the correlation coefficient of Panama Current and Peru Current are 0.279 and 0.473 respectively. Due to the domain

limitation of the high resolution, we will use the simulated volume flux transport computed from the low resolution of 0.72 °x 0.36 °domain in following discussions.

To find how these currents are related with each other, the correlation coefficients between these three currents (EUC vs. Peru, EUC vs. Panama and Panama vs. Peru) are calculated. The results show that the correlation coefficient between the Panama (Peru) current volume flux and EUC current volume flux is 0.241 (0.192) (both pass the 95% significance test), while the correlation coefficient between the Panama current and Peru Current is 0.016. This indicates that the Panama current and Peru Current is significantly correlated with the EUC current, while the Panama current is not related to Peru Current.

How does the EUC flux transport propagate across the Galápagos platform? As the EUC runs into the GMR and is topographically split into two streams, how do these streams vary in position and strength, and the route through the islands? (Leetmaa., 1982, Steger et al., 1998). Figure 30 shows the north and south branches of the split streams, and the difference between the north and south branch of EUC volume flux of the simulated EUC volume flux transport at 91.26W from 2005 to 2035 around GMR. The north branch of the EUC accounts for the most (58%) of the EUC volume transport.

The GMR is composed of several regions (Edgar, 2002): the west Galapagos, the far north region, the southeast region, the central region, etc. In order to find the effect of

different currents (EUC, Panama and Peru) on different areas of the Galapagos Archipelago, as well as the key region for EUC upwelling, the correlation coefficients between the computed EUC (Panama/Peru Current) volume flux transport and the SST fields in the simulation using the high resolution (0.06 ° x 0.03 °) domain are calculated (Figure 31). The results show that the western Galapagos upwelling region is affected by the EUC and Panama currents; while central/east Galapagos is affected by both Peru and EUC currents. The north region is affected by the Panama Current only. The southeast region is affected by Peru Current only. These regional differences explain the variability of the responses in different regions of the Galapagos Archipelago to global climate change.

4.3. Empirical mode decomposition (EMD) and Ensemble EMD (EEMD) method

4.3.1. Introduction of the EMD and EEMD

Empirical Mode Decomposition (EMD) can be used [Huang et al 1998, 1999] as an adaptive time-frequency data analysis method. It is quite versatile in a broad range of applications for extracting signals from data generated in noisy nonlinear and non-stationary processes.

Because one of the major drawbacks of the original EMD is the frequent appearance of mode mixing, which is defined as a single IMF either consisting of signals of widely disparate scales, or a signal of a similar scale residing in different IMF components, when

mode mixing occurs, an IMF can cease to have physical meaning by itself, suggesting falsely that there may be different physical processes represented in a mode. To overcome the mode mixing problem, the Ensemble EMD is used [Wu et *al* 2009], which defines the true IMF components as the mean of an ensemble of trials, each consisting of the signal plus a white noise of finite amplitude. With this ensemble approach, we can clearly separate the scale naturally without any *a priori* subjective criterion selection. To generalize this ensemble idea, noise is introduced to the single data set, $x(t)$, as if separate observations were indeed being made as an analog to a physical experiment that could be repeated many times. The added white noise is treated as the possible random noise that would be encountered in the measurement process. Under such conditions, the *i*th "artificial" observation will be

$$x(t) = x(t) + w_i(t) \qquad (2)$$

In the case of only one time series, each multiple-observation ensembles is processed by adding not arbitrary but different realizations of white noise, $w_i(t)$, to that single time series as given in Eq. (2). By adding finite noise, the EEMD eliminated largely the mode mixing problem and preserved physical uniqueness of decomposition. Therefore, the EEMD represents a major improvement of the EMD method.

4.3.2 Analysis of EUC and SEC volume flux using EMD and EEMD method

Figures 32-34 show the intrinsic mode functions of the EUC, Panama Current and Peru Current volume flux transport (C1-C9). The decompositions of these indices using the original EMD are plotted in Figure 32. The lack of correlation clearly represents a typical problem of mode mixing in the original EMD. It is composed of pieces of contagious model mixing. The pieces of oscillations having approximate periods of those appear also in its neighboring IMFs. For examples, if happens in one IMF, it will happen in the following IMFs at the same temporal neighborhood. Consequently, mode mixing reduces the capability of the EMD in identifying the true timescales of consistent oscillations in the individual IMF component. This is clearly shown in Figures 32-34, in which none of the IMF pairs with a rank from 1 to 7 have a higher correlation than 0.3.

To solve this problem and to identify the timescale at which the interaction truly occurs, all time series (EUC, Panama and Peru Current) were reanalyzed using the EEMD. The results are displayed in Figures 35-37. It is clear that the synchronizations between corresponding IMF pairs are much improved, especially for the IMF components 3-7. The detailed correlation between the corresponding IMF components of EUC volume flux transport is displayed in Figure 38. Clearly, the decompositions using the EEMD improve the correlation values significantly. The EEMD results help greatly in the isolation of signals of various scales that reflect the relation between EUC volume flux and SEC volume transport. So the higher correlations between EUC and SEC (including

Panama and Peru Current) at various timescales have been obtained, especially those of annual (components 4 and 5 with mean periods of 1 and 2 years, respectively) and interannual (components 6 and 7 with mean periods of 3 and 5 years, respectively) time scales. For the long interdecadal timescales, especially for C8 and C9, since the number of degrees of freedom of the IMF components is very small due to the lack of oscillation variations, the correlation coefficients corresponding to them can be very misleading; therefore, they should be ignored. These results clearly indicated the correlation between EUC and SEC volume flux occurs on a broad range of timescales, covering annual, inter-annual and decadal from 1 to 10 years.

5. Concluding Remarks

The regional impact of global climate change on the ocean circulation and water volume characteristics around the Galápagos Archipelago is studied using the Hybrid Coordinate Ocean Model (HYCOM). A four-level nested-domain system is used in the study to downscale the global climate change impact to the regional scale centered on the Galapagos Archipelago.

The ocean circulation driven by the past and current climate is simulated using HYCOM with daily atmospheric forcing derived from the NCEP/NCAR reanalysis dataset for the period of 1951-2007 (Expt1). The result indicates that with prescribed atmospheric forcing, the major characteristics of the ocean circulation and its variability

in the Galapagos region, including the ENSO events, annual and seasonal cycles, upwelling system, local and regional current systems, and tropical instability waves, can be reproduced by the nested HYCOM. There is a high correlation (r=0.73) between the simulated Sea Surface Temperature (SST) anomalies and the observed SST anomalies in the Niño3.4 region. The response of the ocean circulation in the Galapagos region to future climate change scenarios is studied using the IPCC AR4 SRES A1b scenario as an example. The monthly IPCC (AR4) SRES A1b Emissions Scenario from 2001-2050 is used as the atmospheric forcing to drive the nested HYCOM in the future climate change scenario simulation (Expt2). The results show that the oceanic variability in the Galapagos region is sensitive to global climate change. The result also indicates that future climate will continue the type of El Nino/La Nina phenomenon as seen in the present day climate; however the presence of a warming trend, at a rate of approximately 0.1-0.4 degrees per decade, creates higher maximum SST during future El Nino than seen in the past. There are different characteristics in future ENSO events, with some events shutting down the EUC and the upwelling almost completely within the upper 50m of water.

The regional impact of global climate change in the Galapagos region varies from region to region. The SST trend is also dependent on the time scales. The upwelling region has the lowest warming trend, and occasionally experiences a decreasing trend at decadal time scales. This indicates that the upwelling zone may be less affected by global warming compared with other regions. Power spectrum analysis shows that the frequency

for the occurrence of ENSO events seems unchanged (4-5yr) by climate change, while the amplitude of ENSO events is increased. There seems to be a nonlinear coupling between El Nino and the long-term warming trend. There is deepening of the core of EUC due to warming and deepening of the mixed layer, resulting in weaker upwelling/La Nina, and enhancing warming/El Nino.

The surface temperature, salinity and current as well as the undercurrent around Galápagos Archipelago are simulated under increasing fine resolution. These variables are specifically compared and analyzed around the Galapagos Marine Reserve with a resolution of $0.06° \times 0.03°$ for El Niño and La Niña cases, respectively. The results show that for the El Niño cases, the EUC will be greatly weakened, leading to weaker upwelling to the west of Isabella Island. While during the La Niña event, the EUC will be greatly strengthened and the EUC may come up to the sea surface. The EUC core is located around 0.5˚N. The volume transport variations in the entire equatorial band of the Pacific and in its eastern part are quantified using both in situ data and an ocean general circulation model, in which the current data from the TAO/TRITON moorings and simulated current at the equator are compared. The effect of different currents (EUC, Panama and Peru) on different areas of the Galapagos Archipelago is studied. The results show that the western Galapagos upwelling region is affected mainly by the EUC and Panama currents; while central/east Galapagos is predominantly affected by both Peru and EUC currents. The north region is affected by the Panama Current only. The southeast region is affected by Peru Current only. These regional differences explain the

variability of the responses in different regions of the Galapagos Archipelago to global climate change. However, a limitation of the assessment is that it is based on one IPCC scenario only. A more reliable way to assess regional response to climate change is to estimate the range of responses using ensemble approach.

Acknowledgements

This project was funded by National Aeronautics Space Association (NASA) Biodiversity and Ecological Forecasting grant NNG04GL98G. The Counterpart US-AID No. 518-A-00-03-00152-00 and UK Darwin Initiative Project No. 14-048 also provided funding for this project. All modeling work is carried out in the Coastal Fluid Dynamical Lab of North Carolina State University using the High-Performance Computing (HPC) system.

Appendix

1. EMD and EEMD

First, we will briefly introduce the original EMD method. The detailed description can be found in the works of Huang et al [1998], Huang et al [1999], and Wu et *al* [2009]. The EMD method is adaptive, with the basis of the decomposition derived from the data. In the EMD approach, the data $x(t)$ is decomposed in terms of several different Intrinsic Mode Function (IMF) components, C_j, i.e.,

$$x(t) = \sum_{j=1}^{n} C_j + r_n \qquad (1)$$

where r_n is the residue of data $x(t)$, after n number of IMFs are extracted [Wu et al 2009]. IMFs are simple oscillatory functions with varying amplitude and frequency, and hence have the following properties:

1. Throughout the whole length of a single IMF, the number of extrema and the number of zero-crossings must either be equal or differ at most by one (although these numbers could differ significantly for the original data set).

2. At any data location, the mean value of the envelope defined by the local maxima and the envelope defined by the local minima is zero.

Therefore, the means of the corresponding IMFs of different white noise series are likely to cancel each other.

The principle of the EEMD is that the added white noise would populate the whole time-frequency space uniformly with the constituting components of different scales. When a signal is added to this uniformly distributed white background, the bits of signal of different scales are automatically projected onto proper scales of reference established by the white noise in the background. Each individual trial may produce very noisy results, for each of the noise-added decompositions consists of the signal and the added white noise. Since the noise in each trial is different in separate trials, it is canceled out in the ensemble mean of enough trials. The ensemble mean is treated as the true answer, for, in the end, the only persistent part is the signal as more and more trials are added in the

ensemble.

References

Bleck, R., 2002. An oceanic general circulation model framed in hybrid isopycnic-Cartesian coordinates. Ocean Modeling, 4, 55-88.

Boersma, P.D. 1977. An ecological and behavioral study of the Galápagos Penguin. Living Bird 15: 43–93.

Boersma, P.D. 1978. Breeding patterns of Galápagos Penguins as an indicator of oceanographic conditions. Science 200: 1481–1483.

Bustamante, R., Collins, K. J. Bensted-Smith, R., 1999.Biodiversity conservation in the Galápagos Marine Reserve. Entomologie Supplement 68: 45-52.

Cayan, D., Latent and sensible heat flux anomalies over the Northern oceans: driving the sea surface temperature, J. Phys. Oceanogr., *22*, 859–881, 1992.

Cayan, 1992: Latent and sensible heat flux anomalies over the northern ocean: The connection to monthly atmospheric circulation. JClim, 5, 354--369

Chassignet, E.P., Smith, L.T., Bleck, R., Bryan, F.O., 1996. A model comparison: numerical simulations of the north and equatorial Atlantic oceanic circulation in depth and isopycnic coordinates. J. Phys. Oceanogr. 26, 1849–1867.

Chassignet, E.P., Smith, L.T., Halliwell, G.R., Bleck, R., 2003. North Atlantic Simulations with the Hybrid Coordinate Ocean Model (HYCOM): impact of the vertical coordinate choice, reference density, and thermobaricity. J. Phys. Oceanogr. 33, 2504–

2526.

Chavez, F.P., Strutton, P.G., Friederich, G.E., Feely, R.A., Feldman, G.C., Foley, D.G., McPhaden, M.J., 1999. Biological and chemical response of the equatorial pacific ocean to the 1997–1998 El Niño. Science 286, 2126–2131.

Conroy, J.L., A. Restrepo, et al., 2009: Unprecedented recent warming of surface temperatures in the eastern tropical Pacific Ocean. Nature Geosci, 2: 46-50.

Edgar, G. J., Banks, S., Farina, J. M., Calvopina, M. and Martınez, C., 2004. Regional biogeography of shallow reef fish and macro-invertebrate communities in the Galápagos archipelago. Journal of Biogeography 31: 1107-1124.

Feldman, G., Clark, D., Halpern, D., 1984. Satellite color observations of the phytoplankton distribution in the eastern equatorial Pacific during the 1982–1983 El Niño, Science 226 (4678), 1069–1071.

Feldman, G..,1986. Patterns of phytoplankton production around the Galápagos Islands. In M.J. Bowman, R.T. Barber & C.N.K. Mooers (Eds.), Lecture Notes on Coastal and Esutarine Studies: Tidal Mixing and Plankton Dynamics (pp. 77-106). Berlin: Springer

Ghil, M., Malanotte-Rizzoli, P., 1991. Data assimilation in meteorology and oceanography. Adv. Geophys. 33, 141–266.

Glynn, P.W. and J.S. Ault. 2000. A biogeographic analysis and review of the far eastern Pacific coral reef region. *Coral Reefs* **19**: 1-23.

Halliwell Jr., G.R., 2004. Evaluation of vertical coordinate and vertical mixing algorithms in the Hybrid-Coordinate Ocean Model (HYCOM). Ocean Modelling. 7, 285–322.

Hayes, S. P. 1985. Sea level and near surface temperature variability at the Galápagos Islands, 1979-1983

Houvenaghel, G. T., 1978. Oceanographic conditions in the Galápagos Archipelago and their relationships with life on the islands. In: Boje, R., Tomczak, M. (Eds.), Upwelling Ecosystems. Springer, Berlin, pp. 181–200.

Houvenaghel, G. T., 1984. Oceanographic setting of the Galápagos Islands. In: Perry, R. (Ed.), Key Environments, Galápagos. Pergamon Press, Oxford, pp. 43–54.

Huang N. E, Shen Z, Long S. R, Wu M. C, Shih E. H, Zheng Q, Tung C. C and Liu H. H, 1998: The empirical mode decomposition method and the Hilbert spectrum for non-stationary time series analysis, *Proc. Roy. Soc. London* **454 (A),** 903–995.

Huang N. E, Shen Z and Long R. S, 1999:, A new view of nonlinear water waves — the Hilbert spectrum, *Ann. Rev. Fluid Mech.* **31,** 417–457.

Kistler, R., E. Kalnay, W. Collins, S. Saha, G. White, J. Woollen, M. Chelliah, W. Ebisuzaki, M. Kanamitsu, V. Kousky, H. van den Dool, R. Jenne, and M. Fiorino, 2001: The NCEP-NCAR 50-Year Reanalysis: Monthly Means CD-ROM and Documentation. Bull. Amer. Meteor. Soc., 82, 247-268.

Large, W.G., Mc Williams, J.C., Doney, S.C., 1994. Oceanic vertical mixing: review and a model with a nonlocal boundary layer parameterization. Rev. Geophys. 32, 363–403.

Levitus, S., Boyer, T., 1994. World Ocean Atlas 1994, Volume 4: Temperature. NOAA Atlas NESDIS 4. US Dept. of Commerce, Washington, DC.

Levitus, S., Burgett, R., Boyer, T., 1994. World Ocean Atlas 1994, Volume 3: Salinity. NOAA Atlas NESDIS 3. US Dept. of Commerce, Washington, DC.

Jennings, S., Brierley, A.S., & Walker, J.W. 1994. The inshore fish assemblages of the Galápagos Archipelago. Biological Conservation, 70, 49-57

Oschlies, A., Model-derived estimates of new production: New results point towards lower values, *Deep-Sea Research II*, **48**, 2173-2197, 2001.

Palacios, D.M. (2004). Seasonal patterns of sea-surface temperature and ocean color around the Galápagos: regional and local influences. *Deep-Sea Research II, 51,* 43-57

Riedinger, M.A., Steinitz-Kannan, M., Last, W.M., Brenner, M.,2002. A similar 6100 C-14C yr record of El Niño activity from the Galápagos Islands. Journal of aleolimnology 27, 1–7.

Rodbell, D.T., Seltzer, G.O., Anderson, D.M., Abbott, M.B., Enfield, D.B., Newman, J.H., 1999. An asymptotically equal to 15,000- Year Record of El Niño-Driven Alluviation in Southwestern Ecuador. Science 283, 516–519.

Steger, J. M., Collins, C. A., Chu, P. C., 1998. Circulation in the Archipielago de Colon (Galápagos Islands), November 1993. Deep-Sea Research II 45, 1093–1114.

Sweet W. V., Morrison J. M., Liu Y., Kamykowski D., Schaeffer B. A., Xie L., Banks S. Tropical instability wave interactions within the Galbpagos Archipelago. Deep sea research part I: oceanographic research papers, vol.56 n.8 pp: 1217-1229

Trenberth, K.E., Hoar, T.J., 1997. El Niño and climate change. Geophysical Research Letters 24, 3057–3060.

Trenberth, K.E., 1997. The Definition of El Niño. Bulletin-American Meteorological Society 78, 2771–2778.

Wiggert, J. D., R.R. Hood, K. Banse and J.C. Kindle. 2005. Monsoon-driven biogeochemical processes in the Arabian Sea. Progress In Oceanography 65 (2-4), pp. 176-213

Wu, Z. and Huang, N. E., 2009: Ensemble Empirical Mode Decomposition: A Noise-Assisted Data Analysis Method. Advances in Adaptive Data Analysis 1 (1) , 1-41.

Wyrtki, K., Kilonsky, B., 1984. Mean water and current structure during the Hawaii-to-Tahiti shuttle experiment. Journal of Physical Oceanography 14, 242–254.

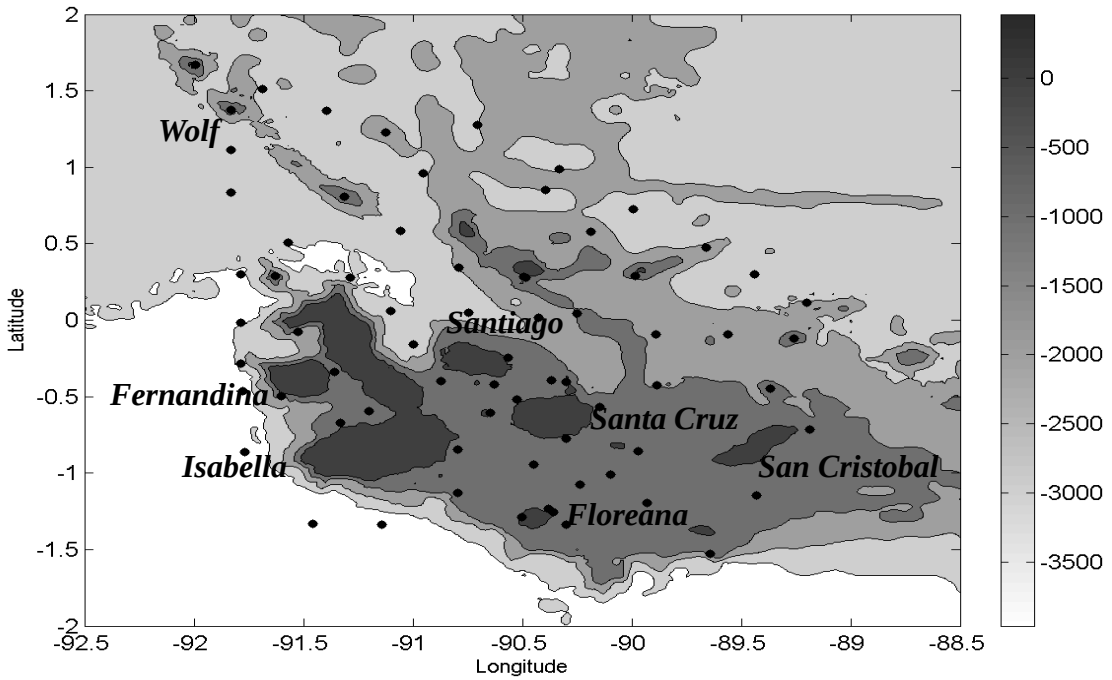

Figure 1: Bathymetry map and sampling stations of the Galápagos Archipelago.

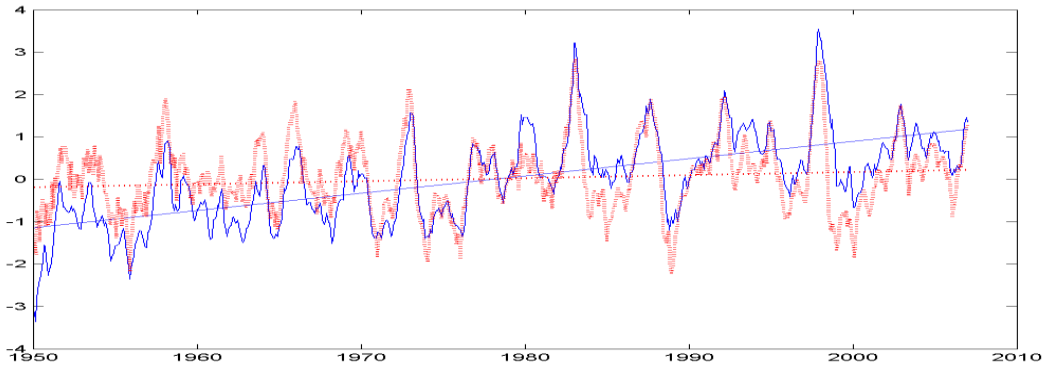

Figure 2: The observed (red, dashed) and HYCOM simulated SST anomalies (blue, solid) in Nino3.4 region from 1950 to 2006.

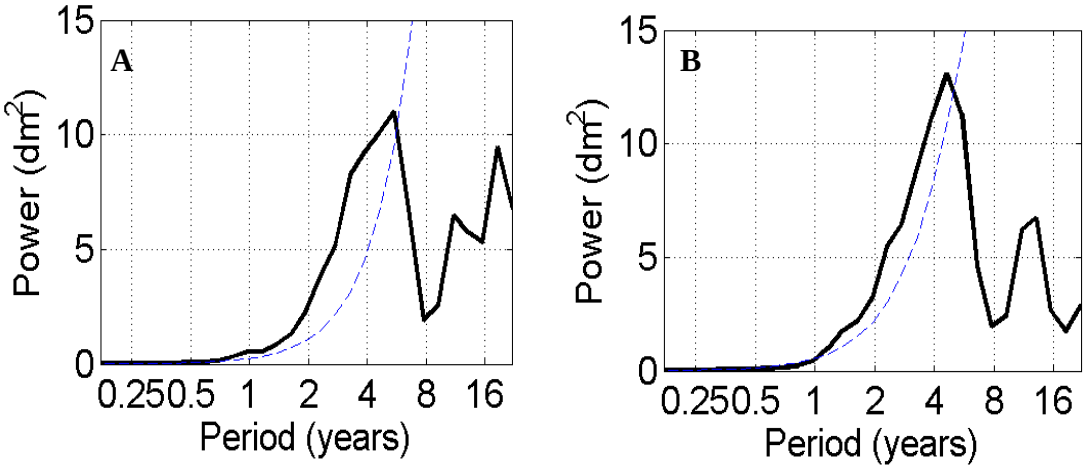

Figure 3: The power spectrum of the SST anomalies in the Niño3 region during 1950-2006: a) Model simulation; b) Observation.

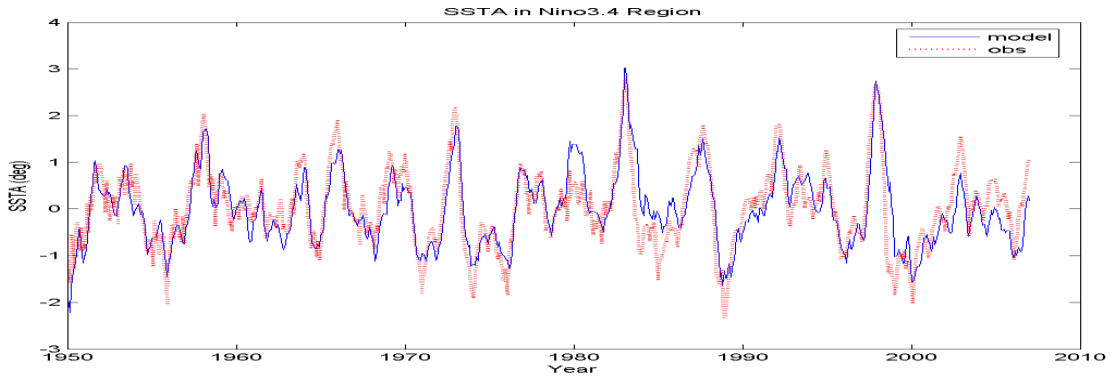

Figure 4: The observed (red, dashed) and HYCOM simulated SST anomalies (blue, solid) in Nino3.4 region from 1950 to 2006 after subtracting the trend.

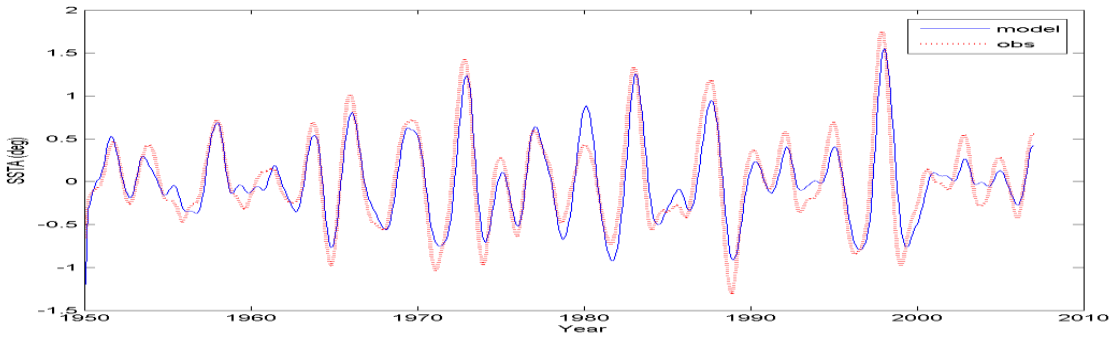

Figure 5: The bandpass filtered observed (red, dashed) and HYCOM simulated SST anomalies (blue, solid) in Nino3.4 region from 1950 to 2006.

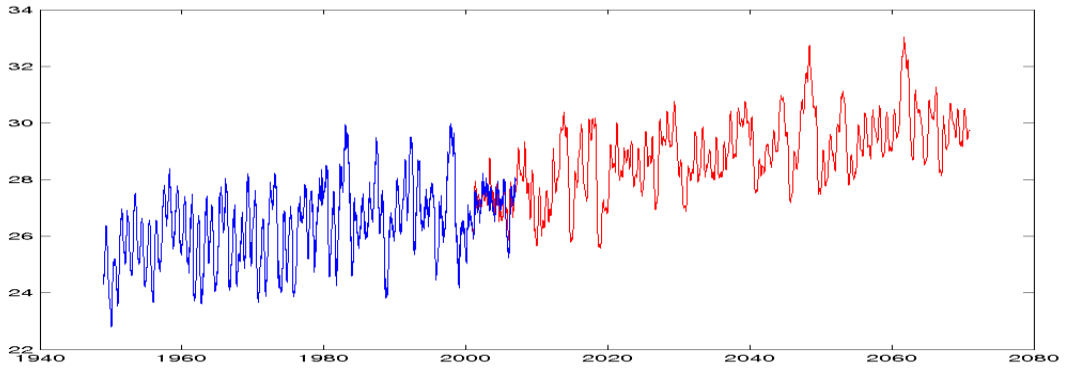

Figure 6: The simulated SST in Nino3.4 Region from 1950 to 2006 (Blue) forced by NCEP atmospheric forcing and simulated SST from 2001 to 2060 (red) forced by IPCC AR4 SERS A1b atmospheric forcing using HYCOM model.

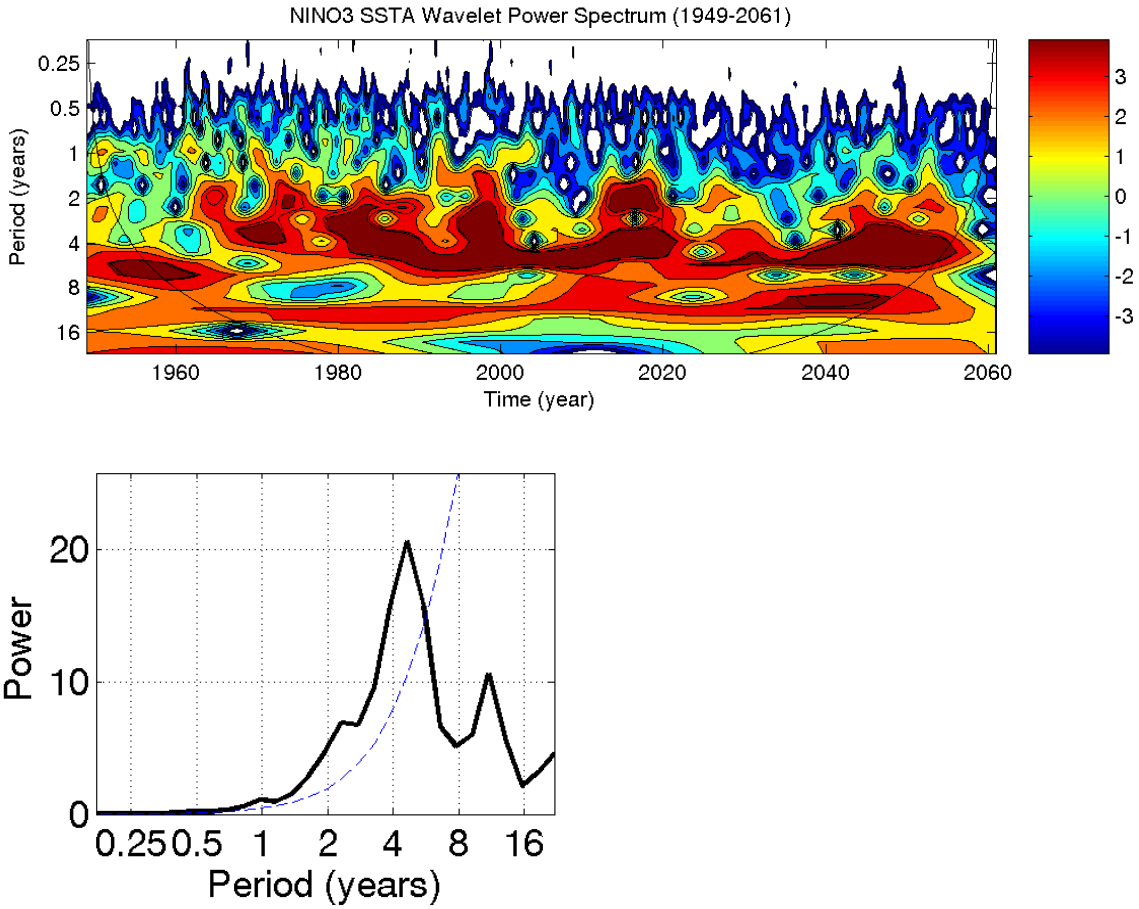

Figure 7: a) The wavelet power spectrum and b) main period of the simulated SSTA in Nino 3.4 region from 1949 to 2061.

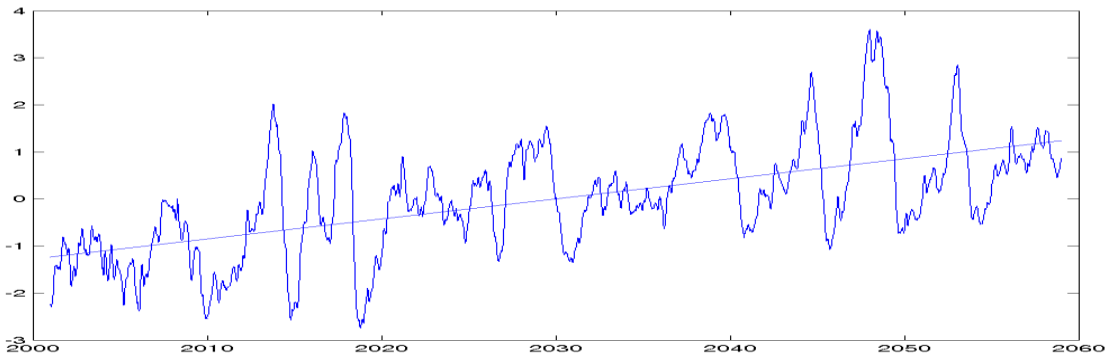

Figure 8: The simulated SSTA in Nino3.4 Region from 2001-2060.

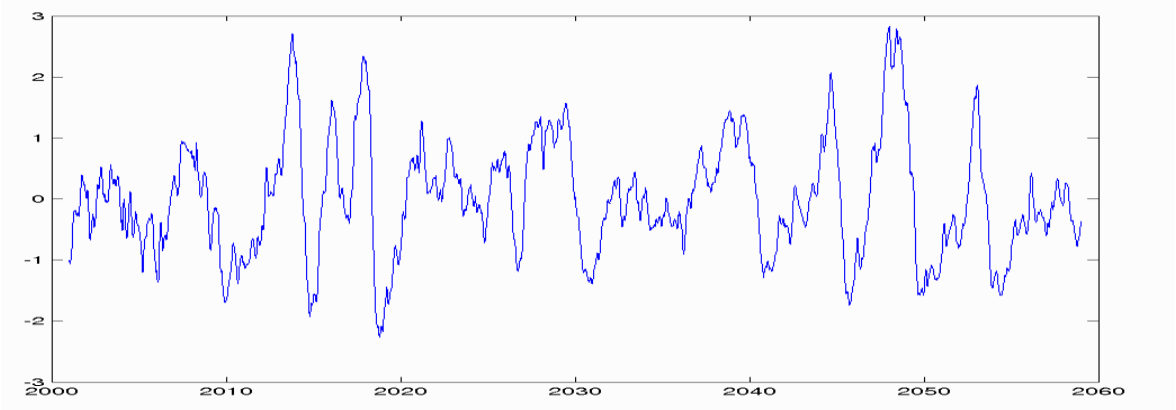

Figure 9: The HYCOM simulated SST anomalies (blue, solid) in Nino3.4 region from 2001-2060 after subtracting the trend.

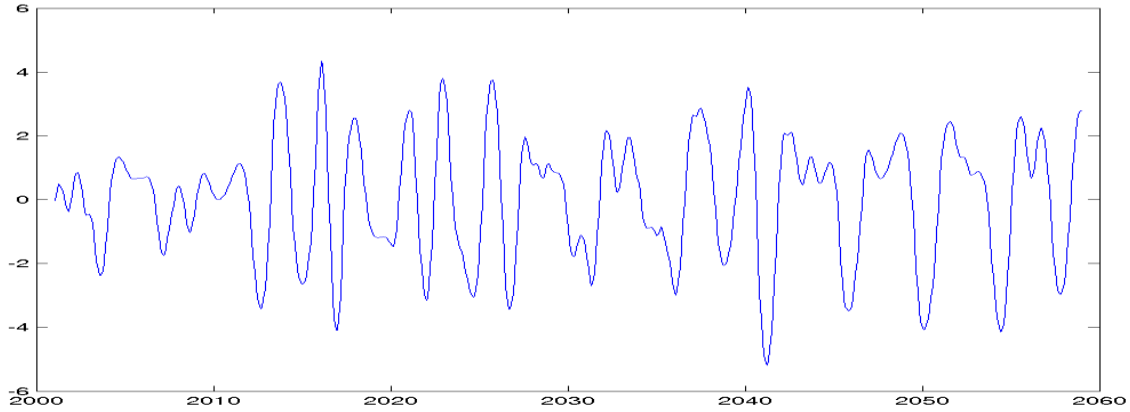

Figure 10: The band-pass filtered HYCOM simulated SST anomalies (blue, solid) in Nino3.4 region from 2001-2060

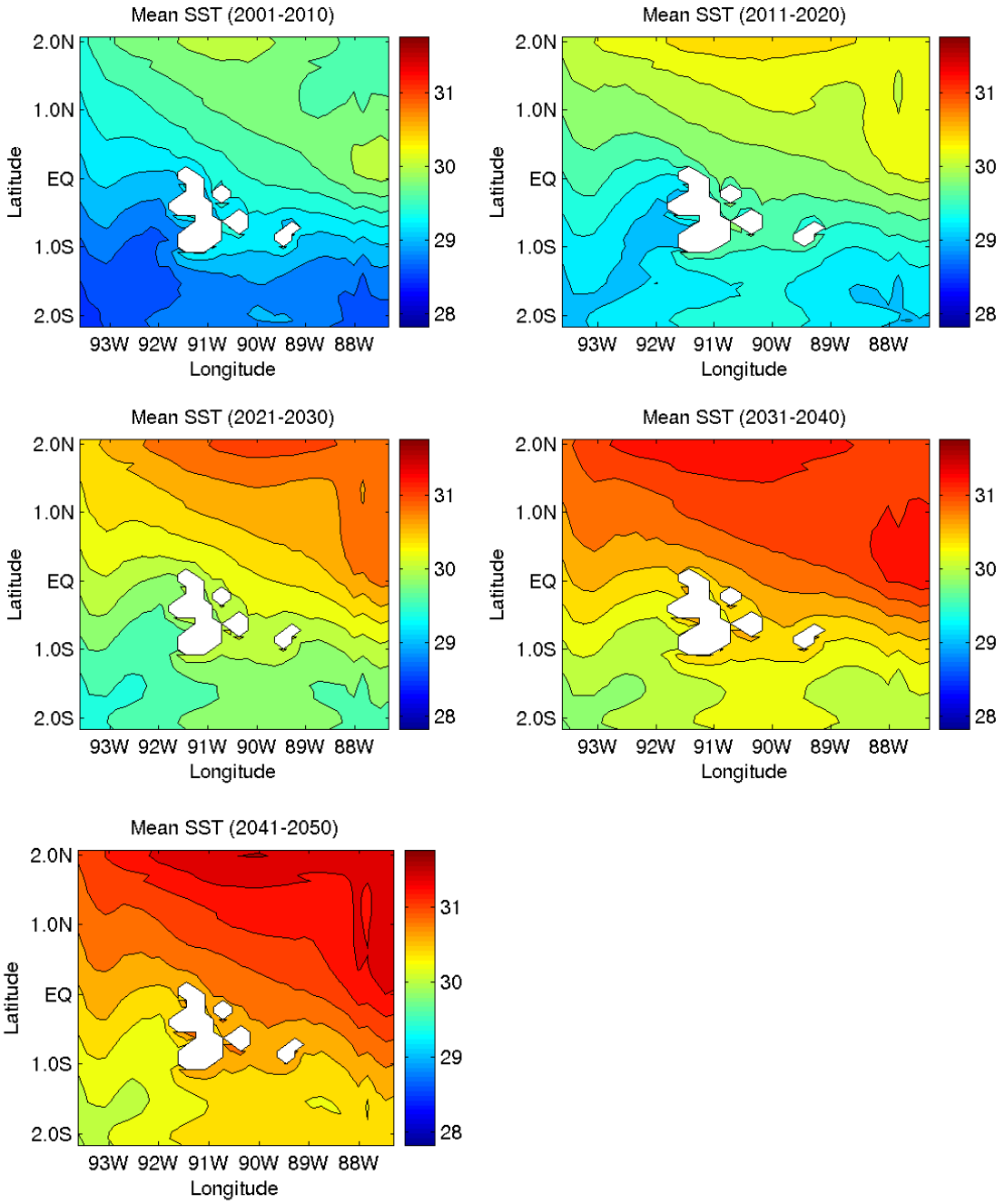

Figure 11: The 10-yr average SST around the GMR under the resolution of 0.18 °x 0.09 °: a) from 2001 to 2010, b) from 2011 to 2020, c) from 2021 to 2030, d) from 2031 to 2040 and e) from 2041 to 2050.

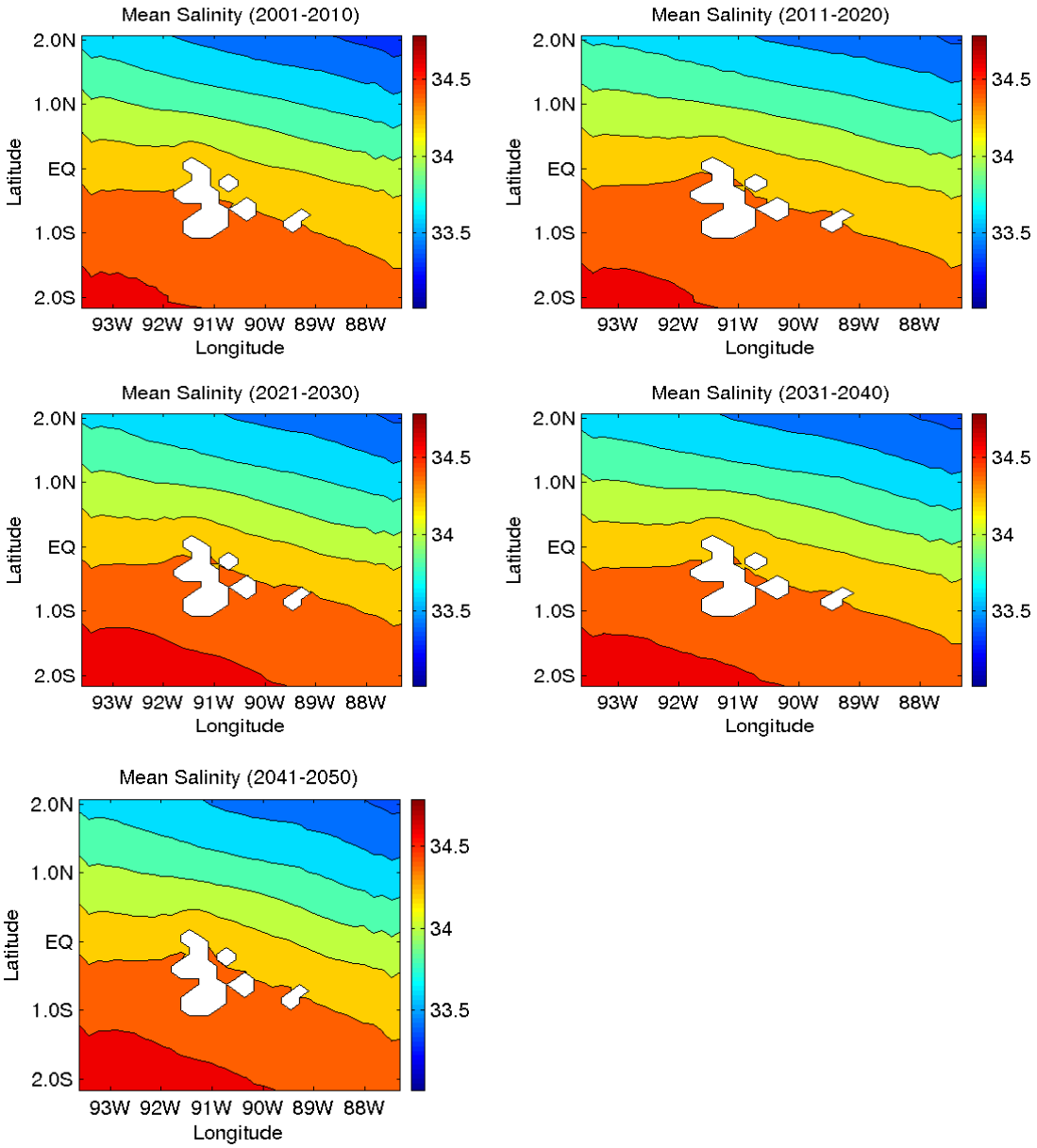

Figure 12: The 10-yr average Sea surface salinity around the GMR under the resolution of 0.18 ° x 0.09 °. a) from 2001 to 2010, b) from 2011 to 2020, c) from 2021 to 2030, d) from 2031 to 2040 and e) from 2041 to 2050.

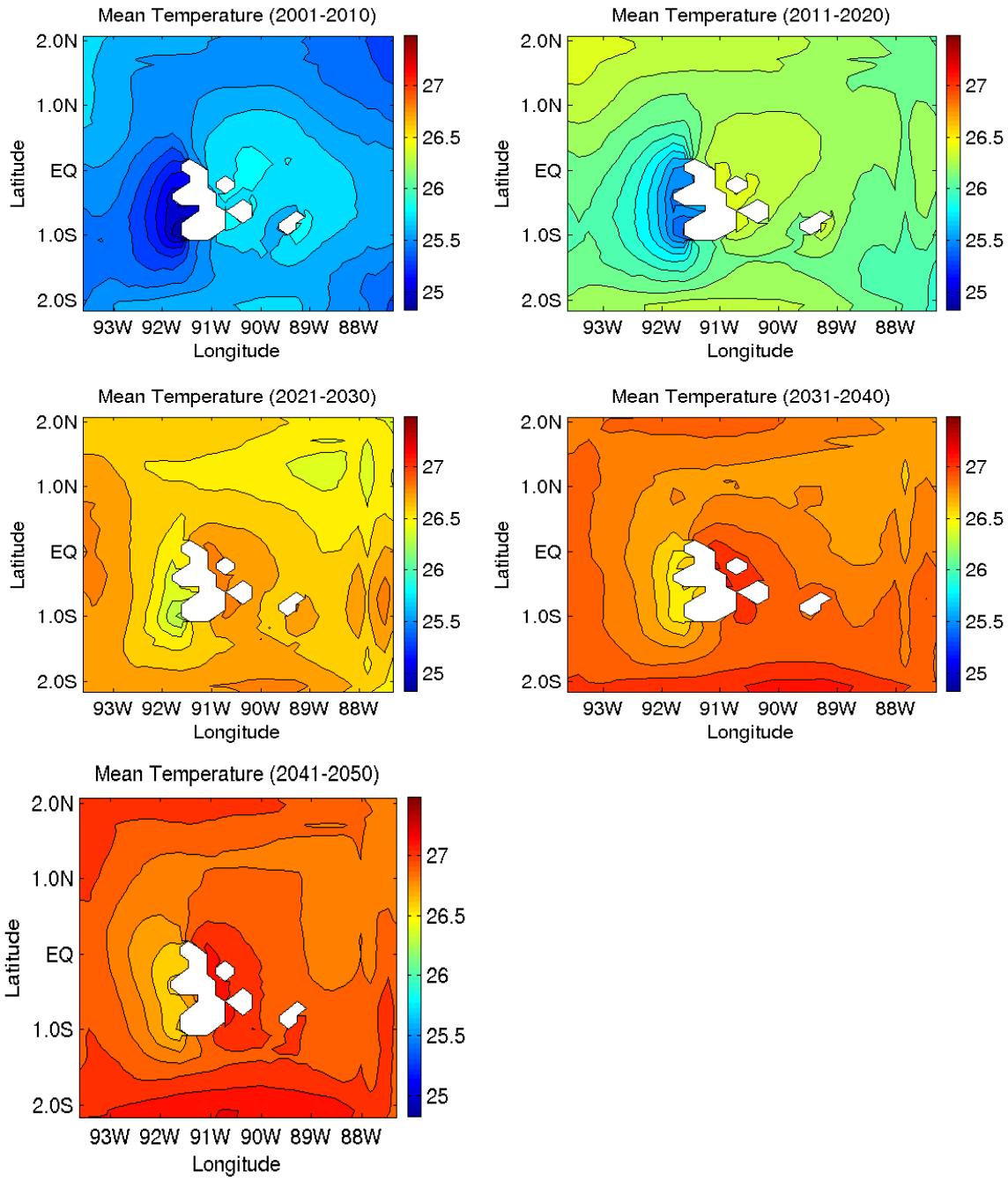

Figure 13: The 10-yr average Sea temperature at 40m around the GMR under the resolution of 0.18 ° x 0.09 °: a) from 2001 to 2010, b) from 2011 to 2020, c) from 2021 to 2030, d) from 2031 to 2040 and e) from 2041 to 2050.

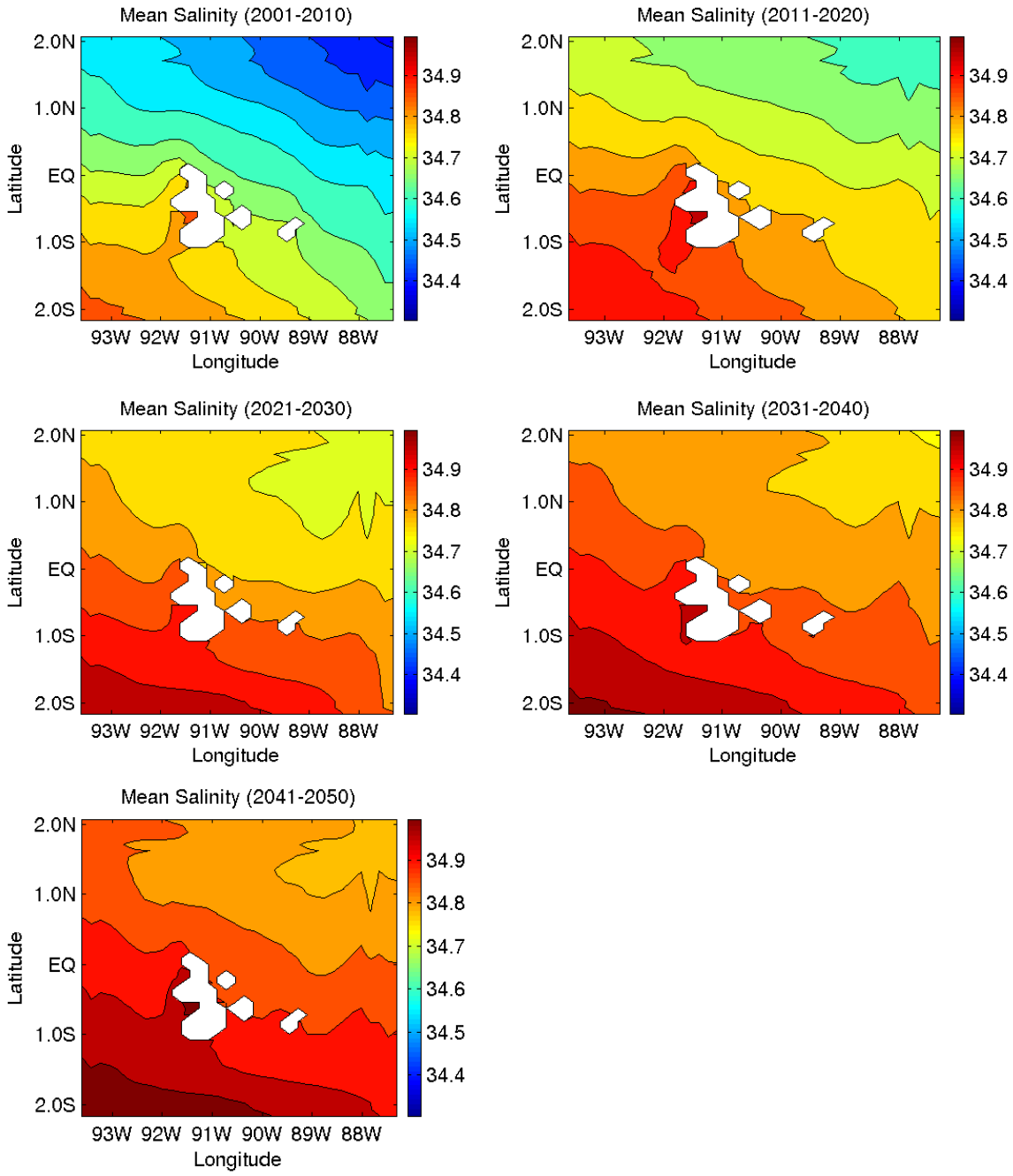

Figure 14: The 10-yr average Sea salinity at 40m around the GMR under the resolution of 0.18 °x 0.09 °. a) from 2001 to 2010, b) from 2011 to 2020, c) from 2021 to 2030, d) from 2031 to 2040 and e) from 2041 to 2050.

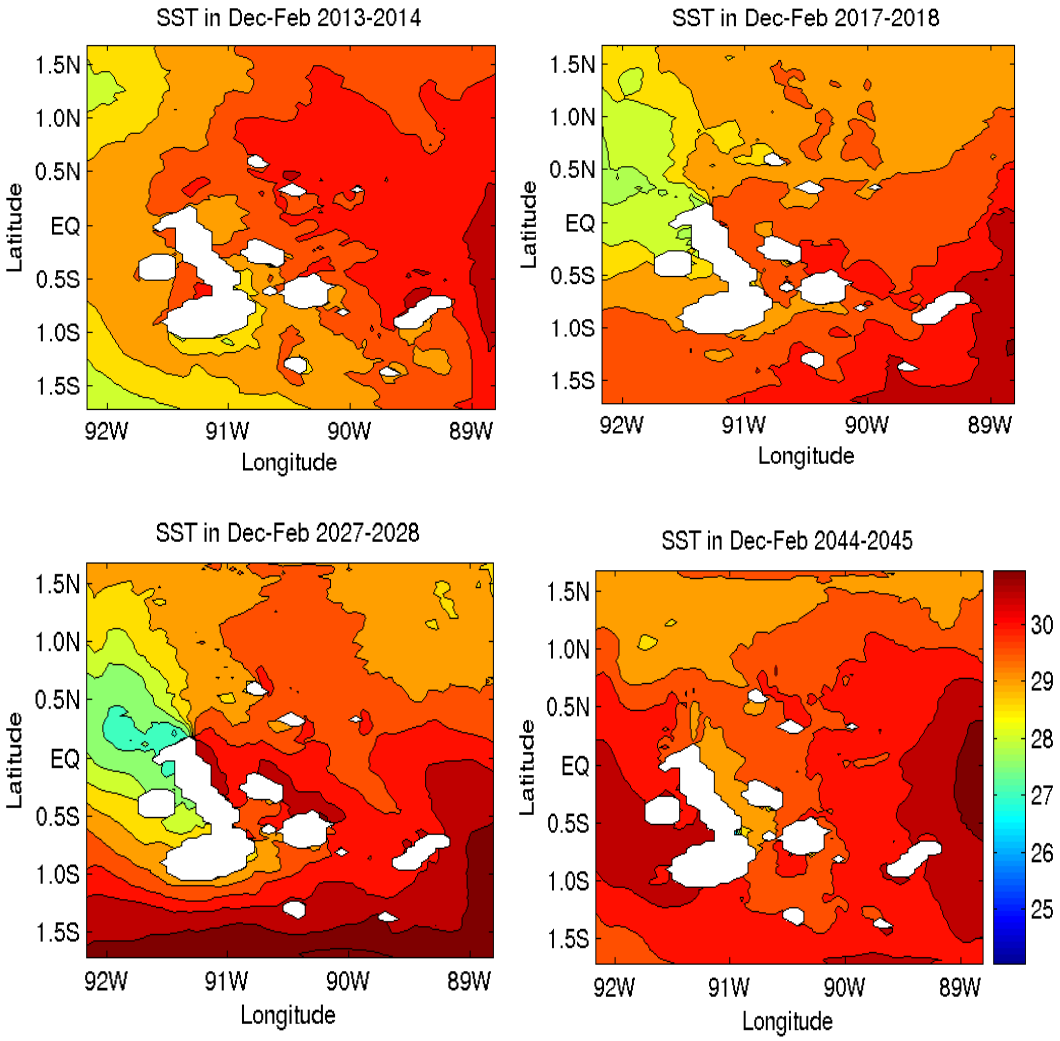

Figure 15: The SST around the GMR during the El Nino cases: a) in Dec-Feb in 2013-2014, b) in Dec-Feb in 2017-2018, c) in Dec-Feb in 2027-2028 and d) in Dec-Feb in 2044-2045.

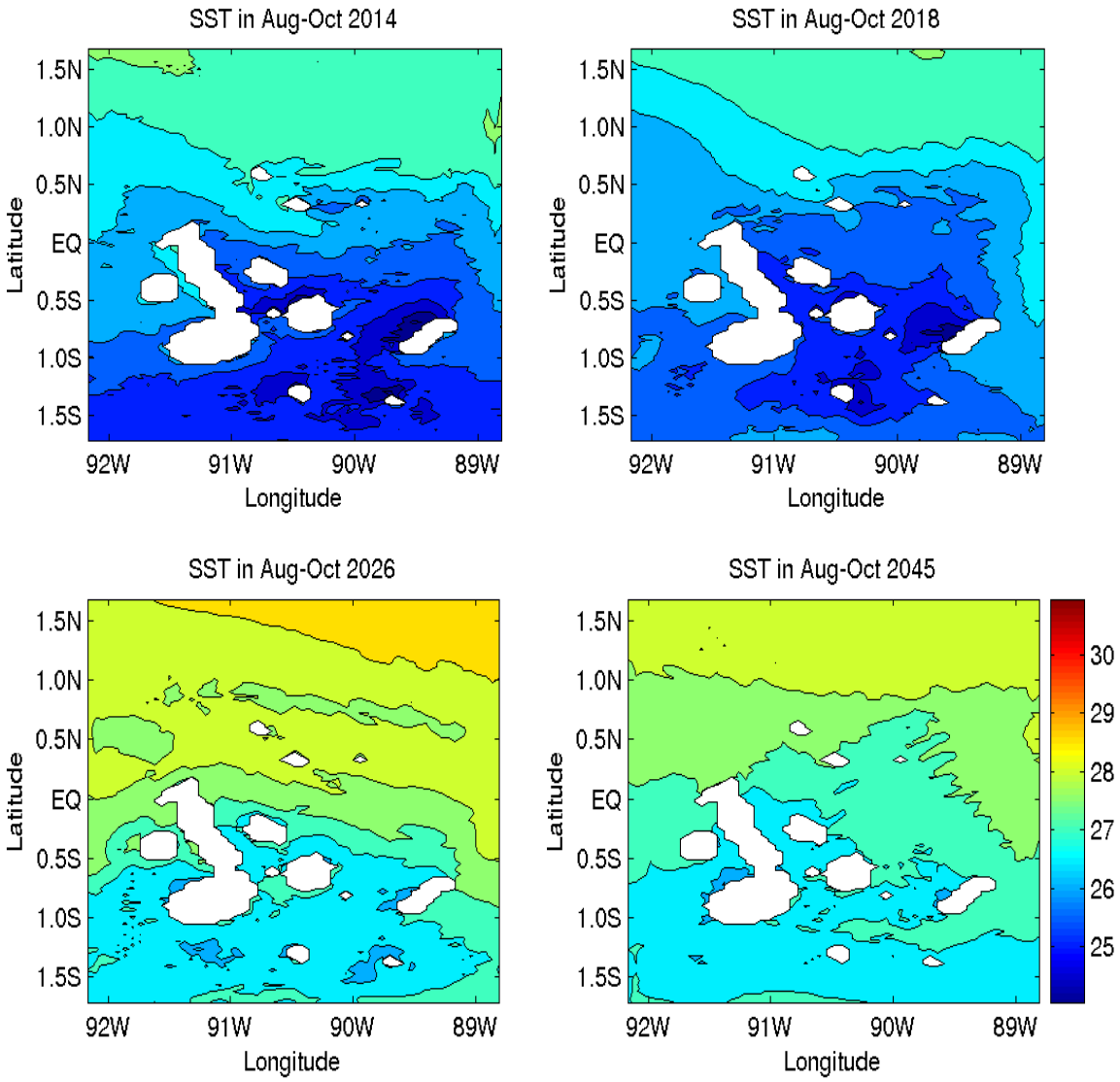

Figure 16: The SST around the GMR during the La Nina cases: a) in Aug-Oct in 2014, b) in Aug-Oct in 2018, c) in Aug-Oct in 2026 and d) in Aug-Oct in 2045.

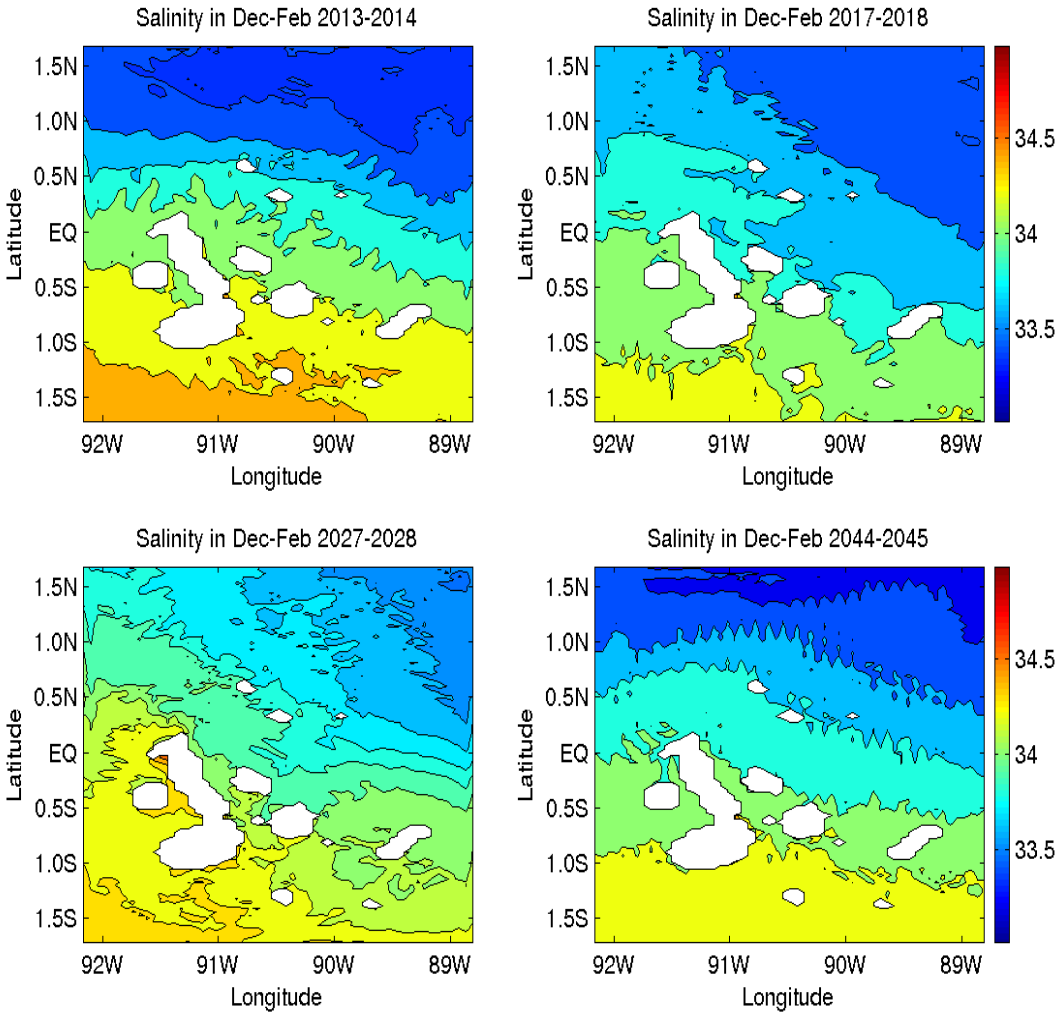

Figure 17: Sea surface salinity around the GMR during the El Nino cases: a) in Dec-Feb in 2013-2014, b) in Dec-Feb in 2017-2018, c) in Dec-Feb in 2027-2028 and d) in Dec-Feb in 2044-2045.

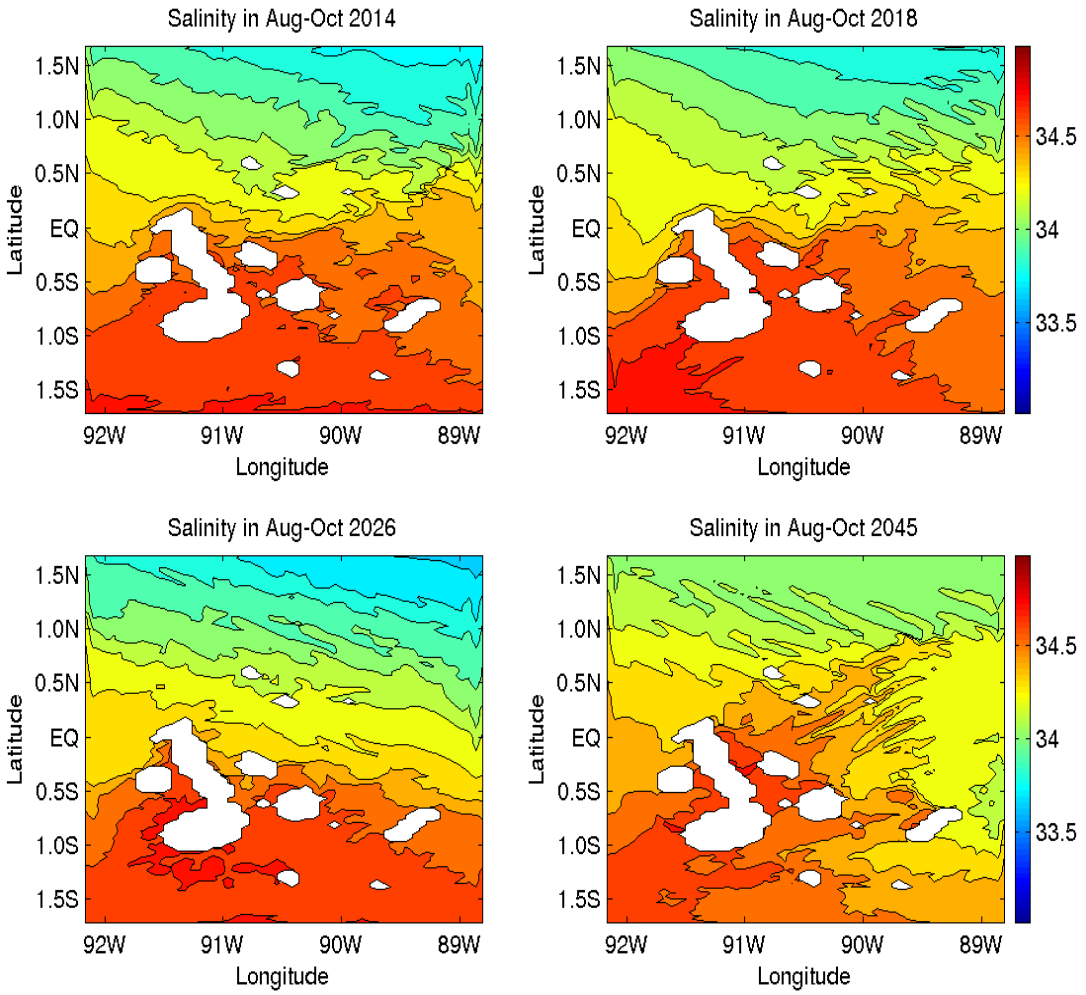

Figure 18: Sea surface salinity around the GMR during the La Nina cases: a) in Aug-Oct in 2014, b) in Aug-Oct in 2018, c) in Aug-Oct in 2026 and d) in Aug-Oct in 2045.

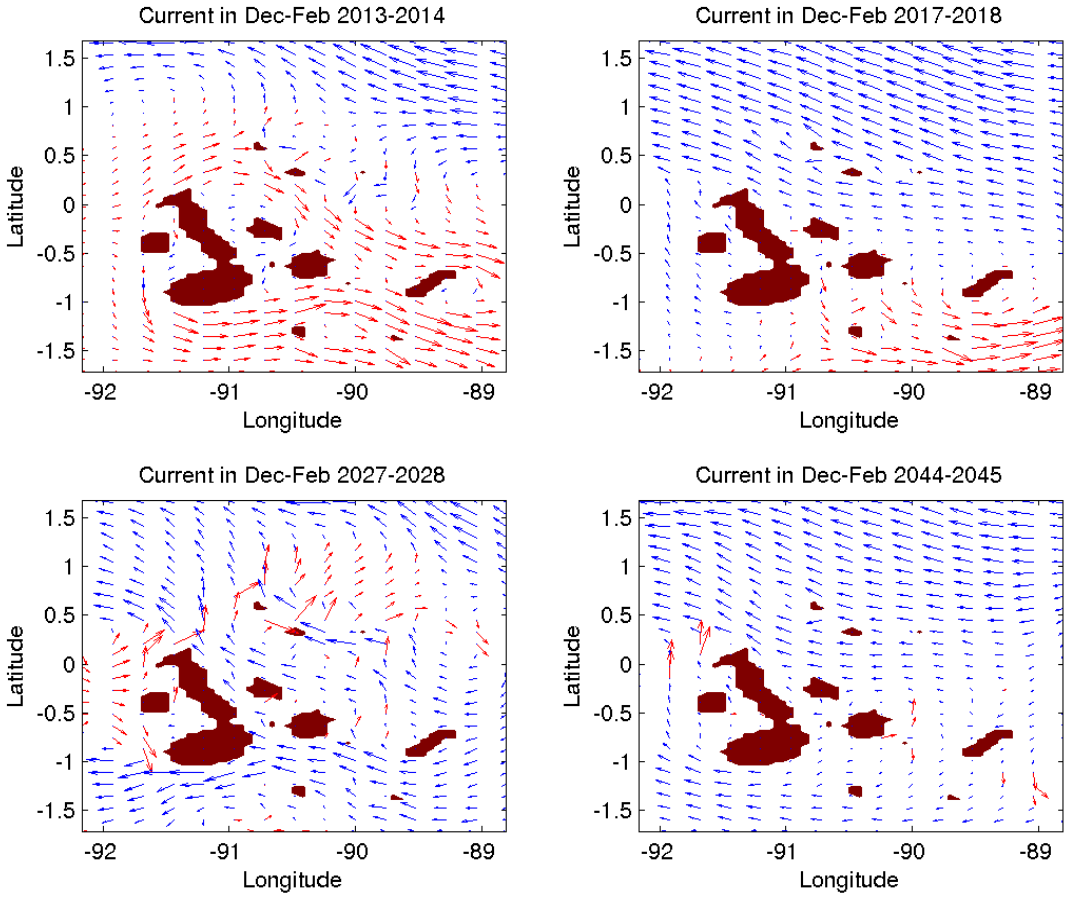

Figure 19: The surface current around the GMR during the El Nino cases: a) in Dec-Feb in 2013-2014, b) in Dec-Feb in 2017-2018, c) in Dec-Feb in 2027-2028 and d) in Dec-Feb in 2044-2045.

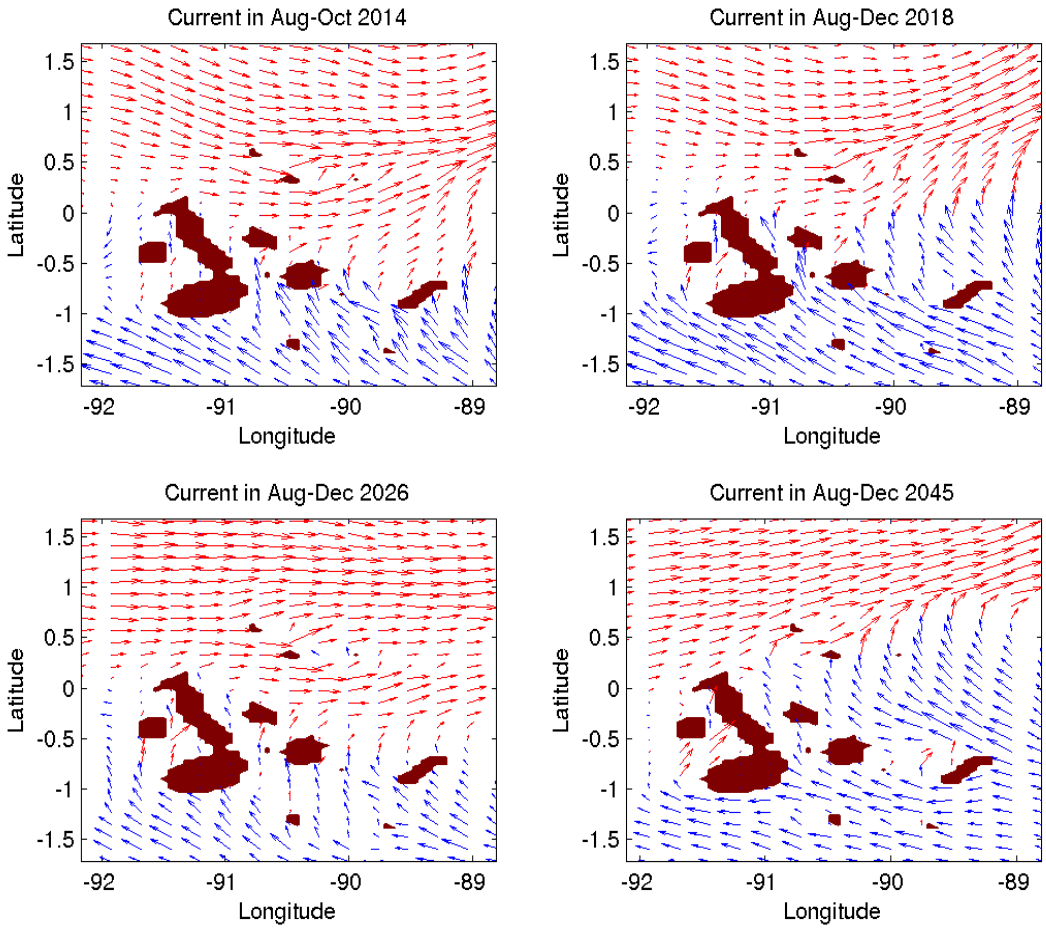

Figure 20: The surface current around the GMR during the La Nina cases: a) in Aug-Oct in 2014, b) in Aug-Oct in 2018, c) in Aug-Oct in 2026 and d) in Aug-Oct in 2045.

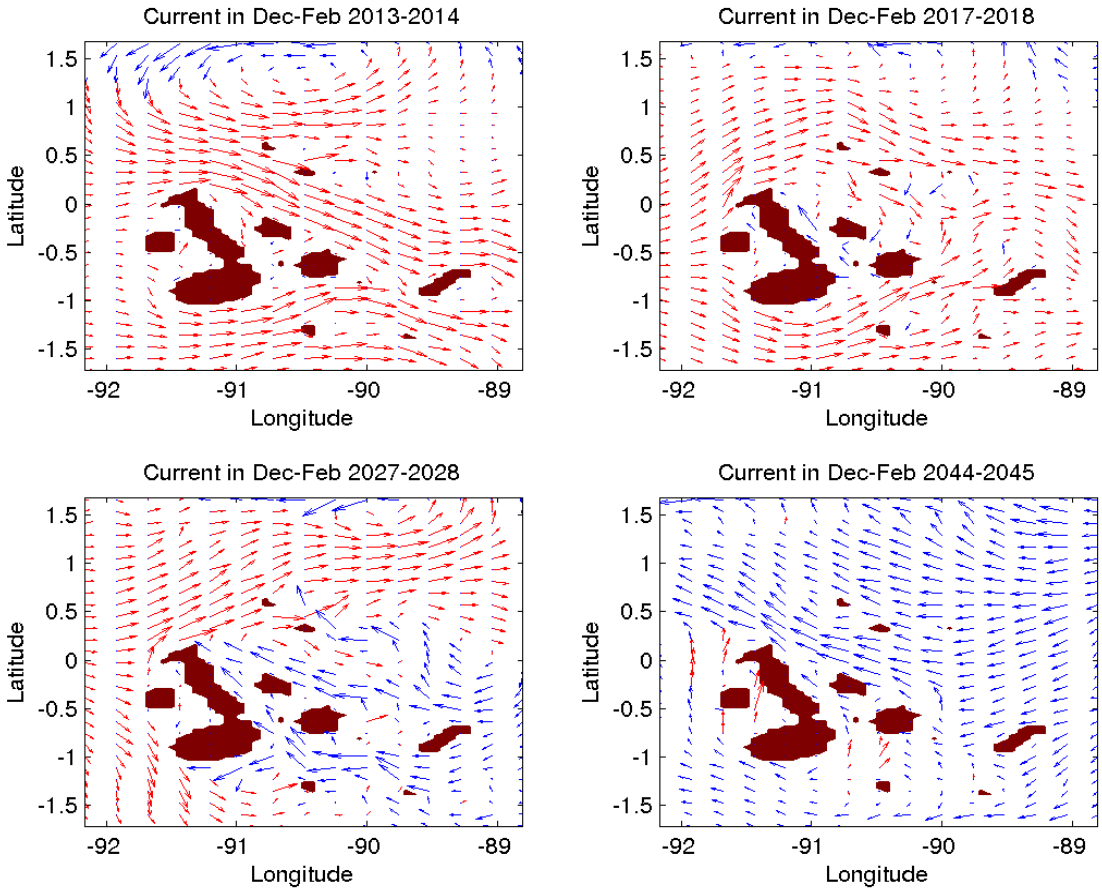

Figure 21: The current at 40m around the GMR during the El Nino cases: a) in Dec-Feb in 2013-2014, b) in Dec-Feb in 2017-2018, c) in Dec-Feb in 2027-2028 and d) in Dec-Feb in 2044-2045.

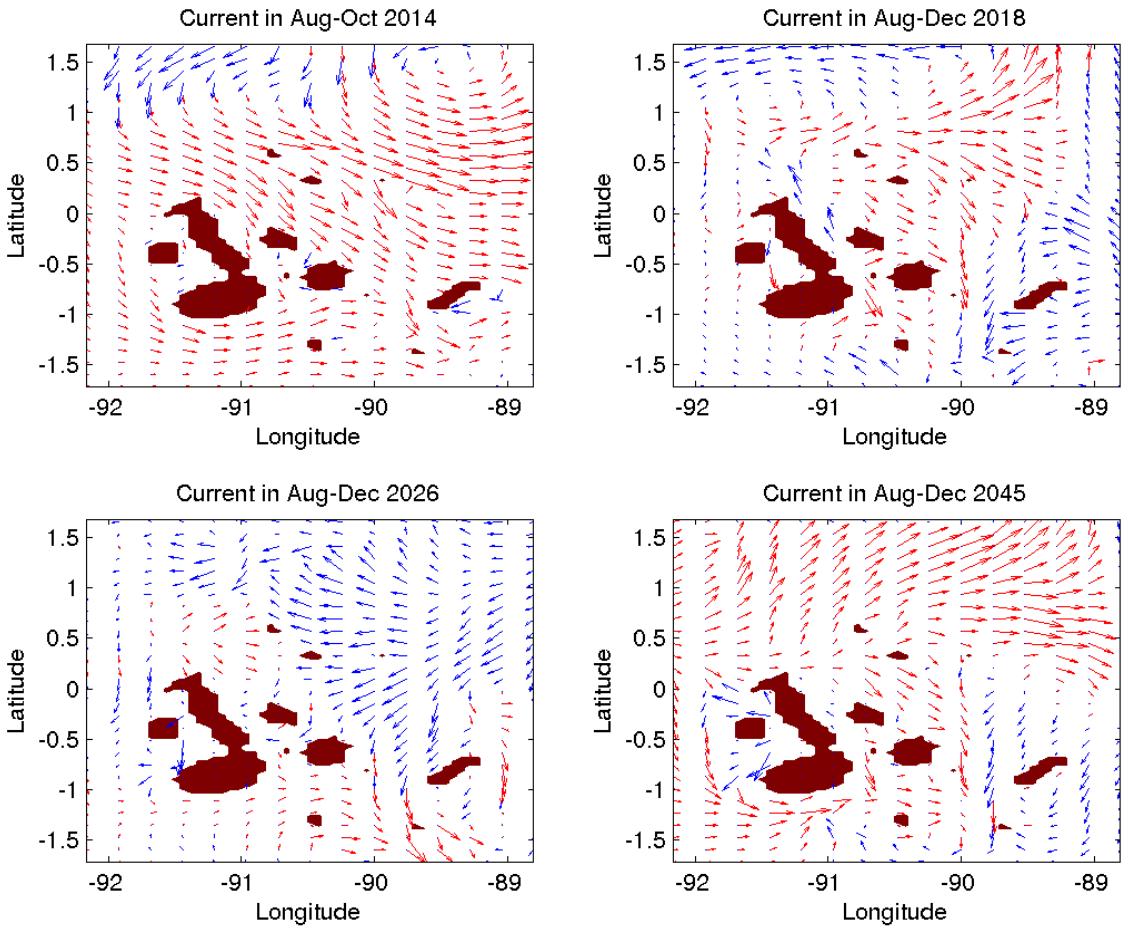

Figure 22: The current at 40m around the GMR during the La Nina cases: a) in Dec-Feb in 2013-2014, b) in Dec-Feb in 2017-2018, c) in Dec-Feb in 2027-2028 and d) in Dec-Feb in 2044-2045.

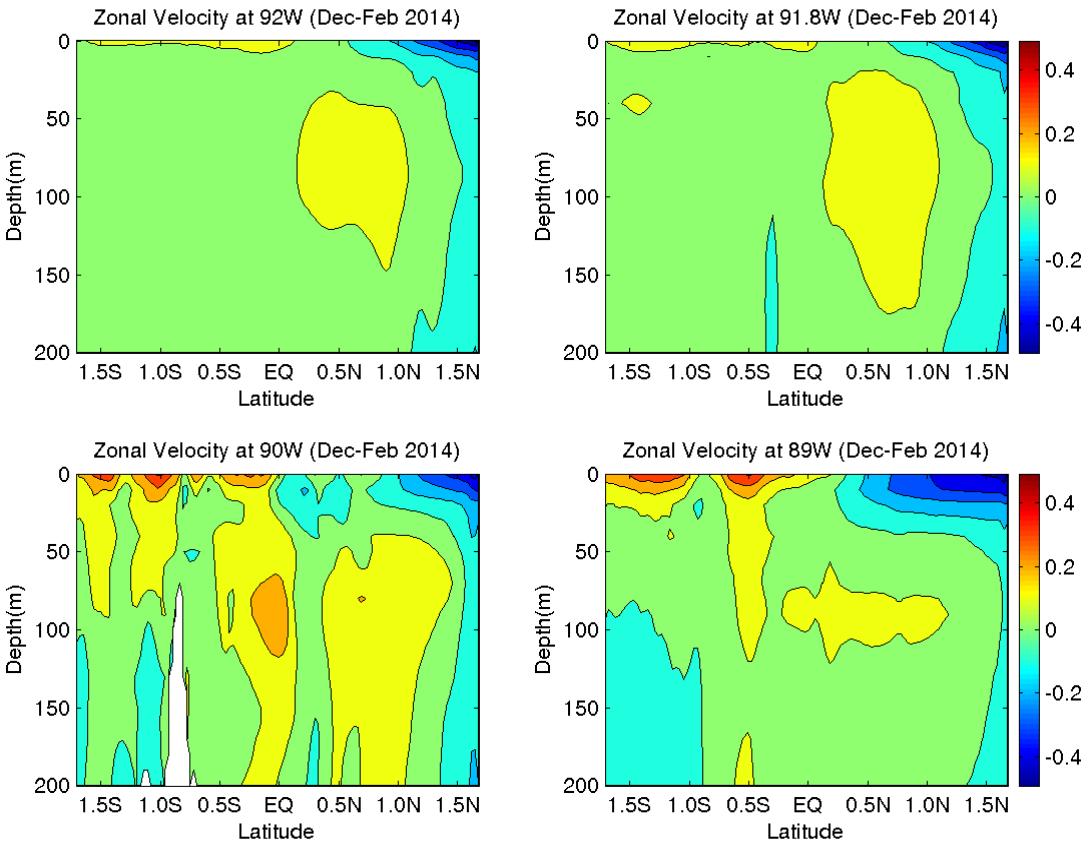

Figure 23: Vertical sections of zonal current (m/s) along 92W, 91.8W, 90W and 89W for the upper 200 m around the GMR in Dec-Feb 2014 El Niño event.

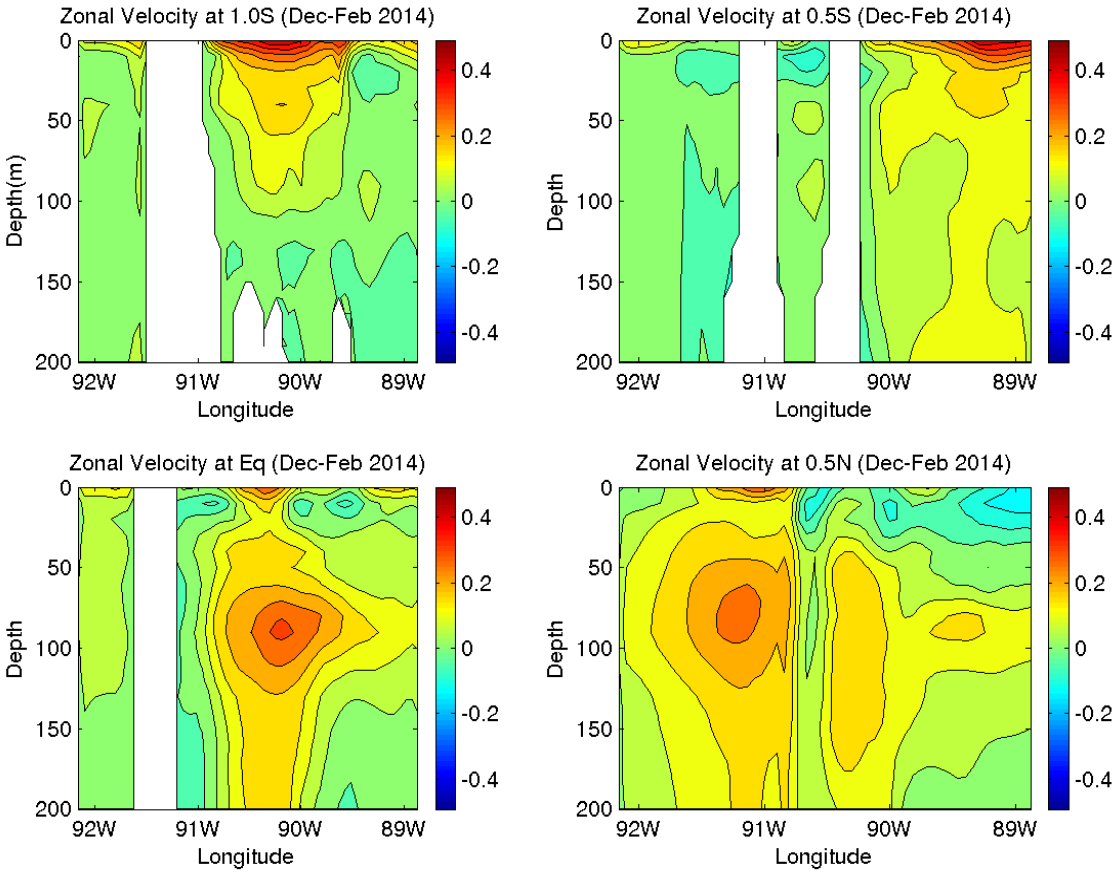

Figure 24: Vertical sections of zonal current (m/s) along 1S, 0.5S, EQ and 0.5N for the upper 200 m around the GMR in Dec-Feb 2014 El Niño event.

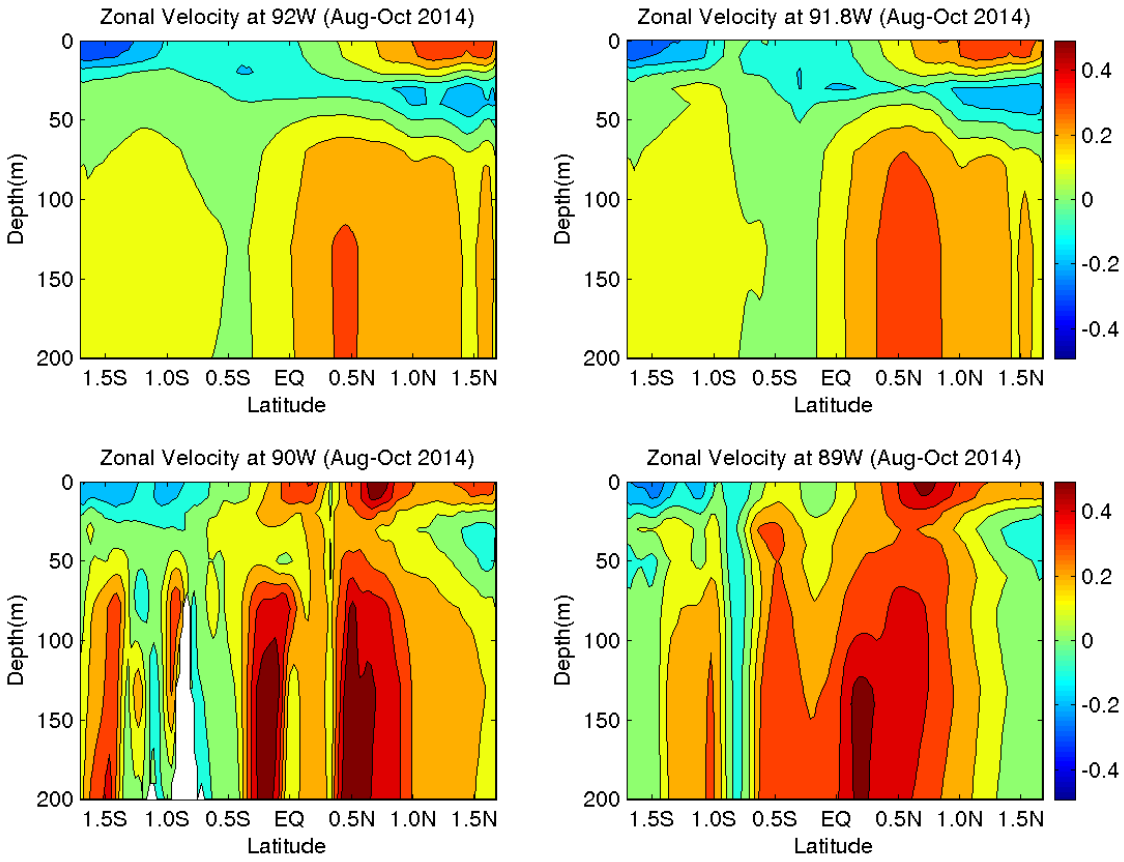

Figure 25: Vertical sections of zonal current (m/s) along 92W, 91.8W, 90W and 89W for the upper 200 m around the GMR in Aug-Oct 2014 La Niña event.

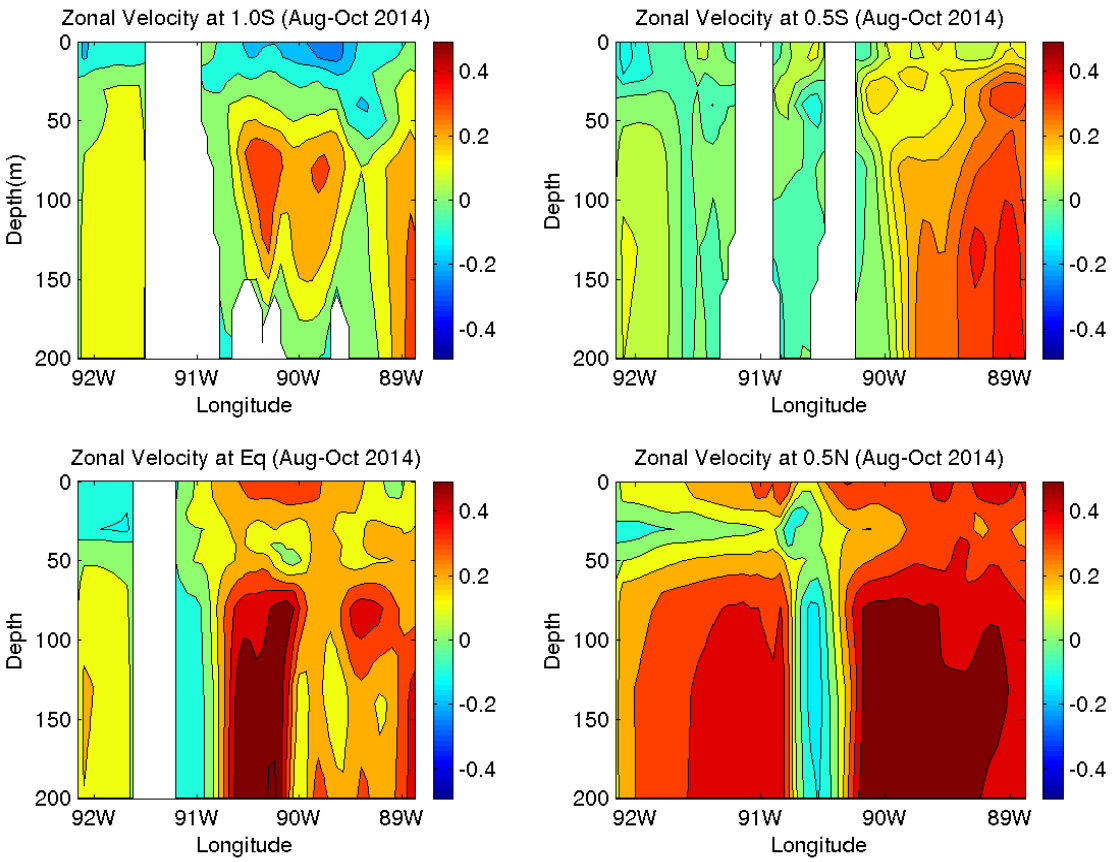

Figure 26: Vertical sections of zonal current (m/s) along 92W, 91.8W, 90W and 89W for the upper 200 m around the GMR in Aug-Oct 2014 La Niña event.

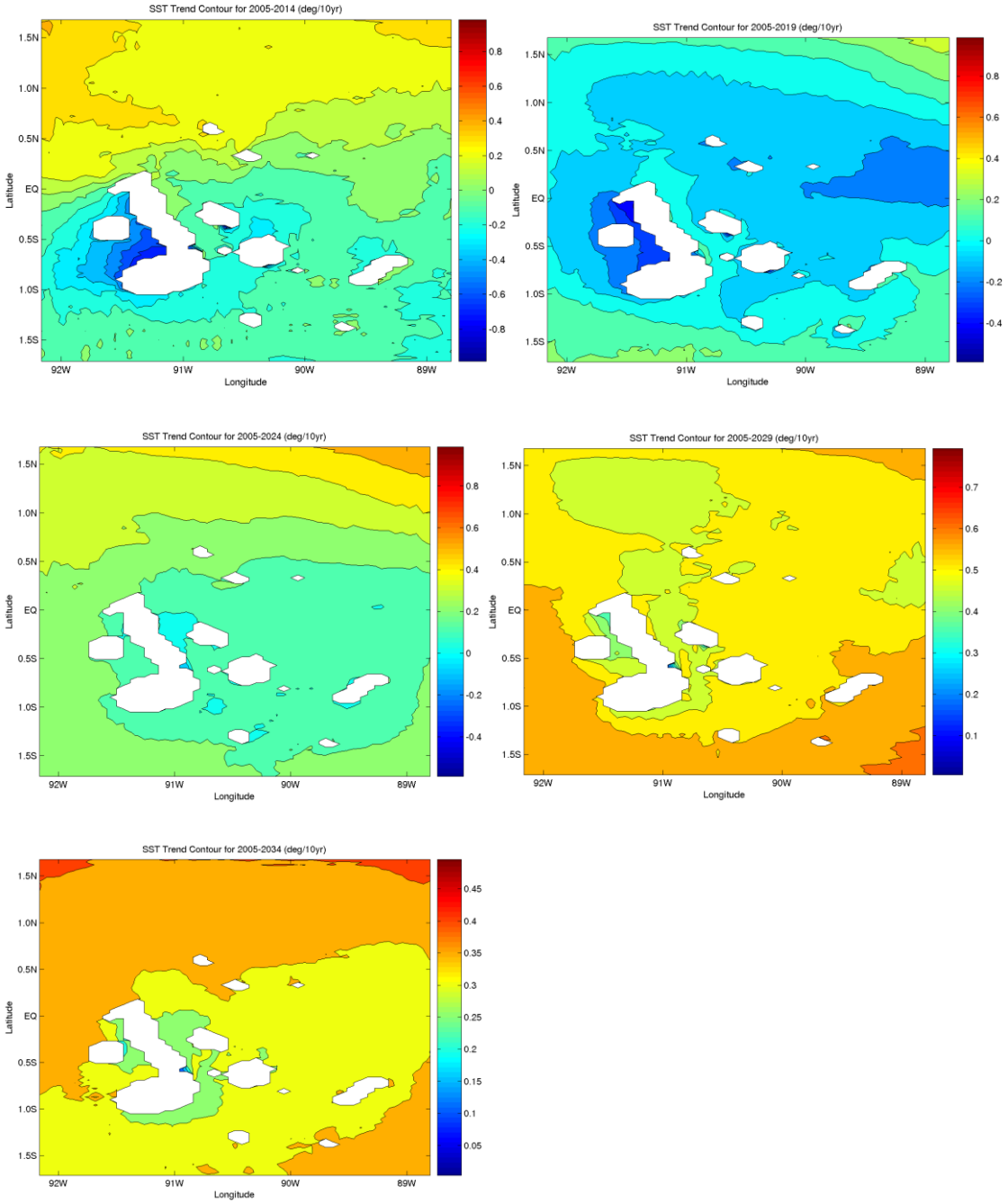

Figure 27: The SST trend contour around GMR for a) 10yr from 2005-2014, b) 15yr from 2005-2019, c) 20yr from 2005-2024, d) 25yr from 2005-2029 and e) 30yr from 2005-2029.

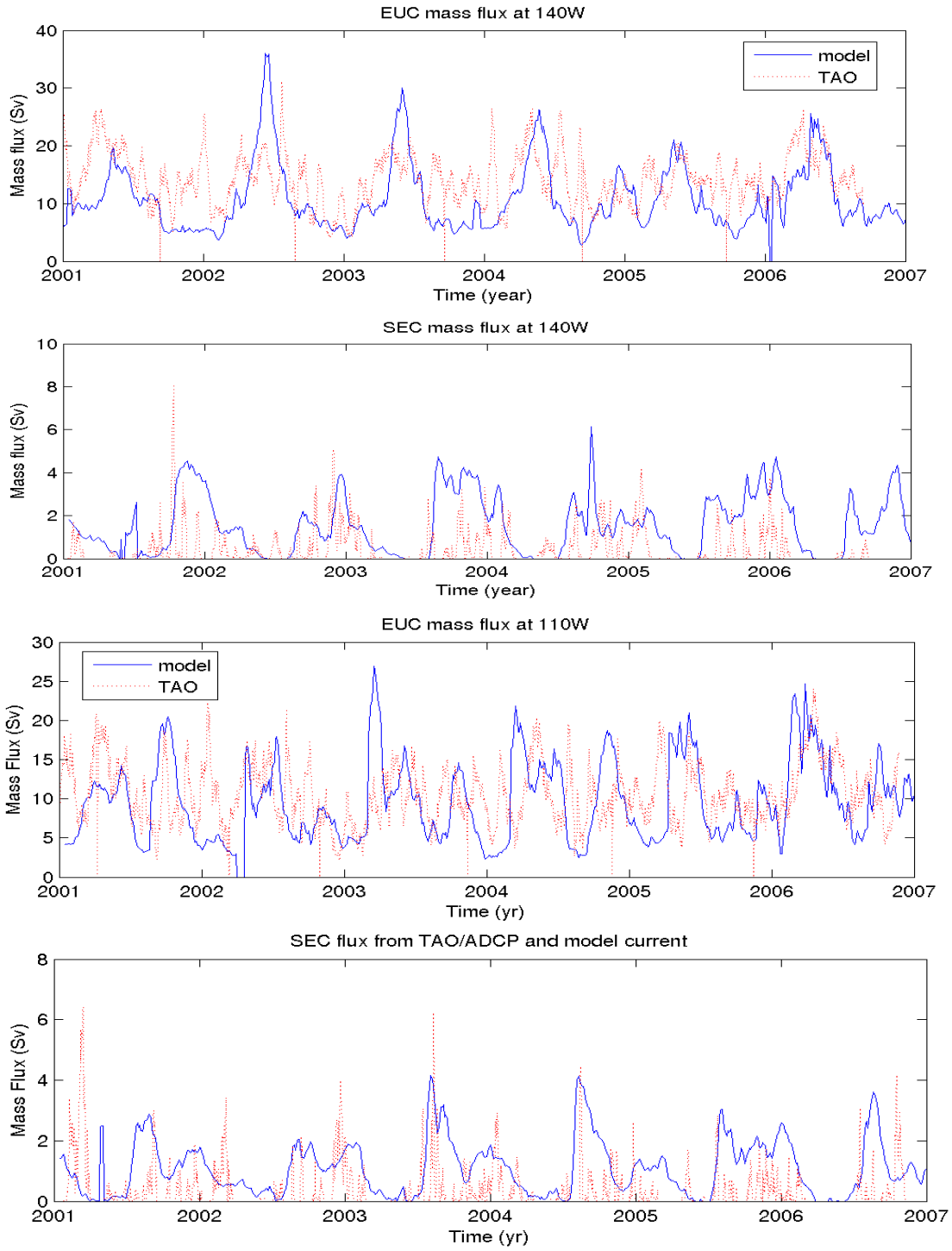

Figure 28 the compared model and TAO EUC (SEC) volume flux transport at 140 ºW and 110 ºW.

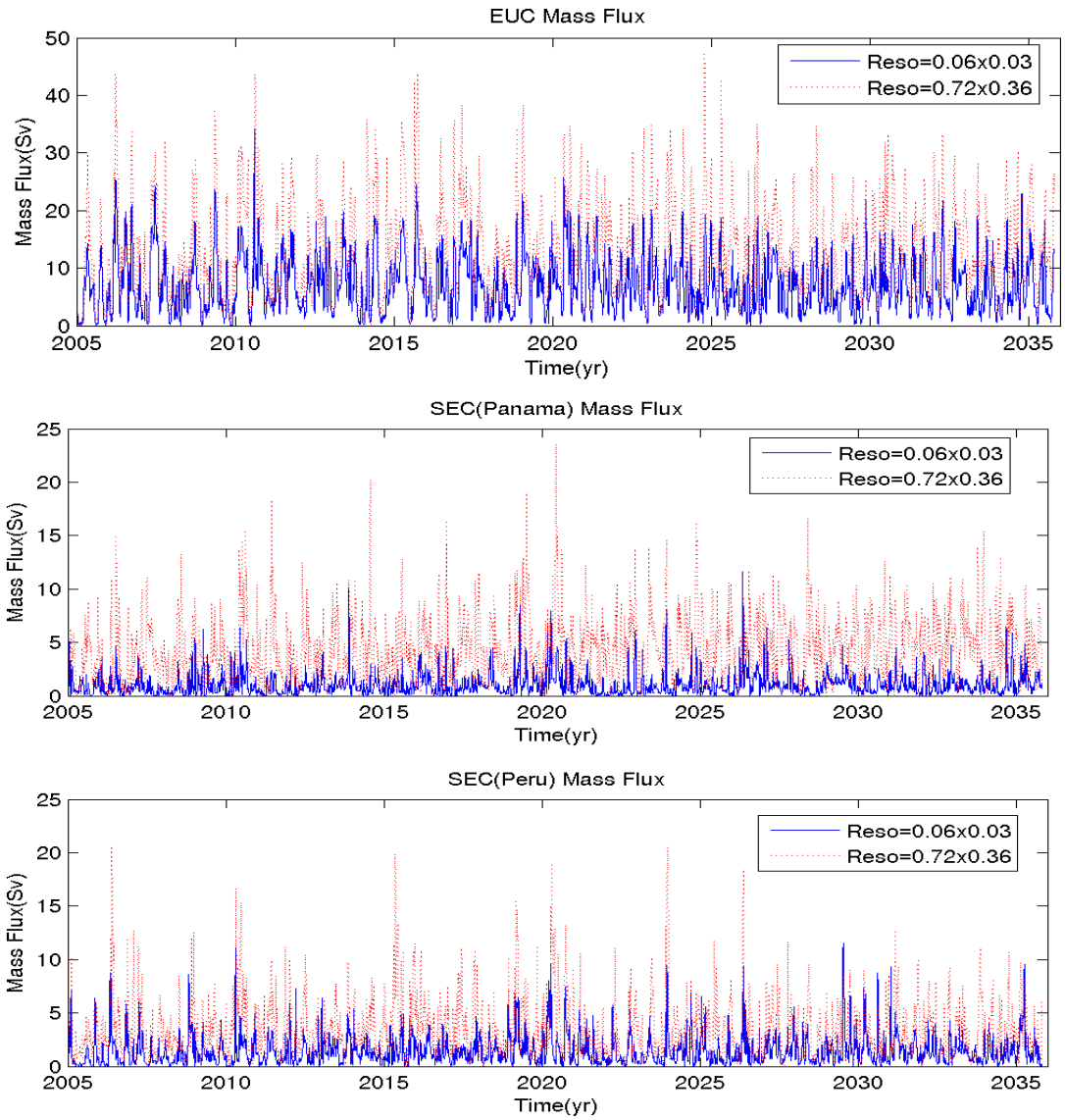

Figure 29: The simulated EUC, SEC (including Panama current and Peru Current) volume flux transport from 2005 to 2035 around GMR. The blue line is the simulated flux transport with a high resolution of 0.06x0.03, while the red line means the simulated flux transport with a relatively low resolution of 0.72x0.36.

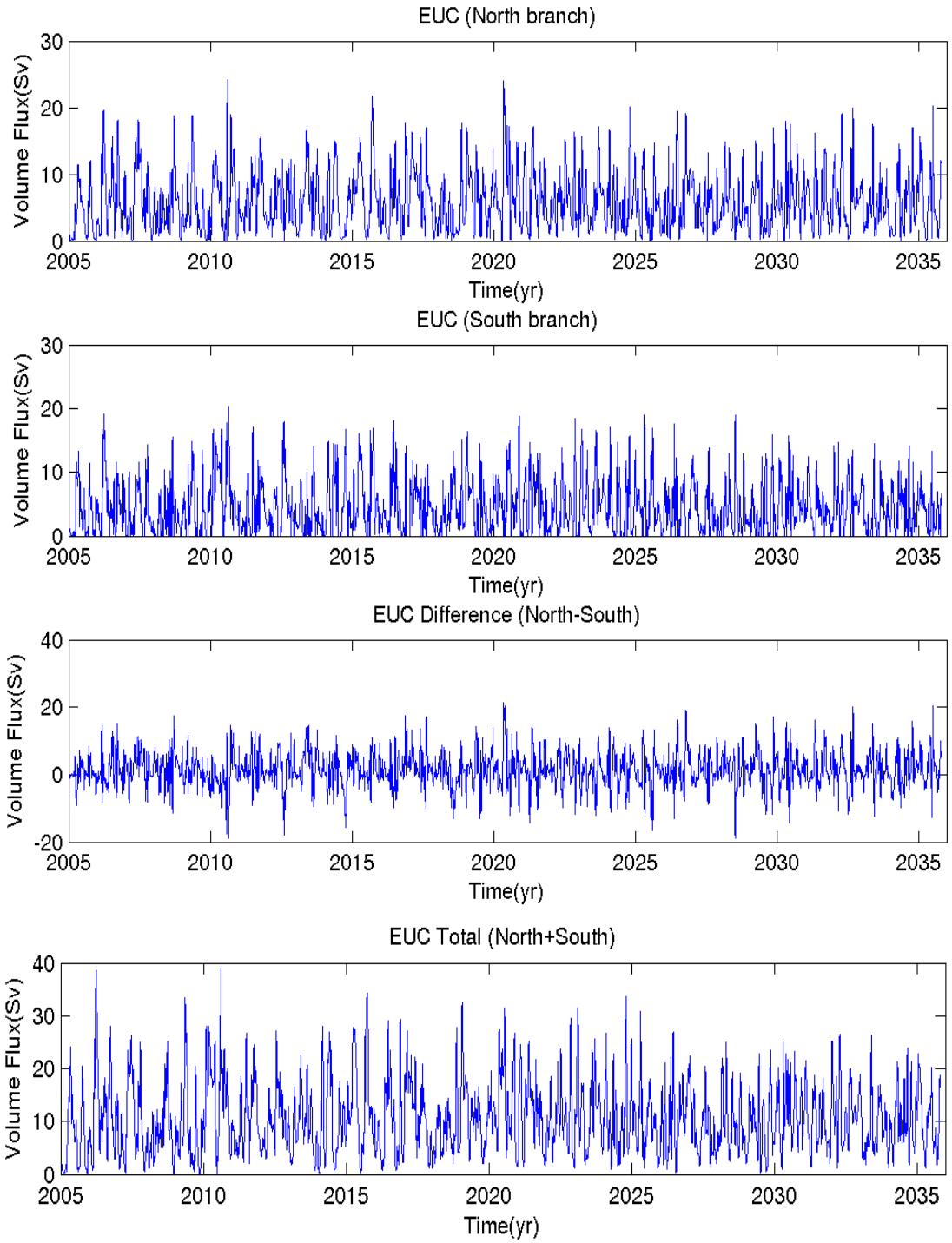

Figure 30: The a) north branch, b) south branch, c) difference between the north branch and the south branch, d) the whole (south + north) simulated EUC volume flux transport at 91.26W from 2005 to 2035 around GMR.

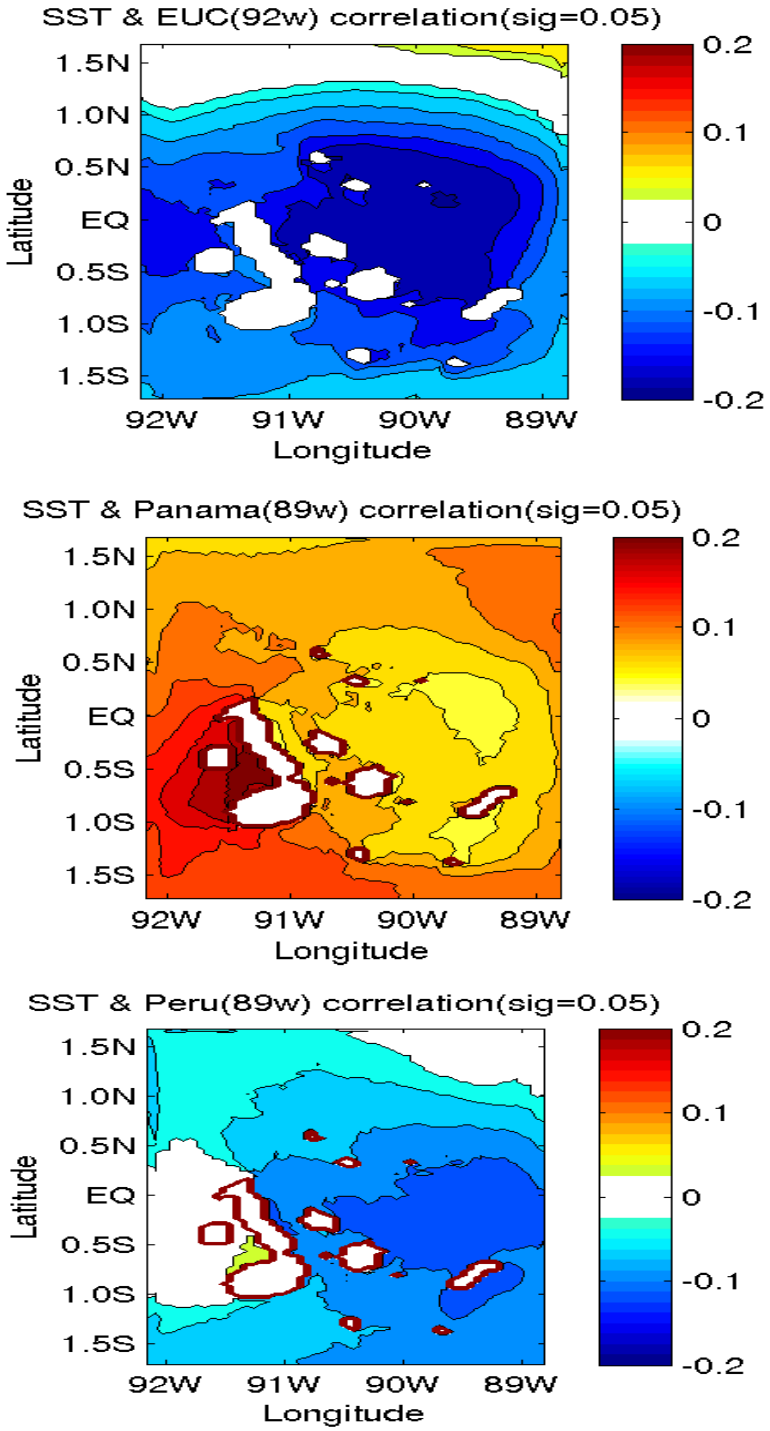

Figure 31: The contour of correlation coefficients between the simulated a) EUC, b) Panama Current, c) Peru Current volume flux transport under the low resolution of 0.72 x 0.36 degree and SST fields under the high resolution of 0.06 x 0.03.

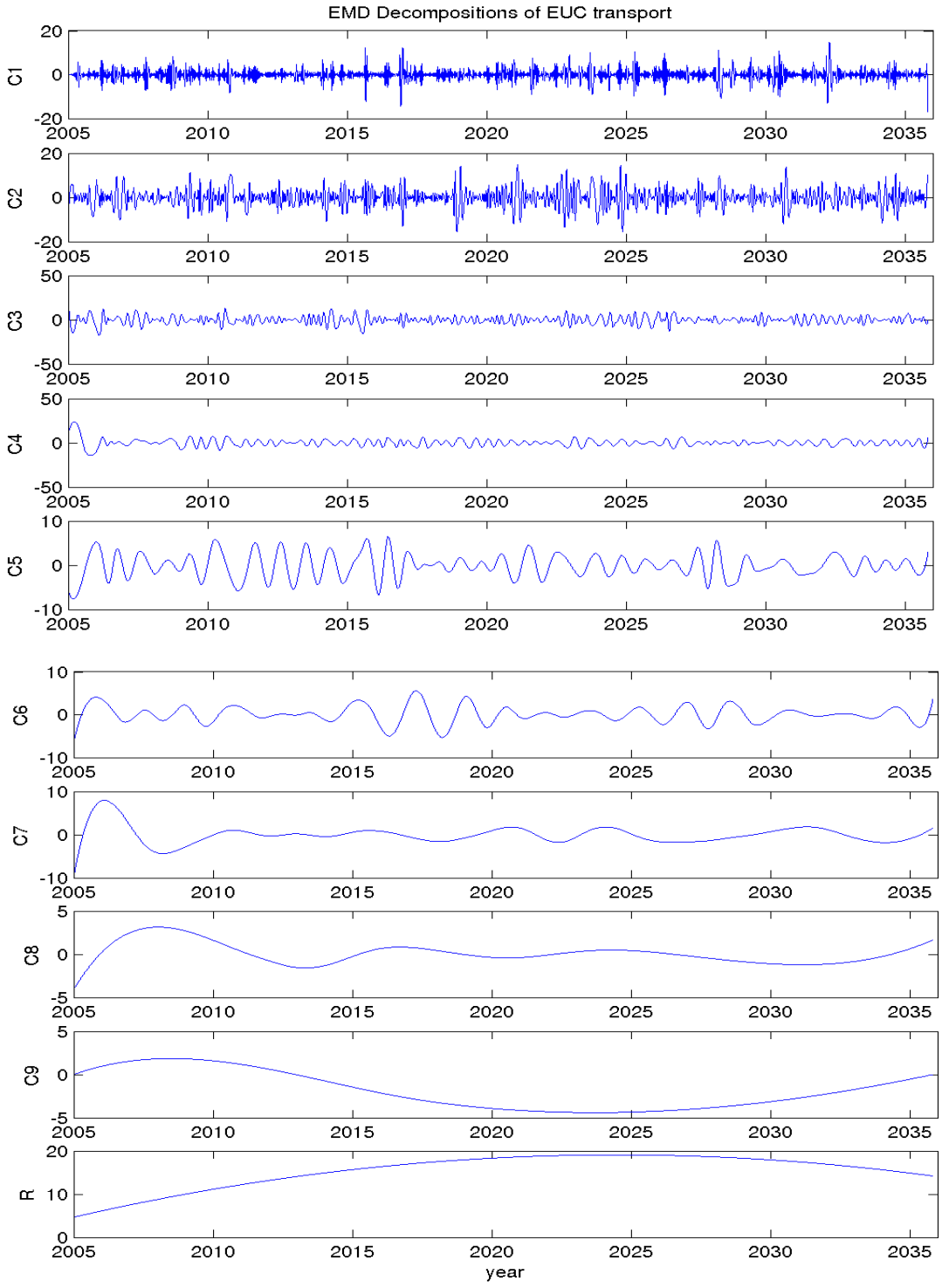

Figure 32: The intrinsic mode functions of the EUC volume flux transport (C1-C9).

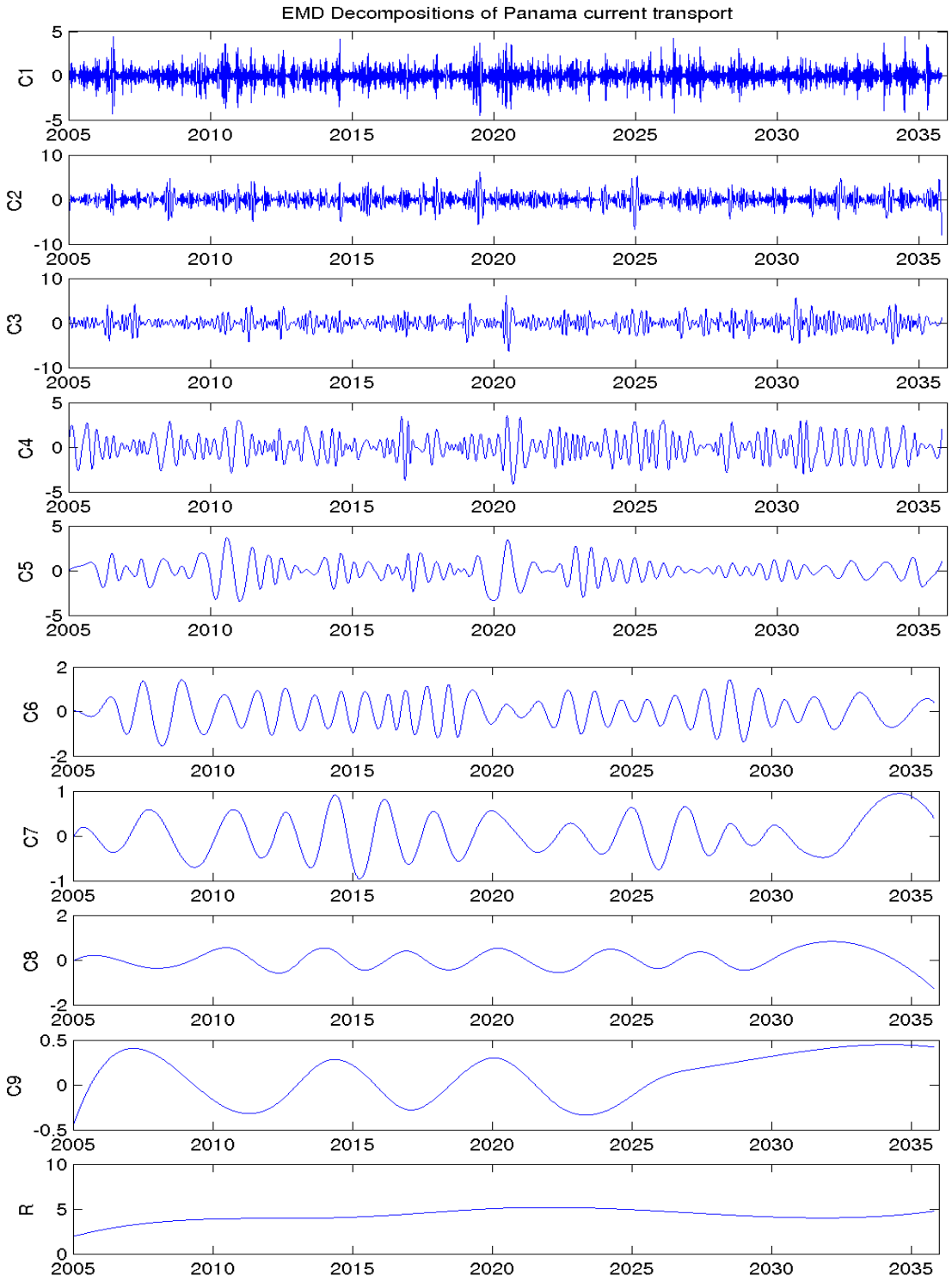

Figure 33: The intrinsic mode functions of the Panama Current volume flux transport (C1-C9).

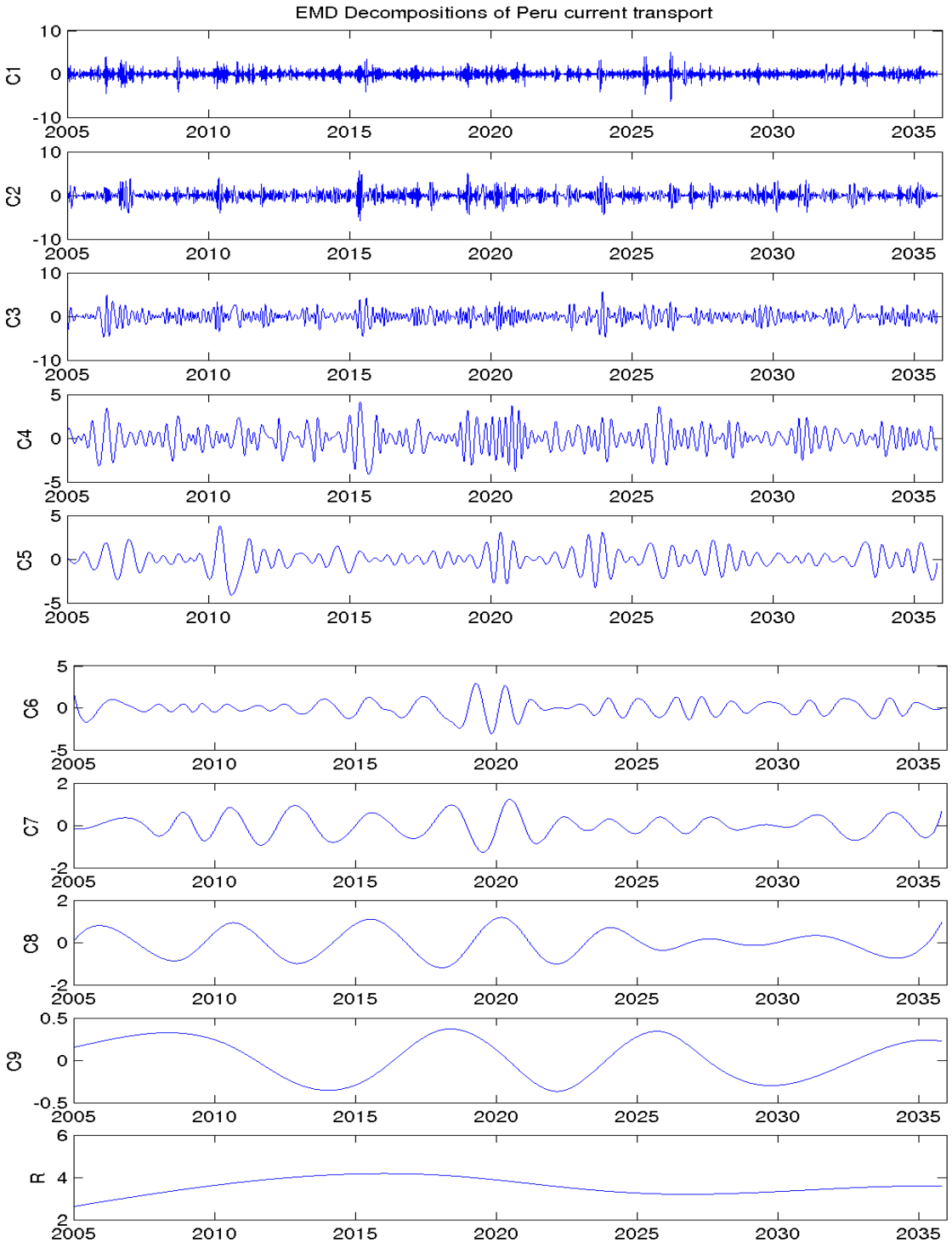

Figure 34: The intrinsic mode functions of the Peru Current volume flux transport (C1-C9).

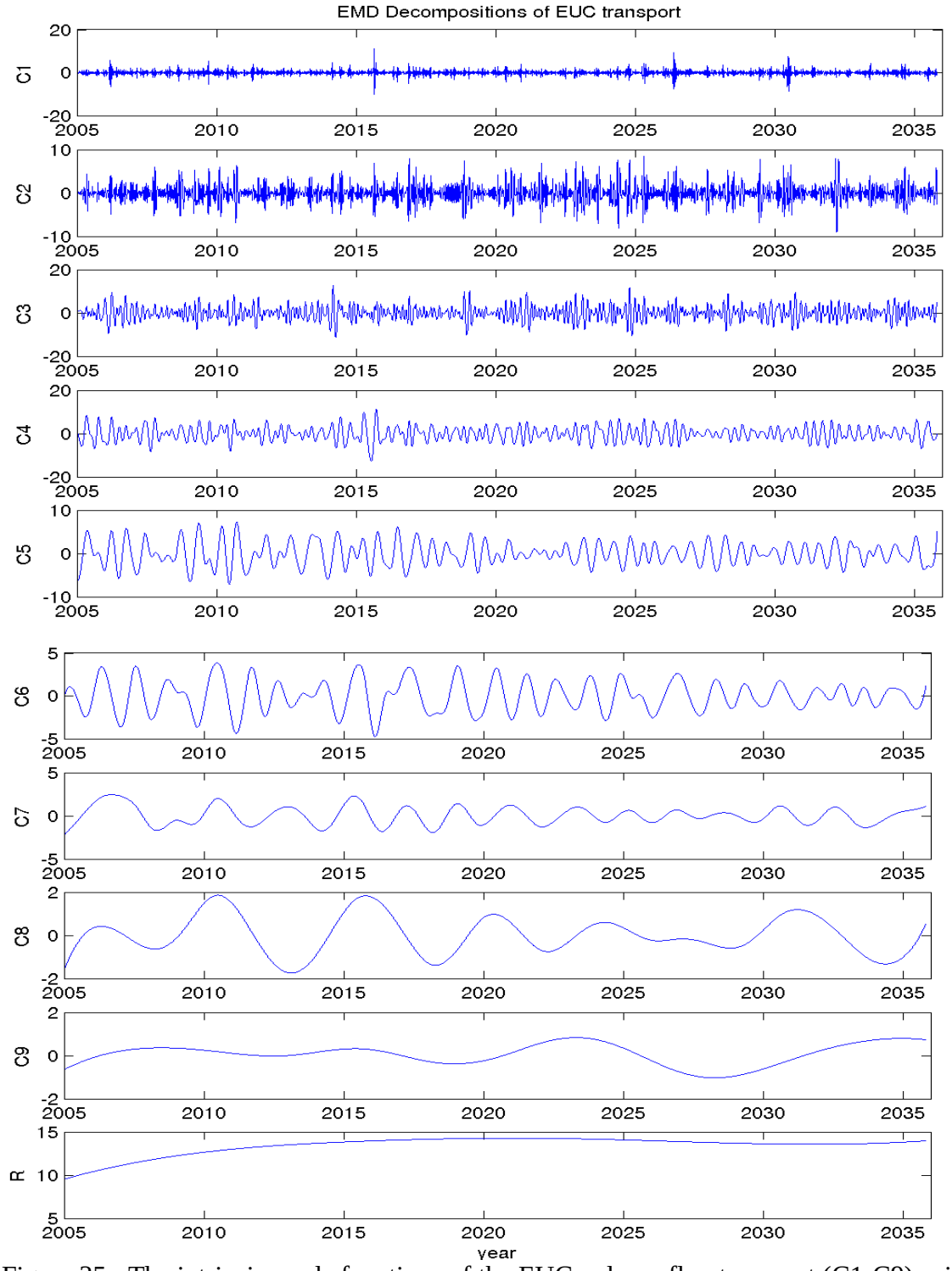

Figure 35: The intrinsic mode functions of the EUC volume flux transport (C1-C9) using EEMD (standard deviation is 0.4).

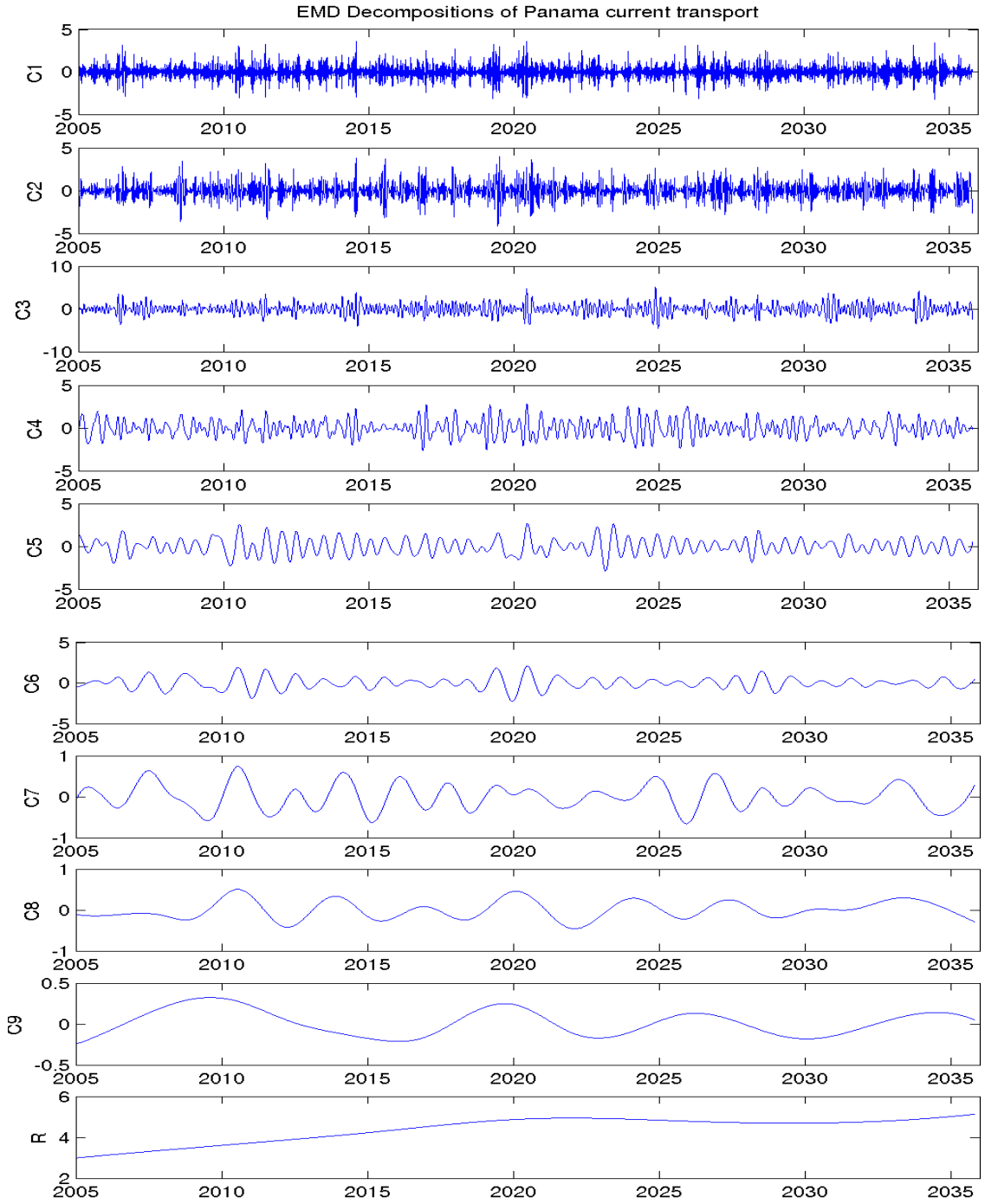

Figure 36: The intrinsic mode functions of the EUC volume flux transport (C1-C9) using EEMD (standard deviation is 0.4).

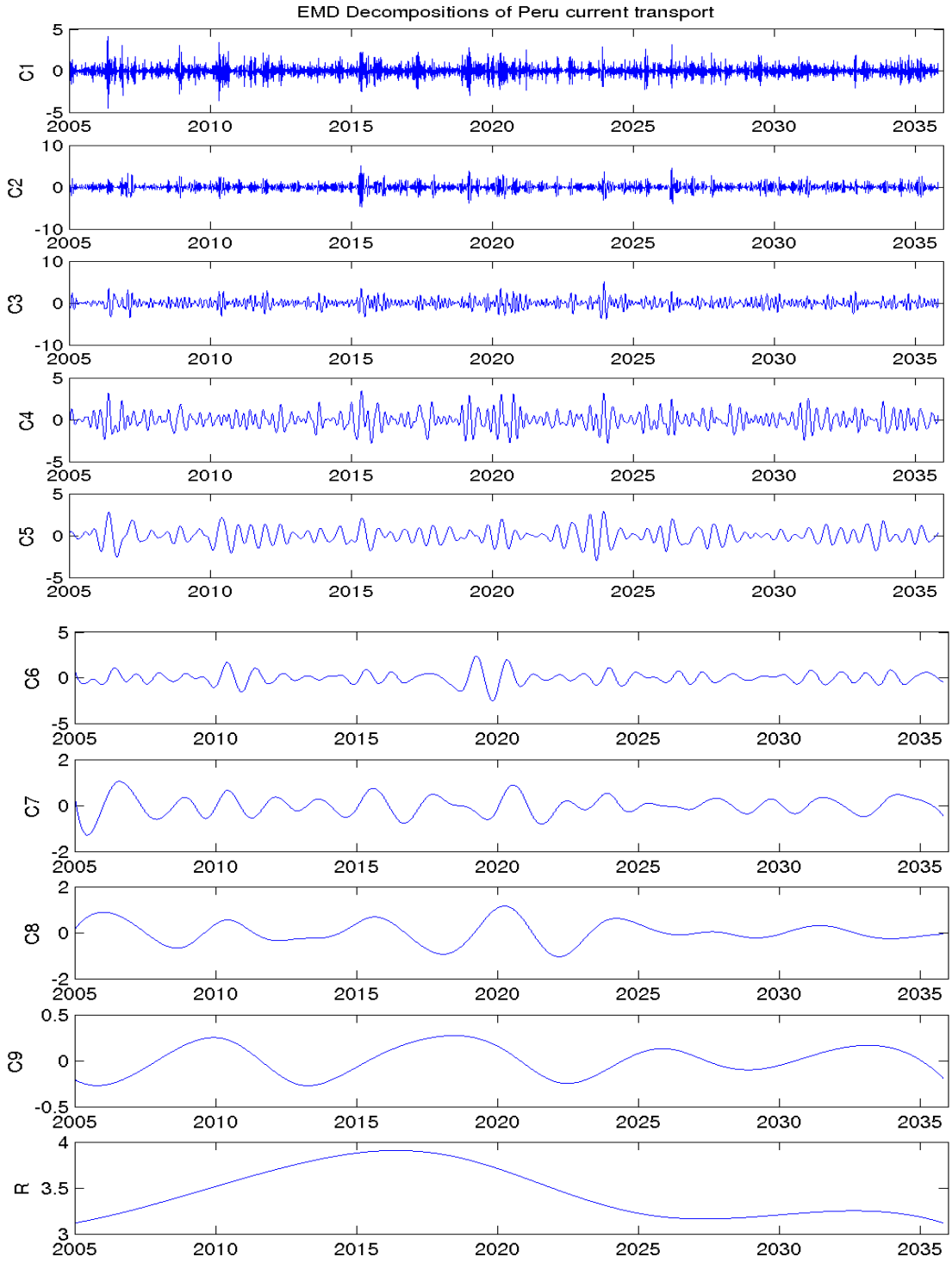

Figure 37: The intrinsic mode functions of the EUC volume flux transport (C1-C9) using EEMD (standard deviation is 0.4).

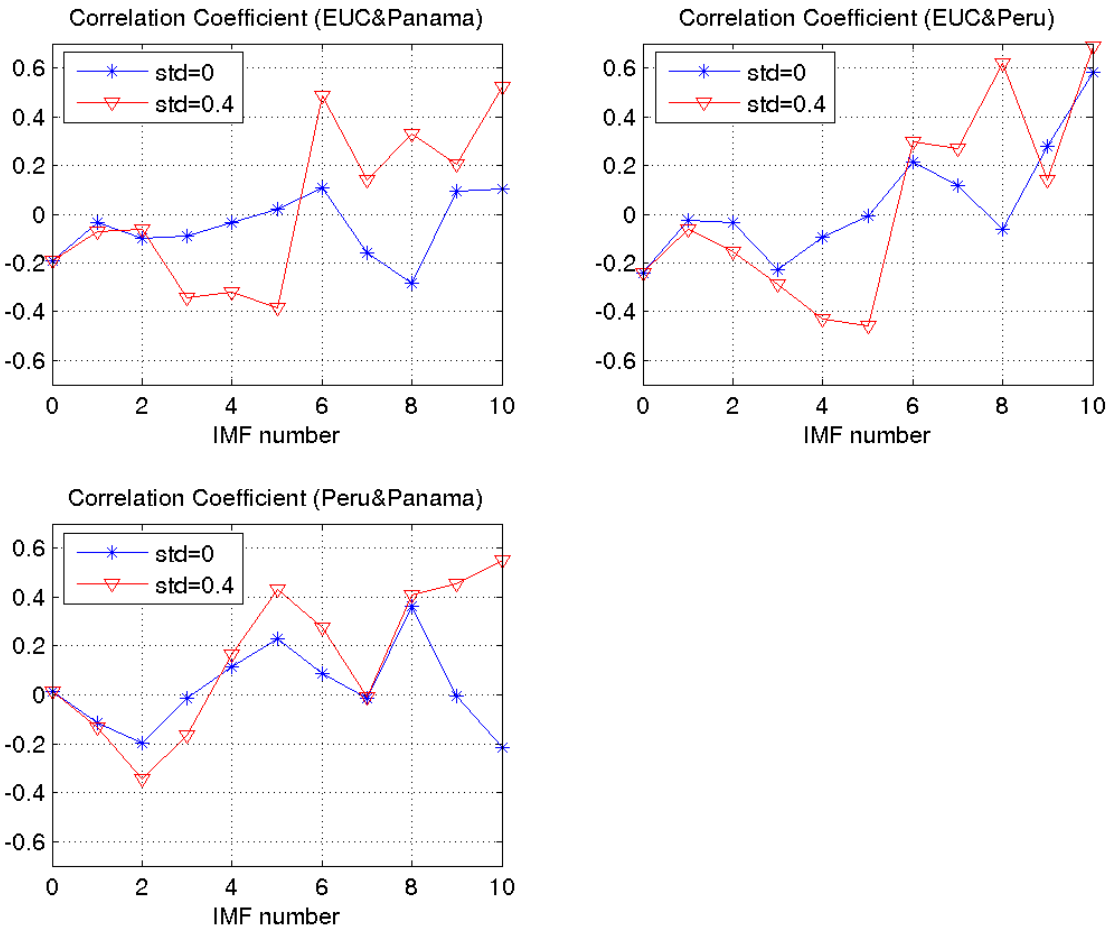

Figure 38: The intrinsic mode functions of the EUC volume flux transport (C1-C9).

Chapter 7

Concluding Remarks and Future Work

1. Concluding Remarks

The ocean circulation around the Galápagos Archipelago is simulated using the University of Miami's Hybrid Coordinate Ocean Model (HYCOM) using a high-resolution (.04 degree resolution) nested domain. The model generally reproduces the major ocean circulation features around the Galapagos showing that the 0.04 degree resolution is sufficient for studying the circulation and water mass structure local to the Galápagos. A variety of winds forcing were tried with high frequency wind forcing (daily, 6-hrly) proving to be more reliable than the monthly forcing. The Archipelago has a large range in temperature and salinity associated with four different current systems and topographically and wind forced upwelling. West of Isabella and Fernandina Islands are the largest and most consistent upwelling zones, resulting from the collision of the Equatorial Undercurrent with the islands, bring relatively colder and salty waters to the surface in a region of topographically induced upwelling. This upwelling zone marks the location of high biological production at the surface with the EUC shoaling to approximately 20m from its normal depth of 50m just to the west of the islands. This results not only a strong upwelling zone just to the west of the islands, but also in shallow mixed layers over the entire western portion of the Archipelago. The model results, which agree quite well with observations of the EUC by the TAO array, show a

seasonal cycle in the speed and transport of the EUC, reaching a maximum during the late spring/early summer and minimum in the late fall. This seasonal cycle is disrupted during El Niño when the collapse of the westerlies results in a greatly weakened to a total lack of the undercurrent. The far northern region of the Archipelago is characterized with warmer, fresher water and had the deepest mixed layer depth as a result of Panama Current waters from the northeast. The water masses over the remainder of the region result from a mixing of cool Peru Current waters and upwelled Cold Tongue waters entering from the east to the southeast mixing with the upwelled EUC waters.

The regional impact of global climate change on the ocean circulation and water mass characteristics around the Galápagos Archipelago is studied using the Hybrid Coordinate Ocean Model (HYCOM). A four-level nested-domain system is used in the study to downscale the global climate change impact to the regional scale centered on the Galapagos Archipelago. First, the ocean circulation driven by the past and current climate is simulated using HYCOM with daily atmospheric forcing derived from the NCEP/NCAR reanalysis dataset for the period of 1951-2007. The result indicates that with prescribed atmospheric forcing, the major characteristics of the ocean circulation and its variability in the Galapagos region, including the ENSO events, annual and seasonal cycles, upwelling system, local and regional current systems, and tropical instability waves, can be reproduced by the nested HYCOM.

The response of the ocean circulation in the Galapagos region to future climate change scenarios is studied using the IPCC AR4 SRES A1b scenario as an example. The results

show that the oceanic variability in the Galapagos region is sensitive to global climate change. However, the regional impact of global climate change in the Galapagos region varies from region to region. The SST trend is also dependent on the time scales. The upwelling region has the lowest warming trend, and occasionally experiences a decreasing trend at decadal time scales. This indicates that the upwelling zone may be less affected by global warming compared with other regions. Power spectrum analysis shows that the frequency for the occurrence of ENSO events seems unchanged (4-5yr) by climate change, while the amplitude of ENSO events is increased. for the El Niño cases, the EUC will be greatly weakened, leading to weaker upwelling to the west of Isabella Island. While during the La Niña event, the EUC will be greatly strengthened and the EUC may come up to the sea surface. The EUC core is located around 0.5˚N. The volume transport variations in the entire equatorial band of the Pacific and in its eastern part are quantified using both in situ data and an ocean general circulation model, in which the current data from the TAO/TRITON moorings and simulated current at the equator are compared. The north branch of the EUC accounts for the most (58%) of volume transport. The effect of different currents (EUC, Panama and Peru) on different areas of the Galapagos Archipelago is studied. The results show that the western Galapagos upwelling region is affected mainly by the EUC and Panama currents; while central/east Galapagos is predominantly affected by both Peru and EUC currents. The north region is affected by the Panama Current only. The southeast region is affected by Peru Current only. These regional differences explain the variability of the responses in different regions of the Galapagos Archipelago to global climate change. These regional

differences explain the variability of the responses in different regions of the Galapagos Archipelago to global climate change. However, a limitation of the assessment is that it is based on one IPCC scenario only. A more reliable way to assess regional response to climate change is to estimate the range of responses using ensemble approach.

2. Future Work

1) Coupled Physical –Biological Modeling

As an integral part of recent large-scale observational programs such as JGOFS (Joint Global Ocean Flux Study) and GLOBEC (Global Ocean Ecosystems Dynamics), models have been developed to simulate biogeochemical cycling in specific oceanographic regions. As part of the Regional Ecosystem Modeling 'Testbed' Project (Friedrichs et al., 2006), inter-comparisons are being carried out to critically examine which ecosystem structures and formulations are best able to simulate observed data across regions. One of the regions that have been studied in this program is the IronExII region around the Galápagos (Coale et al., 2006). Initial results have indicated that a simple NPZD models can fit data well at individual sites such as the Galápagos.

Wiggert et al. (2004) conclude that at present the greatest challenge in understanding the biogeochemistry of the Arabian sea appears to be understanding and reproducing in models the observed levels of physical variability (e.g., upwelling and rapid mixing events, filaments and mesoscale eddies). They show that these higher frequency physical

processes are directly responsible for the major biogeochemical events that are, in turn, responsible for a large fraction of the annual production and export fluxes. Until these processes are resolved and their biogeochemical effects accounted for, our understanding of Arabian Sea biogeochemistry will be severely hampered. Hood *et al.* (2003) go on to say that changes in the physical environment result in more drastic changes in the resulting phytoplankton distributions in their coupled model studies than those incurred by varying the degree of ecosystem model complexity. Therefore, rather than starting with a more complicated ecosystem model, such as the 10 compartment model of Chai et al. (2002), future work of the biological variability associated with the physical oceanographic setting around the GMR should be studied using a Nutrient-Phytoplankton-Zooplankton-Detritus (NPZD) ecosystem model coupled to a hydrodynamic model that will resolve the observed scales in physical variability within the GMR.

The physical model system described above will be used to determine the three dimensional motions of water within the oceanic domain; the dynamics are forced by meteorological and tidal influences. The inclusion of tides is important in this study since the dynamics within the islands are essentially the same as in a coastal environment, therefore the tides can have important implications regarding larval dispersal (Wolanski and Spagnol, 2000). Within the sub-domain of the GMR, the model domain has a grid size of 0.04 ° x 0.02 ° (about 4.45 km x 2.21 km) that is centered on the GMR (92.16 ° W - 88.96 ° W, 1.68 ° S - 1.68 ° N). Within this domain the model has a

vertical resolution of 26 layers that stretch or shrink vertically as a function of total depth according to the hybrid coordinate frame discussed above. The fine resolution within the GMR and will provide pathways and current dynamics to be used in the biological components of the model system. The set z-coordinate layers in the hybrid model facilitate the addition of vertical migration behavior between layers over short distances (10s of meters) in the biological models.

The physical oceanic dynamics generated by HYCOM may be used as the environmental framework for driving coupled biological models. A working version of a general Nutrient-Phytoplankton-Zooplankton-Detritus (NPZD) ecosystem model has been successfully interfaced to HYCOM (Oschlies 2001). The NPZD model will act as food source for key larval species under study. The NPZD ecosystem model is directly coupled to and runs simultaneously with the physical model using the same scheme used to drive the temperature/salinity. That is, the NPZD domain is developed and runs in Eulerian space as coupled conservation advective-diffusive equations in addition to community dynamics equation components (Olascoaga et al., 2005). The unique feature of this NPZD model is the temperature dependent physiological process functions added to both the P and Z compartments of the coupled ecosystem model.

The nutrient- phytoplankton- zooplankton – detritus (NPZD, Oschlies 2001) will be used to simulate the biological response to physical forcing. In the most general form, the NPZD model is coupled to a physical model through the advection-diffusion equation.

Each state variable of the NPZ model will have a separate equation describing its motion in space and time, of the form

$$\frac{\partial C}{\partial t} + u\frac{\partial C}{\partial x} + v\frac{\partial C}{\partial y} + (w + w_s)\frac{\partial C}{\partial z} = K_h(\frac{\partial^2 C}{\partial x^2} + \frac{\partial^2 C}{\partial y^2}) + K_V\frac{\partial^2 C}{\partial z^2} + sms(C) \quad (6.1)$$

where C is the concentration of the state variable (N, P, Z, etc), u, v and w are the horizontal and vertical water velocities determined by the physical model, w_s is the vertical swimming or sinking speed of the state variable, and K_h and K_v are the horizontal and vertical eddy diffusivities. The last term is the source-minus-sink term due to biological activity. The *u*, *v* and *w* are obtained from the physical model run (HYCOM) simultaneously with the biological dynamics. All four ecosystem compartments are transported passively by advection and diffusion.

A great deal of attention must be placed on parameter choices. The initial simulations have been carried out using reference values from Oschlies 2001. For the actual Galapagos simulations, the choice of parameters will be determined using the observed data (Schaeffer et al., 2008, Sweet et al., 2007). The physical forcing can be generated by a spin-up of several years using NCEP forcing fields. The nitrogen compartment of the model can be initialized by the annual nitrate field from WOA98. The other compartments (phytoplankton, zooplankton, and detritus) will be initialized with a small concentration (for example. $0.1\,mmolN \cdot m^{-3}$) in the mixed layer and zero concentration below the mixed layer. HYCOM's velocity fields will be used to determine the advection fields for the NPZD model. Daily advection and horizontal diffusion of the ecosystem

components as well as the effects of diapycnal mixing and mixed layer shoaling/deepening on the concentration of the ecosystem variables will be computed. Biological source/sink terms will be computed using a forward Euler time-stepping scheme. This will result in estimations of the biological responses to the physical forcing.

A more advanced ten-compartment ecosystem model has been developed by Chai Fei (2002). This model contains compartments representing two size of phytoplankton, small phytoplankton cells (P1) and diatoms (P2), micro- and meso-zooplankton (Z1 and Z2), nonliving detrital nitrogen and silica (DN and DSi), dissolved silicic acid (Si), two forms of dissolved inorganic nitrogen: nitrate (N1) and ammonium (N2), and total CO_2 (T CO_2). The one-dimensional version is ready for release, however, the 3D version that are coupled with HYCOM are under development and will be available in the future.

2) Data Assimilation

The simulations of oceanic circulation can be improved by data assimilation. Simulations without data assimilation contain errors due to inadequate knowledge of the ocean's initial/boundary conditions, atmospheric forcing as well as those that are due to deficiencies in the model's dynamics. These errors can be corrected by assimilate available observations into model. Data assimilation is the process by which observations are used to correct the evolving state of the model (Bengtsson et al. 1981). There are several kinds of data assimilation. For example, Kalman filtering (Kalman., 1960)

attempts to exploit the effects of dynamics on the evolution of errors; while optimal interpolation (Carton and Hackert 1990) often assumes the error structure to be temporally stationary and spatially inhomogeneous. Both approaches rely on a covariance-based formalism.

HYCOM has been a leader in the application of data assimilation techniques for operational ocean predictions. The simplest method for assimilating data into HYCOM is optimal interpolation. Current efforts toward at making HYCOM operational are centering on a data-assimilation package the Navy has developed for use with more conventional models. Ensemble Kalman Filter (Evensen, G. 1994) is an advanced data assimilation technique that is implemented in HYCOM.

The EnKF is a sophisticated sequental data assimilation method. It applies an ensemble of model states to represent the error statistics of the model estimate, it applies ensemble integrations to predict the error statistics forward in time, and it uses an analysis scheme which operates directly on the ensemble of model states when observations are assimilated. The EnKF has proven to efficiently handle strongly nonlinear dynamics and large state spaces and is now used in realistic applications with primitive equation models for the ocean and atmosphere. Efforts have been made to implement EnKF in HYCOM by Navy Research Library (NRL), and a version of EnKF code that is tailored for HYCOM can be downloaded at http://enkf.nersc.no/. Further work needs to be done to improve the simulation accuracy.

References:

Bengtsson, L., M. Ghil, and E. Källén, Eds.,.1981: Dynamic Meteorology: Data Assimilation Methods. Academic Press, 330 pp.

Carton, J. A. and E. C. Hackert, 1990: Data assimilation applied to the temperature and circulation in the tropical Atlantic, 1983–84. J. Phys. Oceanogr., **20**:1150–1165

Evans, G. T., and J. S. Parslow. 1985. A model of annual plankton cycles. Biological Oceanography 3:328-347.

Evensen, G., 1994: Inverse methods and data assimilation in nonlinear ocean models. Physica D, 77:108–129.

Evensen, G., D. P. Dee, and J. Schröter, 1998: Parameter estimation in dynamical models. Ocean Modeling and Parameterization, E. P. Chassignet and J. Verron, Eds., NATO Science Series, Vol. 516, Kulwar Academic, 337–398.

Kalman, R. E., 1960: A new approach to linear filtering and prediction problems. Trans. ASME, J. Basic Eng., D82:35–45.

Oschlies, A., 2001. Model-derived estimates of new production: New results point towards lower values. *Deep Sea Research II* 48:2173- 97.

Olascoaga, M. J., Idrisi, N. and Romanou, A. (2005) Biophysical isopycnic-coordinate modelling of plankton dynamics in the Arabian Sea. *Ocean Model*, 8, 55–80.

Schaeffer, B.A., Morrison, J., Kamykowski, D., Feldman, G., Xie, L., Liu, Y., Sweet, W.V., McCulloch, A., & Banks, S., 2008: Phytoplankton biomass distribution and

seasonal change within the Galápagos Marine Reserve. Remote Sensing of Environment. 112(6), pp. 3044-3054

Sweet, W.V., J.M. Morrison, D. Kamykowski, B.A. Schaeffer, S. Banks, A. McCulloch, 2007: Water mass seasonal variability in the Galápagos Archipelago. Deep-Sea Research I 54, 2023-2035.